THÈSE DE DOCTORAT

Présentée en vue

d'obtenir le grade de

DOCTEUR

Filière: Molécules et Matière Condensée

Discipline: Chimie des Matériaux

Par

Paola Beatriz ARANGO PONTON

DOCTORAT délivré par l'UNIVERSITÉ DE LILLE

Optimisation de la pyrolyse catalytique de polyéthylène en présence de zéolithes

Optimization of catalytic pyrolysis of polyethylene in the presence of zeolites

---

Soutenue le 12 Décembre 2023 devant la Commission d'Examen composée de :

Directeurs	Prof. **Jean-François LAMONIER**, Université de Lille, France
	Prof. **Sophie DUQUESNE**, Centrale Lille Institut, France
Rapporteurs	Prof. **Bechara TAOUK**, INSA Rouen Normandie, France
	DR. **Anthony DUFOUR**, Université de Lorraine, France
Examinateurs	Prof. **Stéphane SIFFERT**, Université du Littoral Côte d'Opale, France
	Prof. **Alain MOISSETTE**, Université de Lille, France (Président)
Invitée	Ing. **Sophie HEYMANS**, Néo-Eco, France







This research is co-funded by the European Union through the European Regional Development Fund (FEDER) (50 %), I-Site (30 %), and Néo-Eco (20 %) (Specialist in recovery engineering. support for technological innovations: Focus on waste recovery processes)













Acknowledgement

This project owes its realization to the generous support of numerous individuals, to whom I wish to extend my deepest gratitude. First and foremost, I am immensely thankful to the esteemed directors of the Unité de Catalyse et Chime du Solide (UCCS) and Unité de Matériaux Et Transformations (UMET) laboratories, Franck Dumeignil and Patrice Woisel, for graciously accommodating me within their research facilities.

I would like to acknowledge the invaluable contributions of the PYROCAT team, with special mention to Guillaume Corjon, whose unwavering collaboration, guidance, and assistance were instrumental in developing this project. I also appreciate the Institut Chevreul, a pivotal part of the PYROCAT team.

My heartfelt appreciation extends to the Hauts-de-France Region, I-site, and the company Néo-Eco for their financial support, which enabled the realization of my PhD. I wish to offer particular thanks to Sophie Heymans for her insightful advice and engaging discussions during this period. Additionally, I am grateful to my mentors, Jean-François Lamonier and Sophie Duquesne, for affording me this extraordinary opportunity and warmly welcoming me into the PYROCAT team. Your guidance, shared knowledge, trust, and constructive criticism have been invaluable throughout these years. I would like to seize this opportunity to extend my sincere congratulations to Jean-François on his well-deserved appointment as the Director of the UCCS

I wish to express my gratitude to all the members of UMET for their warm reception, notably Pierre Bachelet, Johan Sarazin, Corinne Henry, Fabienne Samyn, and Séverine Bellayer. I also acknowledge Louis Meunier and Jihane Chaouay for their unwavering support.

Furthermore, I am deeply thankful to the entire UCCS team, including Barbara Declerck-Boulanger, Sandrine Berton, David Poirier, Martine Trentesaux, Stéphane Chambrey, Olivier Gardoll, Elise Berrier, Pardis Simon, Jean-Charles Morin, Mélanie Dubois, Celine Delabre, particularly Melissandre Richard, Jeremy Dhainaut, and Carmen Ciotonea, for their guidance in navigating unfamiliar situations. Special thanks to Mathieu Sauthier and Sebastien Royer for allowing me to collaborate with their respective laboratory teams.

I extend my heartfelt appreciation to my colleagues and friends at UCCS, who have lent their ear and aid, particularly Ana Fellenberg (and Banguela), Alan Barrios, Amaury Decoster, and Jianying Deng, for their unwavering support, attentive listening, and assistance. Ana, thank you very much for your unconditional friendship; you've become my sister. This journey has been challenging, but we made it!

Lastly, my deepest gratitude goes to my family. I thank my parents, Álvaro and Lilian, for their unwavering emotional support, and my grandparents, Fabio and Beatriz who, though absent, have always kept me in their thoughts and affections. I dedicate this achievement to my grandmother, Rosalba, whose strength, tenacity, wisdom, and boundless love have served as a guiding example. To my uncles, Fabio, Fernando, and Sandra, I extend my thanks for their support during critical stages of my life and their love, akin to that of a parent. Finally, to Yamid, my beloved, I am deeply grateful for your moral and

emotional support, your unwavering love, and my hope that, following this endeavour, we may continue building the family we already are.

Abstract

Plastics have been pivotal in various human activities since 1950 due to their remarkable properties. In 2021, global plastic production reached an astonishing 390.7 million metric tons (Mt). The demand for various polymer types, including PE, PP, PVC, PET, PS, and others, within the European Union (EU_{27}+3) in 2021 was predominantly driven by industries such as packaging, construction, automotive, electrical and electronic equipment, household, leisure, sports, and agriculture, among others—this extensive consumption of plastics results in the generation of a substantial volume of waste. In 2020, 29.5 Mt of plastic waste was collected in the EU, with 35 % directed towards recycling, 42 % undergoing energy recovery through incineration, and 23 % disposed of in landfills. One promising approach for recovering plastics as high-quality substances or materials is chemical recycling and catalytic pyrolysis, emerging as a valuable method for producing high-added molecules from plastic waste.

This PhD thesis focused on the catalytic pyrolysis of PE, driven by the complexity of its degradation and the goal of obtaining a pyrolysis oil rich in aromatic compounds, particularly in BTEX. A first selection process using Thermogravimetric Analysis (TGA) was conducted to identify two effective zeolites, Hβ and HZSM-5. These zeolites were subsequently used in the catalytic pyrolysis of PE following two preparation methods: extrusion and powdered mixture. HZSM-5 exhibits a higher selectivity toward aromatics due to its specific properties, while extrusion enhances the catalysis activity even if deactivation is favoured. The acidity of HZSM-5 was then modified through Zn-exchange doping to introduce more Lewis acid sites, thereby enhancing the selectivity for aromatics. The introduction of Zn ions resulted in creating one Lewis acid site at the expense of two Brønsted acid sites. It was thus shown that Zn-exchange doping permits an increase in the selectivity of the pyrolysis reaction for BTEX, even if a decrease in the overall aromatic content of the oil was noticed and attributed to the loss of Brønsted acid sites. Subsequently, the acidity was further modified through different calcination conditions involving static and dynamic airflow. Static conditions generated more dealumination, resulting in a higher density of Lewis acid sites, while dynamic conditions facilitated rapid water drainage during calcination, reducing steam-dealumination. The use of zeolite obtained under dynamic conditions allows for an increase in the aromatics content of the pyrolysis oil. Finally, the deactivation of the catalyst was studied over five cycles. It was demonstrated that after three cycles, the oil yield stabilized even if the oil composition was affected by coke deposition on acid sites.

Résumé

Les plastiques ont joué un rôle essentiel dans diverses activités humaines en raison de leurs propriétés remarquables, ce qui a conduit, en 2021, à une production mondiale de plastique de 390,7 millions de tonnes (Mt). La demande de différents types de polymères, notamment le PE, le PP, le PVC, le PET, le PS et d'autres, au sein de l'Union européenne (UE_{27}+3) en 2021 était principalement stimulée par des industries telles que l'emballage, la construction, l'automobile, les équipements électriques et électroniques, les loisirs, le sport et l'agriculture, entre autres. Cette consommation extensive de plastiques entraîne la génération d'un volume substantiel de déchets. En 2020, 29,5 Mt de déchets plastiques ont été collectés dans l'UE, dont 35 % étaient destinés au recyclage, 42 % ont subi une valorisation énergétique par incinération, et 23 % ont été enfouis dans des décharges. Différentes politiques et réglementations sont mises en place à l'échelle européenne afin d'augmenter le taux de matière recyclée, et une approche prometteuse pour la valorisation des plastiques en tant que ressources est le recyclage chimique, avec la pyrolyse, en particulier la pyrolyse catalytique, émergeant comme une méthode précieuse pour recycler les déchets plastiques, en particulier les plastiques difficiles à recycler mécaniquement.

Cette thèse de doctorat s'intéresse à la pyrolyse catalytique du PE, sujet motivé par la complexité de sa dégradation. L'objectif principal consiste à obtenir une huile de pyrolyse riche en composés aromatiques, principalement des BTEX. Initialement, un processus de présélection utilisant l'Analyse Thermogravimétrique (ATG) a été utilisé pour identifier deux catalyseurs de type zéolites, Hβ et HZSM-5, démontrant une efficacité vis-à-vis de la réactivité de la réaction de pyrolyse. Ces zéolites ont ensuite été utilisées pour la pyrolyse catalytique du polyéthylène via deux méthodes de préparation d'échantillons : l'extrusion et le mélange en poudre. HZSM-5 a montré une sélectivité vis-à-vis des aromatiques plus significative en raison de ses propriétés structurales uniques, tandis que la méthode d'extrusion a démontré une activité accrue mais également un niveau plus élevé de désactivation. L'acidité de la zéolithe HZSM-5 a ensuite été modifiée par échange avec le zinc pour introduire davantage de sites acides de Lewis en vue d'améliorer la sélectivité du catalyseur vis-à-vis des composés aromatiques. L'introduction d'ions Zn entraîne la création d'un site acide de Lewis au détriment de deux sites acides de Brønsted. Cette modification augmente la sélectivité de la réaction vis-à-vis des BTEX parmi les aromatiques totaux, bien qu'une réduction de la teneur globale en composés aromatiques ait été observée et attribuée à la perte de sites acides de Brønsted. Dans la suite de l'étude, l'acidité a été modifiée en utilisant différentes conditions de calcination, impliquant à la fois un écoulement d'air statique et dynamique. Les conditions statiques ont généré plus de désaluminisation, entraînant une densité plus élevée de sites acides de Lewis, tandis que les conditions dynamiques ont facilité un drainage rapide de l'eau pendant la calcination, réduisant la désaluminisation. Ainsi, lorsque la zéolithe préparée par calcination dynamique est utilisée, davantage de composés aromatiques sont produits. Finalement, la désactivation du catalyseur a été étudiée sur cinq cycles pour évaluer les performances de HZSM-5 calciné dans des conditions dynamiques sur la pyrolyse du polyéthylène. Après trois cycles, le rendement en huile s'est stabilisé ; cependant, la composition de l'huile est affectée par le dépôt de coke sur les sites acides.

Contents

Acknowledgement v

Abstract vii

Résumé ix

Contents xi

List of figures xvii

List of Tables xxiii

Symbols, acronyms and abbreviations xxv

General Introduction 1

I. Thesis Plan 2

II. References 4

1. Literature review 5

1.1. Post-consumer Plastic Waste 5

1.2. Recycling 7

1.2.1. Generality 7

1.2.2. Thermal process 9

1.3. Catalytic pyrolysis of polyethylene 17

1.3.1. Overview of Published Review Articles on Plastic Pyrolysis 17

1.3.2. Effects of Main Parameters on Catalytic Pyrolysis of Polyethylene 19

1.3.3. Zeolite catalyst 25

1.3.4. Zeolite ZSM-5 30

1.4. Strategic methodology 32

1.5. References 33

2. Materials and Methods 43

2.1. Introduction 43

2.2. Pyrolysis reactor 43

2.3. A pyrolysis experiment 44

Description of a typical pyrolysis experiment 44

2.4. Analytical tools 45

2.5. Optimisation of the set-up 46

2.5.1. First observations 46

2.5.2. Set-up weaknesses 47

2.5.3. Changes 49

2.5.4. Comparison of results from the new set-up with the literature data 51

2.5.5. Conclusion 53

2.6. Catalysts preparation 53

2.6.1. Feedstock 53

2.6.2. Ammonium ion exchange of zeolites 54

2.6.3. Metallic (M) ion exchange of zeolites 54

2.6.4. Calcination of zeolites 54

2.7. Catalysts characterisation techniques 55

2.7.1. X-ray diffraction (XRD) [26] 55

2.7.2. N_2-physisorption 56

2.7.3. ^{27}Al NMR [31] 59

2.7.4. Temperature-programmed desorption of Ammoniac (NH_3-TPD) [34] 59

2.7.5. Pyridine adsorption-Infrared spectroscopy (Py-IR) 60

2.7.6. RAMAN spectroscopy [46] 62

2.7.7. X-ray photoelectron spectroscopy (XPS) 63

2.7.8. Scanning electron microscopy - Energy dispersive X-ray spectroscopy (SEM-EDS) [52] 64

2.7.9. Electron microprobe analysis (EMPA) [52,53] 64

2.7.10. Inductively coupled plasma optical emission spectrometry (ICP-OES) 64

2.7.11. Thermogravimetric analysis (TGA) 65

2.8. Catalyst/Polymer mixture preparation 67

2.8.1. Pellet polymer and powdered catalyst 67

2.8.2. Extruded mixture 67

2.8.3. Powdered mixture 68

2.9. Conclusion 68

2.10. Reference 68

3. Effect of the nature, the content and the preparation method of zeolite-polymer mixtures on the pyrolysis of linear low-density polyethylene 73

3.1. Summary 73

3.2. Introduction 73

3.3. Experimental 75

3.3.1. Catalyst preparation 75

3.3.2. Samples preparation 76

3.4. Results and discussion 76

3.4.1. Effect of zeolite composition on LLDPE pyrolysis 76

3.4.2. Effect of the preparation method of the mixture 78

3.4.3. Effect of the preparation method of the mixture on the yield and selectivity of the pyrolysis reaction of LLDPE 79

3.4.4. Effect of the ratio catalyst/polymer on the yield and selectivity of the pyrolysis reaction of LLDPE 86

3.5. Conclusions 89

3.6. References 90

4. Effect of zinc doping of ZSM-5 zeolite combined with multiphase catalytic pyrolysis on the cracking of polyethylene 95

4.1. Summary 95

4.2. Introduction 95

4.3. Experimental 97

4.4. Results and Discussion 98

4.4.1. Zeolite characterisation 98

4.4.2. Pyrolysis of PE 105

4.5. Conclusion 112

4.6. References 113

5. The effect of calcination conditions on the catalytic performances of HZSM-5 zeolite for the polyethylene pyrolysis 117

5.1. Summary 117

5.2. Introduction 117

5.3. Experimental 119

5.4. Result and discussion 120

5.4.1. Effect on calcination conditions on structural and textural properties of HZSM-5 120

5.4.2. Effect of calcination conditions on Al distribution in HZSM-5 122

5.4.3. Effect of calcination conditions on HZSM-5 acid properties 125

5.4.4. Effect of calcination conditions on LLDPE catalytic pyrolysis 126

5.5. Conclusions 130

5.6. References 130

6. Study of cycles effect on the performances of HZSM-5 zeolite in the polyethylene catalytic pyrolysis 137

6.1. Introduction 137

6.2. Experimental 139

6.3. Catalytic performances of HZSM-5 up to five pyrolysis reaction cycles 139

6.4. Characterisation of spent catalysts 141

6.4.1. TG analysis 141

6.4.2. RAMAN Spectroscopy 142

6.4.3. XPS 144

6.4.4. SEM-EDS 145

6.4.5. XRD 146

6.4.6. N_2-physisorption 146

6.4.7. Acidity by NH_3-TPD 147

6.5. Discussion and conclusions 150

6.6. References 151

General Conclusion and Prospect for Future Work 157

I. The main conclusions of this thesis 157

II. The main contributions of this thesis to the catalytic pyrolysis of polyethylene 158

III. Perspective for future work 159

List of figures

Figure I. Evolution of plastic post-treatment in Europe of plastic collected from 2006 to 2020. Adapted from ref [2]. 2

Figure 1.1. Circularity of Plastics. Copyright ref [10]. 7

Figure 1.2. Routes for recycling of solid plastic waste from ref.[16]. 8

Figure 1.3. Flow chart summary of lab-scale research diagnostics for pyrolysis of waste plastic and plastic mixture adapted from ref [25] 10

Figure 1.4. Influence of temperature, polymer complexity and residence time on end-products. Copyright ref [15] 14

Figure 1.5. Diagram showing (a) continuous-stirred tank reactor; (b) batch and semi-batch reactor; (c) fixed-bed reactor; (d) conical spouted bed reactor; and (e) auger/screw reactor. Copyright ref [73] ... 19

Figure 1.6. Influence of catalyst type and temperature reaction on LDPE cracking from ref.[103] 24

Figure 1.7. Key properties of zeolites relevant to the catalytic pyrolysis of polyethylene 29

Figure 1.8. Framework structure and channel system of a ZSM-5 zeolite. Copyright from ref [144]... 30

Figure 1.9. Representation of the strategic methodology of this PhD thesis. 32

Figure 2.1. Schematic representation of the first pyrolysis facility by KLAIMY (2019) [1]; 1 Gas valve; 2 and 3 Flowmeters; 4 Cold room; 5 Stainless steel tube; 6 Spoon; 7 Electric oven; 8 Cold traps; 9 water-sealed bottle. 44

Figure 2.2. Schematic of the process used to perform the experiments. 44

Figure 2.3. Evidence in photos of the losses of the wax-liquid fraction inside the reactor. 46

Figure 2.4. Schematic representation of the first pyrolysis facility by KLAIMY (2019) [1] and the detected points to improve. 48

Figure 2.5. Photos of the original (a) and modified (b) cold traps **(Change #2)** 48

Figure 2.6. Schematic representation of the pyrolysis facility (2nd set-up) and its changes 49

Figure 2.7. Diagram of pyrolysis results from the first set-up to the optimised set-up. The reaction temperature and the nitrogen flow were 550 °C and 200 mL.min^{-1}, respectively. 50

Figure 2.8. First version (a) and new design (b) of the cold traps after pyrolysis experiment. 50

Figure 2.9. Final schematic representation of the pyrolysis facility (2nd setup); 1 Gas valve; 2 Flowmeter; 3 Cold room; 4 Stainless steel tube; 5 Spoon; 6 Electric heater; 7 Heating zone; 8 Hot Chamber; 9 Thermocouple; 10 Cold traps; 11 water-sealed bottle..... 51

Figure 2.10. Yield composition of pyrolysis of Pure LDPE from this study and references. 52

Figure 2.11. Fraction yield of the decomposition of pure LLDPE (a). Composition of the oil pyrolysis fraction (b) and carbon distribution of the oil fraction (c) at 550 °C at different nitrogen flow: 200 $mL.min^{-1}$ (LLDPE-200), 400 $mL.min^{-1}$ (LLDPE-400), 600 $mL.min^{-1}$ (LLDPE-600).and 800 $mL.min^{-1}$ (LLDPE-800)..... 53

Figure 2.12. System set-up for the ion exchange process. 54

Figure 2.13. (a) Profile of the calcination procedure, photos of furnace used for calcination on dynamic conditions (b) and static conditions (c). 55

Figure 2.14. Geometrical condition for diffraction from lattice planes from reference [26]..... 56

Figure 2.15. BET equipment used to perform the catalyst analysis. 57

Figure 2.16. (a) The IUPAC classification of adsorption isotherms: Microporous (type I), non-porous or macroporous (types II, III and VI), mesoporous (types IV and V) and (b) Types of hysteresis loops obtained by nitrogen physisorption [27]..... 58

Figure 2.17. Schema of the operation of an NMR system (a). ^{27}Al MAS NMR spectra of HZSM-5 zeolites with different treatments and doping from ref [32] (b), collected from a frequency at 79.5 MHz and spinning speed of 10 kHz. 59

Figure 2.18. The NH_3-TPD equipment used in this study (a). NH_3-TPD profiles of different HZSM-5 zeolites from ref [32] (b), the desorption was made from 177 °C to 550 °C at 10 $°C.min^{-1}$. 60

Figure 2.19. Pyridine adsorption to the zeolite surface (a). FTIR spectra of adsorbed pyridine at different temperatures of a ZSM-5 zeolite calcinated first under nitrogen and then under air from (a) ref [35]..... 61

Figure 2.20. Raman spectra of a spent HZSM-5 after cracking of polyethylene ref [47]. 62

Figure 2.21. XPS equipment used in this study..... 63

Figure 2.22. Components of an ICP-OES instrument from ref. [55]..... 65

Figure 2.23. Evaluation of catalytic activity through TG (a) and DTG (b) profiles of thermal and catalytic degradation of pure LDPE over different catalysts from ref [57], and evaluation of the coke deposition through TG (c) and DTG (d) profiles of used Mo/H-ZSM-5 catalysts obtained after a 5 recycle reaction including oxidative regeneration at 450, 550, 700, and 850 °C. from ref [58]..... 66

Figure 2.24. Schema of a Mix arrangement **(A)** of pellet polymer and powdered catalyst, Mix/Layer arrangement **(B)** and the layer arrangement **(C)**..... 67

Figure 3.1. TGA conversion (a) and DTG (a) curves of LLDPE degradation and its respective mixtures under nitrogen atmosphere, using a ratio catalyst:polymer, 1:1. (a) no catalyst, (b) NaY (5.1), (c) Hβ (360), (d) HZSM-5 (23), (e) HY (5.1), and (f) Hβ (25). 78

Figure 3.2. TGA **(a)** and DTG **(b)** curves obtained during the pyrolysis under nitrogen atmosphere of a LLDPE/ Hβ (25) (a) and LLDPE/ HZSM-5 (23) (a) mixtures achieved by simple powder mixing (red lines) : (a) (TG) and (a) DTG; or by extrusion (black lines) : (c) (TG) and (d) DTG, using a ratio catalyst:polymer 1:10..... 79

Figure 3.3. Possible pathways scissions of the catalytic pyrolysis of polyethylene with zeolite acid catalysts from ref [55]. 80

Figure 3.4. Reaction mechanism illustration of olefinic and aromatic cycles on acid active sites from ref [56]..... 80

Figure 3.5. Yield result of pyrolysis of LLDPE with Hβ (25) (a) and composition of oil/wax (b) from the decomposition of LLDPE with Hβ (25) using powdered polymer (Powdered) or catalyst extruded with polymer (Extruded). 81

Figure 3.6. Yield result of pyrolysis of LLDPE with HZSM-5 (23) (a) and composition of oil/wax (b) from the decomposition of LLDPE with HZSM-5 (23) using powdered polymer (Powdered) or catalyst extruded with polymer (Extruded)..... 83

Figure 3.7. TG (a) and DTG (b) curves of Hβ (25) and HZSM-5 (23) zeolites after reaction using powdered catalyst-polymer mixture (Powdered) or catalyst extruded with polymer (Extruded) under air. 84

Figure 3.8. XRD of Hβ (25) (a) and HZSM-5 (23) (b) zeolites before reaction (Fresh) and after reaction using powdered catalyst-polymer mixture (Powdered) or catalyst extruded with polymer (Extruded). 85

Figure 3.9. TG (a) and DTG (b) curves obtained during the pyrolysis of LLDPE under nitrogen atmosphere at 10 °C . min^{-1} with Hβ (25) zeolite using different catalyst: polymer ratios : (a) 0:100, (b) 1:100, (c) 1:50, (d) 1:30, (e) 1:20, (f) 1:10, (g) 1:5..... 87

Figure 3.10. TG (a) and DTG (b) curves obtained during the pyrolysis of LLDPE under nitrogen atmosphere at 10 °C.min^{-1} with HZSM-5 (23) zeolite using different catalyst: polymer ratios: (a) 0:100, (b) 1:100, (c) 1:50, (d) 1:10..... 87

Figure 3.11. Comparison of the effect of the concentration of catalyst on the decomposition of LLDPE in the presence of Hβ (25) (a) and HZSM-5 (23) (b) zeolites on relative activity from the TG curves obtained in this study (red) and in ref [21] (black) at 10 °C . min^{-1} under nitrogen atmosphere. 89

Figure 4.1. XRD patterns of HZSM-5 and ZnZSM-5 catalysts. 98

Figure 4.2. N_2-physisorption isotherms at -196 °C (a) and BJH pore size distribution (b) of HZSM-5 and ZnZSM-5 catalysts. 99

Figure 4.3. XPS core-level spectra of Zn 2p (a) of ZnZSM-5 and XPS core-level spectra of Si 2p (b), Al 2p (c) and O 1s (d) of the HZSM-5 and ZnZSM-5 zeolites. 100

Figure 4.4. Electron microprobe images of HZSM-5 and ZnSM-5 zeolites. 101

Figure 4.5. NH_3-TPD curves of HZSM-5 (blue) and ZnZSM-5 (yellow) zeolites. 102

Figure 4.6. Pyridine FT-IR of HZSM-5 and ZnZSM-5 zeolites after desorption at 150, 250, 350, and 450 °C (a). And their respective Brønsted (b) and Lewis (c) acid sites distribution as functions of the strength of the acid site, very weak (150 °C), weak (250 °C), medium (350 °C) and strong (>450 °C). 104

Figure 4.7. Zinc species reported in the literature from ref [13] 105

Figure 4.8. TG (a) and DTG (b) curves under N_2 of pure LLDPE the corresponding mixtures with ZSM-5 Zeolites. 105

Figure 4.9. Liquid composition (a) and BTEX composition (b) results of pyrolysis of LLDPE with protonated (HZSM-5) and Zn-doped (ZnZSM-5) zeolites at 500 °C under nitrogen. 107

Figure 4.10. Liquid composition (a) and BTEX composition (b) results of pyrolysis of LLDPE with protonated (HZSM-5) and Zn-doped (ZnZSM-5) zeolites at 450 °C and 500 °C under nitrogen. 112

Figure 5.1. XRD patterns of the native NH_4^+-ZSM-5 zeolite and the calcined HZSM-5 DC and HZSM-5 SC zeolites. 120

Figure 5.2. N_2 physisorption curves (a) and pore size distribution (b) of the calcined HZSM-5 DC and HZSM-5 SC zeolites. 121

Figure 5.3. ^{27}Al MAS NMR of ZSM-5 samples: native NH_4^+-ZSM-5 (Purple), HZSM-5 DC (Blue), and HZSM-5 SC (Green). 122

Figure 5.4. XPS core-level spectra of Si 2p (a), Al 2p (b) and O 1s (c) of the native NH_4^+-ZSM-5 zeolite and the calcined HZSM-5 DC and HZSM-5 SC zeolites. 124

Figure 5.5. Pyridine FT-IR of HZSM-5 DC and HZSM-5 SC zeolites after desorption at 150, 250, 350, and 450 °C (a). And their respective Brønsted (b) and Lewis (c) acid sites distribution as functions of the strength of the acid site, very weak (150 °C), weak (250 °C), medium (350 °C) and strong (>450 °C). 125

Figure 5.6. TG (a) and DTG (b) curves under N_2 of LLDPE and the corresponding mixtures with the HZSM5 Zeolites. 126

Figure 5.7. Yield result of pyrolysis of LLDPE at 480 °C (Purple), LLDPE + HZSM-5 DC (Blue), and LLDPE + HZSM-5 SC (Green). 128

Figure 5.8. Product carbon distribution (a) and composition (b) of the oil/wax from the decomposition of LLDPE at 480 °C (Purple), LLDPE + HZSM-5 DC (Blue), and LLDPE + HZSM-5 SC (Green). 129

Figure 6.1. Possible states of deactivation of acid sites of the zeolite after coke deposition from ref. [13]. 138

Figure 6.2. Yield result of pyrolysis of LLDPE with HZSM5 zeolite after first use (1-cycle) and after using it five times (5-cycle). 140

Figure 6.3. Carbon distribution of the wax+oil of pyrolysis of LLDPE with HZSM5 zeolite after first use (1-cycle) and after using it five times (5-cycle). 140

Figure 6.4. Composition of oil/wax product (a) and total BTEX (b) from liquid yield composition of catalytic pyrolysis of LLDPE after fifth use of HZSM-5 DC catalyst. 141

Figure 6.5. TG (a) and DTG (b) curves of HZSM-5 DC zeolites after one and five reactions under air. 142

Figure 6.6. RAMAN Spectroscopy curves of HZSM-5 DC fresh and after one and five cycles of reaction. 143

Figure 6.7. XPS core-level spectra of Si 2p (a), Al 2p (b), O 1s (c) and C 1s (d) of HZSM-5 DC fresh and after five cycles of reaction 145

Figure 6.8. SEM images of fresh (a) and spent HZSM-5 DC zeolite after five cycles (b). 146

Figure 6.9. XRD of HZSM-5 DC zeolite before reaction (Fresh) and after one and five cycles of reaction. 147

Figure 6.10. N_2-physisorption isotherms at -196 °C (a) and BJH pore size distribution (b) and total specific surface area (BET surface), external and micropore surface area (c) of HZSM-5 zeolites before reaction (Fresh) and after five reaction cycles. 148

Figure 6.11. NH_3-TPD curves of HZSM-5 fresh and after five cycles of reactions 149

Figure 6.12. Schema of coke formation from reference [5]. 150

List of Tables

Table 1.1 Different types of pyrolysis and operating parameters from ref [26], [27] 11

Table 1.2 Plastic types and their characteristics, applications and role in pyrolysis adapted from ref [2], [30]–[35] 13

Table 1.3. Synthesis of the free radical mechanism of the thermal degradation of polyethylene from references [44], [45] 15

Table 1.4 Overview of a selection of reviews covering various studied factors for waste plastic pyrolysis. 18

Table 2.1 Comparison of liquid yield (wt. %) of the pyrolysis of PS from KLAIMY 2019 [1] study and the bibliography. 47

Table 3.1 Main characteristics of the catalysts used in the study 76

Table 3.2 Characteristic data obtained from TGA and DTG for LLDPE and its respective mixture with different catalysts under nitrogen atmosphere (ratio catalyst:polymer, 1:1) 77

Table 3.3 Carbon distribution by family of products from pyrolysis of LLDPE with Hβ (25) using powdered polymer (Powdered) or catalyst extruded with polymer (Extruded). 82

Table 3.4 Textural properties of Hβ (25) and HZSM-5 (23) zeolites before reaction (Fresh) and after reaction using powdered catalyst-polymer mixture (Powdered) or catalyst extruded with polymer (Extruded). 85

Table 3.5 Data extracted from TG and DTG curves obtained in the course of the LLDPE pyrolysis (10 °C.min^{-1}) under nitrogen atmosphere (100 mL.min^{-1}) 88

Table 4.1 Textural properties and relative crystallinity of the ZSM-5 zeolites. 99

Table 4.2 XPS and ICP-OES results of ZSM-5 zeolites. 101

Table 4.3 NH_3-TPD results of HZSM-5 zeolites from different types of doping 103

Table 4.4 Total, Brønsted and Lewis acid sites of ZSM-5 Catalysts Measured by Pyridine FT-IR 103

Table 4.5. Temperature of maximum decomposition rate and total weight loss of LLDPE and polymer mixtures with ZSM-5 zeolites. 106

Table 4.6 Yield result of pyrolysis of LLDPE with HZSM-5 and ZnZSM-5 zeolites at 500 °C. 106

Table 4.7 Yield result of pyrolysis of LLDPE with HZSM-5 and ZnZSM-5 zeolites at 450 °C and 500 °C. 111

Table 5.1 Textural properties and relative crystallinity of the calcined HZSM-5 DC and HZSM-5 SC zeolites. 121

Table 5.2 Si/Al superficial ratio from XPS. Al atoms distribution from ^{27}Al MAS NMR and XPS. And Total, Brønsted and Lewis acid sites measured by Pyridine FT-IR in ZSM-5 zeolites. 123

Table 5.3 Temperature of maximum, 5 %, 50 % and 95 % of decomposition and total weight loss of LLDPE and polymer mixtures with both HZSM5. 127

Table 6.1 Characteristic fraction of deconvoluted area of lines assignee in the Raman spectra and peak position of the spent HZSM-5 DC zeolite after one and five reaction cycles. 143

Table 6.2 XPS surface atomic concentration of the fresh and used catalysts after five cycles. 144

Table 6.3 NH_3-TPD and pore volume results of fresh and spent (after five cycles) HZSM-5 zeolite. 149

Symbols, acronyms and abbreviations

Al	Aluminium
BE	Binding energy
BET	Brunauer-Emmett-Teller theory
BJH	Barret-Joyner-Halenda theory
BTEX	Benzene, Toluene, Ethylbenzene and Xylenes
BTX	Benzene, Toluene and Xylenes
C	Carbon
CH_4	Methane
CO	Carbon monoxide
CO_2	Carbon dioxide
e.g.	Latin exempli gratia, meaning for example
EDS	Energy dispersive X-ray spectroscopy
EMPA	Electron microprobe analysis
EPS	Expanded polystyrene
et al.	Latin et alii, meaning and co-workers
EU_{27}+3	European Union plus Norway, Switzerland and the United Kingdom
GC	Gas chromatography
H	Hydrogen
H_2	Hydrogen gas
H_2S	Hydrogen Sulphide
H_2-TPR	hydrogen temperature-programmed reduction
HCl	Hydrochloric acid
HDPE	High-density polyethylene
HHV	High heat value
i.e.	Latin id est, meaning that is
ICP-OES	inductively coupled plasma optical emission spectrometry
IR	Infrared spectroscopy
LDPE	Low-density polyethylene
LLDPE	Linear low-density polyethylene
MDPE	Middle-density polyethylene
MPW	Municipal plastic waste
MS	Mass spectrometry
Mt	Million tonnes
N	Nitrogen
N_2	Dinitrogen

NH_3	Ammonia
NMR	Nuclear magnetic resonance
NO_x	Nitrogen oxides
P	pressure
P_0	atmospheric pressure
PE	Polyethylene
PET	Polyethylene terephthalate
PP	Polypropylene
PS	Polystyrene
PSW	Plastic solid waste
PUR	Polyurethane
PVC	Polyvinyl Chloride
S	Sulphur
SEM	Scanning electron microscope
TGA	Thermogravimetric analysis
TPD	Temperature-programmed desorption
XDR	X-ray diffraction
XPS	X-ray photo-electron spectroscopy
θ	Bragg angle (XRD)
λ	stoichiometric factor or wavelength of source radiation (XRD)

General Introduction

Plastics play a crucial role in various industries and are integral to our daily lives, contributing significantly to our economy. The widespread utilization of plastics is justified by their favourable physical and chemical properties, cost-effectiveness compared to alternative materials [1], and their applicability in diverse market sectors, including packaging, building and construction, among others [2].

Plastics predominantly derive from petrochemical sources, utilizing approximately 4 % of global fossil feedstocks, and this proportion is estimated to range between 4 % and 6 % in Europe [3]. In terms of global production in 2021, Europe ranks as the third largest producer of plastics, generating 57.2 million tons (Mt) domestically. This places Europe behind Asia (including China) and North America, accounting for 49 % and 18 % of global production, respectively, which amounted to 390.7 Mt [2]. France exhibits the third highest demand among European countries, constituting 9.4 % of the European market [2].

The overall demand for various polymer types (PE, PP, PVC, PUR, PET, PS, EPS, and others) within Europe (EU27+3) in 2021 was primarily driven by industries such as packaging, building and construction, automotive, electrical and electronic, household, leisure or sports, and agriculture, among others. Such consumption of plastics leads to a large volume of waste production. In 2020, a total of 29.5 million tons (Mt) of plastic waste were collected, with 35 % being directed towards recycling, 42 % undergoing energy recovery through incineration, and 23 % being disposed of in landfills [2].

Production of plastic waste and, in particular, mismanaged plastic waste is also associated with detrimental effects on the environment [4]. A significant concern arises from the non-biodegradable nature of most plastic materials. Regrettably, over the past few years, a staggering amount, ranging from 8 to 12 million tons of plastic waste has accumulated in our oceans [5]. These marine environments are now inundated with microplastics or concentrated patches of marine litter, which become entangled in ocean currents and impose severe ecological damage upon marine ecosystems. Consequently, plastic pollution poses a potential threat to human health through the contamination of the food chain [6]. The packaging industry is primarily responsible for this environmental predicament [7]. The problem is exacerbated as plastic waste production increases in tandem with population growth, particularly in developing nations, where the demand for plastic is escalating [1]. It is worth noting that approximately 40 % of total plastic production is dedicated to single-use plastic items [7].

As an indication of growing awareness regarding the environmental challenges associated with waste management, including plastic waste, a transition is underway in the treatment of post-consumer waste. This shift involves moving away from the linear economic model of production and traditional disposal methods such as landfills, energy recovery, and mechanical recycling. Instead, the focus is on reducing resource consumption, redesigning materials to be more eco-friendly, extending product lifespans through reuse, setting waste limits, and valorising or recycling waste. This transition aligns with the principles of a circular economy, which have been embraced since 2008 [6]. In Europe, the

implementation of circular economy practices has yielded significant results. Between 2006 and 2020, recycling rates increased by 117.7 %, the utilization of post-consumer plastic waste in energy recovery grew by 77.1 %, and landfill volumes decreased by 46.4 % [2]. These changes are illustrated in Figure I, which depicts the variations observed during this time period. The European Commission has set ambitious targets, aiming to achieve 100 % plastic packaging recyclability in a cost-effective way by 2030 [6].

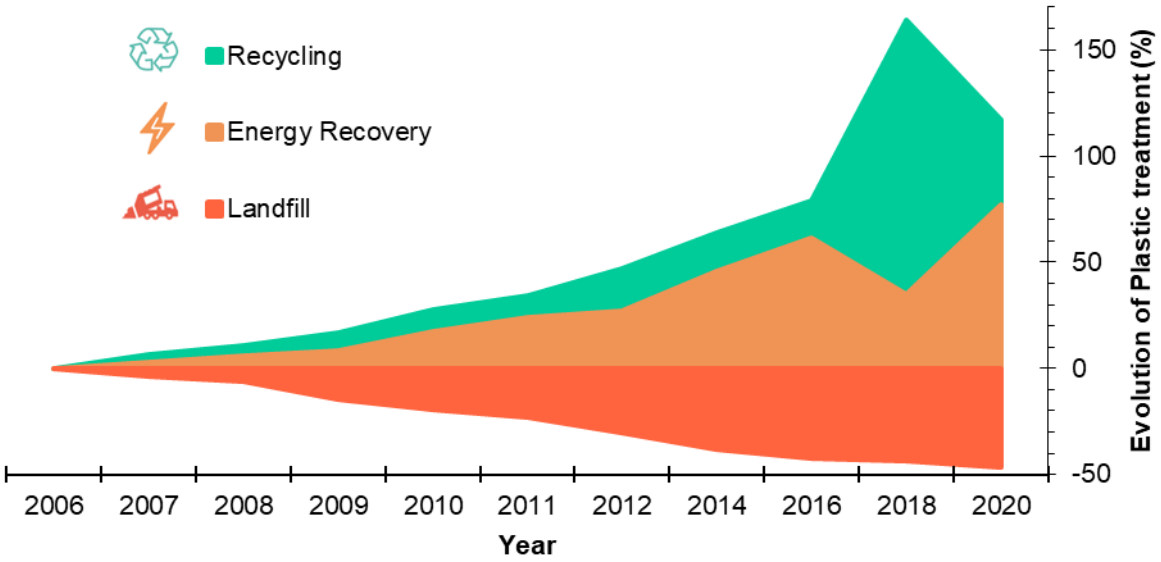

Figure I. Evolution of plastic post-treatment in Europe of plastic collected from 2006 to 2020. Adapted from ref [2].

Achieving these objectives presents a significant challenge. Landfilling continues to pose a threat to soil contamination, while incineration, although providing energy recovery, leads to emissions of pollutants, particularly CO_2. Additionally, the mechanical recycling of plastics faces limitations, including the degradation of polymer properties over its lifespan, resulting in diminished strength and toughness compared to virgin polymers.

A promising solution that offers a means to extract value from plastic waste involves chemical recycling and, in particular, catalytic pyrolysis. This process involves the cracking of plastics, yielding oils with high potential chemical value. Catalytic pyrolysis is performed under an inert atmosphere, typically at lower temperatures compared to thermal pyrolysis when combining the polymer with a catalyst. The use of a closed system in catalytic pyrolysis helps to mitigate the generation of pollutants.

I. Thesis Plan

Considering the advantages associated with catalytic pyrolysis of plastic, the PYROCAT team, comprising researchers from the CHEVREUL Institute (UMET and UCCS Laboratories) and the Neo-Eco company, conducted first the PhD thesis of Sophie KLAIMY. This thesis focused on various aspects, including the thermal cracking of a model mixture of plastic waste commonly used in packaging, the

investigation of its decomposition mechanism [8], the optimization of the catalytic process for polyethylene (the predominant polymer in packaging) using a commercial zeolite ZSM-5, and the exploration of different parameters such as reaction temperature, polymer/catalyst ratio, and various Si/Al ratios. Furthermore, the study evaluated the influence of several acid catalysts synthesized in the laboratory on yield and selectivity [9]. The experiments were performed using an improved homemade reactor specifically designed for this project.

To advance the knowledge in this field and identify the most suitable catalytic option, the present research aims to identify an optimal catalytic formulation for plastic waste pyrolysis and optimize the pyrolysis process. Consequently, this thesis encompasses three primary objectives:

- Select, develop, and optimize catalytic materials capable of selectively converting polyethylene during catalytic pyrolysis, with the aim of minimizing the formation of solid by-products (pyrolysis coke) and maximizing the production of the liquid phase (oil). This will involve exploring novel catalytic formulations specifically designed for the treatment of polyethylene in catalytic pyrolysis.
- Optimise the catalytic pyrolysis process to enhance the generation of aromatic compounds, particularly benzene, toluene, ethylbenzene, and xylene (BTEX), in the liquid phase. The focus will be on maximizing the yield of these valuable compounds with improved selectivity.
- Investigate the capability of the optimized catalysts to maintain their activity and selectivity over multiple pyrolysis cycles. The stability and performance of the catalysts will be assessed to determine their suitability for prolonged use in the catalytic pyrolysis process.

These objectives were developed in the following chapters:

The ***first chapter*** provides a comprehensive review of various post-consumer plastic waste treatment methods, with a specific focus on pyrolysis. The literature review explores the influence of plastic feedstock composition, reactor types, reaction conditions, and catalysts, particularly highlighting the significance of zeolite ZSM-5.

The ***second chapter*** describes the optimization of the experimental setup and outlines the materials and methods employed throughout the thesis. This includes details regarding the plastic samples used, various commercial catalysts, characterization techniques for material analysis, and the pyrolysis process itself.

The ***third chapter*** is divided into three parts. The first part investigates the pyrolysis of polyethylene via thermogravimetric analysis (TGA), focusing on the influence of different types of zeolite catalysts. The second part evaluates the effect of the preparation method to mix the polymer and the catalyst prior to performing the pyrolysis. The last part is dedicated to the study of the effect of catalyst-to-polymer ratio.

The ***fourth chapter*** explores the specific reaction conditions required to achieve the desired improvement in BTEX selectivity. With that purpose, it compares the performance of zeolite ZSM-5 and

doped zeolite Zn-ZSM-5 simultaneously with three different types of catalyst-polymer contact to assess whether the modification and/or the process enhances BTEX selectivity.

The ***fifth chapter*** investigates whether there are any differences in the pyrolysis of polyethylene resulting from two different calcination methods of the zeolite as the method used to modify its acidity. The chapter explores the effects of these calcination techniques on the pyrolysis process and associated outcomes.

The last and ***sixth chapter*** focuses on evaluating the stability of zeolite ZSM-5 after undergoing five cycles of pyrolysis. The chapter examines any potential changes in catalytic performance or material degradation over repeated pyrolysis cycles.

This PhD thesis (PYROCAT project) was financially supported by the European Union through the European Regional Development Fund (ERDF), I-Site, and Néo-Eco, a specialist in recovery engineering and technological innovation for waste recovery processes.

II. References

[1] S.M. Al-Salem, A. Antelava, A. Constantinou, G. Manos, A. Dutta, A review on thermal and catalytic pyrolysis of plastic solid waste (PSW), J. Environ. Manage. 197 (2017) 177–198. https://doi.org/10.1016/j.jenvman.2017.03.084.

[2] Plastics Europe, Plastic Europe 2022, 2022. https://plasticseurope.org/knowledge-hub/plastics-the-facts-2022/.

[3] British Plastics Federation, Oil Consumption, (2019). https://www.bpf.co.uk/press/Oil_Consumption.aspx (accessed November 4, 2019).

[4] Plastics Europe, Plastics Europe Association of Plastics Manufacturers Plastics—The Facts 2022, 2022. https://plasticseurope.org/knowledge-hub/plastics-the-facts-2022/ (accessed August 26, 2022).

[5] Secourue, une tortue a déféqué l'équivalent de 26 pailles - Sciences et Avenir, (n.d.). https://www.sciencesetavenir.fr/animaux/animaux-marins/secourue-une-tortue-a-defeque-l-equivalent-de-26-pailles-en-plastique_140927 (accessed March 19, 2020).

[6] European Commission, A European Strategy for Plastics, Eur. Com. (2018) 24. https://doi.org/10.1021/acs.est.7b02368.

[7] E. Joltreau, of International Plastic Waste Trade Stakes at Play and Perspectives, 2019 (2019) 1–6.

[8] S. KLAIMY, J.F. LAMONIER, M. CASETTA, S. HEYMANS, S. DUQUESNE, Recycling of plastic waste using flash pyrolysis – Effect of mixture composition, Polym. Degrad. Stab. 187 (2021) 109540. https://doi.org/10.1016/j.polymdegradstab.2021.109540.

[9] S. Klaimy, C. Ciotonea, J. Dhainaut, S. Royer, M. Casetta, S. Duquesne, G. Tricot, J.-F. Lamonier, Flash catalytic pyrolysis of polyethylene over (alumino)silicate materials, CHEMCATCHEM Catal. (2019). https://doi.org/10.1002/cctc.201901819.

Chapter 1

1. Literature review

Plastics are synthetic compounds, defined by IUPAC as *"material which contains as an essential ingredient a high polymer and which, at some stage in its processing into finished products, can be shaped by flow*" [1]. They have been integral to human activity since 1950 due to their versatility [2]. Plastics are present in our daily lives, serving as the foundation for various products such as bottles, films, and boxes (especially in packaging), and they are essential components in industries spanning construction, transportation, electronics, energy, and more [3]. In 2019, slightly over 99 % of global plastic production relied on petrochemical resources [4], although they can also be derived from biomass like cellulose, natural gas, coal, or salt [5].

The production of plastics designed for their intended applications necessitates various processes, such as polyaddition or polycondensation [5]. Plastics can be broadly categorized into two prominent families: Thermoplastics and Thermosets. In the latter's case, exposure to heat followed by cooling induces structural changes [6], which are irreversible [7]. Consequently, the recyclability of Thermosets poses a considerable challenge. Materials unsaturated polyester or epoxy exemplify common Thermosets [7].

In contrast, Thermoplastics can be melted and solidified repeatedly without altering their fundamental structure, offering the potential for recyclability [7]. Among these, key polymers in the packaging industry include polyethylene (PE), polypropylene (PP), polystyrene (PS), and polyethylene terephthalate (PET) [8]. PE, the dominant material in packaging, covers high-density polyethylene (HDPE) in products such as shampoo bottles, milk containers, and freezer bags, as well as low-density polyethylene (LDPE) for food packaging films [8]. PP finds its application in bottle caps and plastic bags, while PET is commonly employed in water and beverage bottles. Polystyrene is favoured for fabricating hot beverage cups and protective packaging materials [8].

1.1. Post-consumer Plastic Waste

Plastic has generated severe environmental, social and human health problems for various reasons. First, those materials are durable, which is why they are used; it is the plastic paradox. Second, there is an escalating global demand for plastics, particularly in developing nations, coupled with the allocation of approximately 40 % of total plastic production for single-use purposes [9] and the inadequate waste management practices in some developing regions, which sometimes accept waste from developed countries [8].

These plastic wastes are distinguishable as either municipal or industrial plastic waste. The latter category typically contains relatively uncontaminated plastics and is amenable to repalletization and remoulding. Conversely, municipal plastic waste (MPW), comprising predominantly polyethylene (PE), polypropylene (PP), polystyrene (PS), and polyvinyl chloride (PVC), among others, is chiefly attributed

to the packaging industry, representing approximately 60 % of total plastic waste within the European Union [9]. MPW often arrives contaminated and, in certain instances, commingled with other plastics or materials, especially in the absence of well-defined separation policies, rendering mechanical recycling a complex effort. In Europe, just 35 % of the approximately 29.5 million tons of used plastic collected in 2020 underwent recycling, 42 % were channelled into energy recovery processes, and 23 % were relegated to landfills [10].

Incineration, while capable of converting recovered plastics into electricity or combined heat and power, poses the risk of releasing greenhouse gases and hazardous substances into the atmosphere. This is particularly pronounced when incinerating mixed plastic waste, notably in the presence of PVC, which can generate dioxins, polychlorinated biphenyls, and furans [11], [12].

Regrettably, landfilling remains the predominant destination for post-consumer conventional plastic waste, accounting for a global share of 79 % [13], despite its associated drawbacks. Landfill sites are becoming increasingly scarce, and they entail enduring risks of soil and groundwater contamination due to the by-products of plastic decomposition, which can manifest as persistent organic pollutants [12].

In sound waste management practice, the environmental management hierarchy prefers reduction, reuse, recycling, and energy recovery, with landfilling as a last resort [12]. Illustrating this approach, the Indian Government has enacted bans on producing and using specific plastics [8]. At the same time, the United Kingdom has shifted responsibility for plastic disposal to packaging producers, with an ultimate target of eliminating plastic waste by 2042 and investment in plastic innovation research [8]. Parallel policies have been implemented by the European Commission under the "European strategy for plastics in a circular economy" [14].

Comparing 2020 to 2006 in Europe, a positive trend in plastic collection has been observed, with recycling rates surging by 117.7 %. Conversely, the utilization of plastics for energy recovery through incineration has risen by 77.1 %, while landfilling has diminished by 46.4 % [10]. This underscores the European Union's dedication to adhering to established agreements for responsible plastic waste disposal by the circular economy strategy for plastics in Europe [14]. The circular economy seeks to incorporate the recovery of plastic waste intended for recycling into monomers and oligomers, enabling their re-polymerization after purification for use in equivalent applications to virgin polymers derived from fossil fuels [15], as depicted in **Figure 1.1**.

Recycling plastics results in the management of plastic waste in non-destructive and economically viable manners, including reuse or reprocessing into valuable products, with proper collection as the foremost step [8]. A prime illustration is the successful recycling of PET bottles through hydrolysis, which converts PET back into monomers for subsequent re-polymerization [8]. However, the complexity of recycling arises in situations such as trays, tubs, pots, and containers, which consist of diverse plastic and non-plastic materials, thereby complicating the separation process [8].

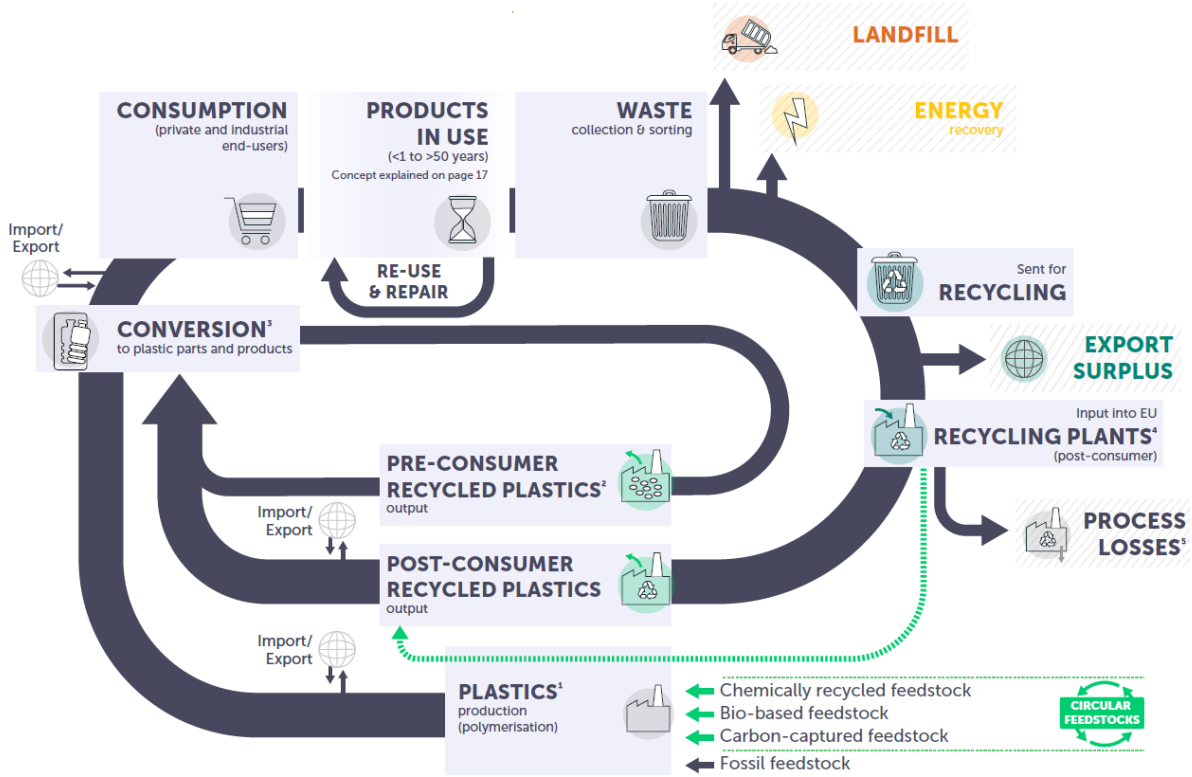

Figure 1.1. Circularity of Plastics. Copyright ref [10].

1.2. Recycling

1.2.1. Generality

A multitude of activities exist for the recovery and recycling of plastic materials, which can be categorized into four principal classifications: primary, secondary, tertiary, and quaternary recycling, as visually depicted in **Figure 1.2**.

- ***Primary or closed-loop recycling*** includes the mechanical reprocessing of uncontaminated plastic into materials with properties akin to their original state. This method is unsuitable for municipal plastic waste, which typically carries contaminants [12], [16]. A drawback is that primary recycling encounters limitations for plastic packaging, with the potential for up to seven recycling cycles before polymer degradation occurs [16].
- ***Secondary recycling*** results in the mechanical reprocessing of plastic waste into new products with reduced properties, thereby representing a form of downgrading [12], [16].
- ***Tertiary or chemical recycling*** seeks to recover plastics as valuable chemical constituents or raw materials [12], [16].
- ***Quaternary recycling*** involves energy recovery through the combustion of plastic waste [12], [16].

Of these recycling approaches, secondary and tertiary recycling align most closely with the objectives of the circular economy. Solis et al. [16] characterize ***mechanical recycling*** as a process yielding

materials distinct from the original plastics and possessing diminished performance criteria and lifespans. Moreover, this method can sometimes prove costlier than utilizing virgin plastics. In instances involving plastic mixtures and/or contaminated plastics, mechanical recycling necessitates procedures such as grinding, washing, separation, drying, re-granulation, extrusion, and compounding [17]. This reliance on additional steps, including implementing intricate separation and classification systems, cleaning and drying processes, size reduction mechanisms, and waste rejection systems, can escalate recycling expenses while diminishing process efficiency. Consequently, there is an initial loss of material amounting to approximately 10 %, accompanied by a parallel reduction in material quality. The need for these supplementary steps is contingent on the nature of the waste and the ultimate process quality [16].

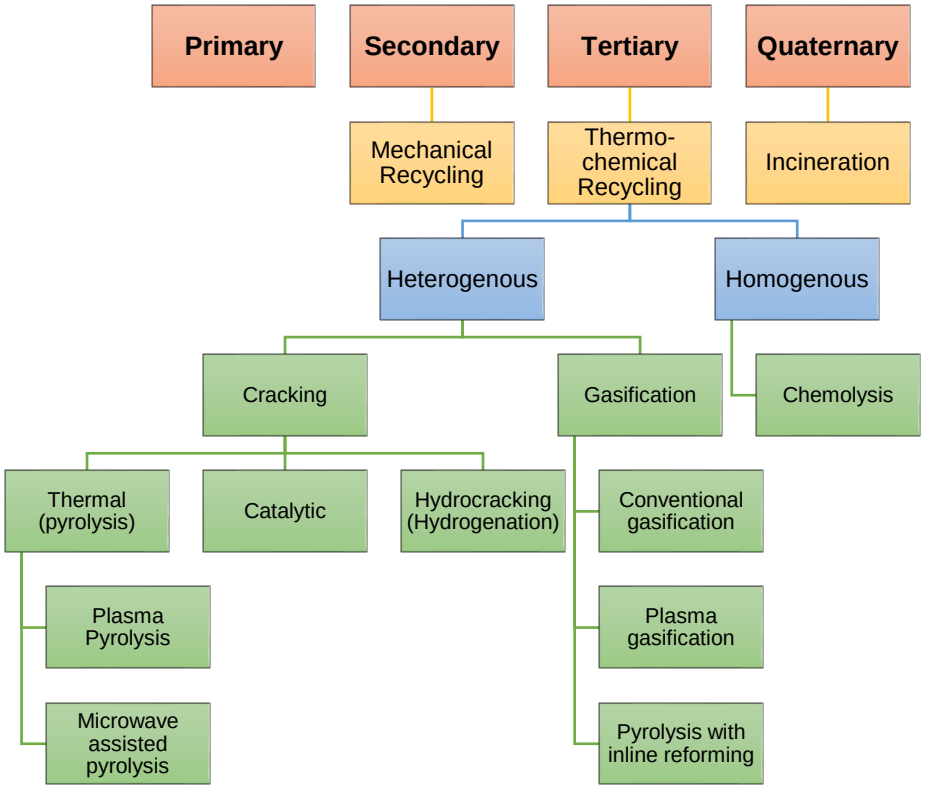

Figure 1.2. Routes for recycling of solid plastic waste from ref.[16].

In contrast, ***chemical recycling*** [12], [16], [17] can recover plastics as high-quality substances or materials, such as the petrochemical constituents of the polymer, other high-value chemicals, or even fuels. These recycling techniques can accommodate polymer mixtures or contaminated polymers, thus facilitating the closure of circular economy cycles more efficiently. However, chemical recycling is frequently not economically advantageous, as the costs associated with petrochemical-origin raw materials are typically lower than the production expenses incurred through this recycling modality. Chemical recycling divides heterogeneous mixtures into two overarching categories: pyrolysis and gasification.

1.2.2. Thermal process

Combustion

The combustion or incineration process of plastic waste entails the oxidative degradation of the material to harness energy in the form of heat. The objective of incineration is to optimize the utilization of this energy, derived from a cost-effective and readily available raw material, while minimizing adverse environmental impacts [18], [19]. This is achieved through meticulous control of the combustion temperature. However, it is noteworthy that the conventional approach does not involve pre-treatment or classification of the polymers used, leading to a lack of precise control over incineration by-products [19]. Consequently, this results in a variable combustion calorific value and the potential production of contaminants [19], [20]. Addressing these challenges necessitates the implementation of pollutant control measures to adhere to the emissions standards established by individual countries [20].

Gasification

Gasification is a process that facilitates the decomposition of polymers or polymer mixtures into a gaseous amalgamation primarily comprised of CO and H_2, recognized as synthesis gases (syngas). Trace amounts of CO_2, CH_4, and other lightweight hydrocarbons are also present. This controlled process occurs within a controlled oxidizing atmosphere, encompassing air, steam, or oxygen, constituting an endothermic transformation. This synthesis gas is the foundational precursor for numerous high-value chemical compounds, notably methanol synthesis, Fischer-Tropsch synthesis for fuel production, and the water-gas shift reaction [16], [21].

Advancements in the industrial implementation of gasification systems have made noteworthy strides when contrasted with pyrolysis techniques. However, it is essential to underscore that further research endeavours are warranted in equipment design and process optimization. A distinctive feature of plasma-based processes is their capacity to reduce reaction temperatures, curbing the production of tars while concurrently manifesting heightened resilience to subpar raw materials [16], [21]. Despite this emerging technology currently exhibits energy inefficiency, particularly in comparison to established hydrogen production methodologies such as Steam Methane Reforming or Nuclear Electrolysis, where the value of hydrogen production up to three times lower than when using plasma co-gasification [22].

One of the notable limitations of gasification resides in generating undesirable byproducts such as NH_3, H_2S, NO_x, alkali metals, and tars. Managing these byproducts necessitates meticulous system control and introduces an additional purification step. This augmentation, though conducive to refining the synthesis gas quality, concurrently escalates production expenses. However, these elevated costs can be offset by handling larger volumes of raw materials. Furthermore, when oxygen is utilized, the requisite separation from atmospheric air escalates operational expenses [16], [21].

Pyrolysis

Pyrolysis is a thermochemical process involving thermal cracking in an oxygen-free environment. This method is primarily employed to degrade plastic waste, particularly those challenging to depolymerize. It is an alternative to incineration or landfill disposal when mechanical recycling proves unfeasible [16], [21], [23].

The thermal cracking of plastic waste through pyrolysis yields three intricate fractions: liquid, comprised predominantly of hydrocarbons; gas, consisting of light hydrocarbons with a high calorific value suitable for energy generation; and solid residue in the form of carbon [16], [21], [23], [24]. The efficiency and specificity of this process hinge upon factors such as reaction temperature, residence time, and reactor design [16], [23]. However, it is worth noting that plastic pyrolysis necessitates substantial energy input, exhibits limited tolerance to polyvinyl chloride (PVC), and is susceptible to contamination from impurities in the feedstock [16].

Figure 1.3 overviews lab-scale plastic pyrolysis, including plastic feedstocks, varying conditions and reactor types, and diverse analytical methodologies. This depiction covers the dynamic variations in kinetics, thermal behaviour, and synergistic effects of polymer mixtures. Additionally, it highlights the diverse product categories generated through pyrolysis.

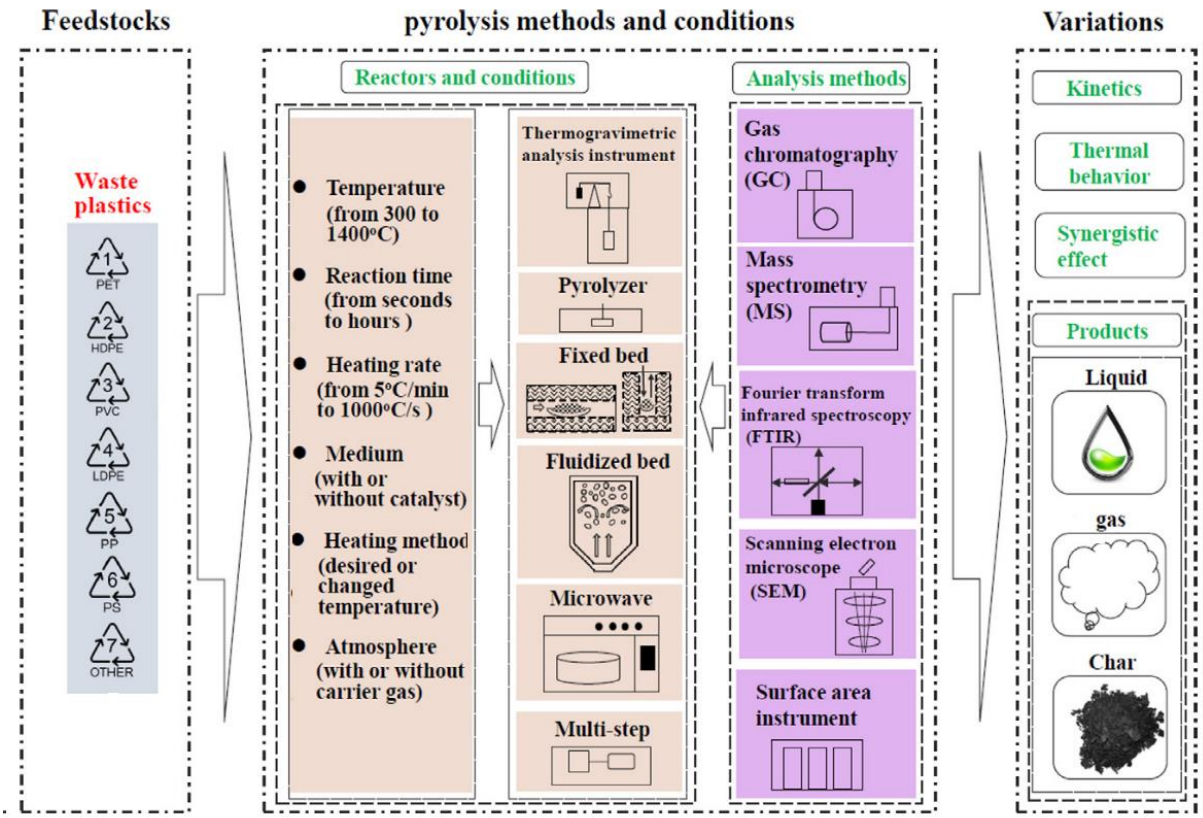

Figure 1.3. Flow chart summary of lab-scale research diagnostics for pyrolysis of waste plastic and plastic mixture adapted from ref [25]

Commonly encountered plastic waste materials include polyethylene (PE), polypropylene (PP), polystyrene (PS), polyvinyl chloride (PVC), polyethylene terephthalate (PET) or combinations thereof, among others [7]. Over the past two decades, extensive research has focused on plastic waste pyrolysis, predominantly targeting high, medium, or low-density polyethylene, polypropylene, polystyrene, polyethylene terephthalate, or various mixtures. These plastic wastes are predominantly sourced from the packaging industry, which accounts for a substantial 60 % of the total plastic waste in the European Union [9].

Type of pyrolysis

Pyrolysis can be categorized into three distinct types, each delineated in **Table 1.1**, with primary differences in heating rate, particle size employed in the system, residence time, and reactor type.

Table 1.1 Different types of pyrolysis and operating parameters from ref [26], [27]

Operating Conditions	Conventional	Fast	Flash
Heating Rate (°C.s^{-1})	0.1-1	10-200	>1000
Particle size (mm)	5-50	<1	<0.2
Vapor residence time (s)	450-550	0.5-10	<0.5
Reactor configurations	Fixed bed, vacuum reactors	Ablative, auger, fluidized bed, circulating fluidized bed reactors	Fluidized bed, circulating fluidized bed reactors, downer reactors, pyrolyzers

Thermal cracking can be augmented through the following three methodologies:

- **Catalytic Pyrolysis:** This approach integrates catalysts, which may interact with the polymer either in the liquid phase, constituting a one-step process, or in the vapour phase, involving a two-step procedure wherein the cracking vapours react with the catalyst within a fixed bed [16], [20], [23]. The utilization of catalysts and the various factors influencing selectivity will be expounded upon subsequently (section **1.3**).
- **Fluid Catalytic Cracking (FCC):** A solvent is introduced here, enabling the plastic to dissolve in the solvent and facilitating continuous feeding. Catalysts are also instrumental in this process [20].
- **Hydrocracking:** This technique employs a hydrogen-rich atmosphere under high pressures (approximately 70 atm) [16], [20], [23]. It requires an initial step for separating the organic material from the plastic waste, termed liquefaction [16], [20]. This method yields higher-quality products at lower reaction temperatures [16], [20].

The valorisation of plastic waste presents an opportunity to enhance recycling methods beyond conventional mechanical recycling, providing plastic waste with added value. Over the past decade, catalytic pyrolysis of plastic waste has emerged as a promising avenue for valorisation, converting it into high-quality pyrolysis oil rich in BTX (benzene, toluene, xylene) compounds. BTX compounds find applications in solvents, fibres, films, and the plastic industry, rendering this approach particularly engaging [28].

Type of feedstocks

Notably, plastic waste carries a substantial carbon content, except PVC, leading to a rich diversity of plastics and various end products. **Table 1.2** presents key characteristics, elemental analyses, and typical products resulting from the thermal cracking of these polymers. In pyrolysis, PVC, due to its potential to generate hazardous substances such as hydrogen chloride (HCl), necessitates a dechlorination step to prevent catalyst poisoning or damage to the reactor. This constitutes a drawback in the pyrolysis of mixed plastic waste. On the other hand, PS comprises styrene monomers characterized by heat resistance and durability. In comparison, PET is composed of dimethyl terephthalate monomer. Both PS and PET exhibit elevated aromatic content, accounting for the prevalence of aromatic fractions in the final product [22].

Polyethylene, constituting approximately 40 % of post-consumer plastic waste (PSW), is widely recognized as the primary plastic utilized in packaging applications [29]. HDPE boasts high crystallinity and limited branching, rendering it more degradation-resistant. In contrast, LDPE features increased branching, resulting in decreased resistance. Polypropylene exhibits commendable chemical and heat resistance. These three polymers yield substantial quantities of fuel-rich oils [30].

The processing of mixed plastics offers an advantage by eliminating the need for a separation step. Nonetheless, certain limitations persist. For instance, the co-pyrolysis of PVC and PET leads to the complete degradation of PET. This mixture proves sensitive to contaminants but displays a high tolerance for low PVC percentages [30].

Vollmer et al. [15] elucidate the significant factors influencing polymer degradation or depolymerization. The complexity of reaction mechanisms joints on the structural intricacy of the polymer; greater complexity facilitates depolymerization. Elevated temperatures yield increased quantities of short-chain products. In the case of polyethylene, a polymer with intricate depolymerization properties, shorter retention times favour β-scission, predominantly yielding ethylene, while longer times promote carbon and hydrogen transfer reactions, enhancing selectivity towards BTX (benzene, toluene, and xylene). **Figure 1.4** provides insight into the distribution of polymer pyrolysis products and the intricacies of reaction mechanisms. This complexity amplifies in the absence of functional groups and heteroatoms, with temperature and retention time exerting considerable influence, especially in the case of HDPE [15].

Table 1.2 Plastic types and their characteristics, applications and role in pyrolysis adapted from ref [2], [30]–[35]

Plastic types	Characteristics	As pyrolysis feedstock	Elemental composition (wt. %) and higher heating values (MJ/kg)	Main Products at < 400 °C	Main Products at > 700 °C	Pyrolysis oil composition
PS	Heat resilience Lightness High strength Reasonable durability	Requires low temperature in comparison to PP and PE plastic types Produces less viscous oil in comparison to PE and PP plastic types	C: 91.48 H: 7.41 N: – S: 0.19 Others: 0.92 HHV: 38.53	Styrene, its oligomers	Styrene, its oligomers Poly Aromatic Hydrocarbons	Styrene Toluene Ethylbenzene Benzene Xylene Cumene Benzene Naphthalene Anthracene Di and triphenylbenzene
HDPE	It is a long polymer chain Highly crystalline High-strength properties polymer	Requires high temperature > 500 °C due to its long chain structure It converts into wax instead of liquid fuel in thermal pyrolysis	C: 85.49 H: 14.23 N: – S: 0.28 Others: – HHV: 43.92	Waxes Paraffins	Gases Light oils	1- and 3-methylcyclopentene 1-hexene Cyclohexene, 1-octene 1-nonene 1-decene Benzene Toluene Xylene
LDPE	Less tensile strength Less hardness Excellent water resistant Desirable polymer for various applications	Wax formation occurs on the external site of the catalyst, while further cracking of wax into gases and liquid occurs in the internal site of the catalyst	C: 85.44 H: 14.31 N: – S: 0.25 Others: – HHV: 43.28			Benzene Toluene Xylene Di and trimethylbenzene Indane Indene Naphthalene Fluorene Acenapthene
PP	Good heat and chemical resistance Low density High rigidity High hardness	Requires high temperature Difficult to degrade under thermal pyrolysis Produces liquid yield with high aromatic compounds under catalytic pyrolysis	C: 83.80 H: 13.85 N: – S: 0.33 Others: 2.02 HHV: 38.1	Waxes Oils	Gases Light oils	Benzene Toluene Xylene Ethylbenzene Indene Biphenyl 1-heptene 1-octene 2-methy l-1-pentene
PVC	Resistant to fire Versatile plastic	Produce hazardous chlorine gas Dechlorination via low temperature (250-320 °C) or physical or chemical adsorption The presence of chlorine and the deposition of coke affect the catalytic activity of the catalyst	C: 39.17 H: 4.96 N: – S: 0.58 Others: 55.29	HCl Benzene	Toluene	Azulene Biphenyl Phenanthrene 9H-fluorene Naphthalene and its monomers

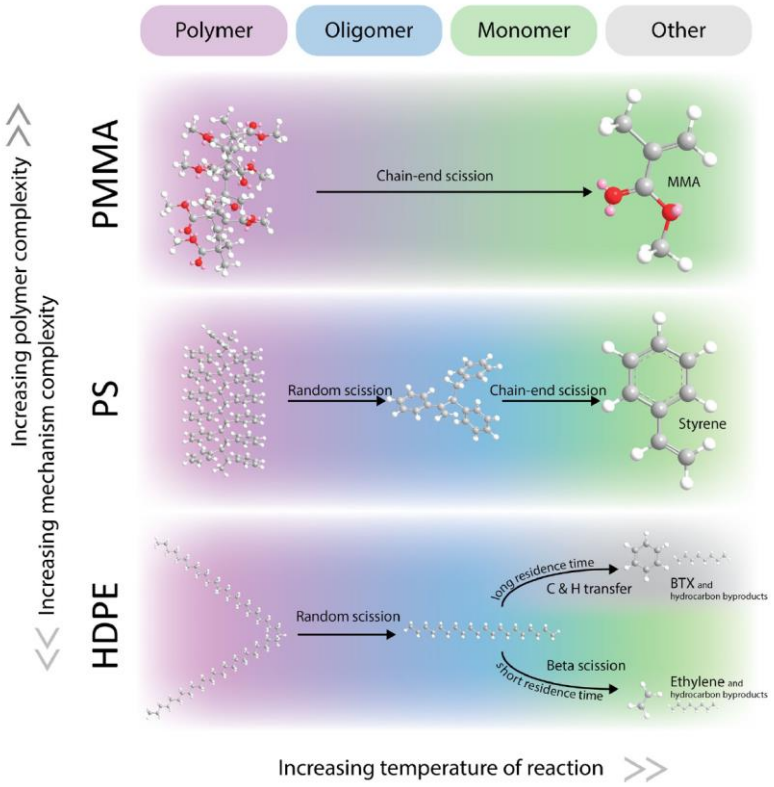

Figure 1.4. Influence of temperature, polymer complexity and residence time on end-products. Copyright ref [15]

Owing to its intricate reaction mechanisms and prevalence within the plastic waste, the thermal depolymerization of polyethylene has acquired significant attention within the research community. In the following section, a comprehensive elucidation of its thermal depolymerization will be found, containing both the free radical mechanisms observed in thermal pyrolysis and the carbocation mechanisms intrinsic to catalytic pyrolysis.

Reaction mechanisms of PE thermo-cracking

Free radical mechanism. The degradation mechanism of polyethylene (PE) primarily operates through a free radical process. This process is notably intricate, given the many species produced, their intermediates, and potential reactions. This complexity becomes even more pronounced with larger carbon chains and structural branches in the polymer [20], [36]. Efforts by various researchers have categorized these degradation models into two principal methods: deterministic (kinetic) and statistical (stochastic) [20]. Generally, the decomposition mechanism can be described in three stages: initiation, propagation, and termination [20], [37], [38]. These stages involve a vast array of species, encompassing over a thousand, a staggering 24,000 elementary reactions, and roughly 20 reaction families [20], [34], [39]. These stages are delineated as follows and are succinctly summarized in **Table 1.3**.

The ***initiation*** phase arises from random scissions, often due to structural imperfections (weak links), primarily within C-C bonds. It necessitates substantial activation energies and gives rise to primary radicals [36], [37]. These radicals exhibit varying carbon chain lengths (see **Table 1.3**) [40].

Table 1.3. Synthesis of the free radical mechanism of the thermal degradation of polyethylene from references [44], [45]

Initiation:	$CH_2 - CH_2 - CH_2 - CH_2 - CH_2 - CH_2 \rightarrow CH_2 - CH_2 - \dot{C}H_2 + \dot{C}H_2 - CH_2 - CH_2$
Propagation:	$CH_3 - (CH_2)_n - CH_2 - \dot{C}H_2 + CH_2 - CH_2 - CH_2 \rightarrow CH_3 - (CH_2)_n - CH_2 - CH_3 + CH_2 - \dot{C}H - CH_2$
	(Hydrogen abstraction, paraffin production)
	$CH_2 - CH_2 - CH_2 - CH_2 - CH_2 - \dot{C}H_2 \rightarrow CH_2 - CH_2 - \dot{C}H_2 + CH_2 = CH_2$
	(β-scission of the primary radical
	$CH_2 - CH_2 - \dot{C}H - CH_2 - CH_2 - CH_2 - CH_3 \rightarrow \dot{C}H_2 + CH_2 = CH - CH_2 - CH_2 - CH_2 - CH_3$
	(β-scission, olefin production)
Termination:	$\dot{C}H_2 + \dot{C}H_2 \rightarrow CH_2 - CH_2$
	(Recombination)

After initiation, the ***propagation*** stage endeavours to stabilize these free radicals through random reactions such as β-scission and H-abstraction [37]. β-scission leads to the formation of olefins and new radicals via the scission of paraffins and olefins radicals. H-abstraction, on the other hand, creates paraffins and more stable radicals through hydrogen transfer between a primary radical and a hydrocarbon chain [37], [40]–[42]. These mechanisms yield hydrocarbons spanning a carbon number range of 1 to 50 [36], [37]. Intramolecular hydrogen transfer reactions involve the abstraction of a nearby hydrogen atom from an adjacent molecule, producing a specific set of low molecular weight products (LMWP) when followed by mid-chain β-scission. Intermolecular hydrogen transfer, on the other hand, entails the abstraction of a hydrogen atom from the same chain, yielding a diverse set of LMWP when followed by mid-chain β-scission [39]. The latter mechanism tends to be dominant due to the higher availability of hydrogen atoms [32]. Random reactions in the propagation stage are contingent on factors like the molecular weight of the PE chain [39], impurities [43], and the reaction conditions [34]. They significantly influence the decomposition of PE, determine the selectivity of final products, and require lower activation energy compared to the initial stage. β-scission, which necessitates more energy, leads to the production of lower-carbon products, and its prevalence increases with higher temperatures [36]. Long residence times influence tertiary reactions, resulting in higher hydrogen, methane and coke yield. These reactions also give rise to cyclic compounds and aromatics, which are highly dependent on increasing temperature. Aromatics are formed from the Diels-Alder mechanism, followed by dehydrogenation involving paraffinic and olefinic hydrocarbons [37]. Polyaromatic hydrocarbons (PAH) result from the polycondensation of aromatics and similarly depend on temperature and residence time [36].

In the final ***termination*** stage, two free radicals recombine to form stable molecules [15], [20], [36], [46]. Due to its long-chain structure, thermal pyrolysis of PE tends to produce more wax than liquid oil [34]. This predominance of wax is especially notable in the primary devolatilization reaction [37].

Carbocation mechanism. A prominent route in the pyrolysis of polyethylene facilitated by acid catalysts also involves three distinct stages. The application of acid catalysts decreases the activation energy of cracking reactions, particularly in the initial phase. This reduction results in the production of lighter hydrocarbons [47], [48]. Low molecular weight products can either evaporate and diffuse through the polymer or partake in other reactions as they enter the pores of the catalyst [49]. Compared to thermal decomposition, the carbon number distribution of the final products is lower [50]. In the liquid phase, the predominant products are primarily branched hydrocarbons [48], [51]. The formation of carbocations, which are positively charged ions, marks the ***initiation*** stage and relies on the nature and strength of acid sites [41], [50].

At the acid sites of the catalyst, two primary types of carbocations emerge: carbenium ions, formed by the abstraction of a hydride ion (removing one hydrogen and two electrons) at Lewis acid sites, and carbonium ions, resulting from the protonation of the hydrocarbon at Brønsted acid sites [41], [42], [50]–[54]. A higher concentration of Brønsted acid sites favours β-cracking mechanisms and promotes the proteolysis of pentacoordinated carbonium ions. In contrast, a greater abundance of Lewis acid sites encourages cyclization and hydrogen transfer processes, ultimately enhancing the selectivity for aromatic compounds [54].

The ***propagation*** and ***termination*** stages witness the involvement of these carbocations in various reactions, including the cracking of C-C bonds, isomerization, hydrogen transfer, alkylation, oligomerization, cyclization, and aromatization [42], [50], [52], [53], [55]–[57]. Tertiary carbocations exhibit increased stability, and a positively charged carbon in a tertiary position further enhances their stability [53]. The stability of tertiary carbocations and their formation is contingent upon the degree of branching, implying that for LDPE, cracking yields more tertiary hydrocarbons compared to HDPE, which possesses a linear structure [52], [58].

C-C bond cracking arises from β-scission, producing olefins and additional carbocations. The latter continues the chain reaction and forms new short-chain olefins (oligomerization) [53]. Isomerization leads to the rearrangement of carbocations, producing tertiary ions, which then undergo cracking to create branched molecules [51], [53]. Hydrogen transfer occurs as olefins are adsorbed on neighbouring active sites, with one olefin converting to paraffin while the other reorganizes in a cyclization reaction to form cyclic or aromatic compounds [48], [51]–[53], [59]. These aromatics can be positively charged by protonation and subsequently condensed to yield polyaromatic compounds [59]–[61]. The nature of the resultant compounds is influenced not only by reaction conditions but also by the nature and strength of the acid sites of the catalyst [55].

According to the findings synthesized by Abbas-Abadi et al. [59], two dominant pathways are recognised in the cracking of polyolefins: the monomolecular and the bimolecular mechanisms. The monomolecular

mechanism involves the direct cracking of the backbone through protolytic scission, yielding carbenium ions and shorter paraffins. This leads to the production of short-chain saturated hydrocarbons and hydrogen. The carbocation generated in this mechanism is an unstable penta-coordinated carbonium-ion, which necessitates high activation energy for the protolytic scission. However, it prevails at low conversions and low carbenium-ion concentrations. The bimolecular mechanism, conversely, encompasses a hydrogen-abstraction process followed by β-scission in the backbone. It requires less activation energy than the monomolecular mechanism and is dominant in the initiation step of polyolefin cracking. This mechanism necessitates a higher quantity of carbenium-ions and results in a significant production of butene and propylene.

Catalytic cracking thus has distinct advantages over thermal cracking. First, it allows for a reduction in reaction temperature due to the catalyst's ability to lower the activation energy of cracking reactions. This temperature reduction is contingent upon the nature and strength of the acid sites [50], [62]. Second, the use of acid catalysts enhances the selectivity of PE cracking, resulting in a narrower distribution of carbon atom numbers in the pyrolysis products [50]. This allows for the production of specific desired products [52] and is highly dependent on steric hindrance (shape selectivity) [51], [52], [59], [62], pore systems, and chemical composition [41], [50], [51], [59], [63] of the catalyst.

1.3. Catalytic pyrolysis of polyethylene

1.3.1. Overview of Published Review Articles on Plastic Pyrolysis

Several reviewers have meticulously explored the numerous factors influencing the catalytic pyrolysis of plastics in general, including polyethylene. A synthesis of these critical reviews is presented in **Table 1.4**. This tabular presentation offers a comprehensive chronological overview of the factors examined in various publications, highlighting the key insights derived from prior and recent research.

Notably, each author's distinctive approach is evident, offering updated perspectives and avoiding redundancy. It is noteworthy, however, that despite the comprehensive coverage of factors influencing catalytic pyrolysis in these reviews, there is a relative paucity of focus on producing aromatic components. This is the case of the work conducted by Lok et al. [64]; they primarily emphasized ZSM-5 zeolites promoted for the production of aromatics in the thermochemical conversion of biomass and waste.

On the other hand, it should be noted that these reviews do not focus on PE but rather on Plastic Solid Waste. As this PhD work centres on PE, the subsequent section of this chapter will focus on PE.

Table 1.4 Overview of a selection of reviews covering various studied factors for waste plastic pyrolysis.

Title (Published date)	Journal	Feedstock	Reactor	Reaction temperature	Pressure	Residence time	Type of Catalyst	Catalyst acidity	Catalyst characterization	Catalyst-Polymer ratio	Catalyst deactivation	Others
A review on pyrolysis of plastic wastes (2016) [30]	Energy Convers. Manag.	■	■	■	■	■	■					■
Catalytic pyrolysis of plastic waste: A review (2016) [32]	Process Saf. Environ. Prot.	■		■		■	■	■	■			
Plastics to fuel: a review (2016) [67]	Renew. Sustain. Energy Rev.						■	■				■
A review on thermal and catalytic pyrolysis of plastic solid waste (PSW) (2017) [29]	J. Environ. Manag.	■	■	■	■	■	■					
Thermochemical routes for the valorization of waste polyolefinic plastics to produce fuels and chemicals. A review (2017) [63]	Renew. Sustain. Energy Rev.		■				■					
Conversion of waste plastic to fuel products (2020) [68]	Mater. Today Procee.						■					■
Review of catalyst materials in achieving the liquid hydrocarbon fuels from municipal mixed plastic waste (MMPW) (2020) [69]	Mater. Today Commun.	■	■	■	■	■	■	■	■			
The Use of Heterogeneous Catalysis in the Chemical Valorization of Plastic Waste (2020) [70]	ChemSusChem	■	■	■			■			■		
Thermal and catalytic decomposition of waste plastics and its coprocessing with petroleum residue through pyrolysis process (2020) [65]	J. Clean. Prod.	■	■	■			■					■
Hydrogen and Carbon Nanotubes from Pyrolysis-Catalysis of Waste Plastics: A Review (2020) [71]	Waste Biomass Valori.	■	■				■			■	■	
Deactivation and Regeneration of Zeolite Catalysts Used in Pyrolysis of Plastic Wastes—A Process and Analytical Review (2021) [60]	Catalysts		■				■		■		■	■
Thermochemical Recycling of Waste Plastics by Pyrolysis: A Review (2021) [72]	Energy & Fuels	■	■	■	■	■	■					■
Pyrolysis for plastic waste management: An engineering perspective (2022) [73]	J. Environ. Chem. Engineer.	■	■				■	■	■	■		■
Conversion of mixed waste plastic into fuel for diesel engines through pyrolysis process: A review (2022) [74]	Applied Energy	■	■	■	■		■					
A review on catalytic pyrolysis of plastic wastes to high-value products (2022) [75]	Energy Convers. Manag.	■	■	■	■	■	■				■	■
Production and utilization of pyrolysis oil from solidplastic wastes: A review on pyrolysis process and influence of reactors design (2022) [76]	J. Environ. Manag.	■	■				■					■
Valorization of plastic wastes for production of fuels and value-added chemicals through pyrolysis – A review (2022) [53]	Ther. Sci Engineer. Progress	■	■	■			■					■
Challenges and opportunities of light olefin production via thermal and catalytic pyrolysis of end-of-life polyolefins: Towards full recyclability (2023) [59]	Progress Energy Comb. Sci.	■	■	■		■	■	■				■
Recent Research Advancements in Catalytic Pyrolysis of Plastic Waste (2023) [77]	ACS Sustainable Chem. Eng.						■					■

1.3.2. Effects of Main Parameters on Catalytic Pyrolysis of Polyethylene

Influence of the type of reactor

As investigated in the previously mentioned review articles, the catalytic pyrolysis processes of polyethylene have mainly utilized batch or semi-batch reactors due to their operational simplicity and easy parameters control. Additionally, the study identified alternative reactor types, including fluidized bed reactors, fixed bed reactors, conical spouted bed reactors (CSBR), and microwave-assisted reactors. The diversity in reactor designs significantly influences heat transfer mechanisms, residence times, and thus, the ultimate product composition. Several of these reactor types are depicted in **Figure 1.5**.

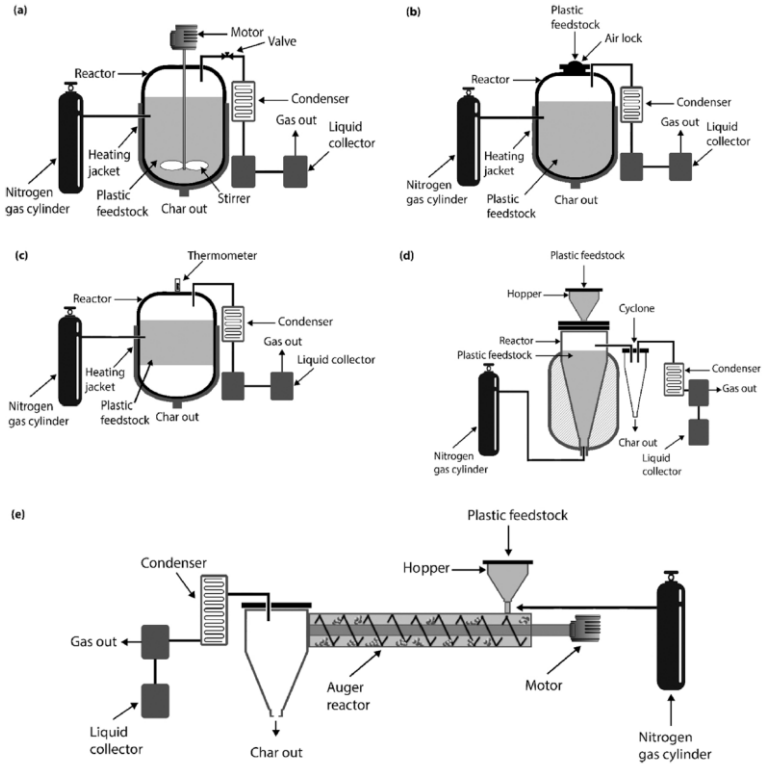

Figure 1.5. Diagram showing (a) continuous-stirred tank reactor; (b) batch and semi-batch reactor; (c) fixed-bed reactor; (d) conical spouted bed reactor; and (e) auger/screw reactor. Copyright ref [73]

Batch reactors are closed systems where the reaction takes place. As a central problem, the final products vary from batch to batch, and the repeatability of the process is challenging to scale up [30], [65]. ***Batch*** systems imply that the sample is subjected to a temperature gradient while reaching the desired temperature, considering that a slow temperature ramp (in $°C.min^{-1}$) results in a lower maximum degradation temperature for polyethylene [66].

Semi-batch reactors have an inlet for continuous feed and outlet. The end products are continuous in terms of selectivity [30], [65]. In ***Semi-batch*** reactors, the main parameter to control is the stirring rate. For example, Abbas-Abadi et al. [78], [79] studied the degradation of polyethylene using a 20 wt. % of

Fluidized Catalytic Cracking (FCC) catalyst at 450 °C with nitrogen in a semi-batch reactor, either without a stirrer or with a stirrer up to 300 rpm. They found an increase in condensable products, reaching a maximum of 91-93 % at 50 rpm, while non-condensable products reach their minimum at 2.2-4.1 %, and coke decreases by 2.2-9.1 %. The aromatics content increases by 1.3 %, and olefins decrease by 4.5-6.5 %, while the carbon distribution of condensable products tends to concentrate between C_5-C_9, with a maximum when using a stirring rate of 50-100 rpm. The results indicate that a stirrer can enhance heat transfer, particularly in the centre of the reactor. In the absence of a stirrer, such as in a ***batch reactor***, weak radiative heat transfer leads to plastic agglomeration in the centre of the reactor, resulting in a substantial temperature gradient and increased residence time.

On the other hand, a high stirring capacity can positively impact product outcomes, whereas a significant difficulty is the formation of coke that deactivates the catalyst over time.

The great advantage of both reactors (***batch*** and ***semi-batch reactor***) is that the liquid yield is more significant when compared with other types of reactors due to the direct contact between the raw material and the catalyst [30], [65].

Fluidized bed *and* ***fixed bed reactors*** are easy to design, but the size of the raw material is a limitation since it has to be adapted. The process is usually more expensive for the ***fixed bed reactor*** since it involves a thermal cracking at a higher temperature followed by a contact of the cracking vapours with the catalyst at a controlled temperature. These results are usually comparable with those obtained when there is direct contact with the catalyst. In a ***fluidized bed reactor***, better polymer-catalyst contact is generated, it has good heat transfer, and the process variables are better controlled. This reactor is the best option for a larger-scale process [30], [65]. A drawback of the ***fluidized bed reactor*** is its non-isothermal nature, with temperature fluctuations between the bed and the reactor head. This results in the different components produced at different rates, although the residence times are generally short. The homogeneity of the mixture can be partially lost before pyrolysis occurs, and the catalytic character of the process may be less effective as the uniform mixture falls onto the inert bed in counterflow to the carrier gas flow [80].

Comparing HDPE cracking in a ***fluidized bed*** (fast pyrolysis) reactor with 20 wt. % of zeolite HZSM-5 at 800 °C to one carried out in a pyrolyzer (flash pyrolysis), where the contact between the polymer and the catalyst is more homogeneous, the pyrolyzer favours the gaseous fraction and the formation of lighter hydrocarbons [80]. It results in minimal coke production at temperatures above 700 °C, whereas below this temperature (between 500 °C and 600 °C), the roles are reversed, and the pyrolyzer produces a more significant amount of solid residues, ranging from 40 to 70 %, with fewer light hydrocarbons [81].

Artetxe et al. [82], [83] compare HDPE pyrolysis with HZSM-5 at 500 °C using a ***fixed bed reactor,*** i.e. a two-step system and a ***conical spouted bed reactor (CSBR),*** i.e. a one-step system, and show that a similar quantity and distribution of compounds were obtained. However, limitations of the ***CSBR*** system were observed. The mass of the bed used in the ***CSBR*** is limited by the hydrodynamic conditions required for adequate heat and mass transfer velocities and to prevent fluidization problems. As a result,

the catalyst's space-time (g_{cat}.min.g_{HDPE}^{-1}) was 2-4 times higher than that of the ***fixed bed reactor***, as hydrodynamic conditions do not constrain the latter. This understanding is based on the CSBR system following the subsequent sequence: plastic melting, coating of catalyst particles with molten plastic, pyrolysis of molten plastic, and catalytic transformation of molten plastic in pyrolysis volatiles. In contrast, the ***fixed bed reactor*** does not have catalytic pyrolysis and cracking reactions competing at the same acid sites, offering operational advantages and scalability. However, the ***CSBR*** system also has its advantages, such as preventing bed fluidization, higher yield per reactor volume, and lower yields of secondary reaction products [62].

Recently, ***microwave*** technology has attracted high interest in pyrolysis. ***Microwave-assisted*** pyrolysis aims to accelerate chemical reactions and improve energy efficiency. Its advantages include rapid and efficient heating, selective heating, increased energy conversion efficiency, and shorter processing times, which result in liquid products with lower viscosity, lower density, and higher quality than conventional pyrolysis. Pyrolyzing LDPE with HY zeolite in two steps at 450 °C, the amount of aromatic compounds exceeds 20 % [84]. This technology requires a microwave absorber mixture to absorb energy and reach the desired temperatures, directly heating the product. This type of heating is fast, so pyrolysis is faster, and therefore, there is a decrease in production costs. The efficiency of microwave heating depends on the dielectric properties of the material, so it differs for each material, which has been an excellent challenge for industries [30], [65].

Finally, Serrano et al. [85] employed a ***screw kiln reactor*** to degrade LDPE with two hot zones heated to 400-500 °C. The polymer was melted at 300 °C and mixed with a 50 wt. % MCM-41 catalyst beforehand. Complete conversion was achieved at 450 °C and 500 °C with a screw speed of 8.5 rpm in both zones, resulting in a C_5-C_{12} productivity of 74.2 %. Compared to a ***batch*** system, the gas production was reduced, possibly due to the reactor favouring oligomerization reactions.

Effect of the processing conditions

The scientific community has fully investigated the factors that influence the composition of the oil resulting from the catalytic pyrolysis of polyethylene, temperature, reaction time, and catalyst properties.

Temperature is one of the most extensively studied parameters in the catalytic pyrolysis of polyethylene. The choice of temperature profoundly affects the product distribution. High temperatures typically lead to increased gas and liquid yields, favouring the production of valuable hydrocarbons. However, excessively high temperatures can promote undesirable side reactions, such as coke formation. Researchers have optimised the temperature range to balance product yield and composition.

Abbas-Abadi et al. [78], [79] used a 20 wt. % FCC catalyst with LLDPE in a first study and HDPE in second study, both in a semi-batch reactor with stirring at 50 rpm under nitrogen and increasing the reaction temperature from 420 °C to 510 °C; they found that condensable products decrease by 9 % (first study [78] at 510°C) and 9.6 % (second study [79] at 510°C), with a maximum at 450 °C. In contrast, non-condensable products and coke increased by 6.8 % and 2.1 % (first study at 510°C) and 6.2 % and 3.4 % (second study at 510°C), respectively. The content of aromatics and olefins increases by 2.3 %

and 1.8 %(first study at 510°C) and 7.3 % and 4.3 % (second study at 510°C), respectively. At the same time, the carbon distribution of condensable products tends to concentrate between C_5-C_9; with increasing temperature, activation energies decrease, promoting chain cracking and facilitating reactions like the Diels–Alder reaction followed by dehydrogenation.

Artetxe et al. [82] investigated the effect of pyrolysis temperature on HDPE pyrolysis with HZSM-5 in a fixed-bed reactor, ranging from 350 to 500 °C. They found a substantial increase, doubling the light olefins and nearly quadrupling the aromatics when the temperature increases. Secondary reactions such as oligomerization, isomerization, hydrogen transfer, or Diels-Alder became more prominent at higher temperatures. A similar trend was observed with the FCC catalyst when temperatures between 450 and 550 °C were applied [86].

The ***residence time*** also assumes a pivotal role in the pyrolysis of polyethylene. Extended residence times of gas phase facilitate secondary reactions, such as isomerization, aromatization, and hydrogenation/dehydrogenation reactions. Consequently, a liquid phase transformation is evident, producing gases and coke. The presence of coke signifies the occurrence of elimination reactions within certain carbon chains, yielding lighter compounds and hydrogen [87]. When studying the effect of residence time in HDPE cracking in a fluidized bed reactor with 20 wt. % of zeolite HZSM-5 at 800 °C, Hernandez et al. [80] found that residence time promotes secondary reactions, increasing the production of light hydrocarbons like methane, ethane, or ethylene. It also increases the production of aromatics like benzene from a yield of 0.09 to 8.2 % when the V/m ratio increases from 0 to 1500. Hernandez et al. [80] introduced the V/m ratio as a parameter that exhibits a rough proportionality to the degree of tar cracking. In this context, V represents the volume of the upper section of the reactor, which is devoid of sand, while m denotes the mass of the sample deposited onto the bed. This parameter is closely associated with the concept of residence time.

Using an FCC catalyst to pyrolyse LLDPE (first study) or HDPE (second study) at 450 °C in a semi-batch reactor with stirring at 50 rpm under nitrogen, Abbas-Abadi et al. [78], [79] increased the ***catalyst concentration*** from 10 % to 60 %. Condensable products decreased by approximately 5.5 %. In contrast, non-condensable products increased by 2.5 % (first study) and 3.1 % (second study), as well as coke with an increase of 2.8 %. The content of aromatics and olefins increases by 0.8 % and 5.0 % (first study) and 3.1 % and 7.2 % (second study), respectively, while the carbon distribution of condensable products tends to concentrate between C_5-C_9. They conclude that a higher catalyst concentration increases the degradation of high molecular weight olefinic molecules on the catalyst's external surface, forming smaller molecules that can enter the zeolite pores for further cracking, improving the reaction's selectivity.

Serrano et al. [88] employed a screw kiln reactor to pyrolyze LDPE, featuring two distinct heating zones at 450 °C and 500 °C, respectively. The polymer was mixed with lubricating oil (30 wt. % of lubricant) to enhance the ***polymer-catalyst contact,*** and an MCM-41 type catalyst was used. Compared to a previous study conducted without lubricant [85], this lubricant-infused system exhibited a significantly higher quantity of C_5-C_{12} compounds, primarily comprising olefins, with an increase of approximately 50

%. Marcilla et al. [89] used two mixing methods to enhance the HDPE and HZSM-5 catalyst interaction. In one approach, the materials were mixed in powder form, while in the other, the molten plastic was mixed directly with the catalyst. Notably, the latter molten mixture exhibited more substantial gas yields, increased aromatic compound production, minimized solid waste, and reduced levels of olefins and paraffins compared to the powdered mixture.

Another noteworthy parameter for evaluation pertains to the ***nature of carrier gas***. Abbas-Abadi et al. [78], [79] employed different carrier gases: H_2, He, N_2, ethylene, propylene, and argon to perform the pyrolysis. Using 20 wt. % of FCC catalyst with LLDPE or HDPE at 450 °C in a semi-batch reactor at 50 rpm, condensable products reach a maximum with H_2 at 95-96 %, followed by He at ~94 %, N_2 at 91-93 %, ethylene at ~94 %, propylene at ~88 %, and finally Argon at 86-88 %. Meanwhile, non-condensable products reach a maximum with propylene and argon and coke with nitrogen and argon. The aromatics content is consistent across all carrier gases, ranging from 2.3 % to 5.7 %, except for H_2, which exhibits a 1.8-2.9 % range. Olefins range from 61.3 % to 76.5 %, except when H_2 is used, reaching around 45.5 %. The carbon distribution of condensable products tends to concentrate between C_5-C_9. This study demonstrates that as the temperature increases, lower molecular-weight inert carrier gases accelerate more pyrolysis than heavier molecular-weight gases. Heavier inert carrier gases show that the pyrolysis oil comprises slightly broader carbon number distribution compounds, with C_7 remaining the dominant compound in all atmospheres. In comparison, reactive carrier gases perform better. Reactive carrier gases generate internal heat, dilute products, and influence equilibriums, kinetics, and mechanisms. When hydrogen is used as a carrier gas, hydrogen atoms decompose on the catalyst's surface and subsequently undergo hydrogenation reactions with adsorbed olefins on active sites. The resulting paraffins easily desorb from active sites without further reactions.

Effect of the Catalyst Nature and Properties

The choice of the catalyst plays a pivotal role in determining the efficiency and selectivity of polyethylene catalytic cracking. Alumino-silicates have gained prominence due to their well-defined microporous structures, which offer shape selectivity and control over product distribution [90]–[93]. Mesoporous alumino-silicates with extended external surfaces exhibit more significant activity in polyethylene degradation, primarily because polyethylene can interact more easily with acid sites [94]. Zeolites, in particular, are known for their ability to catalyse the cracking of long hydrocarbon chains, producing valuable hydrocarbons with reduced coke formation. Their unique properties make them suitable for tailoring the product spectrum to meet specific market demands. These distinctive characteristics will be further elucidated in section **1.3.3**.

Additionally, fluidized catalytic cracking (FCC) catalysts, initially designed for petroleum refining, have been adapted for polyethylene cracking. These catalysts are versatile and effective in breaking down complex hydrocarbon structures, yielding a wide range of products [86], [95]–[97]. Due to their low cost and abundance, clays have also been explored as catalysts for polyethylene cracking. Although their catalytic activity may be modest compared to zeolites, clays offer an economically viable option for large-

scale applications. Their use has demonstrated the feasibility of converting plastic waste into valuable products [98]–[101]

Serrano et al. [102] initiated the study of LDPE cracking using three different acid catalysts (amorphous alumino-silica, MCM-41, and USY) within a stirred semi-batch reactor at 120 rpm under nitrogen. They began cracking at temperatures ranging between 380 °C and 420 °C. A maximum of the liquid phase was observed at 420 °C, though complete conversion was not achieved. Van Grieken et al. [103] investigated PE cracking within a stirred semi-batch reactor at 120 rpm under nitrogen using various catalysts at temperatures ranging from 340 °C to 420 °C (**Figure 1.6**). They found higher liquid-phase conversion with nano-ZSM-5 and MCM-41 at 380 °C and 420 °C, respectively, with a minimal solid-phase contribution. Other similar studies employing stirred semi-batch reactors, fixed-bed reactors, and Py-GC/MS analysis showed a trend: the zeolite ZSM-5 obtained the highest selectivity for aromatics, while MCM-41 had higher selectivity for olefins [104]–[106].

García et al. [107] synthesized hybrid materials of ZSM-5 and MCM-41 catalysts and employed them for HDPE cracking with a polymer/catalyst ratio of 100/1 at 380 °C in a stirred semi-batch reactor under nitrogen. This cracking was compared with pure ZSM-5 and MCM-41, with all catalysts featuring a Si/Al ratio of approximately 30. The hybrid material with a lower meso-external surface area (465 $m^2.g^{-1}$) and higher acidity (0.163 $mmol.g^{-1}$) exhibited the highest HDPE conversion. It showed lower selectivity for C_1-C_5 olefins and paraffins and higher selectivity for products in the C_6-C_{12} range. This study shows that while Si/Al ratios were crucial for acidity, material structure also played a significant role.

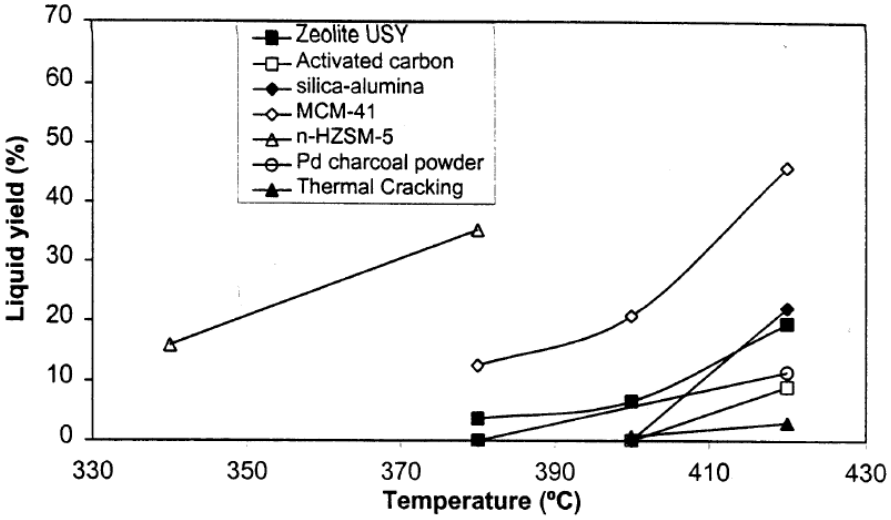

Figure 1.6. Influence of catalyst type and temperature reaction on LDPE cracking from ref.[103]

Aguado et al. [108] pyrolyzed LDPE in a pyrolyser coupled with a gas-chromatography / mass spectroscopy (Py-GC/MS) heated to 700 °C with a heating rate of 10 $°C.ms^{-1}$ using helium as the carrier gas and various catalysts. They conclude that β and ZSM-5 zeolites exhibited higher selectivity for single-ring aromatic products. In comparison, MCM-41 and SBA-15 acidic catalysts displayed higher selectivity for light hydrocarbons but also produced a wide range of branched olefins and alkyl-derived

aromatic products due to their weaker acidic properties and larger pore dimensions. Amorphous silica exhibited low activity and conversion. In another study [109], they synthesized three types of mordenite with different Si/Al ratios (from 7.8 to 10.2) and external surface areas (from 9 to 57 $m^2.g^{-1}$) and used them in LDPE cracking with a polymer/catalyst ratio of 50/1 at 420 °C in a stirred semi-batch reactor under nitrogen. Conversion was highest for mordenite with a Si/Al ratio of 10.2 and an external surface area of 57 $m^2.g^{-1}$. Higher Si/Al ratios and more significant external surface areas led to greater selectivity for the C_6-C_{12} range, while mordenite with lower Si/Al and surface area exhibited higher aromatics production. These results suggest that primary cracking products from terminal chain conversion can undergo subsequent cracking on the high proportion of easily accessible acid sites in mordenite samples with higher external surface areas.

Additionally, zeolitic acid sites promote secondary cyclization, oligomerization, or aromatization reactions. Other solid catalysts, such as H-Ferrierite or aluminosilicates, have also been studied alongside zeolites in the thermal degradation of polyethylene. They exhibit lower activity due to their reduced total specific surface area and total acidity [90], [110], [111]. The same trend has been observed with various types of pillared and restructured clays in which zeolite ZSM-5, in these cases, showed better activity and better selectivity towards aromatics [98], [101], even when altering its acidity. This modification resulted in a significant increase in olefins [101]. Borsella et al. [100] evaluated the stability in the HDPE degradation with a fluidized bed reactor of iron-alumina pillared montmorillonite, and they found the montmorillonite decreased the activity after 2 min, whereas HZSM-5 continued stable after 15 min. The quantity of waxes was higher with the montmorillonite [112].

The literature review thus shows the interest in using zeolite in the field of catalytic pyrolysis of polyethylene, as a consequence, this is further discussed in the following part.

1.3.3. Zeolite catalyst

Zeolites are solid crystalline structures described as crystalline aluminosilicate sieves with open pores and ion exchange capacity and are obtained using a three-dimensional interlacing where oxygen atoms join the tetrahedral sides. They are made of silica and alumina, and their relationship determines their reactivity, effectiveness, and acidity and affects the final product of plastic waste pyrolysis [30], [65], [69]. It is well known that the Si/ Al ratio (an Al^{3+} substitutes Si^{4+}, an additional positive charge is necessary to maintain neutrality [100]) is a key parameter for consideration of the scission activity of catalysts because catalysts with higher Si/Al ratio can crack the C– C bonds with higher degree [113]. This ratio also determines the proportion of Brønsted and Lewis acid sites, although the latter also depends on other factors, such as calcination of the zeolite structure [114], [115]. The bridging Si–OH–Al groups are related to the proton donating Brønsted and the lattice aluminium and the unsaturated coordination of aluminium either bound to the framework or in extra-framework positions with the Lewis electron-acceptor sites [114].

Among the extensively investigated zeolites (or zeolite-content material) for polyethylene cracking, ZSM-5, β, Y zeolites, and FCC catalysts stand out. Due to its acidic nature, determined by the Si/Al

ratio, zeolites promote β-scission reactions, forming shorter molecules [113]. Elordi et al., in their preliminary studies from 2007, employed a CSBR to pyrolyze HDPE in the presence of zeolites under a nitrogen atmosphere, aiming to obtain a gasoline-rich oil. In their initial study [116], they used 100 g of HY zeolite at 500 °C with batches of 3 g of plastic, resulting in a BTEX (benzene, toluene, ethylbenzene, and xylene) production of 12.8 %. In the subsequent second [117] and third studies [95], under similar conditions but with HZSM-5 zeolite at 500 °C and FCC catalyst at 475 °C, they achieved 14.4 % and 4.1 % in BTEX, respectively. These two studies were continued by comparing HZSM-5 and HY zeolites with Hβ, utilizing a continuous feed of HDPE up to 1000 g [62]. These zeolites were agglomerated with alumina and bentonite. HZSM-5 zeolite contained the highest concentration of Brønsted acid sites compared to Lewis acid sites, followed by HY and Hβ. The results of this pyrolysis were influenced by pore size and the acidic strength of the zeolites. There exists a clear relationship between the yield of light olefins and the pore size of the catalytic zeolite. Thus, the zeolite with the smallest pore size, HZSM-5, produces a greater quantity of light olefins, followed by Hβ and HY. It should be noted that large pores, such as those found in B zeolite, lead to significant yields of liquid products [118]. The catalyst with the largest pore size yields the highest amount of butenes, while propylene is the primary product for the catalyst with smaller pores, and ethylene yield is also significantly higher for the latter. Yields of non-aromatic C_5-C_{11} compounds and >C_{11} hydrocarbons are higher for the catalysts with larger pore sizes. Pore size in Hβ and HY zeolites is a key aspect influencing deactivation. Both zeolite-based catalysts, Hβ and HY, exhibit a similar deactivation trend. Coke yields obtained for both are similar, and wax yields are of a similar order, clearly evidencing a lower catalytic cracking. At the opposite, coke deposition is much lower for the HZSM-5 zeolite-based catalyst, and the wax yield is negligible. The yield of single-ring aromatic compounds increases with acid strength. Therefore, HZSM-5 zeolite-based catalyst yields more aromatics than HY, and in turn, HY yields more than Hβ.

They further studied the deactivation of these three zeolites under identical conditions [119], finding that HZSM-5 zeolite best-mitigated deactivation due to coke. In a more in-depth analysis of the nature of the coke deposited on zeolites [120], it was concluded that the severity of zeolite shape selectivity not only governs the product distribution but also influences coke deposition. Precursors of aromatic nature tend to grow, reaching a point of steric hindrance and forming aliphatic chains. Hβ zeolite primarily generates coke of aromatic origin; however, it yields the highest amount of olefins. HZSM-5 coke can be depicted as benzene-like molecules with long and numerous attached aliphatic chains, whereas HY zeolite coke exhibits the highest aromatic condensation, with the presence of aromatic rings ranging from 4 to 7, along with few and short aliphatic chains.

Another study involving the degradation of LDPE mixed with 20 wt. % of zeolites Hβ and HZSM-5 [121] in a fixed bed reactor at 500 °C reveals that HZSM-5 zeolite produces a higher amount of olefins and less coke (char production is around 4.5 %) compared to Hβ zeolite (char production is around 12 %). This demonstrates the zeolites' pore system's significant influence on the evolved gas's composition.

Renzini et al. [122] compared HZSM-11 and Hβ zeolites in LDPE cracking. Both catalysts had similar total acidity, but HZSM-11 presents higher Brønsted than Lewis acid sites. Brønsted acid sites are

essential for initial cracking and aromaticity; Lewis acid sites favour cyclization and aromatization reactions [123]. Moreover, Hβ zeolites have a higher specific surface area. This study shows that Hβ zeolite allows a higher relative activity of 88 °C, whereas HZSM-11 was 44 °C. For HZSM-11, after 11 cycles, the quantity of coke was stable, around 8 %, while there was no production of waxes. It is also shown that after 11 cycles, a relative activity of 40 °C is obtained, demonstrating a shift of only 4 °C. Hβ finishes the 11 cycles with around 15 % coke, while waxes appear after six cycles, with a relative activity of only 3 °C. It means that at the beginning, the specific surface area is an essential parameter to determine the activity, whereas, at the end, the nature of the acid sites and the coke deposition affect the deactivation of the catalyst. A similar study was conducted by Lerici et al. [124] with the same zeolites but doped with zinc. They obtained similar behaviour in liquid, gas and coke yield and stability. The quantity of aromatic was higher with doped zeolites, especially with Zn-ZSM-11 zeolite.

Marcilla et al. [125] tested the deactivation of Protonic ultra-stable Y zeolite (HUSY) zeolite and HZSM-5 at 10 °C min^{-1} until rising 550 °C and 30ml min^{-1} of nitrogen flow in LDPE cracking. HUSY zeolite has almost two times more acidity than HZSM-5, and with five cycles of use, almost 50 % of the acidity is reduced. The zeolite HZSM-5, after 13 cycles, has a reduction of 31 % of its acidity. With LDPE, after 13 cycles, HZSM-5 zeolite has a T_{max} of 446 °C, whereas, with only five cycles, HUSY has a 467 °C of T_{max}. The deactivation caused by the coke deposition using the HUSY catalyst was faster compared to HZSM-5 deactivation. At the same carbon range, HUSY favours the production of olefins and paraffins in the HDPE cracking, whereas HZSM-5 obtains mainly olefins [50], [126], [127]. In the cracking of HDPE and LDPE, with HZSM-5 zeolite, it is obtained between 7 % and 20 % more aromatics in the liquid phase, and the carbon number distribution is shorter compared with HUSY zeolite [50]. Lin et al. [126], [128] obtained 2.5 more coke using HUSY zeolite and 1.5 more BTX using HZSM-5 at 360 °C in a fluidized bed reactor. In a batch reactor, the cracking of HDPE at 450 °C and a catalyst:polymer ratio of 1:20 aromatics compounds are 50 % higher using ZSM-5 compared with Y zeolite [111]. Elordi et al. [62] concluded that monomolecular cracking primarily occurs within the channels of zeolite HZSM-5, whereas bimolecular cracking and hydrogen transfer reactions are more prominent within zeolite HY due to its larger pores. HZSM-5 zeolite selectively generates gaseous olefins while impeding the formation of coke precursor reactions. In contrast, the cracking products in HY zeolite contain a higher proportion of paraffins, promoting coke formation. This is further encouraged by the cages that intersect channels within HY zeolite. Zeolite Hβ, with intermediate acid strength and pore size, exhibits behaviour between HZSM-5 and HY zeolites.

Previous studies on the deactivation of zeolites HUSY and HZSM-5 [125], [129] during polyethylene degradation in TGA have shown that HZSM-5 retains activity even after up to 13 reaction cycles without regeneration, accumulating up to 8 % coke [125], [129], [130]. In contrast, HUSY zeolite preserves activity for up to 5 reaction cycles, with a coke accumulation of up to 20 % [50], [125], [129]. This difference is attributed to the larger pores in HUSY. After these reaction cycles, the products generated become more akin to those produced in the thermal process, an indicator of deactivation [129].

Hernandez et al. [81], [131], [132] studied the effect of HDPE cracking in a fluidized bed reactor with 20 wt. % of zeolite HZSM-5 or HUSY at temperatures ranging from 400 to 800 °C. They observed that an

increase in temperature favoured the production of light hydrocarbons and reduced the amount of solid residues, except at 800 °C with HZSM-5. The aromatics production increased with temperature, with the maximum amount of BTX at 700 °C for HUSY and 500 °C for HZSM-5. A harder, insoluble coke increased with temperature [133]. They concluded that using HZSM-5 zeolite offered significant advantages, including higher gas production at lower temperatures, a narrower product distribution favouring the C_3 to C_5 range, greater selectivity for olefins and aromatics [50], and the coke generated is mostly soluble [133], [134], which means it is less hard due to pore constraints preventing polycondensation reactions, leading to the formation of polyaromatic compounds [134]. This, in turn, results in a less aggressive regeneration process.

Effect of the main properties of zeolite

The performance of polyethylene catalytic pyrolysis involves three primary properties of zeolites: ***crystallinity***, ***surface area***, and ***acidity*** (**Figure 1.7**). The degradation of polyethylene on zeolites involves a series of consecutive reactions, including cracking at the entrance of the pores and on the external surface of the zeolites, followed by further cracking within their pores. When a small amount of catalyst is loaded, the acid sites at the pore entrances and on the external surface are insufficient to initiate catalytic cracking. Consequently, catalytic cracking on the external surface becomes more significant than the additional cracking within the pores [118]; this means that the catalytic activity of the zeolites depends mainly on the accessibility to the active sites, while the product selectivity is mainly determined by the acidic strength of the zeolite catalyst [135].

As described above, the ***acidity*** depends on the Si/Al ratio. Aguado et al. [136] synthesized three different β zeolites with varying Si/Al ratios (39 and 85) and one with titanium atoms introduced into the structure during synthesis. PE cracking was carried out at 400 °C for 30 minutes using a 50 wt. % catalyst in a batch reactor. Maximum conversion, around 50 %, was achieved with β zeolites (Si/Al ratio 39) and β with Ti. These two catalysts exhibited selectivity exceeding 60 % for C_5-C_{12} products, resembling gasoline-type products. In another study [110], the zeolite Hβ shows higher activity in LDPE pyrolysis as the Si/Al ratio decreases, owing to the increased presence of Brønsted acid sites.

Zhou et al. [137] modified a zeolite in desilication with sodium carbonate. The results show a diminution of desilication's Si/Al ratio product; the total specific surface area increased from 334 to 371 $m^2\ g^{-1}$. The liquid yield increased from 45.3 wt. % to 67.3 wt. % and the aromatics are reduced from 23.3 vol. % to 0.8 vol. %, while the olefins are favourited with a rise from 13.8 vol. % to 34.6 vol. % for the pyrolysis of LDPE at 390 °C demonstrating that the desilication has a negative effect on the production of high aromatics yields.

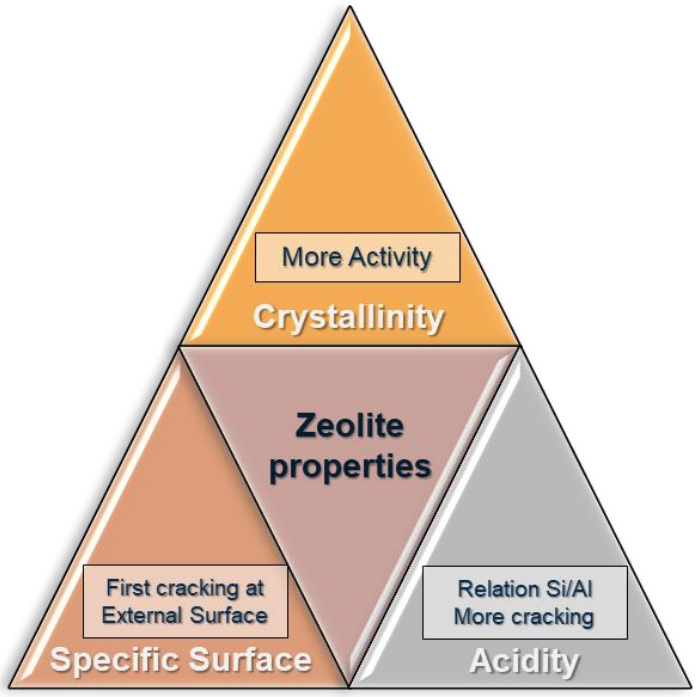

Figure 1.7. Key properties of zeolites relevant to the catalytic pyrolysis of polyethylene

Nanocrystalline zeolites have a larger ***external surface***, allowing a shorter diffusion path and more accessible active sites in the middle of a reaction. The removal of coke is also easier because more is found on the surface than a conventional zeolite [138], [139]. Serrano et al. [138] investigated nano-ZSM-5 with three different Si/Al ratios (ranging from 30 to 59) and ***crystal size*** and ***external surface*** areas (ranging from 78 to 242 $m^2.g^{-1}$). The highest activity was achieved with the zeolite that exhibited an optimal combination of small ***crystal size*** and high acid strength. Indeed, ***crystal size*** is a significant parameter that influences the catalytic cracking behaviour of zeolites, particularly in processes occurring at the surface and associated with the initial degradation steps [140]. Increasing Si/Al decreased acidity; however, cracking of LDPE and HDPE with a polymer/catalyst ratio of 100/1 at 340 °C in a stirred semi-batch reactor under nitrogen yielded higher conversion with the moderately acidic catalyst featuring the largest external surface area.

Another study [58] demonstrated that PE branching hindered polymer entry into zeolite micropores, making external acidic sites the primary cracking sites due to their accessibility. Indeed, the ***external surface*** area played a significant role in deactivating such catalysts; greater external surface area resulted in less coke formation and facilitated a less aggressive and more straightforward regeneration process[141]. Aguado et al. [108] compared an HZSM-5 zeolite with a n-HZSM-5 (nanocrystalline). Both have the same Si/Al ratio of 30 and total specific surface area but an ***external surface*** difference of 73 $m^2\ g^{-1}$ for nanocrystalline zeolite. The latter showed a selectivity in aromatics higher by 7.5 wt. %. Also, this zeolite has better distribution in the range of C_5-C_{12} [139], [142] and better conversion [138].

This literature review shows that ZSM-5 zeolite has gained prominence for its catalytic activity in polyethylene degradation. It is thus further detailed in the following part.

1.3.4. Zeolite ZSM-5

ZSM-5 zeolite, classified within the pentasil family, features a microporous MFI structure with pore dimensions ranging from 5.4 to 5.6 Å [100] (**Figure 1.8**). Due to their robust acidity, HZSM-5 zeolites exhibit remarkable activity in cracking, isomerization, and aromatization reactions that proceed through carbocation intermediates [82]. The zeolite's acidity and pore architecture facilitates extensive molecule cracking, producing low-boiling fractions and gaseous compounds [143]. Its shape-selective properties within the microporous structure impede hydrogen transfer reactions and the formation of polyaromatics, consequently enhancing the selectivity of C_2-C_4 olefins with minimal coke generation. Moreover, the three-dimensional structure of HZSM-5 zeolite promotes the outward diffusion of the precursor to coke formation [82].

The strong acidity and unique sinusoidal pores of ZSM-5 facilitate the rapid degradation of polyethylene [82], [118]. However, the crystallite size of the zeolite must not be too large. Initial cracking steps in ZSM-5 zeolite primarily occur at the strong acid sites [104], [118]. Due to its small micropore size, this initial cracking happens on the external surface, resulting in primary cracking products (C_3-C_5 olefins) through a carbocationic end-chain cracking mechanism [104]. In the case of ZSM-5, the product distribution tends to be narrower due to its smaller pore size and larger crystal size. This leads to more external catalytic sites with less steric hindrance, resulting in less pronounced diffusion limitations for forming higher molecular weight products [108]. HZSM-5 zeolite promotes the end- chain cracking mechanism [58].

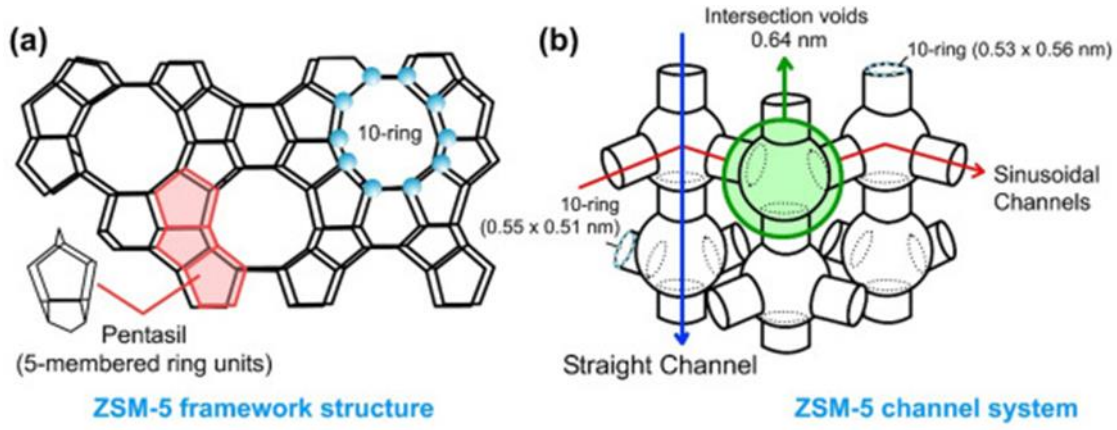

Figure 1.8. Framework structure and channel system of a ZSM-5 zeolite. Copyright from ref [144].

Doped/Modified ZSM-5.

Peral et al. [123] cracked LDPE with ZSM-5 zeolite featuring four different structures and a polymer/catalyst ratio of 100/1 between 340 °C and 380 °C in a stirred semi-batch reactor under nitrogen. They compared two 2D ZSM-5 samples with nanocrystalline and hierarchical ZSM-5 materials regarding textural, acidic, and catalytic properties. Their results indicated that while accessibility issues were critical in converting bulky polyethylene molecules, the acidic characteristics, especially the nature

and strength of acid sites, also played an important role. Materials with larger external surface areas exhibited a higher concentration of less active Lewis acid sites. A nearly linear relationship was observed between activity per unit external surface area and Brønsted acid site concentration, while Lewis site concentration displayed random dispersion. This finding suggests that primary LDPE cracking through terminal chain conversion is primarily catalysed by Brønsted acid sites, explaining why ZSM-5 materials with high Lewis acidity exhibit lower intrinsic activity.

In order to optimise the properties of ZMS-5 zeolite, several authors modify or dope the catalyst. Among them, Zhou et al. [137] impregnated lanthanum by ion-exchange method with $LaCl_3$ on a normal and desilicated zeolite. Even when the synthesis was the same, the results show a rise of La^{3+} content, a product of the low Si/Al and the steric interference for high valence La^{3+} to stay in the channels of the ZSM-5 zeolites; the S_{BET} does not change. The cracking of LDPE on zeolite indicates an increase in liquid yield from 45.3 wt. % to 49.8 wt. % for the zeolite desilicated with La^{3+}, and the aromatics are reduced from 23.3 vol. % to 14.2 vol. %, for the same catalyst. The impregnated normal zeolite does not show any change in yield and selectivity.

The Ga-ZSM-5 was also used for the cracking of industrial waste composed mainly of polyethylene and of municipal plastic wastes composed of polyethylene and polypropylene, in a pilot plant with two systems of cracking, the first one in order to thermal-degrade the waste following a dechlorination station, and the second one a catalytic cracking station. On the cracking of the municipal plastic waste at the same operations conditions, liquid yield increased from 33.3 wt. % to 44.3 wt. % and aromatics from 19.1 wt. % to 35.1 wt. % compared with thermal cracking [145].

Finally, Ma et al. [146] studied the cracking of high-impact polystyrene over HZSM-5 doped with Fe and Ni. There is a diminution of the S_{BET} and the external surface from 100 $m^2\ g^{-1}$ to 39 $m^2\ g^{-1}$ and 76 $m^2\ g^{-1}$ for Fe-doped and Ni-doped, respectively. The liquid yield is similar, between 64.4 wt. % and 61.2 wt. %. The Fe-doped has more production of single-ring compounds, but the Ni-doped has more production of Toluene. Galko et al. [147] evaluated Ni/ZSM-5 zeolite with 10 wt. % Ni content in the pyrolysis of different types of plastic waste to obtain more BTX yield, it is evident that the increasing BTX is confronted with HZSM-5.

Conclusion

One limitation of ZSM-5 zeolite lies in its external surface, which constitutes the initial contact point with plastic. It becomes evident that ZSM-5 nanocrystalline structures outperform conventional ones due to their enhanced external surface area. This, in turn, allows for improved access to acid sites and reduced coke formation within the pores, which might otherwise lead to deactivation.

Several variables, such as residence time, temperature, and the Si/Al ratio, can promote the production of aromatic compounds. Conversely, desilication tends to decrease these yields. Introducing certain metals, like gallium and nickel, can positively influence BTX production. On the other hand, Lanthanum,

while resulting in a slight reduction in coke production, does not exhibit significant alterations in oil production.

Despite the extensive use of HZSM-5 zeolite in plastic waste cracking, ongoing research is aimed at finding this catalyst's optimal modification. Enhancing its physicochemical properties remains a subject of investigation, with the ultimate goal of industrial applications that yield improved selectivity, activity, and stability.

1.4. Strategic methodology

This part aims to provide readers with a clear overview of the strategic methodology applied during this doctoral research. The main objective of this thesis is to optimize the pyrolysis process and the material capable of selectively transforming polyethylene while minimizing the production of solid products, specifically pyrolysis coke, and maximizing a liquid phase rich in aromatic oils with a high content of BTEX. This is achieved through the selection and optimization of the catalyst, the optimization of the pyrolytic process, and/or the modification of the catalyst. Additionally, the ability of the optimized catalyst to maintain its catalytic activity over multiple reuse cycles is investigated.

The literature review in this chapter explored different recycling approaches, and we identified catalytic pyrolysis as a promising approach for recycling plastics that are difficult to depolymerize polyethylene. We have also examined the influence of the type of catalyst and reaction conditions on polyethylene pyrolysis, concluding that, to maximize the production of BTEX compounds, it is essential to use zeolites, especially zeolite ZSM-5, due to its acidity, porosity, specific surface area, and shape selectivity.

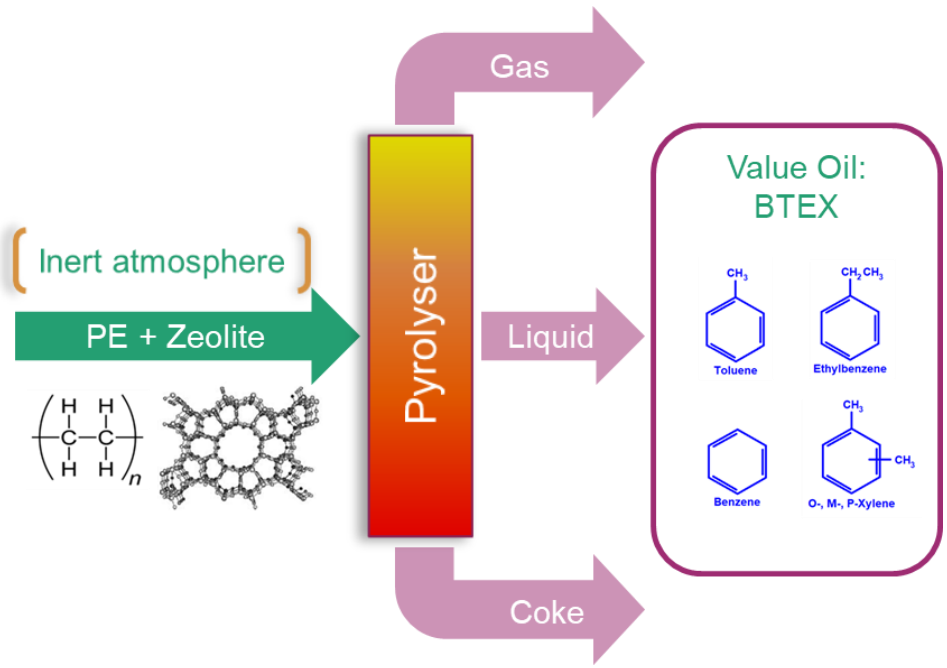

Figure 1.9. Representation of the strategic methodology of this PhD thesis.

Both the selection and optimization of the catalyst and the proper contact between the polymer and the catalyst are crucial factors influencing the catalyst **activity**, the **liquid yield** and the **selectivity** for

obtaining aromatic compounds. To better understand the catalytic process, we have characterized the catalysts using one or more of the following methods (detailed in **Chapter 2**) to assess their physicochemical properties in their pure state and after experiencing partial or complete deactivation: XRD, N_2-physisorption, ^{27}Al NMR, NH_3-TPD, Py-IR, Raman Spectroscopy, XPS, SEM-EDS, EMPA, ICP-OES and TGA.

In **Chapter 3**, thermogravimetric analysis was used to assess the activity of each preselected catalyst based on existing literature, aiming to identify two catalysts and compare their performance in producing aromatic compounds. This step was carried out using two methods for preparing the samples before reaction: extrusion of the polymer and catalyst and powdered mixture of both materials to achieve homogeneity in the respective mixtures.

Once the zeolite was selected, it was doped with zinc to modify its acidic nature and enhance its aromatization capacity. The contact of the catalyst with polyethylene was also compared in the liquid phase (Mix arrangement), with polyethylene pyrolysis vapours (layer arrangement), and with polyethylene pyrolysis vapours pre-cracked with half of the catalyst to be used (mix/layer arrangement). The results of these experiments are presented in **Chapter 4**.

Additionally, calcination was explored as a method to modify the acidic nature of the catalyst without affecting its textural properties. This was achieved by manipulating the calcination atmosphere used for zeolite protonation. Details of these modifications and their impact on polyethylene pyrolysis are described in **Chapter 5**.

Given that the viability of industrial processes hinges on cost reduction, it is crucial to evaluate the stability of a catalyst over multiple cycles. To understand the effects on polyethylene cracking and the limits of continuous catalyst use, the spent and deactivation of the catalyst were assessed after 5 cycles of reuse. This analysis can provide insights into the recommended number of cycles before catalyst activity is lost and the selection of a regeneration method that minimizes catalyst degradation. Details of catalyst deactivation are described in **Chapter 6**.

1.5. References

[1] "ISO 472:2013(en), Plastics — Vocabulary." https://www.iso.org/obp/ui/#iso:std:iso:472:ed-4:v1:en (accessed Oct. 24, 2023).

[2] A. Oasmaa *et al.*, "Pyrolysis of plastic waste: Opportunities and challenges," *J. Anal. Appl. Pyrolysis*, vol. 152, no. October 2019, p. 104804, 2020, doi: 10.1016/j.jaap.2020.104804.

[3] "Thermoplastics :: PlasticsEurope." https://www.plasticseurope.org/en/about-plastics/what-are-plastics/large-family/thermoplastics (accessed May 27, 2021).

[4] L. Filiciotto and G. Rothenberg, "Biodegradable Plastics: Standards, Policies, and Impacts," *ChemSusChem*, vol. 14, no. 1, pp. 56–72, 2021, doi: 10.1002/cssc.202002044.

[5] "How plastics are made :: PlasticsEurope." https://www.plasticseurope.org/en/about-plastics/what-are-plastics/how-plastics-are-made (accessed May 30, 2021).

[6] "Plastics – the Facts 2019: An analysis of European plastics production, demand and waste data," 2019, pp. 1–39.

[7] R. Geyer, “Production, use, and fate of synthetic polymers,” in *Plastic Waste and Recycling*, Elsevier, 2020, pp. 13–32.

[8] T. M. Letcher, “Introduction to plastic waste and recycling,” in *Plastic Waste and Recycling*, Elsevier, 2020, pp. 3–12.

[9] E. Joltreau, “of International Plastic Waste Trade Stakes at Play and Perspectives,” vol. 2019, no. September, pp. 1–6, 2019.

[10] Plastics Europe, “Plastic Europe 2022,” 2022. [Online]. Available: https://plasticseurope.org/knowledge-hub/plastics-the-facts-2022/.

[11] D. Damodharan, B. Rajesh Kumar, K. Gopal, M. V. De Poures, and B. Sethuramasamyraja, “Utilization of waste plastic oil in diesel engines: a review,” *Rev. Environ. Sci. Biotechnol.*, vol. 18, no. 4, pp. 681–697, 2019, doi: 10.1007/s11157-019-09516-x.

[12] J. Hopewell, R. Dvorak, and E. Kosior, “Plastics recycling: Challenges and opportunities,” *Philos. Trans. R. Soc. B Biol. Sci.*, vol. 364, no. 1526, pp. 2115–2126, 2009, doi: 10.1098/rstb.2008.0311.

[13] “10 Shocking Facts About Plastic | National Geographic.” https://www.nationalgeographic.co.uk/10-shocking-facts-about-plastic (accessed Aug. 29, 2022).

[14] European Commission, “A European Strategy for Plastics,” *Eur. Com.*, p. 24, 2018, doi: 10.1021/acs.est.7b02368.

[15] I. Vollmer *et al.*, “Beyond Mechanical Recycling: Giving New Life to Plastic Waste,” *Angew. Chemie - Int. Ed.*, 2020, doi: 10.1002/anie.201915651.

[16] M. Solis and S. Silveira, “Technologies for chemical recycling of household plastics – A technical review and TRL assessment,” *Waste Manag.*, vol. 105, pp. 128–138, 2020, doi: 10.1016/j.wasman.2020.01.038.

[17] P. Das, J. C. P. Gabriel, C. Y. Tay, and J. M. Lee, “Value-added products from thermochemical treatments of contaminated e-waste plastics,” *Chemosphere*, vol. 269, p. 129409, 2021, doi: 10.1016/j.chemosphere.2020.129409.

[18] J. W. Bujak, “Thermal utilization (treatment) of plastic waste,” *Energy*, vol. 90, pp. 1468–1477, 2015, doi: 10.1016/j.energy.2015.06.106.

[19] D. Xu, G. Huang, L. Guo, Y. Chen, C. Ding, and C. Liu, “Enhancement of catalytic combustion and thermolysis for treating polyethylene plastic waste,” *Adv. Compos. Hybrid Mater.*, vol. 5, no. 1, pp. 113–129, 2022, doi: 10.1007/s42114-021-00317-x.

[20] O. Dogu *et al.*, “The chemistry of chemical recycling of solid plastic waste via pyrolysis and gasification: State-of-the-art, challenges, and future directions,” *Prog. Energy Combust. Sci.*, vol. 84, p. 100901, 2021, doi: 10.1016/j.pecs.2020.100901.

[21] K. Ragaert, L. Delva, and K. Van Geem, “Mechanical and chemical recycling of solid plastic waste,” *Waste Manag.*, vol. 69, no. August, pp. 24–58, 2017, doi: 10.1016/j.wasman.2017.07.044.

[22] A. Midilli, H. Kucuk, M. Haciosmanoglu, U. Akbulut, and I. Dincer, “A review on converting plastic wastes into clean hydrogen via gasification for better sustainability,” *Int. J. Energy Res.*, vol. 46, no. 4, pp. 4001–4032, 2022, doi: 10.1002/er.7498.

[23] S. Kumar, A. K. Panda, and R. K. Singh, “A review on tertiary recycling of high-density polyethylene to fuel,” *Resour. Conserv. Recycl.*, vol. 55, no. 11, pp. 893–910, 2011, doi: 10.1016/j.resconrec.2011.05.005.

[24] A. G. Buekens and H. Huang, “Catalytic plastics cracking for recovery of gasoline-range hydrocarbons from municipal plastic wastes,” *Resour. Conserv. Recycl.*, vol. 23, no. 3, pp. 163–181, 1998, doi: 10.1016/S0921-3449(98)00025-1.

[25] Z. Wang, K. G. Burra, T. Lei, and A. K. Gupta, “Co-pyrolysis of waste plastic and solid biomass

for synergistic production of biofuels and chemicals-A review," *Prog. Energy Combust. Sci.*, vol. 84, p. 100899, 2021, doi: 10.1016/j.pecs.2020.100899.

[26] A. Matayeva, F. Basile, F. Cavani, D. Bianchi, and S. Chiaberge, *Development of Upgraded Bio-Oil Via Liquefaction and Pyrolysis*, 1st ed., vol. 178. Elsevier B.V., 2019.

[27] M. Pahnila, A. Koskela, P. Sulasalmi, and T. Fabritius, "A Review of Pyrolysis Technologies and the Effect of Process Parameters on Biocarbon Properties," *Energies*, vol. 16, no. 19, 2023, doi: 10.3390/en16196936.

[28] W. A. Sweeney and P. F. Bryan, "BTX Processing," *Kirk-Othmer Encycl. Chem. Technol.*, no. X, 1990, doi: 10.1002/0471238961.02202419230505.a01.pub2.

[29] S. M. Al-Salem, A. Antelava, A. Constantinou, G. Manos, and A. Dutta, "A review on thermal and catalytic pyrolysis of plastic solid waste (PSW)," *J. Environ. Manage.*, vol. 197, no. 1408, pp. 177–198, 2017, doi: 10.1016/j.jenvman.2017.03.084.

[30] S. D. Anuar Sharuddin, F. Abnisa, W. M. A. Wan Daud, and M. K. Aroua, "A review on pyrolysis of plastic wastes," *Energy Convers. Manag.*, vol. 115, pp. 308–326, 2016, doi: 10.1016/j.enconman.2016.02.037.

[31] D. Chen, L. Yin, H. Wang, and P. He, "Pyrolysis technologies for municipal solid waste: A review," *Waste Manag.*, vol. 34, no. 12, pp. 2466–2486, 2014, doi: 10.1016/j.wasman.2014.08.004.

[32] R. Miandad, M. A. Barakat, A. S. Aburiazaiza, M. Rehan, and A. S. Nizami, "Catalytic pyrolysis of plastic waste: A review," *Process Saf. Environ. Prot.*, vol. 102, pp. 822–838, 2016, doi: 10.1016/j.psep.2016.06.022.

[33] J. Scheirs and W. Kaminsky, *Feedstock Recycling and Pyrolysis of Waste Plastics: Converting Waste Plastics into Diesel and Other Fuels*. wiley, 2006.

[34] R. Miandad, M. A. Barakat, A. S. Aburiazaiza, M. Rehan, I. M. I. Ismail, and A. S. Nizami, "Effect of plastic waste types on pyrolysis liquid oil," *Int. Biodeterior. Biodegrad.*, vol. 119, pp. 239–252, 2017, doi: 10.1016/j.ibiod.2016.09.017.

[35] M. Heydariaraghi, S. Ghorbanian, A. Hallajisani, and A. Salehpour, "Fuel properties of the oils produced from the pyrolysis of commonly-used polymers: Effect of fractionating column," *J. Anal. Appl. Pyrolysis*, vol. 121, pp. 307–317, 2016, doi: 10.1016/j.jaap.2016.08.010.

[36] P. T. Williams and E. A. Williams, "Fluidised bed pyrolysis of low density polyethylene to produce petrochemical feedstock," *J. Anal. Appl. Pyrolysis*, vol. 51, no. 1, pp. 107–126, Jul. 1999, doi: 10.1016/S0165-2370(99)00011-X.

[37] C. Abdy, Y. Zhang, J. Wang, Y. Cheng, I. Artamendi, and B. Allen, "Investigation of high-density polyethylene pyrolyzed wax for asphalt binder modification: Mechanism, thermal properties, and ageing performance," *J. Clean. Prod.*, vol. 405, no. January, p. 136960, 2023, doi: 10.1016/j.jclepro.2023.136960.

[38] S. M. Al-Salem and P. Lettieri, "Kinetic study of high density polyethylene (HDPE) pyrolysis," *Chem. Eng. Res. Des.*, vol. 88, no. 12, pp. 1599–1606, 2010, doi: 10.1016/j.cherd.2010.03.012.

[39] N. Gascoin *et al.*, "Kinetic modelling of high density polyethylene pyrolysis: Part 1. Comparison of existing models," *Polym. Degrad. Stab.*, vol. 97, no. 8, pp. 1466–1474, 2012, doi: 10.1016/j.polymdegradstab.2012.05.008.

[40] N. Gascoin, G. Fau, P. Gillard, and A. Mangeot, "Experimental flash pyrolysis of high density polyethylene under hybrid propulsion conditions," *J. Anal. Appl. Pyrolysis*, vol. 101, pp. 45–52, 2013, doi: 10.1016/j.jaap.2013.02.014.

[41] D. Almeida and M. de F. Marque, "Thermal and Catalytic Pyrolysis of Polyethylene Plastic Waste in Semi," *Polimeros*, vol. 26, no. 1, pp. 1–8, 2015, doi: http://dx.doi.org/10.1590/0104-1428.2100.

[42] K. Akubo, M. A. Nahil, and P. T. Williams, "Aromatic fuel oils produced from the pyrolysis-

catalysis of polyethylene plastic with metal-impregnated zeolite catalysts," *J. Energy Inst.*, vol. 92, no. 1, pp. 195–202, 2019, doi: 10.1016/j.joei.2017.10.009.

[43] M. Sogancioglu, E. Yel, and G. Ahmetli, "Pyrolysis of waste high density polyethylene (HDPE) and low density polyethylene (LDPE) plastics and production of epoxy composites with their pyrolysis chars," *J. Clean. Prod.*, vol. 165, pp. 369–381, 2017, doi: 10.1016/j.jclepro.2017.07.157.

[44] H. Bockhorn, A. Hornung, U. Hornung, and D. Schawaller, "Kinetic study on the thermal degradation of polypropylene and polyethylene," *J. Anal. Appl. Pyrolysis*, vol. 48, no. 2, pp. 93–109, 1999, doi: 10.1016/S0165-2370(98)00131-4.

[45] N. Horvat and F. T. T. Ng, "Tertiary polymer recycling: Study of polyethylene thermolysis as a first step to synthetic diesel fuel," *Fuel*, vol. 78, no. 4, pp. 459–470, 1999, doi: 10.1016/S0016-2361(98)00158-6.

[46] R. K. Singh, B. Ruj, A. K. Sadhukhan, and P. Gupta, "Impact of fast and slow pyrolysis on the degradation of mixed plastic waste: Product yield analysis and their characterization," *J. Energy Inst.*, vol. 92, no. 6, pp. 1647–1657, 2019, doi: 10.1016/j.joei.2019.01.009.

[47] M. Artetxe, G. Lopez, G. Elordi, M. Amutio, J. Bilbao, and M. Olazar, "Production of light olefins from polyethylene in a two-step process: Pyrolysis in a conical spouted bed and downstream high-temperature thermal cracking," *Ind. Eng. Chem. Res.*, vol. 51, no. 43, pp. 13915–13923, 2012, doi: 10.1021/ie300178e.

[48] N. Miskolczi, J. Sója, and E. Tulok, "Thermo-catalytic two-step pyrolysis of real waste plastics from end of life vehicle," *J. Anal. Appl. Pyrolysis*, vol. 128, no. June, pp. 1–12, 2017, doi: 10.1016/j.jaap.2017.11.008.

[49] R. Miandad *et al.*, "Catalytic pyrolysis of plastic waste: Moving toward pyrolysis based biorefineries," *Front. Energy Res.*, vol. 7, no. MAR, pp. 1–17, 2019, doi: 10.3389/fenrg.2019.00027.

[50] A. Marcilla, M. I. Beltrán, and R. Navarro, "Thermal and catalytic pyrolysis of polyethylene over HZSM5 and HUSY zeolites in a batch reactor under dynamic conditions," *Appl. Catal. B Environ.*, vol. 86, no. 1–2, pp. 78–86, 2009, doi: 10.1016/j.apcatb.2008.07.026.

[51] C. Kassargy, S. and diesel-like fuel production by continuous catalytic pyrolysis of waste polyethylene and polypropylene mixtures over U. zeolite Awad, G. Burnens, K. Kahine, and M. Tazerout, "Gasoline and diesel-like fuel production by continuous catalytic pyrolysis of waste polyethylene and polypropylene mixtures over USY zeolite," *Fuel*, vol. 224, no. November 2017, pp. 764–773, 2018, doi: 10.1016/j.fuel.2018.03.113.

[52] D. P. Serrano, J. Aguado, and J. M. Escola, "Developing advanced catalysts for the conversion of polyolefinic waste plastics into fuels and chemicals," *ACS Catal.*, vol. 2, no. 9, pp. 1924–1941, 2012, doi: 10.1021/cs3003403.

[53] S. Kartik *et al.*, "Valorization of plastic wastes for production of fuels and value-added chemicals through pyrolysis – A review," *Therm. Sci. Eng. Prog.*, vol. 32, no. March, p. 101316, 2022, doi: 10.1016/j.tsep.2022.101316.

[54] M. S. Renzini, U. Sedran, and L. B. Pierella, "H-ZSM-11 and Zn-ZSM-11 zeolites and their applications in the catalytic transformation of LDPE," *J. Anal. Appl. Pyrolysis*, vol. 86, no. 1, pp. 215–220, 2009, doi: 10.1016/j.jaap.2009.06.008.

[55] M. Cocchi *et al.*, "Catalytic Pyrolysis of a Residual Plastic Waste Using Zeolites Produced by Coal Fly Ash," *Catalysts*, vol. 10, no. 10, p. 1113, Sep. 2020, doi: 10.3390/catal10101113.

[56] Y. LIN and M. YANG, "Catalytic conversion of commingled polymer waste into chemicals and fuels over spent FCC commercial catalyst in a fluidised-bed reactor," *Appl. Catal. B Environ.*, vol. 69, no. 3–4, pp. 145–153, Jan. 2007, doi: 10.1016/j.apcatb.2006.07.005.

[57] S. Klaimy, "Pyrolyse thermique et catalytique des polymères utilisés dans les emballages," Université de Lille, 2019.

[58] D. P. Serrano, J. Aguado, J. M. Escola, J. M. Rodriguez, and A. Peral, “Catalytic properties in polyolefin cracking of hierarchical nanocrystalline HZSM-5 samples prepared according to different strategies,” *J. Catal.*, vol. 276, no. 1, pp. 152–160, 2010, doi: 10.1016/j.jcat.2010.09.008.

[59] M. S. Abbas-Abadi *et al.*, “Challenges and opportunities of light olefin production via thermal and catalytic pyrolysis of end-of-life polyolefins: Towards full recyclability,” *Prog. Energy Combust. Sci.*, vol. 96, no. September 2022, p. 101046, 2023, doi: 10.1016/j.pecs.2022.101046.

[60] V. Daligaux, R. Richard, and M. H. Manero, “Deactivation and regeneration of zeolite catalysts used in pyrolysis of plastic wastes—a process and analytical review,” *Catalysts*, vol. 11, no. 7, 2021, doi: 10.3390/catal11070770.

[61] S. P. da S. Ribeiro *et al.*, “Influence of the zeolite acidity on its synergistic action with a flame-retarding polymeric intumescent formulation,” *J. Mater. Sci.*, vol. 55, no. 2, pp. 619–630, 2020, doi: 10.1007/s10853-019-04047-w.

[62] G. Elordi *et al.*, “Catalytic pyrolysis of HDPE in continuous mode over zeolite catalysts in a conical spouted bed reactor,” *J. Anal. Appl. Pyrolysis*, vol. 85, no. 1–2, pp. 345–351, 2009, doi: 10.1016/j.jaap.2008.10.015.

[63] G. Lopez, M. Artetxe, M. Amutio, J. Bilbao, and M. Olazar, “Thermochemical routes for the valorization of waste polyolefinic plastics to produce fuels and chemicals. A review,” *Renew. Sustain. Energy Rev.*, vol. 73, no. November 2016, pp. 346–368, 2017, doi: 10.1016/j.rser.2017.01.142.

[64] C. M. Lok, J. Van Doorn, and G. Aranda Almansa, “Promoted ZSM-5 catalysts for the production of bio-aromatics, a review,” *Renew. Sustain. Energy Rev.*, vol. 113, no. July, p. 109248, 2019, doi: 10.1016/j.rser.2019.109248.

[65] P. Kasar, D. K. Sharma, and M. Ahmaruzzaman, “Thermal and catalytic decomposition of waste plastics and its co-processing with petroleum residue through pyrolysis process,” *J. Clean. Prod.*, vol. 265, p. 121639, 2020, doi: 10.1016/j.jclepro.2020.121639.

[66] A. Marcilla, A. Gómez, A. García, and M. Mar Olaya, “Kinetic study of the catalytic decomposition of different commercial polyethylenes over an MCM-41 catalyst,” *J. Anal. Appl. Pyrolysis*, vol. 64, no. 1, pp. 85–101, 2002, doi: 10.1016/S0165-2370(01)00174-7.

[67] B. Kunwar, H. N. Cheng, S. R. Chandrashekaran, and B. K. Sharma, “Plastics to fuel: a review,” *Renew. Sustain. Energy Rev.*, vol. 54, pp. 421–428, 2016, doi: 10.1016/j.rser.2015.10.015.

[68] B. S. S. Phanisankar, N. Vasudeva Rao, and J. E. Manikanta, “Conversion of waste plastic to fuel products,” *Mater. Today Proc.*, no. xxxx, 2020, doi: 10.1016/j.matpr.2020.02.880.

[69] K. Moorthy Rajendran, V. Chintala, A. Sharma, S. Pal, J. K. Pandey, and P. Ghodke, “Review of catalyst materials in achieving the liquid hydrocarbon fuels from municipal mixed plastic waste (MMPW),” *Mater. Today Commun.*, vol. 24, no. January, p. 100982, 2020, doi: 10.1016/j.mtcomm.2020.100982.

[70] L. O. Mark, M. C. Cendejas, and I. Hermans, “The Use of Heterogeneous Catalysis in the Chemical Valorization of Plastic Waste,” *ChemSusChem*, vol. 13, no. 22, pp. 5808–5836, 2020, doi: 10.1002/cssc.202001905.

[71] P. T. Williams, “Hydrogen and Carbon Nanotubes from Pyrolysis-Catalysis of Waste Plastics: A Review,” *Waste and Biomass Valorization*, no. 0123456789, 2020, doi: 10.1007/s12649-020-01054-w.

[72] V. K. Soni, G. Singh, B. K. Vijayan, A. Chopra, G. S. Kapur, and S. S. V. Ramakumar, “Thermochemical Recycling of Waste Plastics by Pyrolysis: A Review,” *Energy and Fuels*, vol. 35, no. 16, pp. 12763–12808, 2021, doi: 10.1021/acs.energyfuels.1c01292.

[73] T. Xayachak *et al.*, “Pyrolysis for plastic waste management: An engineering perspective,” *J. Environ. Chem. Eng.*, vol. 10, no. 6, p. 108865, 2022, doi: 10.1016/j.jece.2022.108865.

[74] S. M. R. Mirkarimi, S. Bensaid, and D. Chiaramonti, “Conversion of mixed waste plastic into fuel for diesel engines through pyrolysis process: A review,” *Appl. Energy*, vol. 327, no. March, p. 120040, 2022, doi: 10.1016/j.apenergy.2022.120040.

[75] Y. Peng *et al.*, “A review on catalytic pyrolysis of plastic wastes to high-value products,” *Energy Convers. Manag.*, vol. 254, no. January, p. 115243, 2022, doi: 10.1016/j.enconman.2022.115243.

[76] M. Sekar, V. K. Ponnusamy, A. Pugazhendhi, S. Nižetić, and T. R. Praveenkumar, “Production and utilization of pyrolysis oil from solidplastic wastes: A review on pyrolysis process and influence of reactors design,” *J. Environ. Manage.*, vol. 302, no. October 2021, 2022, doi: 10.1016/j.jenvman.2021.114046.

[77] R. Mishra, A. Kumar, E. Singh, and S. Kumar, “Recent Research Advancements in Catalytic Pyrolysis of Plastic Waste,” *ACS Sustain. Chem. Eng.*, vol. 11, no. 6, pp. 2033–2049, 2023, doi: 10.1021/acssuschemeng.2c05759.

[78] M. S. Abbas-Abadi, M. N. Haghighi, and H. Yeganeh, “The effect of temperature, catalyst, different carrier gases and stirrer on the produced transportation hydrocarbons of LLDPE degradation in a stirred reactor,” *J. Anal. Appl. Pyrolysis*, vol. 95, pp. 198–204, 2012, doi: 10.1016/j.jaap.2012.02.007.

[79] M. S. Abbas-Abadi, M. N. Haghighi, and H. Yeganeh, “Evaluation of pyrolysis product of virgin high density polyethylene degradation using different process parameters in a stirred reactor,” *Fuel Process. Technol.*, vol. 109, pp. 90–95, 2013, doi: 10.1016/j.fuproc.2012.09.042.

[80] M. D. R. Hernández, A. García, A. Gómez, J. Agulló, and A. Marcilla, “Effect of residence time on volatile products obtained in the HDPE pyrolysis in the presence and absence of HZSM-5,” *Ind. Eng. Chem. Res.*, vol. 45, no. 26, pp. 8770–8778, 2006, doi: 10.1021/ie060728+.

[81] M. del R. Hernández, A. Gómez, A. García, J. Agulló, and A. Marcilla, “Effect of the temperature in the nature and extension of the primary and secondary reactions in the thermal and HZSM-5 catalytic pyrolysis of HDPE,” *Appl. Catal. A Gen.*, vol. 317, no. 2, pp. 183–194, 2007, doi: 10.1016/j.apcata.2006.10.017.

[82] M. Artetxe, G. Lopez, M. Amutio, G. Elordi, J. Bilbao, and M. Olazar, “Light olefins from HDPE cracking in a two-step thermal and catalytic process,” *Chem. Eng. J.*, vol. 207–208, pp. 27–34, 2012, doi: 10.1016/j.cej.2012.06.105.

[83] M. Artetxe, G. Lopez, M. Amutio, G. Elordi, J. Bilbao, and M. Olazar, “Cracking of high density polyethylene pyrolysis waxes on HZSM-5 catalysts of different acidity,” *Ind. Eng. Chem. Res.*, vol. 52, no. 31, pp. 10637–10645, 2013, doi: 10.1021/ie4014869.

[84] K. Ding *et al.*, “Catalytic microwave-assisted pyrolysis of plastic waste over NiO and HY for gasoline-range hydrocarbons production,” *Energy Convers. Manag.*, vol. 196, no. June, pp. 1316–1325, 2019, doi: 10.1016/j.enconman.2019.07.001.

[85] D. P. Serrano, J. Aguado, J. M. Escola, and E. Garagorri, “Conversion of low density polyethylene into petrochemical feedstocks using a continuous screw kiln reactor,” *J. Anal. Appl. Pyrolysis*, vol. 58–59, pp. 789–801, 2001, doi: 10.1016/S0165-2370(00)00153-4.

[86] I. Barbarias *et al.*, “Catalytic cracking of HDPE pyrolysis volatiles over a spent FCC catalyst,” *Chem. Eng. Trans.*, vol. 43, pp. 2029–2034, 2015, doi: 10.3303/CET1543339.

[87] J. A. Onwudili, N. Insura, and P. T. Williams, “Composition of products from the pyrolysis of polyethylene and polystyrene in a closed batch reactor: Effects of temperature and residence time,” *J. Anal. Appl. Pyrolysis*, vol. 86, no. 2, pp. 293–303, 2009, doi: 10.1016/j.jaap.2009.07.008.

[88] D. P. Serrano, J. Aguado, J. M. Escola, and E. Garagorri, “Performance of a continuous screw kiln reactor for the thermal and catalytic conversion of polyethylene-lubricating oil base mixtures,” *Appl. Catal. B Environ.*, vol. 44, no. 2, pp. 95–105, 2003, doi: 10.1016/S0926-3373(03)00024-9.

[89] A. Marcilla, M. Hernández, and A. García, “Study of the polymer-catalyst contact effectivity and

the heating rate influence on the HDPE pyrolysis," *J. Anal. Appl. Pyrolysis*, vol. 79, no. 1–2, pp. 424–432, 2007, doi: 10.1016/j.jaap.2006.10.017.

[90] S. Klaimy *et al.*, "Flash Catalytic Pyrolysis of Polyethylene over (Alumino)silicate Materials," *ChemCatChem*, vol. 12, no. 4, pp. 1109–1116, 2020, doi: 10.1002/cctc.201901819.

[91] S. Chaianansutcharit *et al.*, "Catalytic degradation of polyolefins over hexagonal mesoporous silica: Effect of aluminum addition," *J. Anal. Appl. Pyrolysis*, vol. 80, no. 2, pp. 360–368, 2007, doi: 10.1016/j.jaap.2007.04.009.

[92] N. D. Hesse and R. L. White, "Polyethylene Catalytic Hydrocracking by PtHZSM-5, PtHY, and PtHMCM-41," *J. Appl. Polym. Sci.*, vol. 92, no. 2, pp. 1293–1301, 2004, doi: 10.1002/app.20083.

[93] L. B. Pierella, S. Renzini, and O. A. Anunziata, "Catalytic degradation of high density polyethylene over microporous and mesoporous materials," *Microporous Mesoporous Mater.*, vol. 81, no. 1–3, pp. 155–159, 2005, doi: 10.1016/j.micromeso.2004.11.015.

[94] A. Marcilla, A. Gómez, and D. Berenguer, "Study of the influence of the characteristics of different acid solids in the catalytic pyrolysis of different polymers," *Appl. Catal. A Gen.*, vol. 301, no. 2, pp. 222–231, 2006, doi: 10.1016/j.apcata.2005.12.018.

[95] M. Olazar, G. Lopez, M. Amutio, G. Elordi, R. Aguado, and J. Bilbao, "Influence of FCC catalyst steaming on HDPE pyrolysis product distribution," *J. Anal. Appl. Pyrolysis*, vol. 85, no. 1–2, pp. 359–365, 2009, doi: 10.1016/j.jaap.2008.10.016.

[96] K. H. Lee *et al.*, "Thermal and Catalytic Degradation of Waste High-density Polyethylene (HDPE) Using Spent FCC Catalyst," *Korean J. Chem. Eng.*, vol. 20, no. 4, pp. 693–697, 2003, doi: 10.1007/BF02706909.

[97] K. H. Lee and D. H. Shin, "Catalytic degradation of waste polyolefinic polymers using spent FCC catalyst with various experimental variables," *Korean J. Chem. Eng.*, vol. 20, no. 1, pp. 89–92, 2003, doi: 10.1007/BF02697190.

[98] A. De Stefanis, P. Cafarelli, F. Gallese, E. Borsella, A. Nana, and G. Perez, "Catalytic pyrolysis of polyethylene: A comparison between pillared and restructured clays," *J. Anal. Appl. Pyrolysis*, vol. 104, pp. 479–484, 2013, doi: 10.1016/j.jaap.2013.05.023.

[99] M. Liu, J. K. Zhuo, S. J. Xiong, and Q. Yao, "Catalytic degradation of high-density polyethylene over a clay catalyst compared with other catalysts," *Energy and Fuels*, vol. 28, no. 9, pp. 6038–6045, 2014, doi: 10.1021/ef501326k.

[100] E. Borsella, R. Aguado, A. De Stefanis, and M. Olazar, "Comparison of catalytic performance of an iron-alumina pillared montmorillonite and HZSM-5 zeolite on a spouted bed reactor," *J. Anal. Appl. Pyrolysis*, vol. 130, no. July 2017, pp. 249–255, 2018, doi: 10.1016/j.jaap.2017.12.015.

[101] L. Dai *et al.*, "Chemical upcycling of waste polyolefinic plastics to low-carbon synthetic naphtha for closing the plastic use loop," *Sci. Total Environ.*, vol. 782, p. 146897, 2021, doi: 10.1016/j.scitotenv.2021.146897.

[102] D. P. Serrano, R. Van Grieken, J. Aguado, R. A. García, C. Rojo, and F. Temprano, "Study on the initial steps of the polyethylene cracking over different acid catalysts," *Stud. Surf. Sci. Catal.*, vol. 130 B, pp. 1589–1594, 2000, doi: 10.1016/s0167-2991(00)80427-9.

[103] R. Van Grieken, D. P. Serrano, J. Aguado, R. García, and C. Rojo, "Thermal and catalytic cracking of polyethylene under mild conditions," *J. Anal. Appl. Pyrolysis*, vol. 58–59, pp. 127–142, 2001, doi: 10.1016/S0165-2370(00)00145-5.

[104] D. P. Serrano *et al.*, "Feedstock recycling of agriculture plastic film wastes by catalytic cracking," *Appl. Catal. B Environ.*, vol. 49, no. 4, pp. 257–265, 2004, doi: 10.1016/j.apcatb.2003.12.014.

[105] D. P. Serrano, J. Aguado, J. M. Escola, J. M. Rodríguez, and G. San Miguel, "An investigation into the catalytic cracking of LDPE using Py-GC/MS," *J. Anal. Appl. Pyrolysis*, vol. 74, no. 1–2,

pp. 370–378, 2005, doi: 10.1016/j.jaap.2004.11.026.

[106] J. Aguado, D. P. Serrano, G. San Miguel, M. C. Castro, and S. Madrid, “Feedstock recycling of polyethylene in a two-step thermo-catalytic reaction system,” *J. Anal. Appl. Pyrolysis*, vol. 79, no. 1-2 SPEC. ISS., pp. 415–423, 2007, doi: 10.1016/j.jaap.2006.11.008.

[107] R. A. García, D. P. Serrano, and D. Otero, “Catalytic cracking of HDPE over hybrid zeolitic-mesoporous materials,” *J. Anal. Appl. Pyrolysis*, vol. 74, no. 1–2, pp. 379–386, 2005, doi: 10.1016/j.jaap.2004.11.002.

[108] J. Aguado, D. P. Serrano, and G. San Miguel, “Analysis of products generated from the thermal and catalytic degradation of pure and waste polyolefins using Py-GC/MS,” *J. Polym. Environ.*, vol. 15, no. 2, pp. 107–118, 2007, doi: 10.1007/s10924-007-0051-x.

[109] J. Aguado, D. P. Serrano, J. M. Escola, and A. Peral, “Catalytic cracking of polyethylene over zeolite mordenite with enhanced textural properties,” *J. Anal. Appl. Pyrolysis*, vol. 85, no. 1–2, pp. 352–358, 2009, doi: 10.1016/j.jaap.2008.10.009.

[110] J. Agullo *et al.*, “Catalytic pyrolysis of low density polyethylene over H-β, H-Y, H-Mordenite, and H-Ferrierite zeolite catalysts: Influence of acidity and structures,” *Kinet. Catal.*, vol. 48, no. 4, pp. 535–540, 2007, doi: 10.1134/S002315840704009X.

[111] Y. H. Seo, K. H. Lee, and D. H. Shin, “Investigation of catalytic degradation of high-density polyethylene by hydrocarbon group type analysis,” *J. Anal. Appl. Pyrolysis*, vol. 70, no. 2, pp. 383–398, 2003, doi: 10.1016/S0165-2370(02)00186-9.

[112] K. Gobin and G. Manos, “Polymer degradation to fuels over microporous catalysts as a novel tertiary plastic recycling method,” *Polym. Degrad. Stab.*, vol. 83, no. 2, pp. 267–279, 2004, doi: 10.1016/S0141-3910(03)00272-6.

[113] N. Miskolczi, F. Ateş, and N. Borsodi, “Comparison of real waste (MSW and MPW) pyrolysis in batch reactor over different catalysts. Part II: Contaminants, char and pyrolysis oil properties,” *Bioresour. Technol.*, vol. 144, pp. 370–379, 2013, doi: 10.1016/j.biortech.2013.06.109.

[114] D. P. Serrano, R. A. García, M. Linares, and B. Gil, “Influence of the calcination treatment on the catalytic properties of hierarchical ZSM-5,” *Catal. Today*, vol. 179, no. 1, pp. 91–101, 2012, doi: 10.1016/j.cattod.2011.06.029.

[115] S. . Campbell, D. . Bibby, J. . Coddington, and R. . Howe, “Dealumination of HZSM-5 Zeolites,” *J. Catal.*, vol. 161, no. 1, pp. 350–358, 1996, doi: 10.1006/jcat.1996.0192.

[116] G. Elordi, M. Olazar, R. Aguado, G. Lopez, M. Arabiourrutia, and J. Bilbao, “Catalytic pyrolysis of high density polyethylene in a conical spouted bed reactor,” *J. Anal. Appl. Pyrolysis*, vol. 79, no. 1-2 SPEC. ISS., pp. 450–455, 2007, doi: 10.1016/j.jaap.2006.11.010.

[117] G. Elordi, G. Lopez, R. Aguado, M. Olazar, and J. Bilbao, “Catalytic pyrolysis of high density polyethylene on a HZSM-5 zeolite catalyst in a conical spouted bed reactor,” *Int. J. Chem. React. Eng.*, vol. 5, 2007, doi: 10.2202/1542-6580.1567.

[118] Y. J. Lee, J. H. Kim, S. H. Kim, S. B. Hong, and G. Seo, “Nanocrystalline beta zeolite: An efficient solid acid catalyst for the liquid-phase degradation of high-density polyethylene,” *Appl. Catal. B Environ.*, vol. 83, no. 1–2, pp. 160–167, 2008, doi: 10.1016/j.apcatb.2008.02.013.

[119] G. Elordi, M. Olazar, G. Lopez, P. Castaño, and J. Bilbao, “Role of pore structure in the deactivation of zeolites (HZSM-5, Hβ and HY) by coke in the pyrolysis of polyethylene in a conical spouted bed reactor,” *Appl. Catal. B Environ.*, vol. 102, no. 1–2, pp. 224–231, 2011, doi: 10.1016/j.apcatb.2010.12.002.

[120] P. Castaño, G. Elordi, M. Olazar, A. T. Aguayo, B. Pawelec, and J. Bilbao, “Insights into the coke deposited on HZSM-5, Hβ and HY zeolites during the cracking of polyethylene,” *Applied Catalysis B: Environmental*, vol. 104, no. 1–2. pp. 91–100, 2011, doi: 10.1016/j.apcatb.2011.02.024.

[121] A. Marcilla, A. Gómez, and F. Valdés, “Catalytic pyrolysis of LDPE over H-beta and HZSM-5 zeolites in dynamic conditions. Study of the evolution of the process,” *J. Anal. Appl. Pyrolysis*,

vol. 79, no. 1-2 SPEC. ISS., pp. 433–442, 2007, doi: 10.1016/j.jaap.2006.09.006.

[122] M. S. Renzini, L. C. Lerici, U. Sedran, and L. B. Pierella, “Stability of ZSM-11 and BETA zeolites during the catalytic cracking of low-density polyethylene,” *J. Anal. Appl. Pyrolysis*, vol. 92, no. 2, pp. 450–455, 2011, doi: 10.1016/j.jaap.2011.08.008.

[123] A. Peral, J. M. Escola, D. P. Serrano, J. Přech, C. Ochoa-Hernández, and J. Čejka, “Bidimensional ZSM-5 zeolites probed as catalysts for polyethylene cracking,” *Catal. Sci. Technol.*, vol. 6, no. 8, pp. 2754–2765, 2016, doi: 10.1039/c5cy02075a.

[124] L. C. Lerici, M. S. Renzini, U. Sedran, and L. B. Pierella, “Tertiary recycling of low-density polyethylene by catalytic cracking over ZSM-11 and BETA zeolites modified with Zn2+: Stability study,” *Energy and Fuels*, vol. 27, no. 4, pp. 2202–2208, 2013, doi: 10.1021/ef302099e.

[125] A. Marcilla, M. I. Beltrán, F. Hernández, and R. Navarro, “HZSM5 and HUSY deactivation during the catalytic pyrolysis of polyethylene,” *Appl. Catal. A Gen.*, vol. 278, no. 1, pp. 37–43, 2004, doi: 10.1016/j.apcata.2004.09.023.

[126] Y. H. Lin and M. H. Yang, “Tertiary recycling of polyethylene waste by fluidised-bed reactions in the presence of various cracking catalysts,” *J. Anal. Appl. Pyrolysis*, vol. 83, no. 1, pp. 101–109, 2008, doi: 10.1016/j.jaap.2008.06.004.

[127] M. Hernández, Á. N. García, and A. Marcilla, “Catalytic flash pyrolysis of HDPE in a fluidized bed reactor for recovery of fuel-like hydrocarbons,” *J. Anal. Appl. Pyrolysis*, vol. 78, no. 2, pp. 272–281, 2007, doi: 10.1016/j.jaap.2006.03.009.

[128] Y. H. Lin, W. H. Hwu, M. D. Ger, T. F. Yeh, and J. Dwyer, “A combined kinetic and mechanistic modelling of the catalytic degradation of polymers,” *J. Mol. Catal. A Chem.*, vol. 171, no. 1–2, pp. 143–151, 2001, doi: 10.1016/S1381-1169(01)00079-6.

[129] A. Marcilla, M. I. Beltrán, and R. Navarro, “TG/FT-IR analysis of HZSM5 and HUSY deactivation during the catalytic pyrolysis of polyethylene,” *J. Anal. Appl. Pyrolysis*, vol. 76, no. 1–2, pp. 222–229, 2006, doi: 10.1016/j.jaap.2005.11.008.

[130] A. Marcilla, M. I. Beltrán, and R. Navarro, “Study of the deactivation process of HZSM5 zeolite during polyethylene pyrolysis,” *Appl. Catal. A Gen.*, vol. 333, no. 1, pp. 57–66, 2007, doi: 10.1016/j.apcata.2007.09.004.

[131] M. D. R. Hernández, A. García, and A. Marcilla, “Study of the gases obtained in thermal and catalytic flash pyrolysis of HDPE in a fluidized bed reactor,” *J. Anal. Appl. Pyrolysis*, vol. 73, no. 2, pp. 314–322, 2005, doi: 10.1016/j.jaap.2005.03.001.

[132] M. Hernández, A. García, and A. Marcilla, “Catalytic flash pyrolysis of HDPE in a fluidized bed reactor for recovery of fuel-like hydrocarbons,” *J. Anal. Appl. Pyrolysis*, vol. 78, no. 2, pp. 272–281, 2007, doi: 10.1016/j.jaap.2006.03.009.

[133] A. Marcilla, A. Gómez, and F. J. Valdés, “Influence of the temperature on the composition of the coke obtained in the catalytic cracking of low density polyethylene in the presence of USY and HZSM-5 zeolites,” *Microporous Mesoporous Mater.*, vol. 109, no. 1–3, pp. 420–428, 2008, doi: 10.1016/j.micromeso.2007.05.040.

[134] A. Marcilla, A. Gómez, and F. J. Valdés, “Evolution of the deactivation mode and nature of coke of HZSM-5 and USY zeolites in the catalytic cracking of low-density polyethylene during successive cracking runs,” *Appl. Catal. A Gen.*, vol. 352, no. 1–2, pp. 152–158, 2009, doi: 10.1016/j.apcata.2008.10.001.

[135] V. P. S. Caldeira, A. Peral, M. Linares, A. S. Araujo, R. A. Garcia-Muñoz, and D. P. Serrano, “Properties of hierarchical Beta zeolites prepared from protozeolitic nanounits for the catalytic cracking of high density polyethylene,” *Appl. Catal. A Gen.*, vol. 531, pp. 187–196, 2017, doi: 10.1016/j.apcata.2016.11.003.

[136] J. Aguado, D. P. Serrano, J. M. Escola, E. Garagorri, and J. A. Fernández, “Catalytic conversion of polyolefins into fuels over zeolite beta,” *Polym. Degrad. Stab.*, vol. 69, no. 1, pp. 11–16, 2000, doi: 10.1016/S0141-3910(00)00023-9.

[137] Q. Zhou, Y. Z. Wang, C. Tang, and Y. H. Zhang, “Modifications of ZSM-5 zeolites and their applications in catalytic degradation of LDPE,” *Polym. Degrad. Stab.*, vol. 80, no. 1, pp. 23–30, 2003, doi: 10.1016/S0141-3910(02)00378-6.

[138] D. P. Serrano, J. Aguado, J. M. Escola, and J. M. Rodríguez, “Influence of nanocrystalline HZSM-5 external surface on the catalytic cracking of polyolefins,” *J. Anal. Appl. Pyrolysis*, vol. 74, no. 1–2, pp. 353–360, 2005, doi: 10.1016/j.jaap.2004.11.037.

[139] A. L. Figueiredo *et al.*, “Catalytic cracking of LDPE over nanocrystalline HZSM-5 zeolite prepared by seed-assisted synthesis from an organic-template-free system,” *J. Anal. Appl. Pyrolysis*, vol. 117, pp. 132–140, 2016, doi: 10.1016/j.jaap.2015.12.005.

[140] C. Covarrubias, F. Gracia, and H. Palza, “Catalytic degradation of polyethylene using nanosized ZSM-2 zeolite,” *Appl. Catal. A Gen.*, vol. 384, no. 1–2, pp. 186–191, 2010, doi: 10.1016/j.apcata.2010.06.034.

[141] D. P. Serrano, J. Aguado, J. M. Rodríguez, and A. Peral, “Catalytic cracking of polyethylene over nanocrystalline HZSM-5: Catalyst deactivation and regeneration study,” *J. Anal. Appl. Pyrolysis*, vol. 79, no. 1-2 SPEC. ISS., pp. 456–464, 2007, doi: 10.1016/j.jaap.2006.11.013.

[142] D. P. Serrano, J. Aguado, J. M. Escola, and J. M. Rodríguez, “Nanocrystalline ZSM-5: A highly active catalyst for polyolefin feedstock recycling,” *Stud. Surf. Sci. Catal.*, vol. 142 A, pp. 77–84, 2002, doi: 10.1016/s0167-2991(02)80014-3.

[143] A. A. Inayat, A. A. Inayat, W. Schwieger, B. Sokolova, and P. Lestinsky, “Enhancing aromatics and olefins yields in thermo-catalytic pyrolysis of LDPE over zeolites: Role of staged catalysis and acid site density of HZSM-5,” *Fuel*, vol. 314, no. January, p. 123071, 2022, doi: 10.1016/j.fuel.2021.123071.

[144] H. Sharbini Kamaluddin, X. Gong, P. Ma, K. Narasimharao, A. Dutta Chowdhury, and M. Mokhtar, “Influence of zeolite ZSM-5 synthesis protocols and physicochemical properties in the methanol-to-olefin process,” *Mater. Today Chem.*, vol. 26, 2022, doi: 10.1016/j.mtchem.2022.101061.

[145] J. Nishino, M. Itoh, H. Fujiyoshi, and Y. Uemichi, “Catalytic degradation of plastic waste into petrochemicals using Ga-ZSM-5,” *Fuel*, vol. 87, no. 17–18, pp. 3681–3686, 2008, doi: 10.1016/j.fuel.2008.06.022.

[146] C. Ma *et al.*, “Pyrolysis-catalytic upgrading of brominated high impact polystyrene over Fe and Ni modified catalysts: Influence of HZSM-5 and MCM-41 catalysts,” *Polym. Degrad. Stab.*, vol. 146, pp. 1–12, 2017, doi: 10.1016/j.polymdegradstab.2017.09.005.

[147] G. Gałko, M. Rejdak, D. Tercki, M. Bogacka, and M. Sajdak, “Evaluation of the applicability of polymeric materials to BTEX and fine product transformation by catalytic and non-catalytic pyrolysis as a part of the closed loop material economy,” *J. Anal. Appl. Pyrolysis*, vol. 154, no. January, 2021, doi: 10.1016/j.jaap.2021.105017.

Chapter 2

2. Materials and Methods

2.1. Introduction

This chapter describes the experimental set-up designed and optimised to study the pyrolysis of polymers, the preparation and characterisation of the catalysts, and the preparation of the samples (polymer + catalyst) for the different experiments performed in this thesis.

The thermal pyrolysis of polystyrene (PS) and polyethylen (PE) alone were first studied to optimise the pyrolysis set-up. In a second step, the catalytic pyrolysis of PE was studied to evaluate the effect of the preparation methods of the mixture polymer/catalyst, and of the catalyst acidity on the yield and composition of the pyrolysis oil. The methods used (i) to prepare the samples for the pyrolysis experiment, (ii) to modify catalyst acidity, and (iii) to evaluate the possible deactivation of the catalyst at the end of each experiment are described in this chapter.

2.2. Pyrolysis reactor

As part of the PhD thesis of Sophie KLAIMY (2019) [1], an experimental set-up was developed to study the thermal and catalytic pyrolysis of pure and mixed plastic waste. This device is shown in **Figure 2.1** and consists of the following items:

- (1) a nitrogen source, nitrogen U from Air Liquide, the carrier gas,
- (2) and (3) two flowmeters in order to be able to use low (< 1.5 $L.min^{-1}$) and high flows (> 1.5 $L.min^{-1}$) of carrier gas,
- (4) a cold room to keep the sample at room temperature before the pyrolysis. This cold room is cooler through a chiller,
- (5) a cylindrical stainless-steel reactor (grade X5CrNi18-10), designed at Centrale Lille with the software Catia, with an internal diameter of 5.6 cm and a length of 70 cm, with a total volume of 1.7L. At 200 $mL.min^{-1,}$ the residence time was 4.3 min at 20 °C and 1.8 min at 450 °C. The reactor is heated to the desired temperature,
- (6) a spoon to put the sample,
- (7) a CARBOLITE GERO 30-3000 °C oven,
- (8) two borosilicate glass cold traps immersed in liquid nitrogen in order to collect the condensable pyrolysis products with a surface immersed in liquid nitrogen of 195 cm^2,
- (9) a sealed water bottle in order to visualise the flow.

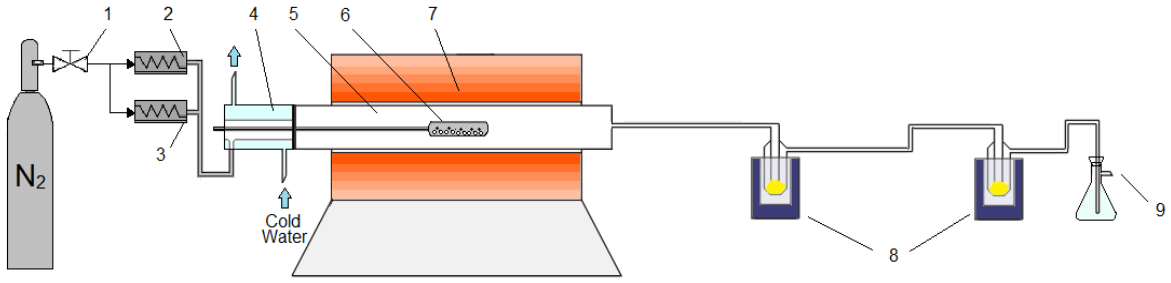

Figure 2.1. Schematic representation of the first pyrolysis facility by KLAIMY (2019) [1]; 1 Gas valve; 2 and 3 Flowmeters; 4 Cold room; 5 Stainless steel tube; 6 Spoon; 7 Electric oven; 8 Cold traps; 9 water-sealed bottle.

2.3. A pyrolysis experiment

In the present PhD thesis work, two types of plastics were used: linear low-density polyethylene (LLDPE), Eltex® PF6220AE, provided by Wipak (Bousbecque, France) in the form of pellets presenting an average particle size of 4 mm and a density of 919 kg m^{-3}, and polystyrene (PS) pellets supplied by Sigma Aldrich.

Description of a typical pyrolysis experiment

The experiments were performed in the set-up previously described, containing a stainless-steel tubular reactor. The pure polymer or polymer-catalyst mixtures were deposited in the spoon and placed in the cold room before the reaction. The temperature of this chamber (**Figure 2.2**) was controlled at 20 °C by a chiller (LAUDA ECO SILVER).

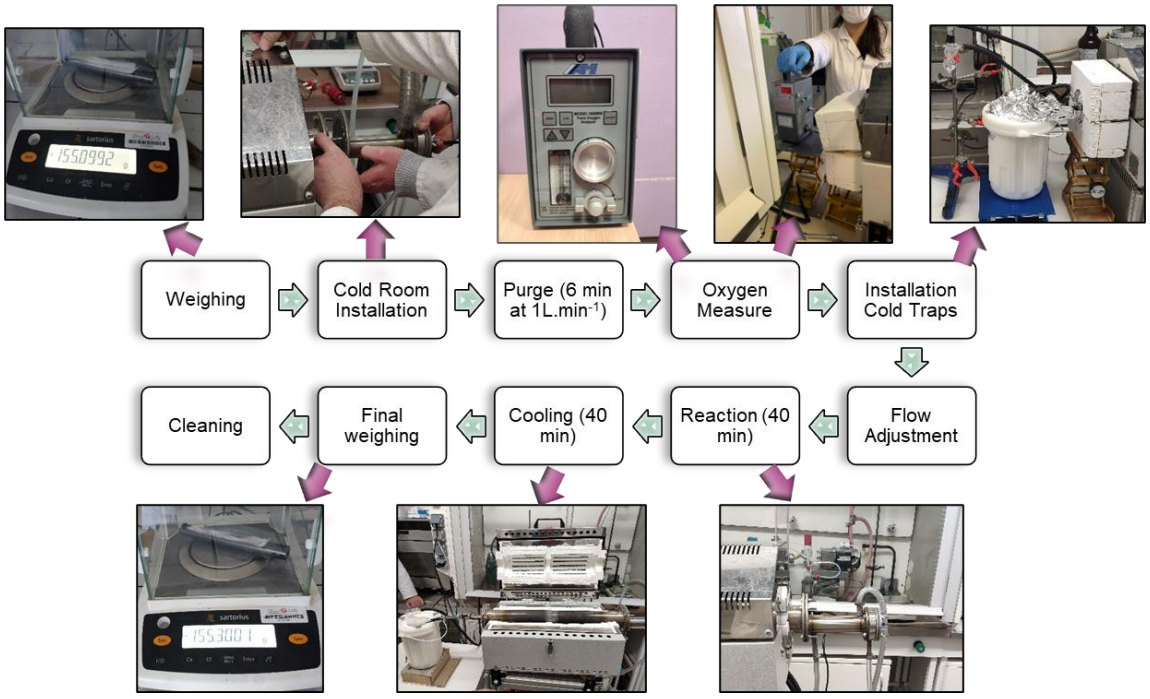

Figure 2.2. Schematic of the process used to perform the experiments.

The cold room was connected to the reactor. The pyrolytic reactor was purged with nitrogen to have an oxygen-free system, and the oxygen content was monitored by means of an oxygen detector placed at the end of the reactor. The reactor was heated to the desired reaction temperature, and the nitrogen flow was adjusted using the flowmeter. Once the pyrolysis temperature was reached, the sample was introduced into the heated zone and placed in the middle of the reactor, where the temperature was homogeneous. The time of the experiment was fixed at 40 min. The condensable pyrolysis gases were condensed in the cold traps immersed in liquid nitrogen. The mass of the liquid phase was determined by the weight difference in the cold traps before and after the reaction. Non-condensable gases were passed through the water-sealed bottle placed inside the fume hood.

The yield values were calculated as follows:

Equation 1 $$\mathrm{Wax+Oil yield(wt.\%)} = \frac{\mathrm{Mass Wax+Oil}}{\mathrm{Mass of LLDPE}} \times 100$$

Equation 2 $$\mathrm{Coke yield(wt.\%)} = \frac{\mathrm{Mass Coke}}{\mathrm{Mass of LLDPE}} \times 100$$

Equation 3 $$\mathrm{Gas yield(wt.\%)} = \frac{\mathrm{Mass of LLDPE - Mass Wax+Oil - Mass Coke}}{\mathrm{Mass of LLDPE}} \times 100$$

Equation 4 $$\mathrm{yield} = \bar{x} \pm t_{\frac{\alpha}{2}} \left(\frac{s}{\sqrt{n}}\right)$$

Where $\bar{x}$ is the average yield value, α is equal to 1 minus the confidence interval, $t_{\frac{\alpha}{2}}$ distribution is found from the t distribution table with the α value and the degrees of freedom, s is the standard deviation, and n is the number of runs. The values of the respective standard errors were calculated based on the average yields of 3 to 5 runs, with a 95 % confidence interval. The standard deviation and the standard errors were obtained for each averaged yield [2].

2.4. Analytical tools

The Wax+Oil fraction was collected from the cold taps by dilution with 15 g approx. of dichloromethane (DCM) from Carlo Erba Reagents. This solvent, compatible with GC columns, was used to dissolve waxes without damaging their chemical structure. The chemical composition of this fraction was analysed with GC-MS gas chromatography, (Shimadzu GC-2010 coupled to a Shimadzu GC-MS-QP2010 Plus mass spectrometer). The GC column is a 30 m*0.25 µm*0.25 µm optima-5 ms capillary column. Before injection, the syringe was rinsed four times with the solvent and four times with the sample. The samples were then injected into the GC-MS instrument and analysed under the following conditions:

- Injection Temperature: 300 °C, to guarantee waxes in liquid or gas state;
- Carrier gas: Helium alphagaz from Air Liquide;

- Pressure: 50.5 kPa;
- Total flow: 54.7 $mL.min^{-1}$;
- Colum Flow: 1.01 $mL.min^{-1}$;
- Purge Flow: 3 $mL.min^{-1}$;
- Split Ratio: 50
- Column Program (chromatographic separation): 40 °C hold for 10 min, ramp of 8 $°C.min^{-1}$ from 40 °C to 280 °C; the temperature of 280 °C hold for 10 min. Total program time: 50 min.
- Mass spectrometric detection: Ionisation mode EI, start time detection at 0.2 min, end time detection at 50 min, full scan mode between m/z from 40 to 800. The Data acquisition and analysis were performed using GCMSsolution software from Shimadzu. The obtained peaks based on their retention times were matched with standard compound peaks of NIST08s mass spectral data library. The different family and BTEX yields were calculated considering the area peak and the Wax+Oil yield.

2.5. Optimisation of the set-up

2.5.1. First observations

The first experiments of this thesis work, performed with the set-up defined in the work of Sophie KLAIMY [1], showed condensation products inside the reactor (**Figure 2.3**). The thermal decomposition at 550 °C of PS led to a wax-liquid yield of only 30 wt. %, whereas literature reports value usually higher than 78 %. Indeed, **Table 2.1** lists some results from the literature on the thermal decomposition of PS under similar conditions to ours, and it shows that it is necessary to improve the experimental pyrolysis set-up to increase the yield.

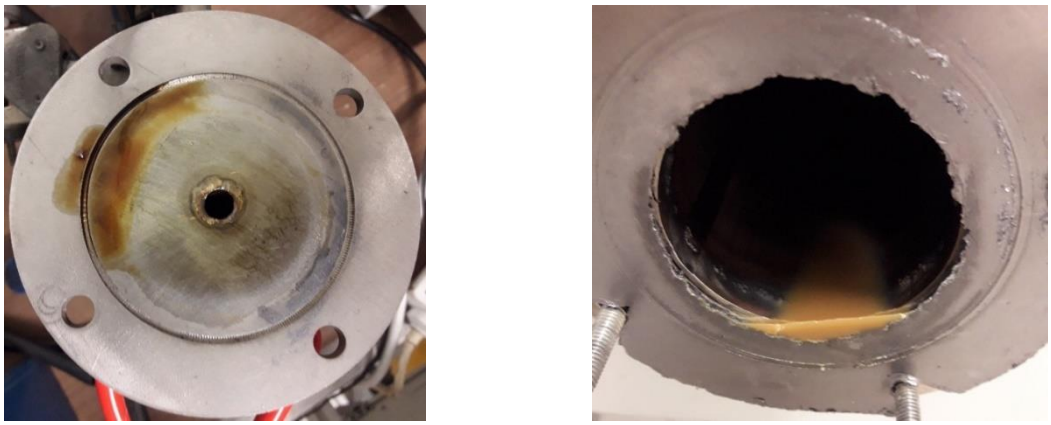

Figure 2.3. Evidence in photos of the losses of the wax-liquid fraction inside the reactor.

Table 2.1 Comparison of liquid yield (wt. %) of the pyrolysis of PS from KLAIMY 2019 [1] study and the bibliography.

Wax-Liquid Yield (wt. %)	**Reaction Temperature (°C)**	**Pyrolysis type**	**Type of PS**	**Reactor type**	**Reference**
42-93	360-425	Slow	EPSW	Batch	[3]
93.04	330	Fast (microwave)	PSW*	Semi-batch	[4]
80.7	434	Slow			
80	400	Slow	PS	Semi-batch	[5]
81.7	400	Slow	PS	Semi-batch	[6]
87	450	Slow	PS	Semi-batch	[7]
80.8	450	Slow	PSW*	Batch	[8]
94	450	Slow	PS	Semi-batch	[2]
75	450	Slow	PS	Batch	[9]
82	500				
78	500	Fast	EPSW**	Distillation set-up	[10]
78	500	Slow	PS	Batch	[11]
80	500	Slow	PS	Batch	[12]
96.6	500	Slow	PSW*	Batch	[13]
86-98.5	514-782	Flash	PS	Fluidised bed	[14]
30	**550**	**Fast**	**PS**	**Batch**	**KLAIMY [15]**
95.3	550	Flash	PSW*	Fluidised bed	[16]
75-92	550	Slow	EPSW**	Batch	[17]
94	550	Flash	PSW *	Semi-batch	[18]

*PSW: Polystyrene waste; ** EPSW: Expanded polystyrene waste

In order to improve the performance but also the accuracy of the experiments that will be conducted during this thesis, we first identified possible weaknesses of the set-up. Modifications were then made. Finally, experiments were carried out, and the results obtained were compared with those of the literature to validate our modifications.

2.5.2. Set-up weaknesses

The identified weaknesses can be observed in **Figure 2.4**. and are listed below:

(a) The existence of two flowmeters could make a complex control of nitrogen flow.
(b) The length of the reactor and the non-insulation of the outlet of the reactor are sources of cold spots that generate unwanted condensation, making condensable products hard to recover.
(c) Other cold spots were observed between the reactor and the first cold trap and between the two cold traps.

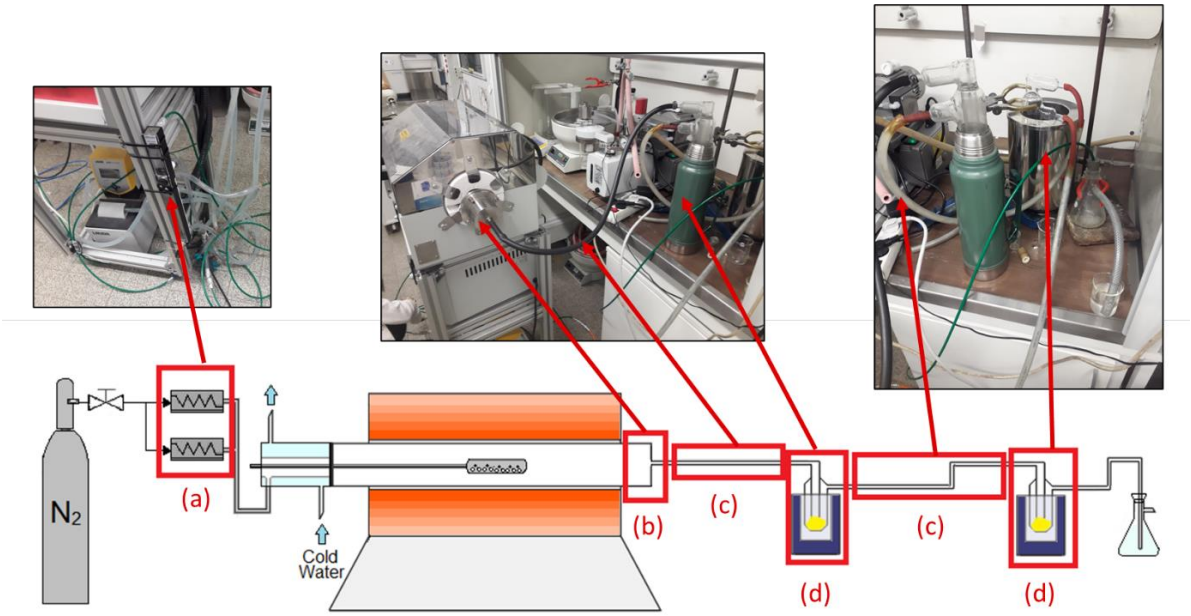

Figure 2.4. Schematic representation of the first pyrolysis facility by KLAIMY (2019) [1] and the detected points to improve.

(d) The containers in which the liquid nitrogen was placed were not large enough to ensure uniform cooling of the traps. Indeed, at the end of the pyrolysis process, it was observed that only the bottom of the cold traps was immersed in liquid nitrogen, representing 43 % of the total surface immersed in liquid nitrogen. The area in blue in **Figure 2.5** (a) represents the heat exchanger surface of the cold trap whereby the gases circulated, and the heat exchange happened, allowing the condensation of the liquid phase inside the trap. During part of the pyrolytic reaction, this surface remained without liquid nitrogen.

(a) (b)

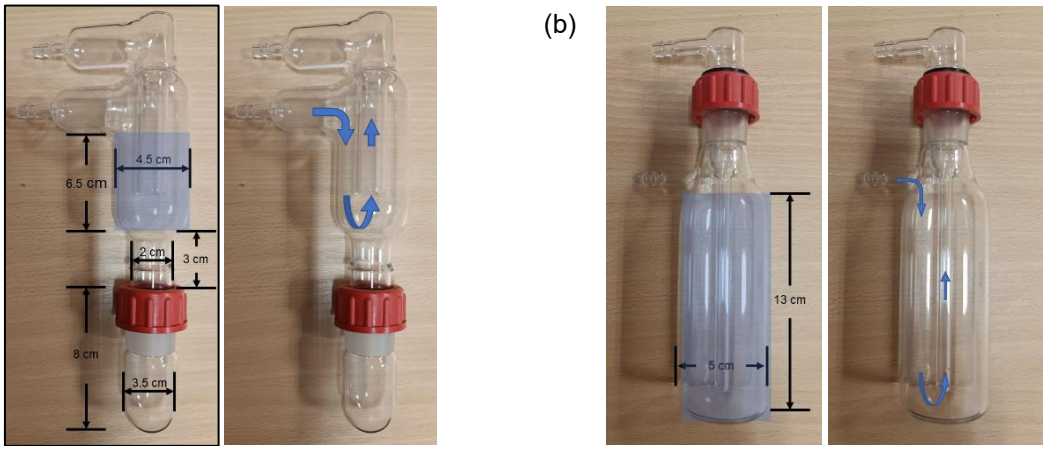

Figure 2.5. Photos of the original (a) and modified (b) cold traps **(Change #2)**

2.5.3. Changes

The details of the changes that have been performed on the initial reactor are illustrated in **Figure 2.6** and described below:

Change #1: Multiple changes were made simultaneously and illustrated in **Figure 2.6** from letters (a) to (e). Those changes are related to the following:

(a) The replacement of the two flowmeters for a digital one, easier to manipulate,
(b) a new reactor: the length of 70 cm was shortened to 60 cm, so the total volume was reduced from 1.7 L to 1.5 L, and the residence time decreased from 4.3 min to 3.7 min at 20 °C, respectively, with the carrier gas at 200 mL.min^{-1},
(c) the reactor outlet was insulated to avoid condensation of waxes,
(d) the distances between the reactor outlet, the first cold trap, and the two cold traps were shortened to avoid cold points,
(e) the liquid nitrogen containers were changed for wider ones in which the cold traps could be immersed more efficiently, so the heat exchange surface of the trap was in contact with the liquid nitrogen.

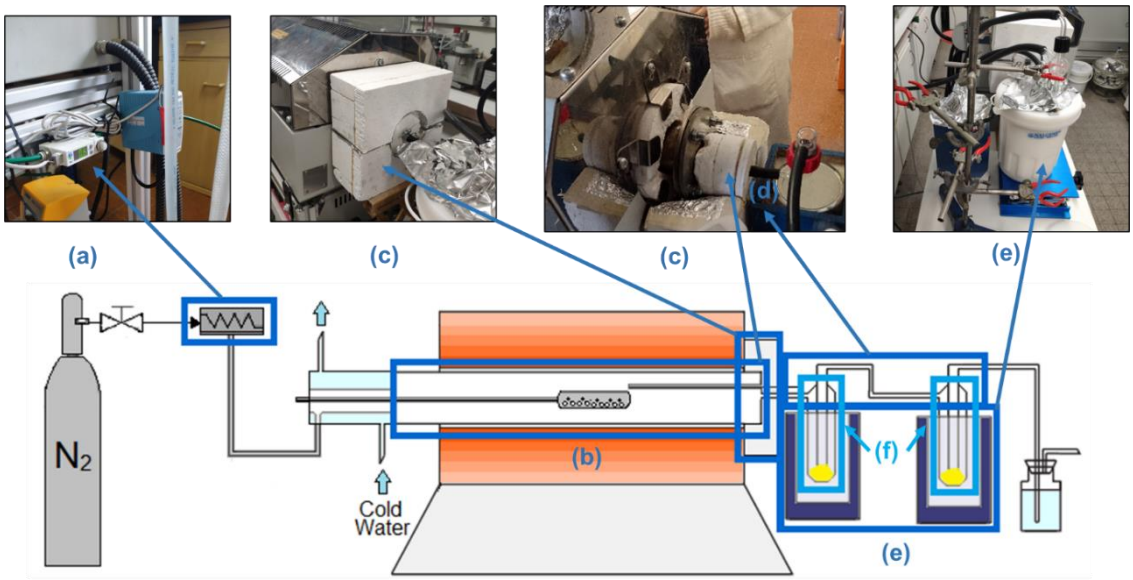

Figure 2.6. Schematic representation of the pyrolysis facility (2nd set-up) and its changes

Changes #2: The cold traps, with a total surface area of 199 cm^2, were changed to lighter ones with a higher total surface of 204 cm^2, which were easier to put on the balance and weigh. The heat exchanger increases from 92 cm^2 to 243 cm^2, as illustrated in **Figure 2.5**. The contact time at 200 mL.min^{-1} between the gas flow and the cold surface also changed from 0.5 min for the first cold trap to 1.3 min for the modified cold trap, corresponding to an increase of more than 155 % of the contact time.

Experiment results

The effects of **Change #1** were studied considering the pyrolysis of polystyrene at 550 °C, while the effects of **Change #2** (made after **Change #1**) were evaluated considering the pyrolysis polyethylene at 550 °C. These results are presented in **Figure 2.7**.

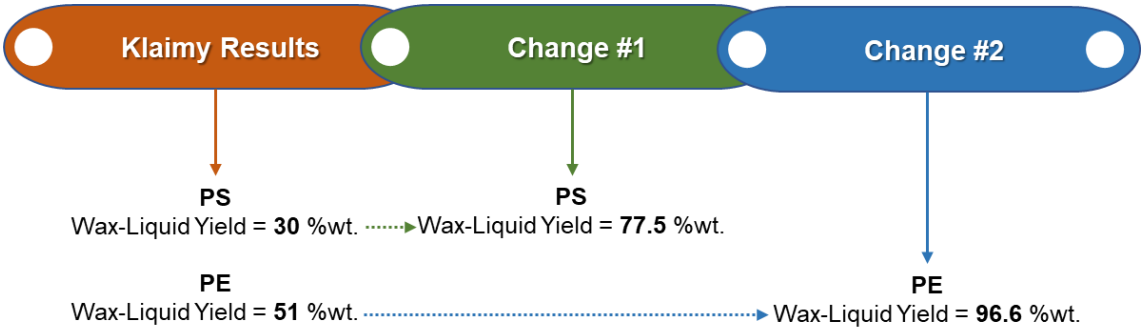

Figure 2.7. Diagram of pyrolysis results from the first set-up to the optimised set-up. The reaction temperature and the nitrogen flow were 550 °C and 200 mL.min^{-1}, respectively.

Our modification #1 compared to the set-up used in the PhD thesis of Sophie KLAIMY [15] allows an increase in liquid phase yield from 30 to 77.5 wt. % for the pyrolysis of PS at 550 °C. No condensation products were observed between the reactor and the first cold trap or between the two cold traps. The reduction in cold spots allows long-chain, easily condensed hydrocarbons to remain in the gaseous state until they reach the first trap. In addition, better contact between the cold traps and the liquid nitrogen allows more condensation inside the traps.

Change #2. With several modifications of the set-up (Changes #1 and #2), the liquid yield in the thermal pyrolysis of PE at 550 °C increased from 51 % (works of KLAIMY [15]) to 96.6 wt. %. This increase was possible due to the first modifications (Change #1) and the improved contact between the gas stream and the cold surface. The new cold traps force the gas to touch the bottom of the trap, which is always in contact with the liquid nitrogen, which guarantees cooling even if the nitrogen level decreases during the experiment. The collection of the condensable liquid fraction is almost complete with the first trap compared to the first set-up. With the first version of the cold traps, some of the liquid was also condensed in the second trap, as shown in **Figure 2.8**.

(a)  (b) 

Figure 2.8. First version (a) and new design (b) of the cold traps after pyrolysis experiment.

Description of the optimised set-up

The characteristics of the optimised set-up (**Figure 2.9**) are described below:

- (1) a nitrogen source, nitrogen U from Air Liquide, the carrier gas.
- (2) a digital flowmeter,
- (3) a cold room to keep the sample at room temperature before the pyrolysis. This cold room is cooled through a chiller.
- (4) a cylindrical stainless-steel reactor (grade X5CrNi18-10), designed at Centrale Lille with the software Catia, has an internal diameter of 5.6 cm and a 60 cm length with a total volume of 1.5 L. At 200 mL.min$^{-1,}$ the residence time was 3.7 min at 20 °C and 1.5 min at 450 °C.
- (5) a spoon to put the sample,
- (6) the CARBOLITE GERO 30-3000 °C oven,
- (10) two borosilicate glass cold traps immersed in liquid nitrogen in order to collect the condensable pyrolysis products with a heat interchange surface of 243 cm^2,
- (11) and a sealed water bottle.

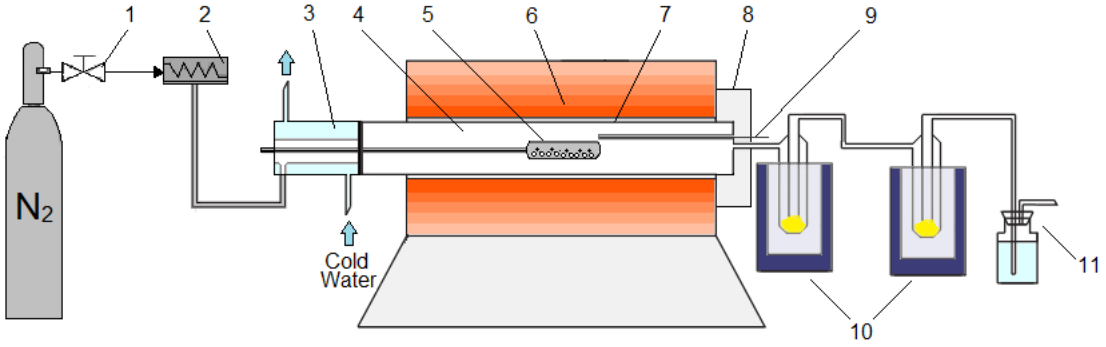

Figure 2.9. Final schematic representation of the pyrolysis facility (2nd setup); 1 Gas valve; 2 Flowmeter; 3 Cold room; 4 Stainless steel tube; 5 Spoon; 6 Electric heater; 7 Heating zone; 8 Hot Chamber; 9 Thermocouple; 10 Cold traps; 11 water-sealed bottle

2.5.4. Comparison of results from the new set-up with the literature data

Flash pyrolysis of low-density polyethylene was studied at 550 °C with the optimised set-up, using nitrogen as carrier gas at 200 mL.min^{-1}. The yield of the three fractions (gas, char and condensable) was evaluated and compared with the literature (**Figure 2.10**). The wax-liquid yield value was 96.6 % and is close to those obtained by Marcilla et al. [19] in a batch reactor using slow pyrolysis and by Williams et al. [20] in a fluidised bed reactor (fast pyrolysis), whereas in KLAIMY's study [15], only 51 % of the liquid fraction was recovered.

Comparing our results with those from the literature gives reliability to the data obtained. The changes improved the temperature distribution within the reactor and decreased the residence time of the gases in the reactor from 1.8 to 1.5 min at 450 °C. It was then decided to re-evaluate one of the parameters

evaluated in KLAIMY 2019 [1] thesis, the effect of carrier gas flow on the performance of the different phases and the distribution of product family and carbon in the wax-liquid phase.

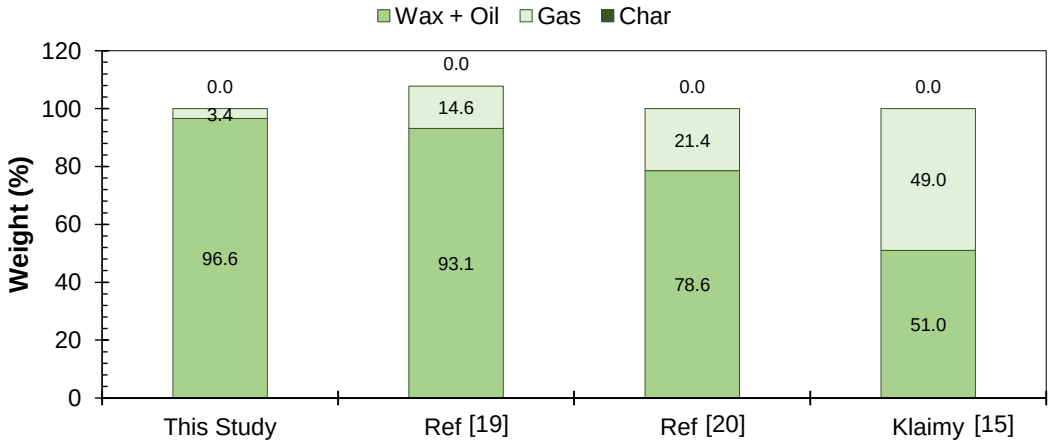

Temperature (°C)	550	550	550	550
Pyrolysis type	Fast	Slow	Fast	Fast
Type of PE	LLDPE	LLDPE	LDPE	LLDPE
Reactor type	Batch	Batch	Fluidised Bed	Batch

Figure 2.10. Yield composition of pyrolysis of Pure LDPE from this study and references.

This effect is critical to re-optimise because a high flow can cause the cracking products to move through the reactor too quickly, leading to incomplete decomposition and lower yields of valuable products. On the other hand, a low flow rate facilitates secondary reactions [21] and can result in the over-decomposition of the cracking products, leading to thermal over-degradation and the formation of undesirable by-products [22].

The effect of residence time on the cracking of LLDPE was studied using four different carrier flow rates, 200, 400, 600 and 800 mL.min^{-1}, which correspond to a residence time of 79, 40, 26 and 20 s at 550 °C, respectively. The effect on the phase yield (**Figure 2.11**(**a**)), the product family distribution (**Figure 2.11**(**b**)) and the carbon distribution (**Figure 2.11**(**c**)) were studied. The results were named LLDPE-### where ### refers to the nitrogen flow used in the experiment, i.e. for LLDPE-200, the nitrogen flow rate used was 200m L.min^{-1} for the given temperature.

With the increase of the residence time (low flow rate), an optimised value is observed for the amount of Wax+Oil at 200 mL.min^{-1} (**Figure 2.11** (**a**)), whereas the value is the lowest for 400 mL.min^{-1} and increased for 600 mL.min^{-1} and 800 mL.min^{-1}. Regarding the product family distribution (**Figure 2.11**(**b**)), no clear effect of the residence time is observed since the amount of aromatics, alkanes, and alkenes are similar, whatever the gas flow used. However, aromatic are only observed at 200 mL.min^{-1}. This may be explained by a longer residence time inside the reactor that seems to favour secondary reactions such as hydrogen transfer and β-scission that require higher activation energy and lead to the production of aromatics. Nevertheless, with the increase of the residence time, the carbon distribution (**Figure**

2.11(**c**)) shows an increase in the C_6-C_{12} zone and a decrease in zone ≥C_{13}, which could be related to the presence of more aromatics.

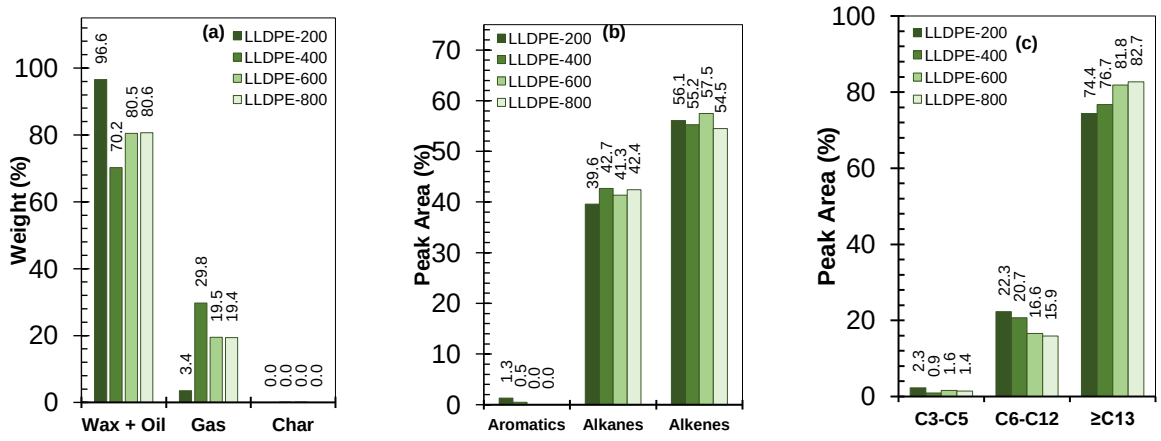

Figure 2.11. Fraction yield of the decomposition of pure LLDPE (a). Composition of the oil pyrolysis fraction (b) and carbon distribution of the oil fraction (c) at 550 °C at different nitrogen flow: 200 mL.min^{-1} (LLDPE-200), 400 mL.min^{-1} (LLDPE-400), 600 mL.min^{-1} (LLDPE-600).and 800 mL.min^{-1} (LLDPE-800).

2.5.5. Conclusion

In a process involving high-temperature reactions, such as the pyrolysis of plastics, it is necessary to optimise an experimental set-up capable of generating reliable and usable data. This first step of the PhD work has shown the weaknesses of the previously used set-up in the laboratory, and relevant changes have allowed a better recovery of the condensable phase from the thermal pyrolysis of PS or LLDPE. The study of the influence of the carrier gas (N_2) flow rate in the thermal pyrolysis of LLDPE showed that the oil fraction was much higher when the residence time was longer (low N_2 flow rate). Therefore, a longer residence time inside the reactor seems to favour reactions such as hydrogen transfer and β-scission that require higher activation energy and lead to the production of aromatics, the reaction products targeted in this study. Therefore, in the subsequent procedures, the carrier gas flow rate was established at 200 mL.min^{-1}, the cold chamber temperature at 20 °C, and the reaction time at 40 minutes. The specific temperature settings and the amount of polymer and catalyst used will be determined according to the individual experiments conducted.

2.6. Catalysts preparation

2.6.1. Feedstock

The commercial ammonium-form zeolite type MFI, ZSM-5 (CBV23), with Si/Al ratio 11.5 (SiO_2/Al_2O_3 = 23), was supplied by Zeolyst International.

The product used for the synthesis of the NH_4^+-zeolite was ammonium nitrate (≥99.0 NH_4NO_3, Sigma Aldrich), and for the doped catalyst was zinc nitrate hexahydrate, $Zn(NO_3)_2$ $6H_2O$, (99.998 % metal basic, Alfa Aesar).

2.6.2. Ammonium ion exchange of zeolites

The ion exchange process of the zeolite was carried out in the presence of 50 cm^3 of 1 M NH_4NO_3 per 1 g of catalyst for 12 h at 70 °C [23]. Then, the NH_4^+-catalyst was filtrated, rinsed three times with 250 mL of deionised water and dried at 120 °C for 12 h [23]. In the case of the protonic (H) form zeolites, the ion exchange step was followed by calcination under air using the program described in session 2.6.4.

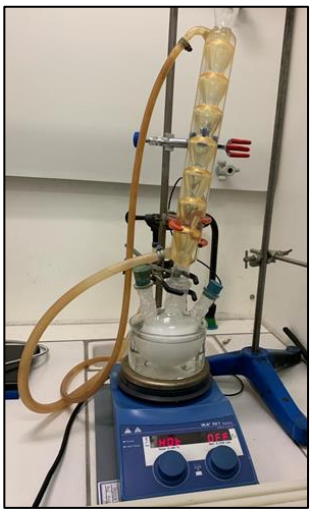

Figure 2.12. System set-up for the ion exchange process.

2.6.3. Metallic (M) ion exchange of zeolites

The M ion exchange process was carried out in order to obtain 2,5 wt. % of metal (Zn) in the zeolite. The metallic nitrate precursor was first solubilised in 50 cm^3 deionised water containing 5 g of NH_4^+-ZSM-5 zeolite. The slurry formed was placed in agitation with reflux for 24 h at 70-80 °C [24] and 500 rpm. The slurry was finally dried at 80 °C [25] and calcined in dynamic conditions (described in session 2.6.4) to obtain the M-H-Zeolite form.

2.6.4. Calcination of zeolites

The zeolite materials were calcined under air flow (dynamic conditions = DC) or under static air (static conditions (SC)). The protocol used for the calcination under air flow is the following: 100 $mL.min^{-1}$ of air (Alphagaz 1 Air Smartop from Air Liquide) passes through a reactor containing 5 grams of zeolite. The pyrex reactor is placed in a tubular furnace (**Figure 2.13** (b)). Static air calcination was performed in a muffle furnace on 2 g of zeolite (**Figure 2.13** (c)). The temperature program was the same, whatever the protocol used. A first temperature ramp of 2 $°C.min^{-1}$ from room temperature to 200 °C is carried out, and the temperature of 200 °C is maintained for 2 h to evacuate the water adsorbed inside the zeolite. A second ramp of 0.5 $°C.min^{-1}$ from 200 °C to 550 °C is then performed, and the temperature of 550 °C is maintained for 8 h [23] (**Figure 2.13** (a)). The samples were labelled DC or SC depending on whether they were prepared under dynamic or static conditions respectively.

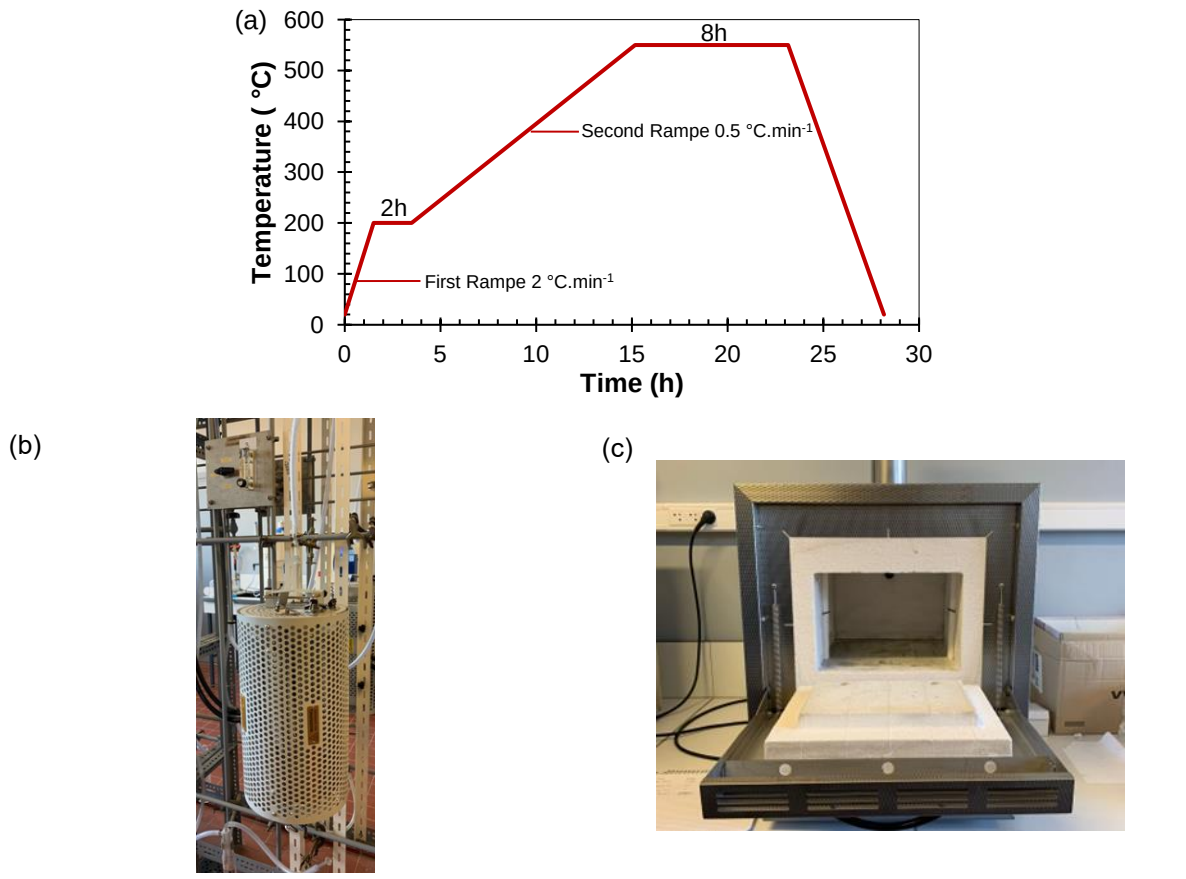

Figure 2.13. (a) Profile of the calcination procedure, photos of furnace used for calcination on dynamic conditions (b) and static conditions (c).

2.7. Catalysts characterisation techniques

The powder catalysts < 5 µm were characterised under the techniques described below, which help to understand the nature and functionality of the catalysts.

2.7.1. X-ray diffraction (XRD) [26]

XRD is a structural analysis technique based on the measure of diffraction of X-ray angles and is used to identify the crystalline phase and other microstructure information, such as the crystallite size in a sample. The geometrical condition is given via Bragg's law in **Equation 5** and described in **Figure 2.14**.

Equation 5 $$2 \cdot d_{hkl} \cdot sin\theta = n \cdot \lambda$$

d_{hkl} is the inter-reticular distance (Å), h, k, l: are the Miller index, 2θ is the angle formed by the incident and diffracted beams (°), λ is the wavelength of the Kα of copper (1.5406 Å), and n is the Bragg diffraction order.

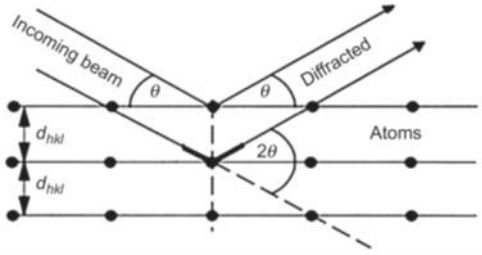

Figure 2.14. Geometrical condition for diffraction from lattice planes from reference [26]

This technique also makes it possible to obtain an approximation of the average apparent size of the crystallites (denoted L) using the Debye-Scherrer **Equation 6**. This equation assumes that the particles are spherical in a size range between 3 and 300 nm. Apparent average crystallite sizes were estimated by full pattern matching of the corresponding XRD structures using the Fullprof Software Suite with the equation:

Equation 6 $$d_{cryst} = \frac{k \times \lambda}{\beta \times cos\theta}$$

where k=geometric factor 0.89, β= the width of the line at half height in radians, λ=the wavelength used and θ the angle of Bragg in radians.

Instrument resolution was evaluated by using LaB_6 as the standard. The powder X-ray diffraction patterns of the samples were obtained on a Bruker AXS D8 Advance diffractometer in Bragg–Brentano geometry, Cu Kα source (λ = 0.154 nm), which was used as the radiation. The XRD pattern was recorded with a step size of 0.01° in 2θ, 1 second per step, and the range of scan was 5° < 2θ < 55°. The samples were checked for crystallinity by comparing the intensity of the strongest peak, 2θ = 23.02° of then, with that of parent ZSM-5 zeolite, which was assumed 100 % crystalline.

2.7.2. N_2-physisorption

The N_2-physisorption in porous materials helps to determine their textural properties. These textural properties are related to the specific pore volume, V_{pore}; the pore size, which is generally the pore width or the distance between the two opposite walls; the pore distribution according to its pore size; and its specific surface per solid mass, S, which is the geometric grain surface and depend on the granulometric distribution, the form and the pore wall surface [27–29].

The shape of the pores can be classified as cylindrical, bottled with ink or slit-shaped pores. Depending on the predominant pore sizes, these materials are classified by IUPAC: microporous materials, (1) having pore diameters of up to 2.0 nm; mesoporous materials (2) having intermediate pore sizes between 2.0 and 50.0 nm; and (3) macroporous materials, having pore sizes greater than 50.0 nm [27].



Figure 2.15. BET equipment used to perform the catalyst analysis.

The nitrogen adsorption is measured at -196 °C in the interval of relative pressure where the statistical monolayer of adsorbed molecules is at the surface, 0.05 <P/P_O<0.35. The physisorption of the first adsorbate layer can be calculated with the Brunauer-Emmett-Teller theory (BET) **Equation 7** [28,30]:

Equation 7

$$\frac{\frac{P}{P_O}}{V\left(1-\frac{P}{P_O}\right)} = \frac{1}{V_m \cdot C} + \frac{C-1}{V_m \cdot C}\left(\frac{P}{P_o}\right)$$

Where V is the adsorbed volume gas in $cm^3.g\text{-}1$ at relative pressure, P/P_O; C is the BET constant equal to $e^{\frac{E_1-E_L}{kT}}$, with E_1 as the heat of adsorption of the first layer and E_L the latent heat of condensation and depending on the temperature T, k is the universal constant gas; V_m is the adsorbate volume on a given sample of catalyst in order to form the adsorbed monolayer; P is the equilibrate pressure; P_O is the saturated vapour pressure at atmospheric pressure**. Equation 8** is used to determine the BET surface, S_{BET}. The monolayer volume, V_m, could be estimated[28].

Equation 8

$$S_{BET} = \frac{\sigma \cdot N_a \cdot V_m \cdot 10^{-10}}{m \cdot V_n}$$

Where σ is the occupied area per adsorbate molecule in $Å^2$, in the case of nitrogen, the value is 0.162 $Å^2$; m is the mass of analysed solid in g; N_a is the Avogadro number, $6.02 \cdot 10^{23}$ molecules per mol; and V_n is the molar volume of the adsorbate in $cm^3.mol^{-1}$.

The adsorption and desorption of the obtained isotherms are classified by the IUPAC, as illustrated in **Figure 2.16** (a). The six types of isotherm (IUPAC classification) are characteristic of microporous adsorbents (type I), non-porous or macroporous (types II, III and VI) or mesoporous (types IV and V) [27]. For type III and V isotherms, C = 1 [28]. These isotherms are rarely superposed, and hysteresis is

typically observed (**Figure 2.16** (b)) and describes the particular aspects of the pore structure and the adsorption mechanism. For example, type H2-H5 hysteresis loops normally have complex pore structures, and their networking effects are important [27].

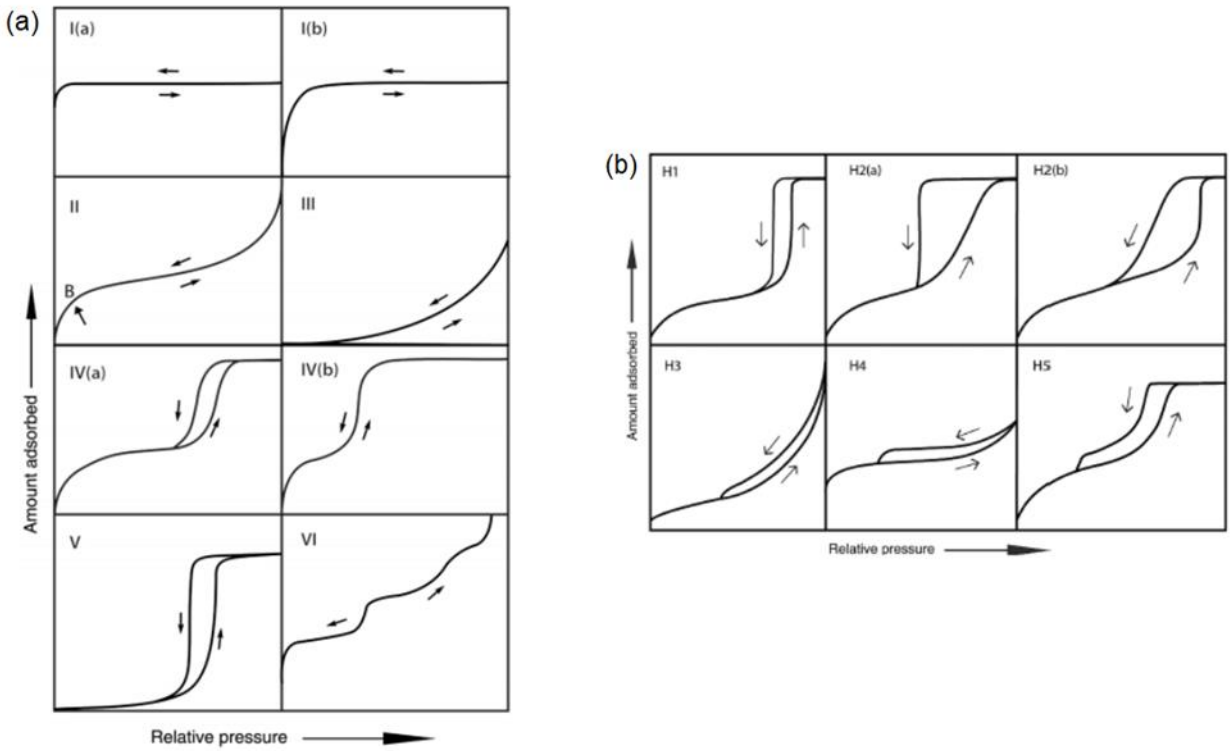

Figure 2.16. (a) The IUPAC classification of adsorption isotherms: Microporous (type I), non-porous or macroporous (types II, III and VI), mesoporous (types IV and V) and (b) Types of hysteresis loops obtained by nitrogen physisorption [27].

The Barrett, Joyner, and Halenda theory, BJH is used to estimate the variation in the thickness of adsorbed film from the decrease of P/P_O in the desorption branch, assuming that the shape of the pore is cylindrical and the adsorbed amount results from both physical adsorption on the pore walls and capillary condensation in mesopores [28].

N_2-physisorption measurements were performed on a Micromeritics TriStarII 3020. The specific surface area was determined using approximately 200 mg of powder sample previously outgassed at 200 °C under vacuum (<0.5 mbar) for a minimum of 2 h in the outgassing station. The analysis chamber has a calibrated volume reservoir, serving as a metering device, two pressure judges and three adsorption cells containing an adsorbent. Through the successive introduction of known quantities of nitrogen, this method makes it possible to plot the adsorption isotherm of the sample. Brunauer-Emmett-Teller theory (BET) was applied to calculate the specific surface areas. Pore size distributions were obtained simultaneously from the isotherms based on the Barret-Joyner-Halenda (BJH) theory. Desorption branches were used to determine S_{BET}, pore size distributions, V_{pore} and d_{pore}.

2.7.3. ^{27}Al NMR [31]

Nuclear magnetic resonance (NMR) spectroscopy is used to study the chemical structure and motion of molecules and materials. The nuclei of particular isotopes with no-zero spins, such as ^{27}Al, respond to a magnetic field by radiofrequency irradiation via specific resonant excitation.

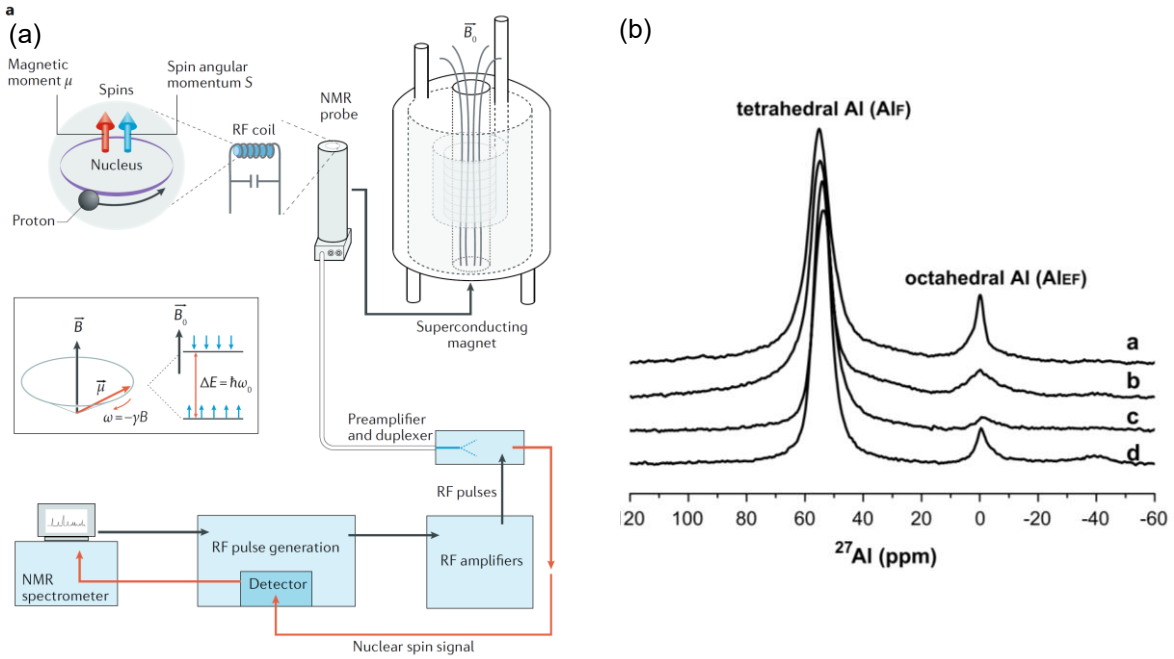

Figure 2.17. Schema of the operation of an NMR system (a). ^{27}Al MAS NMR spectra of HZSM-5 zeolites with different treatments and doping from ref [32] (b), collected from a frequency at 79.5 MHz and spinning speed of 10 kHz.

As illustrated in **Figure 2.17** (b), in NMR spectroscopy, the sample is placed into a radiofrequency (RF) coil inserted into the centre of a strong magnet and exposed to a determined RF pulse, and then the nuclei absorb energy a transition from the lower energy state to the higher energy state. When the RF pulse is turned off, the nuclei return to their lower energy state and emit radiation at the specific frequency, allowing an energy difference (ΔE) measurement. B_0 is the strength of the static magnetic field, and σ is the chemical shift of a nucleus. The value of σ depends on the nuclei of a given isotope in a molecule, causing different frequencies.

In zeolites, the ^{27}Al NMR spectroscopy determines the aluminium distribution in the framework, including the coordination number[33], as shown in **Figure 2.17** (a). In this study, the ^{27}Al MAS-NMR spectra were performed at 400 MHz on an AVANCE III 18.8T spectrometer equipped with a 3.2 mm CP-MAS probe head operating at spinning frequencies, a ν_{rot} of 20–22 kHz.

2.7.4. Temperature-programmed desorption of Ammoniac (NH_3-TPD) [34]

Temperature-programmed desorption of ammonia (NH_3-TPD) is a technique commonly used to determine the density and strength of the acid sites of the zeolite. This method is based on ammonia's

surface desorption as a temperature function [34]. The difference between this method and the pyridine thermal desorption is that the latest can discriminate between Brønsted and Lewis acidity [35].

This method prepares the sample's surface to adsorb the ammonia by a complete degassing. Then, the sample is exposed to ammonia gas at low temperatures, forming a monolayer at the surface. The sample is then heated at a controlled rate under an inert gas such as Helium, while the desorbed ammonia is detected gravimetrically, volumetrically, or by gas chromatography or mass spectrometry. The desorption rate as a function of temperature is plotted as a TPD profile (**Figure 2.18** (b)). The area under the curve gives the density of acid sites, while the desorption temperature is related to the acid strength[34,36].

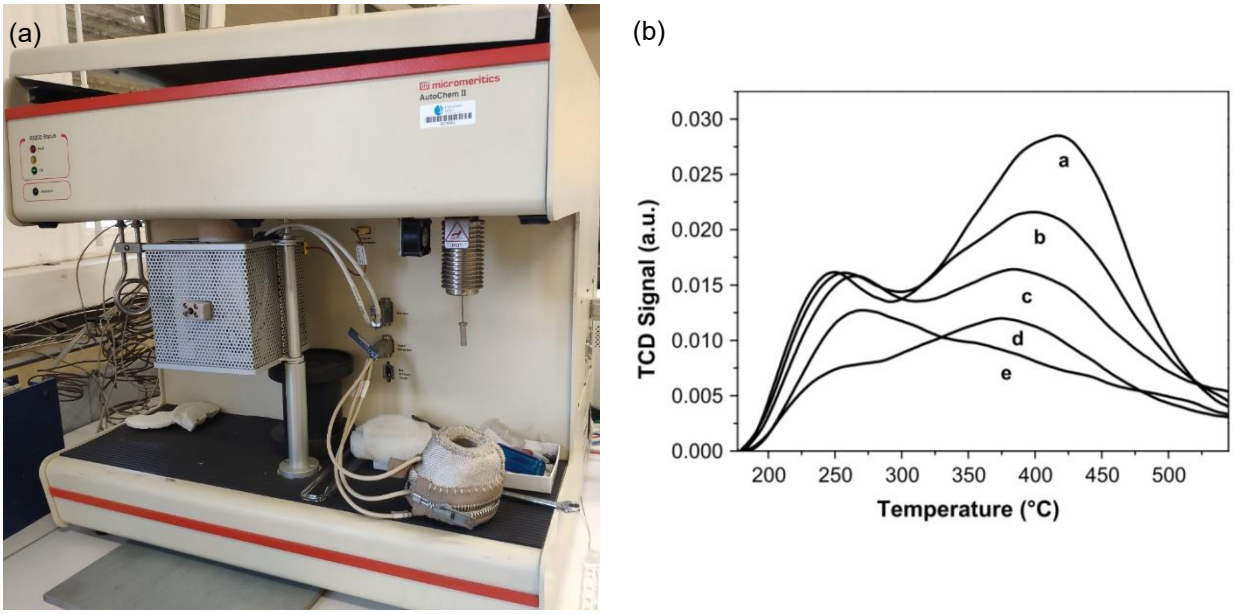

Figure 2.18. The NH_3-TPD equipment used in this study (a). NH_3-TPD profiles of different HZSM-5 zeolites from ref [32] (b), the desorption was made from 177 °C to 550 °C at 10 °C.min^{-1}.

In this study, the total acidity density of acid sites of samples was determined by TPD of ammonia using a Micromeritics Autochem II 2920 Chemisorption Analyser Instrument equipped with a mass spectrometer. 100 mg of sample were purged for 1 h in a He flow at 200 °C before being naturally cooled to room temperature. The sample was then contacted with a 10 % NH_3/He atmosphere for 30 min in a 30 mL min^{-1} flow at 150 °C [23,37]. After adsorption, the temperature was raised at 10 °C min^{-1} up to 700 °C under 30 mL min^{-1} He flow [23]. The quantity of desorbed NH_3 was determined by mass spectrometry using the peak at m/z = 16.

2.7.5. Pyridine adsorption-Infrared spectroscopy (Py-IR)

Pyridine adsorption-infrared spectroscopy (Py-IR) is based on the adsorption of pyridine molecules onto the surface of a sample and the measurement of the infrared (IR) spectra of the adsorbed species. Py-IR provides semiquantitative information about the density and strength of the Brønsted and Lewis acid sites [36]. Brønsted acid sites on aluminosilicate zeolites are formed when Si^{+4} in a tetrahedral position linked to four oxygen atoms are replaced by Al^{+3}, changing from neutral to negative charge. To

neutralise, hydroxyl proton bound to a bridging oxygen atom, balances the negative charge forming a proton donor site (Brønsted acid site, SiOHAl) [34]. Lewis acid sites are formed from Brønsted acid sites, where a loss of a water molecule is formed from a hydroxyl group of Brønsted site and a proton from another Brønsted site [34] and is generally attributed to octahedral aluminium [38]. Typically, this formation is possible at a temperature above 500 °C, creating structural changes in Zeolites [34,39]. Lewis acidity can be assigned not only to the dehydroxylation of Brønsted sites but partially to extra-framework Al [34] formed on thermal or steamed treatment or from framework defects [40]. It has to be noted that Silanol groups are also Brønsted acid sites, but below 150 °C, these sites do not adsorb pyridine [41].

During the experiment, the sample surface is prepared by outgassing and then exposed to pyridine gas at a low temperature. The pyridine molecules interact with the acid sites on the sample's surface. The resulting IR spectrum, measured after adsorption of pyridine adsorption, allows for distinguishing between the Brønsted and Lewis acidity thanks to the pyridine bond: pyridine **protonation** of the pyridine on the Brønsted acid sites forming the ion pyridinium and **adsorption coordinatively** of pyridine on Lewis acid sites. (**Figure 2.19** (a)) [42]. The measurement at different temperatures leads to observing the strength of each acid site [34,36].

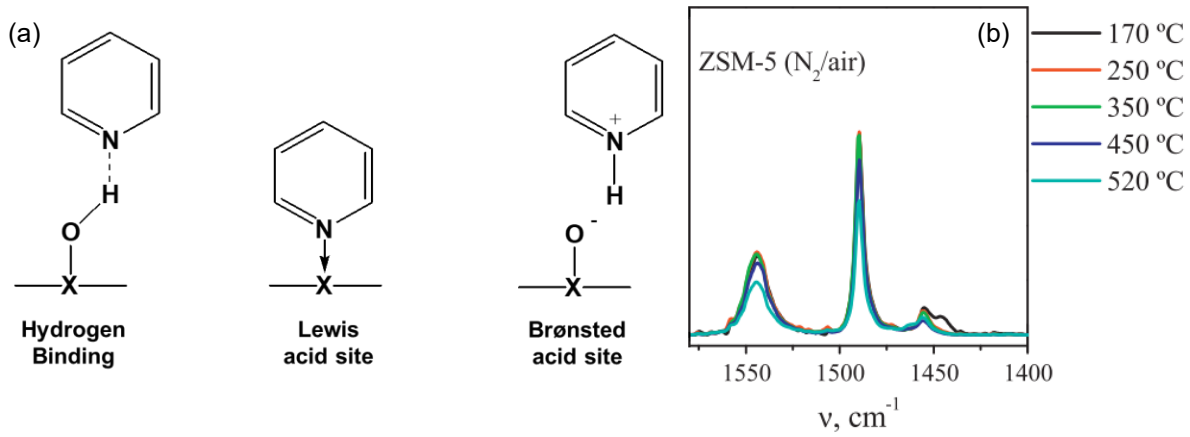

Figure 2.19. Pyridine adsorption to the zeolite surface (a). FTIR spectra of adsorbed pyridine at different temperatures of a ZSM-5 zeolite calcinated first under nitrogen and then under air from (a) ref [35].

The amount of pyridine adsorbed on the surface is directly related to the number of surface acid sites. However, this relation is limited by the shape of the micropores or the zeolite cavities and the pyridine's large diameter compared to ammonia [43].

The experiment was recorded on a Thermo Nicolet 460 protégé instrument equipped with a CSi beam splitter and an MCT detector with a 2 cm^{-1} resolution. The scans were collected from 4000 to 400 cm^{-1}. The sample was shaped into waffles by pressing (14 $Kg.cm^{-2}$, 2,01 cm^2). The adsorption of pyridine (1 Torr) was carried out at room temperature for a maximum 1 min, followed by desorption at 150, 250, 350, and 450 °C. The recorded spectrum of these steps corresponds to very weak, weak, medium, and strong acidity, respectively [44]. Brønsted and Lewis acidities were calculated from the integration of the

adsorption bands at 1545 cm^{-1} and 1450– 1460 $cm^{-1,}$ respectively [45]. Before the analysis, the sample was outgassing at 400 °C under vacuum (<10^{-4} Torr).

2.7.6. RAMAN spectroscopy [46]

Raman spectroscopy is used to study the chemical and structural properties of materials and is based on the inelastic scattering of light by a sample. In our laboratory, the spectrometer used illuminates the sample with a monochromatic light source and a laser and analyses the scattered light. In Raman scattering, a photon from the incident light source is absorbed by a molecule, and a new photon is emitted with a different energy (and thus a different wavelength). The energy difference between the incident photon and the scattered photon is equal to the energy of the vibrational, rotational, or another low-frequency mode of the molecule.

When coke is deposited on a catalyst, it is composed of various hydrocarbons, such as alkanes, alkenes, and aromatics. Each hydrocarbon has its unique Raman spectrum, which can be used to identify and quantify them. The Raman spectra of coke deposited on catalysts can also provide information about the structure of the coke, such as the degree of order and disorder, the size and shape of the coke particles, and the presence of defects. Concerning Raman scattering, the strong fluorescence of the coke when excited by a visible wavelength laser can interfere with the Raman spectrum.

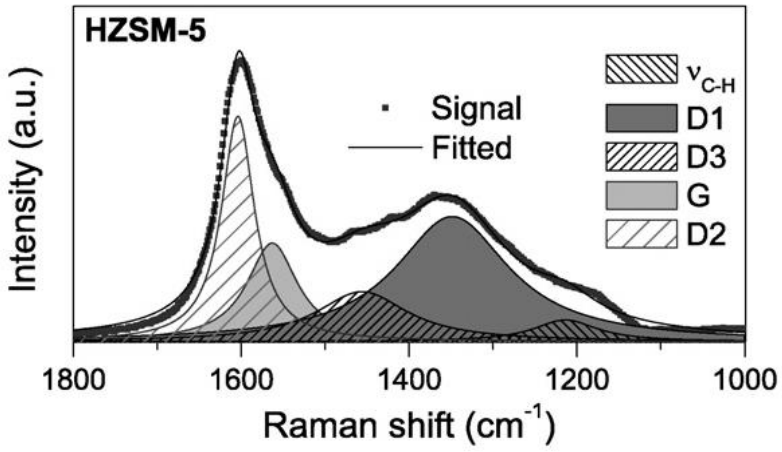

Figure 2.20. Raman spectra of a spent HZSM-5 after cracking of polyethylene ref [47].

The Raman spectroscopy has been performed for coke analysis, subtracting the coke's fluorescence under ambient conditions. The Raman spectra were acquired in confocal mode utilizing the 405 nm line of an Ar^{+}-ion laser (Melles Griot). The laser was focused on the sample, which was positioned within an atmospheric chamber (Harrick Scientific) furnished with a specialized flat silica dome. A 100× long working distance objective (Olympus) was employed for this purpose. The scattered light was directed through a 120 µm pinhole, dispersed using an 1800 grooves spectrometer grating, and subsequently captured by a Peltier-cooled CCD detector (HORIBA LabRAM HR). To prevent any modification of the

sample, the laser power was attenuated using neutral density filters. The spectral range under investigation extended from 200 to 1800 cm^{-1}, with a spectral resolution of 1 cm^{-1}.

2.7.7. X-ray photoelectron spectroscopy (XPS)

X-ray photoelectron spectroscopy (XPS) is used to study the chemical composition, electronic structure, and chemical bonding of materials at the surface and near-surface region, between 2-10 nm depth. The technique is based on the measurement of the kinetic energy and number of photoelectrons emitted from a sample when it is irradiated with X-rays. XPS provides information about the elements present in a sample, their oxidation states, and the chemical bonding of the elements. However, it is limited to a relative precision of 20 %.

When an atom absorbs an X-ray photon, it can cause the ejection of an electron from the innermost occupied electronic level of the atom, which is called the core level. The kinetic energy of the emitted photoelectron is related to the core-level electron's binding energy, which is characteristic of the element and its oxidation state. By measuring the binding energy of the photoelectrons emitted from a sample, XPS can be used to identify the elements present in the sample and their oxidation states.

XPS measurements of the solids were conducted to determine the ratio of Si/Al and the metal content at the catalyst's surface. Samples were prepared by depositing the respective solid on an adhesive Cu tape. XPS analyses were then carried out on an AXIS Ultra DLD Kratos spectrometer equipped with a monochromatic aluminium source (150 W) and charge compensation gun, the energy of the Al source being 1486.6 eV. Binding energy (BE) for Al 2p and O 1s was measured by reference to the Si 2p peak at 102.9 eV, typic of silicon from ZSM-5 zeolites [48–51]. All spectra were fitted with a Voigt function (a 70/30 composition of Gaussian and Lorentzian functions) in order to evaluate the surface Si/Al atomic ratio. Data exploitation was performed using the program CasaXPS.

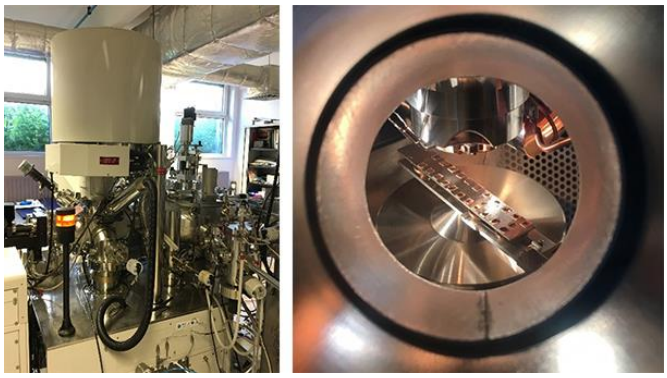

Figure 2.21. XPS equipment used in this study

2.7.8. Scanning electron microscopy - Energy dispersive X-ray spectroscopy (SEM-EDS) [52]

Scanning electron microscopy (SEM) is used to see material morphology and relative composition at the micro- and nanometre scale by high-resolution images of samples. Energy dispersive X-ray spectroscopy (EDS) combines with SEM to identify the elements contained in a sample except for H and He. EDS detector detects X-rays emitted from the sample when it is excited by the electron beam. The energy of the X-rays is characteristic of the elements present in the sample. The concentration measurement is most accurate when the element content is less than 10 wt. %.

The morphological feature of the samples at the micro and nanometre scale was observed on a scanning electron microscope, JEOL JSM-7800F LV, operated at 5 kV.

2.7.9. Electron microprobe analysis (EMPA) [52,53]

Electron Microprobe analysis (EMPA) is a technique used to identify and quantify the chemical composition of small samples, typically measuring only a few micrometres in size. This analysis works by bombarding a micro-volume of a sample with a focused electron beam and collecting the X-ray photons emitted by the different elemental species. Each X-ray spectrum is characteristic of an element, and the intensity quantification is compared to standard samples. The beam is accelerated by a voltage of 1kV to 30kV. The technique can be used to analyse samples in a non-destructive manner. This technique limits quantification when the particle size is less than 1µm. This study used a CAMECA SX 100 electron microprobe to identify the Zn, Ga and Ag distribution on doped zeolites.

2.7.10. Inductively coupled plasma optical emission spectrometry (ICP-OES)

Also called Inductively Coupled Plasma-Atomic Emission Spectrometry (ICP-AES) [54,55], the ICP-OES is a technique used to determine the quantity of an element in a sample in the order of µg per litre [55].

The principle of ICP-OES is to use the energy of plasma heat, usually argon plasma that operates between 8000 and 10000 K [54,55], in order to excite the electrons of atoms or ions and move them to higher energy levels. When the excited electrons return to the ground state, they emit light at particular wavelengths. The ICP-OES measures how much this light emitted at each wavelength is proportional to the number of atoms or ions that make the transition. This information is used to calculate the concentration of the element in the sample using Beer Lambert's law, which describes the relationship between light intensity and a specific element's concentration [55].

The ICP-OES system, **Figure 2.22**, consists of using a nebuliser to turn the liquid sample to analyse into aerosol in argon gas. The aerosol enters a spray chamber where the smallest droplets continue to the plasma torch. A metal coil around the glass torch creates a magnetic field in the plasma torch thanks

to an electric current that passes through. An argon steam flows into the glass, and the plasma is created from a spark discharged into the steam.

The argon gas with the aerosol passes through the plasma torch, and the solvent is evaporated. The molecules break into atoms and ions, and this heat excites their electrons from lowers energy levels into another higher.

A radio-frequency (RF) generator controls the energy level of plasma. The generator controls the RF energy that passes through metal coils around the plasma torch. Later, a light with a precise wavelength is detected when the excited electrons return to a lower energy level. This light goes inside the optical spectrometer, where it is separated at each wavelength. In the detector, the photons of light are measured in the form of peaks from different wavelengths [55].

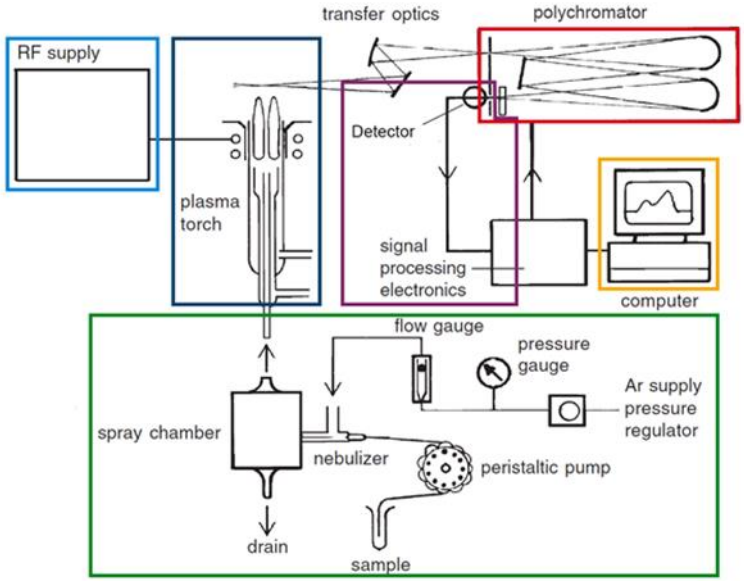

Figure 2.22. Components of an ICP-OES instrument from ref. [55]

In this study, the elemental analysis through inductively coupled plasma optical emission spectrometry (ICP-OES) was used to quantify the ratio of silicon-aluminium (Si/Al) and the metal content on catalysts using an Agilent 5100 ICP-OES from Agilent Technologies, with the previous dissolution of samples in aqua regia solution.

2.7.11. Thermogravimetric analysis (TGA)

Thermogravimetric analysis (TGA) is an analytical technique used to study the thermal behaviour of materials. The technique is based on the measurement of the weight change of a sample as a function of temperature or time while the sample is subjected to a controlled temperature ramp or isotherm. TGA provides information about a material's thermal stability, decomposition, and oxidation and is widely used in chemistry, materials science, and environmental science. In this study, this technique was used

to evaluate the catalyst activity and to characterise the coke. Thermogravimetric analysis (TGA) was performed using a Thermal Analysis instrument, TA Q600.

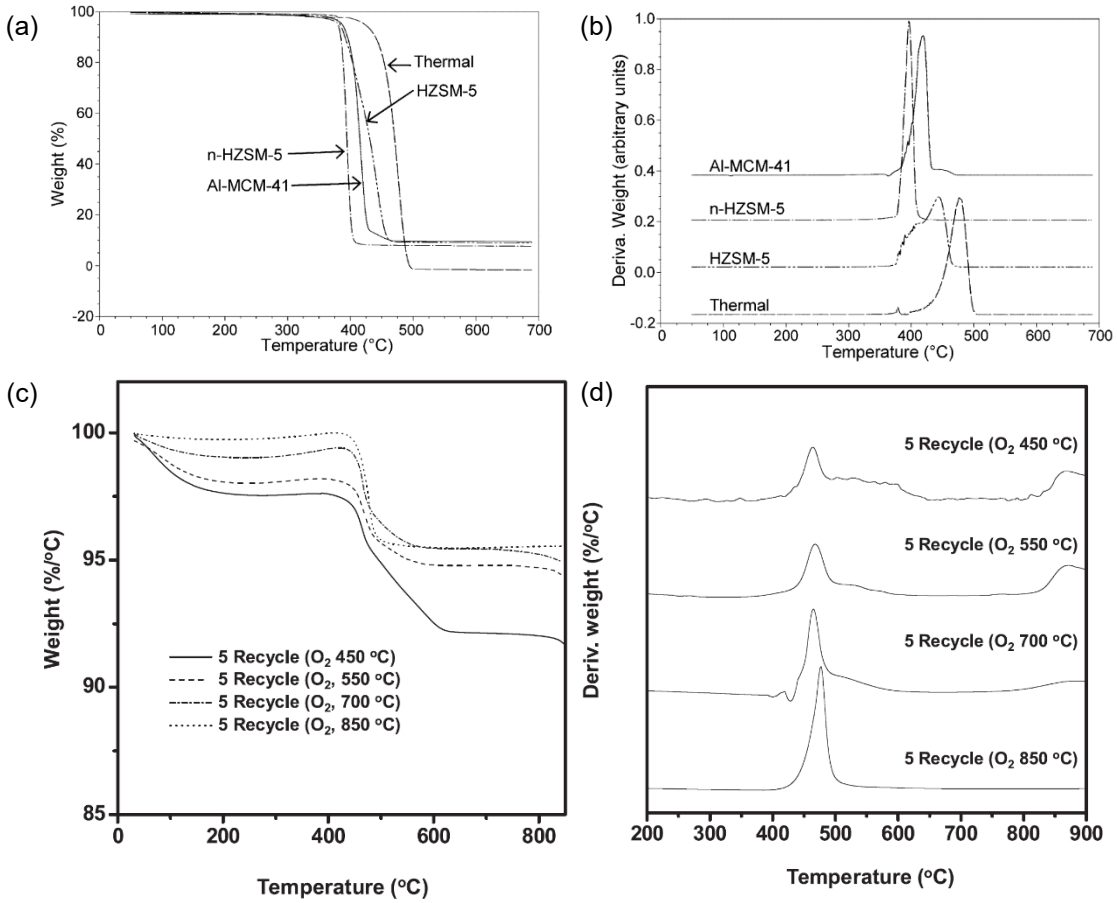

Figure 2.23. Evaluation of catalytic activity through TG (a) and DTG (b) profiles of thermal and catalytic degradation of pure LDPE over different catalysts from ref [57], and evaluation of the coke deposition through TG (c) and DTG (d) profiles of used Mo/H-ZSM-5 catalysts obtained after a 5 recycle reaction including oxidative regeneration at 450, 550, 700, and 850 °C. from ref [58]

For catalyst activity: The weight loss of 15 mg of sample was recorded under pure nitrogen (flow rate = 100 mL min^{-1}) at a heating rate of 10 °C min^{-1} from 50 °C to 900 °C to study the activity of zeolite on the cracking of LLPDE. The principal parameters obtained from the TG analysis are $T_{5\,\%}$ and $T_{95\,\%}$, which represent the temperature when 5 % and 95 % of the LLDPE is pyrolysed, T_{max}, which is the maximal temperature of degradation of LLDPE and $\Delta T_{max,}$ which is the relative catalytic activity of the zeolite, estimated by the difference between the maximum decomposition temperature achieved by the pure polymer and the polymer-zeolite mixture.

The activity of the catalyst ($\Delta T_{max,}$) is thus defined according to the following equation:

Equation *9*

$$\Delta T_{max} = T_{max_{(LLDPE)}} - T_{max_{(LLDPE+Catalyst)}}$$

For coke characterisation: To evaluate the residue (coke-char) mass, the weight loss of 15 mg of catalyst ($Mass_{catalyst}$) obtained at the end of the pyrolysis process was recorded under air at a flow rate of 100 mL. min^{-1}, and a heating rate of 10 °C. min^{-1} from 50 °C to 900 °C. The mass loss at 800°C (Mass

$loss_{TGA}$) is considered to be the quantity of coke and was determined between 350 and 700 °C[56] with the following equation:

Equation *10*

$$Mass\ Coke = \frac{Mass_{catalyst} \times \%Mass\ loss_{TGA}}{1 - \%Mass\ loss_{TGA}}$$

2.8. Catalyst/Polymer mixture preparation

The catalytic pyrolysis of polyethylene was conducted by fixing the catalyst/polymer ratio. However, the effect of the catalyst-polymer mixture preparation was examined, and three different preparations were carried out. The preparation of the different mixtures is described below.

2.8.1. Pellet polymer and powdered catalyst

Mix: The polymer in pellet form and the powdered catalyst with a determinate catalyst:polymer ratio were deposed into the spoon (**Figure 2.24 (A)**) and covered with a quartz wool layer. During the reaction, the polymer in the liquid phase reacts with the powdered catalyst.

Mix/Layer. The notation Mix/Layer refers to the experiments carried out with a part of the powdered catalyst mixed with the pellet polymer and another part between two layers of quartz superposed on top of the first mixture (**Figure 2.24 (B)**). The liquid polymer will react with the powdered catalyst, and the gases produced from this first reaction will react with the powdered catalyst layer.

Layer. The notation layer refers to the experiments carried out with the polymer posed on the bottom of the spoon and the catalyst between two layers of quartz superimposed on top of the polymer (**Figure 2.24 (C)**). The gases produced from the thermal-cracking of the polymer will react with the powdered catalyst layer.

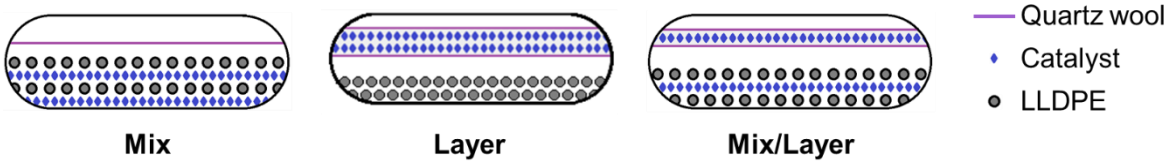

Figure 2.24. Schema of a Mix arrangement **(A)** of pellet polymer and powdered catalyst, Mix/Layer arrangement **(B)** and the layer arrangement **(C)**.

2.8.2. Extruded mixture

The pelleted polymer and powdered catalyst were extruded in a DSM Researche 15 twin-screw microextruder. The quantity of polymer was 10 g, and the amount of catalyst was adjusted according to the target catalyst-to-polymer ratio. The microextruder was heated at 190 °C to melt the polymer, a portion of the polymer was introduced and mixed for about 5 min, and then the catalyst and the remaining polymer were introduced and mixed for about 10 min. The mixing speed used was 50 rpm. At the exit

of the extruder, a rod of 3 mm in diameter was obtained. For these mixtures, the suffix "extruded" is mentioned.

2.8.3. Powdered mixture

The polymer powder was obtained by milling from the LLPDE polymer. The Retsch ZM200 ultracentrifugal mill (speed 8000 rpm) allows obtaining a powder material size of about 0.5 mm. The catalyst:polymer ratio was obtained by manually mixing the two powders. For these mixtures, the suffix "powdered" is mentioned.

2.9. Conclusion

This chapter presented the materials and set-up used in this PhD work, the modifications made to the set-up, and the consequence of these changes. The different analytical techniques and sample preparation were also described. The following chapters will be dedicated to the study of the effect of the catalytic pyrolysis of polyethylene on yield and the composition of the oil fraction, considering variables such as the type of mixture between the polymer and the catalyst, the ratio between the polymer and the catalyst, as well as, the acidity and poisoning effect of the catalyst.

2.10. Reference

[1] S. Klaimy, Pyrolyse thermique et catalytique des polymères utilisés dans les emballages, Université de Lille, 2019.

[2] M. Heydariaraghi, S. Ghorbanian, A. Hallajisani, A. Salehpour, Fuel properties of the oils produced from the pyrolysis of commonly-used polymers: Effect of fractionating column, J. Anal. Appl. Pyrolysis. 121 (2016) 307–317. https://doi.org/10.1016/j.jaap.2016.08.010.

[3] J.S. Kim, W.Y. Lee, S.B. Lee, S.B. Kim, M.J. Choi, Degradation of polystyrene waste over base promoted Fe catalysts, Catal. Today. 87 (2003) 59–68. https://doi.org/10.1016/j.cattod.2003.10.004.

[4] R. Prathiba, M. Shruthi, L.R. Miranda, Pyrolysis of polystyrene waste in the presence of activated carbon in conventional and microwave heating using modified thermocouple, Waste Manag. 76 (2018) 528–536. https://doi.org/10.1016/j.wasman.2018.03.029.

[5] K.H. Lee, Composition of aromatic products in the catalytic degradation of the mixture of waste polystyrene and high-density polyethylene using spent FCC catalyst, Polym. Degrad. Stab. 93 (2008) 1284–1289. https://doi.org/10.1016/j.polymdegradstab.2008.04.009.

[6] S.Y. Lee, J.H. Yoon, J.R. Kim, D.W. Park, Degradation of polystyrene using clinoptilolite catalysts, J. Anal. Appl. Pyrolysis. 64 (2002) 71–83. https://doi.org/10.1016/S0165-2370(01)00171-1.

[7] M. Brebu, T. Bhaskar, K. Murai, A. Muto, Y. Sakata, M.A. Uddin, Thermal degradation of PE and PS mixed with ABS-Br and debromination of pyrolysis oil by Fe- and Ca-based catalysts, Polym. Degrad. Stab. 84 (2004) 459–467. https://doi.org/10.1016/j.polymdegradstab.2004.02.003.

[8] M. Rehan, R. Miandad, M.A. Barakat, I.M.I. Ismail, T. Almeelbi, J. Gardy, A. Hassanpour, M.Z. Khan, A. Demirbas, A.S. Nizami, Effect of zeolite catalysts on pyrolysis liquid oil, Int.

Biodeterior. Biodegrad. 119 (2017) 162–175. https://doi.org/10.1016/j.ibiod.2016.11.015.

[9] Adnan, J. Shah, M.R. Jan, Effect of polyethylene terephthalate on the catalytic pyrolysis of polystyrene: Investigation of the liquid products, J. Taiwan Inst. Chem. Eng. 51 (2015) 96–102. https://doi.org/10.1016/j.jtice.2015.01.015.

[10] Adnan, J. Shah, M.R. Jan, Thermo-catalytic pyrolysis of polystyrene in the presence of zinc bulk catalysts, J. Taiwan Inst. Chem. Eng. 45 (2014) 2494–2500. https://doi.org/10.1016/j.jtice.2014.05.011.

[11] Adnan, J. Shah, M.R. Jan, Recovery of Valuable Hydrocarbons from Waste Polystyrene Using Zinc Supported Catalysts, J. Polym. Environ. 25 (2017) 759–769. https://doi.org/10.1007/s10924-016-0858-4.

[12] H. Ukei, T. Hirose, S. Horikawa, Y. Takai, M. Taka, N. Azuma, A. Ueno, Catalytic degradation of polystyrene into styrene and a design of recyclable polystyrene with dispersed catalysts, Catal. Today. 62 (2000) 67–75. https://doi.org/10.1016/S0920-5861(00)00409-0.

[13] P.T. Williams, R. Bagri, Hydrocarbon gases and soils from the recycling of polystyrene waste by catalytic pyrolysis, Int. J. Energy Res. 28 (2004) 31–44. https://doi.org/10.1002/er.949.

[14] K.B. Park, Y.S. Jeong, B. Guzelciftci, J.S. Kim, Two-stage pyrolysis of polystyrene: Pyrolysis oil as a source of fuels or benzene, toluene, ethylbenzene, and xylenes, Appl. Energy. 259 (2020) 114240. https://doi.org/10.1016/j.apenergy.2019.114240.

[15] S. KLAIMY, J.F. LAMONIER, M. CASETTA, S. HEYMANS, S. DUQUESNE, Recycling of plastic waste using flash pyrolysis – Effect of mixture composition, Polym. Degrad. Stab. 187 (2021) 109540. https://doi.org/10.1016/j.polymdegradstab.2021.109540.

[16] Y. Liu, J. Qian, J. Wang, Pyrolysis of polystyrene waste in a fluidized-bed reactor to obtain styrene monomer and gasoline fraction, Fuel Process. Technol. 63 (2000) 45–55. https://doi.org/10.1016/S0378-3820(99)00066-1.

[17] A. Verma, S. Sharma, H. Pramanik, Pyrolysis of waste expanded polystyrene and reduction of styrene via in-situ multiphase pyrolysis of product oil for the production of fuel range hydrocarbons, Waste Manag. 120 (2021) 330–339. https://doi.org/10.1016/j.wasman.2020.11.035.

[18] A. Zayoud, H. Dao Thi, M. Kusenberg, A. Eschenbacher, U. Kresovic, N. Alderweireldt, M. Djokic, K.M. Van Geem, Pyrolysis of end-of-life polystyrene in a pilot-scale reactor: Maximizing styrene production, Waste Manag. 139 (2022) 85–95. https://doi.org/10.1016/j.wasman.2021.12.018.

[19] A. Marcilla, M.I. Beltrán, R. Navarro, Thermal and catalytic pyrolysis of polyethylene over HZSM5 and HUSY zeolites in a batch reactor under dynamic conditions, Appl. Catal. B Environ. 86 (2009) 78–86. https://doi.org/10.1016/j.apcatb.2008.07.026.

[20] P.T. Williams, E.A. Williams, Fluidised bed pyrolysis of low density polyethylene to produce petrochemical feedstock, J. Anal. Appl. Pyrolysis. 51 (1999) 107–126. https://doi.org/10.1016/S0165-2370(99)00011-X.

[21] M.D.R. Hernández, A. García, A. Gómez, J. Agulló, A. Marcilla, Effect of residence time on volatile products obtained in the HDPE pyrolysis in the presence and absence of HZSM-5, Ind. Eng. Chem. Res. 45 (2006) 8770–8778. https://doi.org/10.1021/ie060728+.

[22] J.A. Onwudili, N. Insura, P.T. Williams, Composition of products from the pyrolysis of polyethylene and polystyrene in a closed batch reactor: Effects of temperature and residence time, J. Anal. Appl. Pyrolysis. 86 (2009) 293–303. https://doi.org/10.1016/j.jaap.2009.07.008.

[23] S. Klaimy, C. Ciotonea, J. Dhainaut, S. Royer, M. Casetta, S. Duquesne, G. Tricot, J.F.

Lamonier, Flash Catalytic Pyrolysis of Polyethylene over (Alumino)silicate Materials, ChemCatChem. 12 (2020) 1109–1116. https://doi.org/10.1002/cctc.201901819.

[24] Y. Ono, K. Kanae, Transformation of butanes over ZSM-5 zeolites. Part 1. - Mechanism of cracking of butanes over H-ZSM-5, J. Chem. Soc. Faraday Trans. 87 (1991) 663–667. https://doi.org/10.1039/FT9918700663.

[25] M. Conte, J.A. Lopez-Sanchez, Q. He, D.J. Morgan, Y. Ryabenkova, J.K. Bartley, A.F. Carley, S.H. Taylor, C.J. Kiely, K. Khalid, G.J. Hutchings, Modified zeolite ZSM-5 for the methanol to aromatics reaction, Catal. Sci. Technol. 2 (2012) 105–112. https://doi.org/10.1039/c1cy00299f.

[26] J. Epp, X-Ray Diffraction (XRD) Techniques for Materials Characterization, Elsevier Ltd, 2016. https://doi.org/10.1016/B978-0-08-100040-3.00004-3.

[27] F.J. Sotomayor, K.A. Cychosz, M. Thommes, Characterization of Micro/Mesoporous Materials by Physisorption: Concepts and Case Studies, Acc. Mater. Surf. Res. 3 (2018) 34–50. https://www.hyomen.org/wp-content/uploads/papers/vol3_no2/sotomayor/sotomayor_40.pdf.

[28] R. Bardestani, G.S. Patience, S. Kaliaguine, Experimental methods in chemical engineering: specific surface area and pore size distribution measurements—BET, BJH, and DFT, Can. J. Chem. Eng. 97 (2019) 2781–2791. https://doi.org/10.1002/cjce.23632.

[29] Z.A. Alothman, A Review: Fundamental Aspects of Silicate Mesoporous Materials, Materials (Basel). 5 (2012) 2874–2902. https://doi.org/10.3390/ma5122874.

[30] K.S.W. Sing, Assessment of Surface Area by Gas Adsorption, 2nd ed., Elsevier Ltd., 2013. https://doi.org/10.1016/B978-0-08-097035-6.00007-3.

[31] B. Reif, S.E. Ashbrook, L. Emsley, M. Hong, Solid-state NMR spectroscopy, Nat. Rev. Methods Prim. 1 (2021). https://doi.org/10.1038/s43586-020-00002-1.

[32] M.G. Ruiz, D.A.S. Casados, J.A. Pliego, C.M. Álvarez, E.S. de Andrés, D.S. Tartalo, R.S. Vaque, M.G. Casas, ZSM-5 zeolites modified with Zn and their effect on the crystal size in the conversion of methanol to light aromatics (MTA), React. Kinet. Mech. Catal. 129 (2020) 471–490. https://doi.org/10.1007/s11144-019-01716-4.

[33] L. Mafra, J.A. Vidal-Moya, T. Blasco, Structural Characterization of Zeolites by Advanced Solid State NMR Spectroscopic Methods, 2012. https://doi.org/10.1016/B978-0-12-397020-6.00004-0.

[34] J. Weitkamp, M. Hunger, ACID AND BASE CATALYSIS ON ZEOLITES, Stud. Surf. Sci. Catal. 168 (2007) 787–835. https://doi.org/https://doi.org/10.1016/S0167-2991(07)80810-X.

[35] D.P. Serrano, R.A. García, M. Linares, B. Gil, Influence of the calcination treatment on the catalytic properties of hierarchical ZSM-5, Catal. Today. 179 (2012) 91–101. https://doi.org/10.1016/j.cattod.2011.06.029.

[36] M. Niwa, N. Katada, K. Okumura, Characterization and Design of Zeolite Catalysts, Springer Berlin Heidelberg, Berlin, Heidelberg, 2010. https://doi.org/10.1007/978-3-642-12620-8.

[37] A. Veses, B. Puértolas, M.S. Callén, T. García, Catalytic upgrading of biomass derived pyrolysis vapors over metal-loaded ZSM-5 zeolites: Effect of different metal cations on the bio-oil final properties, Microporous Mesoporous Mater. 209 (2015) 189–196. https://doi.org/10.1016/j.micromeso.2015.01.012.

[38] A.A. Inayat, A.A. Inayat, W. Schwieger, B. Sokolova, P. Lestinsky, Enhancing aromatics and olefins yields in thermo-catalytic pyrolysis of LDPE over zeolites: Role of staged catalysis and acid site density of HZSM-5, Fuel. 314 (2022) 123071. https://doi.org/10.1016/j.fuel.2021.123071.

[39] M.D. Romero, J.A. Calles, A. Rodriguez, J.C. Cabanelas, The influence of calcination treatment over bifunctional Ni/HZSM-5 catalysts, Ind. Eng. Chem. Res. 37 (1998) 3846–3852. https://doi.org/10.1021/ie980143i.

[40] P. Sazama, B. Wichterlova, J. Dedecek, Z. Tvaruzkova, Z. Musilova, L. Palumbo, S. Sklenak, O. Gonsiorova, FTIR and 27Al MAS NMR analysis of the effect of framework Al- and Si-defects in micro- and micro-mesoporous H-ZSM-5 on conversion of methanol to hydrocarbons, Microporous Mesoporous Mater. 143 (2011) 87–96. https://doi.org/10.1016/j.micromeso.2011.02.013.

[41] F. Jin, Y. Li, A FTIR and TPD examination of the distributive properties of acid sites on ZSM-5 zeolite with pyridine as a probe molecule, Catal. Today. 145 (2009) 101–107. https://doi.org/10.1016/j.cattod.2008.06.007.

[42] S.M. Auerbach, K.A. Carrado, P.K. Dutta, Handbook of Zeolite Science and Technology, 1st Editio, CRC Press, 2003. https://doi.org/10.1201/9780203911167.

[43] G.V.A. Martins, G. Berlier, C. Bisio, S. Coluccia, H.O. Pastore, L. Marchese, Quantification of brønsted acid sites in microporous catalysts by a combined FTIR and NH3-TPD study, J. Phys. Chem. C. 112 (2008) 7193–7200. https://doi.org/10.1021/jp710613q.

[44] A.M. Hernández-Giménez, E. Heracleous, E. Pachatouridou, A. Horvat, H. Hernando, D.P. Serrano, A.A. Lappas, P.C.A. Bruijnincx, B.M. Weckhuysen, Effect of Mesoporosity, Acidity and Crystal Size of Zeolite ZSM-5 on Catalytic Performance during the Ex-situ Catalytic Fast Pyrolysis of Biomass, ChemCatChem. 13 (2021) 1207–1219. https://doi.org/10.1002/cctc.202001778.

[45] M.S. Renzini, U. Sedran, L.B. Pierella, H-ZSM-11 and Zn-ZSM-11 zeolites and their applications in the catalytic transformation of LDPE, J. Anal. Appl. Pyrolysis. 86 (2009) 215–220. https://doi.org/10.1016/j.jaap.2009.06.008.

[46] Deactivation And Regeneration Of Zeolite Catalysts by Guisnet Michel Ribeiro Fernando Ramoa (z-lib.org).pdf, (n.d.).

[47] P. Castaño, G. Elordi, M. Olazar, A.T. Aguayo, B. Pawelec, J. Bilbao, Insights into the coke deposited on HZSM-5, Hβ and HY zeolites during the cracking of polyethylene, Appl. Catal. B Environ. 104 (2011) 91–100. https://doi.org/10.1016/j.apcatb.2011.02.024.

[48] T.L. Barr, The nature of the relative bonding chemistry in zeolites: An XPS study, Zeolites. 10 (1990) 760–765. https://doi.org/10.1016/0144-2449(90)90058-Y.

[49] P. Decyk, K.K. Do, I.W. Seong, Poisoning effect of SO2 on NO reduction by i-butane over Fe/ZSM-5 prepared by sublimation method, J. Catal. 203 (2001) 369–374. https://doi.org/10.1006/jcat.2001.3346.

[50] T.L. Barr, M.A. Lishka, ESCA Studies of the Surface Chemistry of Zeolites, J. Am. Chem. Soc. 108 (1986) 3178–3186. https://doi.org/10.1021/ja00272a004.

[51] J.B. Nagy, P. Bodart, H. Collette, J. El Hage-Al Asswad, Z. Gabelica, R. Aiello, A. Nastro, C. Pellegrino, Aluminium distribution and cation location in various M-ZSM-5-type zeolites (M {double bond, long} Li, Na, K, Rb, Cs, NH4), Zeolites. 8 (1988) 209–220. https://doi.org/10.1016/S0144-2449(88)80310-5.

[52] X. Llovet, A. Moy, P.T. Pinard, J.H. Fournelle, Electron probe microanalysis: A review of recent developments and applications in materials science and engineering, Prog. Mater. Sci. 116 (2021) 100673. https://doi.org/10.1016/j.pmatsci.2020.100673.

[53] R. Theisen, Quantitative Electron Microprobe Analysis, Springer Berlin Heidelberg, Berlin, Heidelberg, 1965. https://doi.org/10.1007/978-3-662-25106-5.

[54] J. Sneddon, M.D. Vincent, ICP-OES and ICP-MS for the determination of metals: Application to oysters, Anal. Lett. 41 (2008) 1291–1303. https://doi.org/10.1080/00032710802013991.

[55] ICP-OES principle, ICP-OES Analysis, ICP-OES FAQ's | Agilent, (n.d.). https://www.agilent.com/en/support/icp-oes/icp-oes-instruments/icp-oes-faq (accessed March 2, 2021).

[56] M.S. Renzini, L.C. Lerici, U. Sedran, L.B. Pierella, Stability of ZSM-11 and BETA zeolites during the catalytic cracking of low-density polyethylene, J. Anal. Appl. Pyrolysis. 92 (2011) 450–455. https://doi.org/10.1016/j.jaap.2011.08.008.

[57] D.P. Serrano, J. Aguado, J.M. Escola, J.M. Rodríguez, G. San Miguel, An investigation into the catalytic cracking of LDPE using Py-GC/MS, J. Anal. Appl. Pyrolysis. 74 (2005) 370–378. https://doi.org/10.1016/j.jaap.2004.11.026.

[58] S.J. Han, S.K. Kim, A. Hwang, S. Kim, D.Y. Hong, G. Kwak, K.W. Jun, Y.T. Kim, Non-oxidative dehydroaromatization of methane over Mo/H-ZSM-5 catalysts: A detailed analysis of the reaction-regeneration cycle, Appl. Catal. B Environ. 241 (2019) 305–318. https://doi.org/10.1016/j.apcatb.2018.09.042.

Chapter 3

3. Effect of the nature, the content and the preparation method of zeolite-polymer mixtures on the pyrolysis of linear low-density polyethylene

Note: This chapter will be published highlighting its scientific contribution and relevance

3.1. Summary

The pyrolysis of polyethylene with different zeolites in powder form was evaluated by TG analysis under a nitrogen atmosphere. Hβ zeolite with the lowest Si/Al ratio shows the best activity. The effect of the extrusion of polyethylene mixed with two zeolites, Hβ (25) and HZSM-5 (23), at different catalyst:polymer ratios was also evaluated. The higher the quantity of catalyst (from 1 % to 16.7 % of the total mixture), the higher the activity that increases in the case of Hβ (25) from 75 °C to 115 °C; nonetheless, Hβ (25) zeolite has a saturation point value when the catalyst:polymer ratio is equal to 1:10. The effect of the pyrolysis of two different preparation methods, extrusion and powdered mixture of polyethylene and the zeolites Hβ (25) and HZSM-5 (23), was also evaluated. Compared with the powder mixtures, the extrusion method limits the diffusion inside the pores and the contact with micropore acid sites, favouring random scission pathway reactions. The textural properties and the acid density have an important effect on the activity, product distribution and aromatization reactions. The Hβ (25) and HZSM-5 (23) were characterized by XRD, N2-physisorption, and TGA before and after pyrolysis. The results show higher deactivation by coke deposition, especially in the micropores after the pyrolysis of the extruded mixtures, with a loss of 79 % and 60 % for HZSM-5 (23) and Hβ (25), respectively.

3.2. Introduction

Pyrolysis is considered a promising way to tackle plastic pollution. It allows polymer decomposition under the action of temperature in the absence of oxygen and leads to the recovery of various essential chemical products [1–3]. Considering different pyrolysis processes, catalytic pyrolysis has several benefits over the non-catalytic route. In recent times, the process of plastic recycling via catalytic pyrolysis has garnered heightened attention within the scientific community, as evidenced by various scientific review articles [4–8]. It significantly reduces the pyrolysis temperature and can direct the reaction to desired liquid pyrolysis products [9]. The main products obtained from catalytic pyrolysis of polyolefins include aromatic hydrocarbons such as benzene, toluene, ethylbenzene and xylene (BTEX), valuable chemicals widely used in the petrochemical industry [10–12]. For example, toluene is one of

the raw materials for caprolactam or polyurethane production, and xylenes are used as solvents [10,13]. Zeolites are the most used catalysts in the pyrolysis of plastics due to their high specific surface area and acidic properties, favouring a lower reaction temperature and promoting higher selectivity in BTEX compared to thermal cracking [14,15,24–26,16–23].

Different types of zeolites have been reported to efficiently affect the pyrolysis of plastics in general and of polyethylene (PE) in particular [4] due to their catalytic activity, control of product distribution and reduction of undesirable by-products. Zeolites are solid crystalline structures described as crystalline aluminosilicate sieves that have open pores and ion exchange capacity and are obtained by means of a three-dimensional interlacing where oxygen atoms join the tetrahedral sides. They are made of silica and alumina, and their relationship determines their reactivity, effectiveness, and acidity and affects the final product of plastic waste pyrolysis [4,27,28]. Boronat et al. [29] highlight the significance of the local geometry of the Al–O(H)–Si group in zeolites as a crucial factor affecting acidity. Specifically, the range of T–O–T angles plays a pivotal role in determining the acidity level of different zeolite materials. Strongly acidic zeolites like HZSM-5 and mordenite exhibit a wider range of T–O–T angles, spanning from 137° to 177° and 143° to 180°, respectively. In contrast, less acidic materials like HY demonstrate narrower T–O–T angle ranges, typically from 138° to 147°. This observation underscores the influence of local geometric variations on the acidity properties of zeolites.

The ratio of polymer to catalyst significantly impacts the quantity and composition of pyrolysis products generated from polyethylene. A study by Mastral et al. [30] investigated the cracking of high-density polyethylene (HDPE) using a nanocrystalline HZSM-5 zeolite catalyst. It was observed that at a temperature of 500 °C, the lowest gas yield during thermal cracking was obtained. Conversely, when the polymer-to-catalyst ratio decreased to 0.93, the gas yield increased significantly to 80.13 %, with a high content of C_4 hydrocarbons. On the other hand, in this case, the liquid phase is made up mainly of cycled and aromatics hydrocarbons, while in thermal cracking, the liquid phase is made up mainly of paraffins (C_{10} - C_{20}) and olefins. Interestingly, when the polymer-to-catalyst ratio exceeded 7, there was a sudden decrease in gas yield.

On the other hand, the efficiency of a catalyst does not only depend on its physicochemical properties and its content, but the contact between the polymer to be recycled and the solid catalyst also plays a determining role in the quality and quantity of products obtained during the catalytic decomposition [27]. The lack of homogeneity between the polymer and the catalyst in the process has led some authors to favour the use of agitation during the reaction [31,32] to obtain a better heat transfer, a higher proportion of the liquid phase (pyrolysis oil) and greater reactivity of the catalysts [33]. Nevertheless, using these reactors implies high operating costs and favours the deactivation of the catalyst, reasons why their use on a large scale is not recommended [33,34]. Another option to get homogeneous contact between the catalyst and the polymer is extrusion, which has recently attracted interest [35]. Extrusion allows excellent control of the pyrolysis residence time and efficient and better contact between the catalyst and the polymer [31]. Marcilla et al. [36] compared a dry powder mixture and a melt extrusion mixture between HDPE (80 %) and zeolite HZSM-5 (20 %) in both flash pyrolysis and slow pyrolysis. Similarly,

Muhammad et al. [37] and Caldeira et al. [38] studied the effect of pre-degradation treatment and thermal homogenisation with an extrudate in catalytic (Y zeolite) pyrolysis of LLDPE and LDPE, respectively. The pre-degradation treatment consists of heating the mixture of polymer and catalyst in powder form to 120 – 180 °C for 10 minutes [37], while the thermal homogenisation consists of an additional step of thermal treatment at 120 °C (isotherm for 6h) before pyrolysis. They show that both processes favoured the catalytic process at lower temperatures. Serrano et al. [39,40] used extrusion in the thermal and catalytic degradation of LDPE through a continuous process using a screw kiln reactor. They evaluated the difference between a screw kiln reactor and a batch reactor in the thermal degradation of LDPE, obtaining a more significant amount of liquid and content in olefins when the extrusion system is used [39]. The authors also showed that using lubricating oil at different concentrations as an additive in the extrudate can significantly improve the catalyst-polymer contact [40]. Most recently, Martey et al. [35] studied the effect of extrusion speed and catalyst composition and concentration on the pyrolysis of LDPE. A hybrid chemical-mechanical approach using reactive twin-screw extrusion (TSE) was used. They showed that LDPE extruded with Y zeolite shows lower degradation temperature and increased short-chain branching. Mesoporous MCM-41 also induces increased branching but does not affect the degradation temperature, possibly due to the low concentration of acid sites, which could generate a fast blockage or deactivation of active sites after extrusion.

This brief literature review highlights the influence of various factors, such as catalyst physicochemical properties and content and preparation method types, on catalytic polymer pyrolysis. While previous studies have investigated these factors individually, a comprehensive and systematic approach is lacking, which is the primary objective of this research. We aim to investigate the impact of polymer-catalyst extrusion compared to an alternative pre-pyrolysis preparation method. To achieve this, a minimum of two catalysts will be selected to evaluate the differences between the two methods and whether these variances correlate with the physicochemical properties of the catalysts. For that purpose, a mixture of LLDPE and zeolite is prepared, and thermogravimetric analysis is used to determine this property. This approach allows the selection of two zeolites with different physicochemical properties. The effect of the preparation method on the pyrolysis of catalyst-polyethylene mixture in the production of BTEX is then examined to discuss if the effect of the preparation method is the same depending on the zeolite type. Finally, the effect of the ratio of zeolite/polymer is studied and discussed.

3.3. Experimental

3.3.1. Catalyst preparation

Before testing, all catalysts were calcinated at 600 °C for 24h in a muffle furnace, except for HZSM-5 samples, which were calcined in flowing air (100 mL.min^{-1}) according to the protocol described in section **2.6.4**. **Table 3.1** shows the main characteristics of the commercial catalysts (reference, supplier, composition and specific surface area given by the supplier).

3.3.2. Samples preparation

In order to evaluate the influence of the catalyst:polymer mixtures in the catalytic pyrolysis of LLDPE, two experimental approaches have been considered. In the first one, the pelleted polymer and the powdered catalyst were extruded, as described in section **2.8.2**. In the following, the suffix "extruded" is mentioned. In the second approach, the catalyst:polymer ratio was obtained by manually mixing the two powders, as described in section **2.8.3**, and the suffix "powdered" is mentioned.

Table 3.1 Main characteristics of the catalysts used in the study

Sample	Supplier	SiO_2/Al_2O_3	S_{BET} ($m^2 . g^{-1}$)	Total Acidity (mmol $NH_3 . g^{-1}$)
Hβ (25)	Alfa Aesar	25	523	1.48 [37]
HY (5.1)	Alfa Aesar	5.1	900	0.61-1.33[38], [39]
HZSM-5 (23)	Zeolyst	23	413	1.40 [37]
Hβ (360)	Alfa Aesar	360	620	0.118[40]
NaY (5.1)	Alfa Aesar	5.1	900	0.40[39]
Hβ (25)	Alfa Aesar	25	523	1.48 [37]

The catalytic pyrolysis of polyethylene with Hβ (25) and HZSM-5 (23) was realized as described in section **2.3,** and the analytical sampling was described in section **2.4.**

3.4. Results and discussion

3.4.1. Effect of zeolite composition on LLDPE pyrolysis

The first step of this study is to investigate the effect of the type of zeolite on the pyrolysis of LLDPE. **Figure 3.1** (a) shows the TGA conversion curves obtained for the thermal pyrolysis of LLDPE and five zeolites-LLDPE mixtures with a catalyst:polymer ratio 1:1. **Figure 3.1** (b) exhibits the corresponding DTG curves. According to the literature, the thermal pyrolysis of LLDPE occurs in a single stage [43], which is confirmed in our study. In the presence of a catalyst, the pyrolysis of PE also occurs in one main stage. However, a shoulder towards the lowest temperatures is visible on the DTG curves (**Figure 3.1** (b)), in particular for the Hβ(25) catalyst. This will be further discussed later in the chapter. An observable initial degradation step is also evident at lower temperatures when NaY is used. This phenomenon can be ascribed to water molecules absorbed within the zeolite framework, which may have been introduced during storage or through the mixing process with the LLDPE [44].

Figure 3.1 also shows that the presence of catalysts allows a noticeable reduction in the maximal temperature of degradation, and this permits the achievement of high activity. In order to easily discuss the effect of the catalyst on the characteristic pyrolysis temperature of LLDPE, **Table 3.2** shows the temperatures T_{max}, $T_{5\,\%}$ and $T_{95\,\%}$, as well as the relative catalytic activity of the zeolites, denoted ΔT_{max}.

Based on ΔT_{max}, the following rank can be established: Hβ (25) ~ HY (5.1) > HZSM-5 > Hβ (360) > NaY. The lowest activity of the NaY zeolite compared to the protonic form of the other studied zeolites can be explained by the difference in the acidity of the material (**Table 3.1**). Indeed, if we compare NaY and HY zeolites, which are two Y zeolite based on sodalite cage that is joined by O-bridges between the hexagonal faces (FAU structure) presenting similar Si/Al ratio (5.1), it is known that the acidity in a proton-type zeolite (HY) is higher than that of sodium-type Y zeolites (NaY). Similarly to what was found by I.C. Neves et al. [45], a decrease in the characteristic temperature of pyrolysis ($T_{5\ \%}$ and $T_{95\ \%}$ in our study and T_{onset} in [45]) is observed compared to PE and is higher in the case of HY. On the other hand, and as expected, Hβ (25) is more active compared to Hβ (360). The difference may be attributed to the fact that the acidity of zeolites is driven by the amount of Brønsted and Lewis acid sites formed by the replacement of Si^{+4} in tetrahedral position by Al^{+3} forming a Si-OH-Al group (Brønsted) [46] and the dehydroxylation of this group (Lewis) [12]. The more aluminium atoms replacing silicon atoms (lower SiO_2/Al_2O_3 ratio), the higher the amount of Brønsted and Lewis acid sites, thus the higher the acidity [47,48]. Agullo et al. [49] reported comparable findings in their study. They conducted experiments by mixing LDPE with 20 wt. % of zeolite Hβ having varying SiO_2/Al_2O_3 ratios (25, 150, and 300). At lower SiO_2/Al_2O_3 ratios, the catalytic activity increased, which was attributed to a higher concentration of Brønsted and Lewis acid sites present in the zeolite. Hβ (25) exhibits superior activity compared to HZSM-5 (23), as illustrated in **Figure 3.1**. According to Tian et al. [44], the cracking of low-density polyethylene (LDPE) by Hβ (ratio polymer:catalyst, 2:1) occurs in two stages. The first stage occurs at lower temperatures (between 250-320 °C) at the catalyst surface, facilitated by greater accessibility of the polymer to acid sites located outside the pores. This leads to more scissions occurring outside the pores. In contrast, HZSM-5 zeolite predominantly cracks LDPE within the pores in an apparent single stage (ratio polymer:catalyst, 2:1). The lower activity of HZSM-5 is attributed to its microporous structure and larger crystal size, which hinder the diffusion of long-chain molecules to the microporous acid sites [50].

Table 3.2 Characteristic data obtained from TGA and DTG for LLDPE and its respective mixture with different catalysts under nitrogen atmosphere (ratio catalyst:polymer, 1:1)

Sample	T_{max} (°C)	ΔT_{max} (°C)	$T_{5\ \%}$ (°C)	$T_{95\ \%}$ (°C)
LLDPE/Hβ (25)	411.0	69.4	360.9	403.4
LLDPE/HY (5.1)	414.2	66.3	354.8	404.5
LLDPE/HZSM-5 (23)	418.7	61.8	358.8	411.5
LLDPE/Hβ (360)	422.6	57.9	373.2	417.0
LLDPE/NaY (5.1)	458.6	21.8	413.0	453.0
LLDPE	481.1	0.0	451.1	478.4

Based on those results, it was decided to look in more detail at the performances of the Hβ (25) catalyst due to its highest catalytic effect by comparing it to the HZSM-5 (23) catalyst. HZSM-5 catalyst was

selected as a reference since it is the most used in polymer pyrolysis [6,51]. Moreover, both zeolites present similar SiO_2/Al_2O_3 ratios, and their specific surface and total acidity are in the same range.

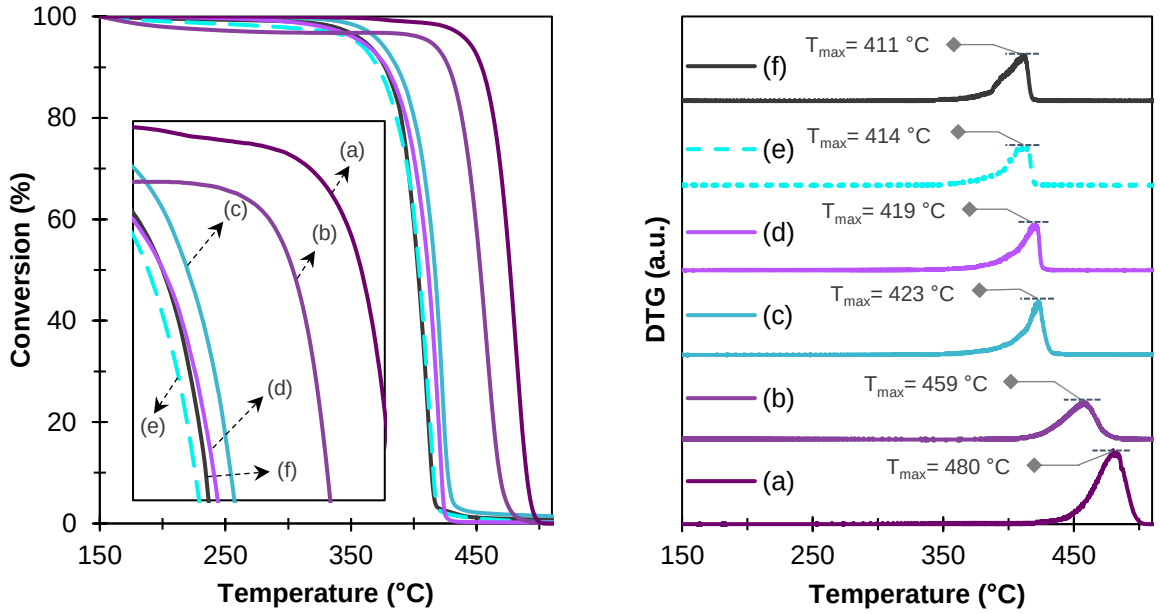

Figure 3.1. TGA conversion (a) and DTG (a) curves of LLDPE degradation and its respective mixtures under nitrogen atmosphere, using a ratio catalyst:polymer, 1:1. (a) no catalyst, (b) NaY (5.1), (c) Hβ (360), (d) HZSM-5 (23), (e) HY (5.1), and (f) Hβ (25).

3.4.2. Effect of the preparation method of the mixture

The effect of the preparation method of the mixture catalyst/polymer on the LLDPE pyrolysis was studied by comparing the results obtained when the polymer and the catalyst (Hβ or HZSM-5) were extruded or simply mixed in powder form, both cases with a catalyst:polymer ratio equal to 1:10. It must be clarified that no effect of extrusion on the polymer alone has been observed, as the recorded mass losses during pyrolysis of the extruded and powdered polymer were found to be identical (not shown).

Figure 3.2 shows the TG and DTG curves obtained during the pyrolysis under nitrogen of a LLDPE/ Hβ (25) and LLDPE/ HZSM-5 (23) mixtures achieved by extrusion or simple powder mixture. The catalytic pyrolysis of the polymer is impacted by the mixing procedure. Indeed, when the polymer-catalyst mixture is prepared by extrusion, the degradation process occurs at lower temperatures. This improved catalytic activity could be explained by better contact between the polymer and the catalyst achieved with the extrusion. Muhammad et al. [37] and Caldeira et al. [38] studied the effect of pre-degradation treatment and thermal homogenisation, respectively, in the catalytic (Y zeolite) pyrolysis of polyethylene. Compared to the normal mixing, the degradation curve (TG) shifted to slightly lower temperatures with pre-degradation treatment. Using the thermal homogenisation process, the degradation curve (TG) shows one mass loss, while two mass losses are clearly identified without thermal homogenisation. Then, it could be suggested that normal mixing of the polymer with the catalyst allows a fraction of the polymer to be decomposed at lower temperatures by the catalytic pathway, while the non-catalytic thermal pathway degrades the remaining polymer. By improving the contact between the polymer and

the catalyst through extrusion, the catalytic pathway is certainly promoted, and the polymer degradation takes place at a lower temperature.

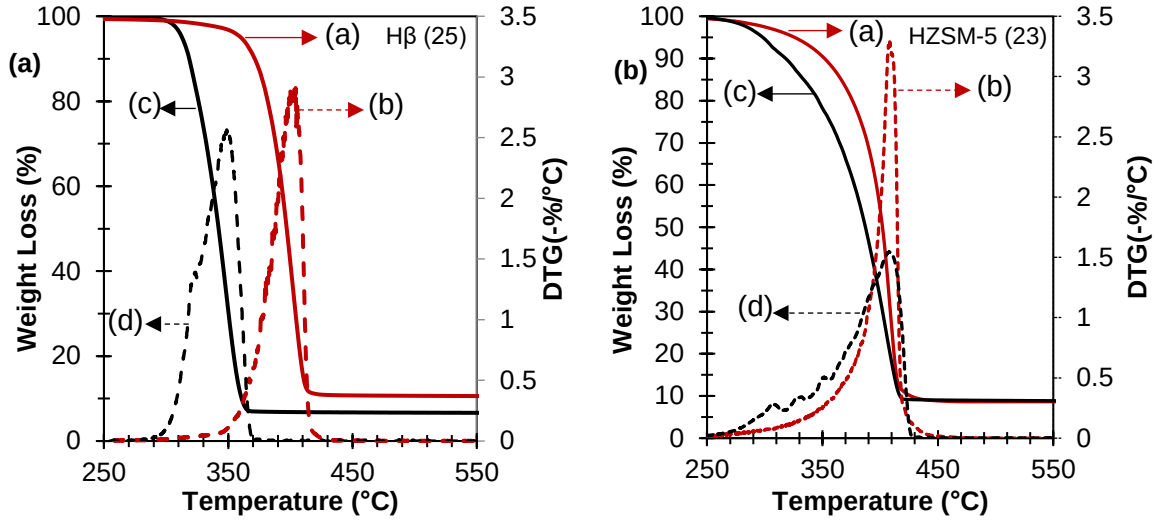

Figure 3.2. TGA **(a)** and DTG **(b)** curves obtained during the pyrolysis under nitrogen atmosphere of a LLDPE/ Hβ (25) (a) and LLDPE/ HZSM-5 (23) (a) mixtures achieved by simple powder mixing (red lines) : (a) (TG) and (a) DTG; or by extrusion (black lines) : (c) (TG) and (d) DTG, using a ratio catalyst:polymer 1:10.

The effect of extrusion is more pronounced when Hβ is employed compared to HZSM-5. As previously mentioned, this result could be explained by the external surface of the Hβ zeolite, which is ~ 6 times larger than that of the HZSM-5 zeolite (**Table 3.4**). These results thus show that the effect of the preparation method could vary from one catalyst to another depending on their physicochemical properties. Since the external surface has a crucial role in the catalytic activity of zeolite in pyrolysis reaction, the preparation method will have a more critical effect when this external surface is important.

3.4.3. Effect of the preparation method of the mixture on the yield and selectivity of the pyrolysis reaction of LLDPE

This part of the study investigated the effect of the preparation method on the yield and selectivity of the pyrolysis reaction of LLDPE. Indeed, the data obtained by TGA only gives information on the activity, *i.e.*, pyrolysis kinetics. The pyrolysis products have been categorized by phase type (gas, wax+oil and coke), by the family of products (paraffins, olefins, aromatics) and according to their carbon distribution (C_3-C_5, C_6-C_{12} and $\geq C_{13}$), these last two considering only the liquid phase. It should be noted that LLDPE conversion is complete at given pyrolysis conditions. However, before going further on the results regarding this question, the selected catalysts are fully characterized, and the mechanism of catalytic cracking of LLDPE is discussed.

LLDPE cracking mechanism

In the polyethylene catalytic cracking mechanism, the transition from macromolecules to lower molecular weight hydrocarbons occurs in three stages: initiation, propagation and termination [52,53].

The initiation stage occurs between the solid surface of the catalyst and the melted polymer, where the first carbocations are formed [52–54]. In this stage, the external surface helps the pre-cracking of macromolecules into oligomers that are then adsorbed on the internal structure of the catalyst, where subsequent and various cracking reactions occur [52–55]. The latter stage is known as the propagation stage. Among these propagation reactions are β-scission, which forms new carbocations (secondary carbocations), hydrogen transfer reactions, or isomerization. The termination stage usually involves recombination reactions, cyclization, etc. [52–54]. Later occurs the desorption of the catalyst and diffusion to the liquid phase (melted polymer) [52].

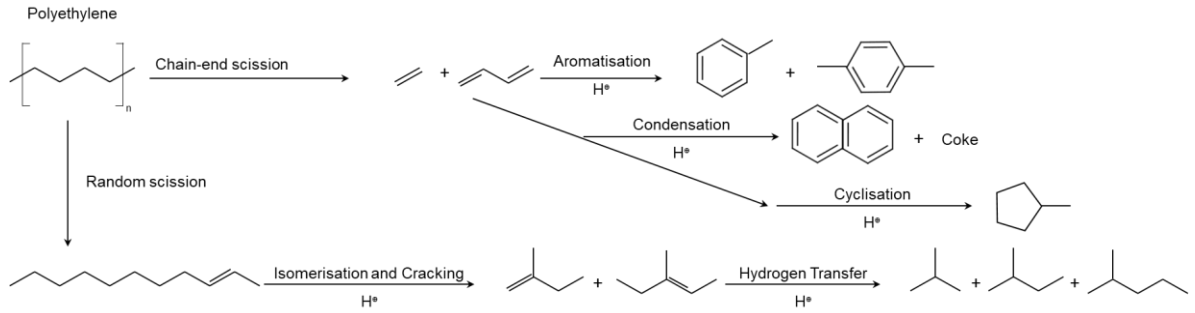

Figure 3.3. Possible pathways scissions of the catalytic pyrolysis of polyethylene with zeolite acid catalysts from ref [55].

It is noteworthy that the product selectivity of catalytic polyethylene cracking depends not only on the polymer quality but also on the catalyst qualities, such as the acid strength and the number of active sites, pore size, and catalyst structure [28,55]. Okonsky et al. [55] explain that the initial catalytic cracking of polyethylene can result in random scission, producing long-chain olefins or chain-end scission, producing short-chain olefins (**Figure 3.3**). On one side, long-chain olefins act on an acid site, leading to cracking and isomerization reactions where paraffins and isomerized olefins are formed. In contrast, short-chain olefins undergo cyclization or aromatization reactions. It is widely acknowledged that the aromatization of olefins occurs between nearby acid sites, where one acid site adsorbs the olefins and produces paraffin through a hydrogen transfer reaction, and another acid site reorganizes the olefins through cyclization or aromatization reactions [7,56], as illustrated in **Figure 3.4**.

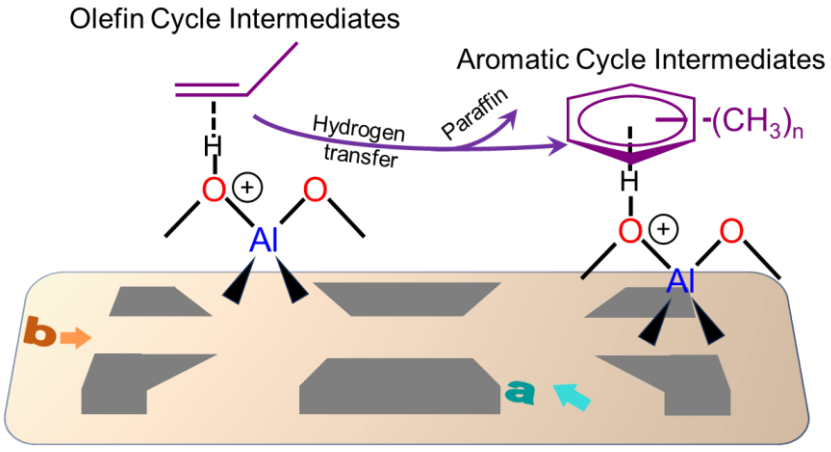

Figure 3.4. Reaction mechanism illustration of olefinic and aromatic cycles on acid active sites from ref [56].

M.S. Abbas-Abadi et al. [8] offer a more detailed insight into this process. Olefin cracking at zeolite's acidic sites induces protonation, leading to a higher concentration of carbenium-ions. Consequently, bimolecular reactions become prevalent in polyethylene cracking. When diolefins and carbenium-ions are present, this bimolecular mechanism stimulates cyclization and Diels-Alder reactions, thus enhancing the production of aromatic compounds.

Catalytic pyrolysis of LLDPE using Hβ (25)

Figure 3.5 (a) shows the effect of the preparation method on the gas/liquid/coke yields in the LLDPE catalytic degradation in the presence of Hβ zeolite. The Hβ/LLDPE extruded mixture yields a higher amount of liquid than the powdered Hβ/LLDPE mixture. Zeolite Hβ has a large pore size with 12-ring three-dimensional channels (5.6 × 5.6 A˚ and 6.6 × 6.7 A˚) perpendicularly intersecting [54]. Its larger external surface (36.9 % of the total surface) promotes the cracking reaction at the external surface, and its large pore size allows faster mass transfer through the channels [57]. Considering the mechanical action of the extrusion and since the external surface of Hβ zeolite is high, LLDPE cracking on the external surface will be favoured, which could explain the more significant amount of liquid phase when the extruded material is used. The coke yields were very low (<1 %) and were similar regardless of the preparation method used.

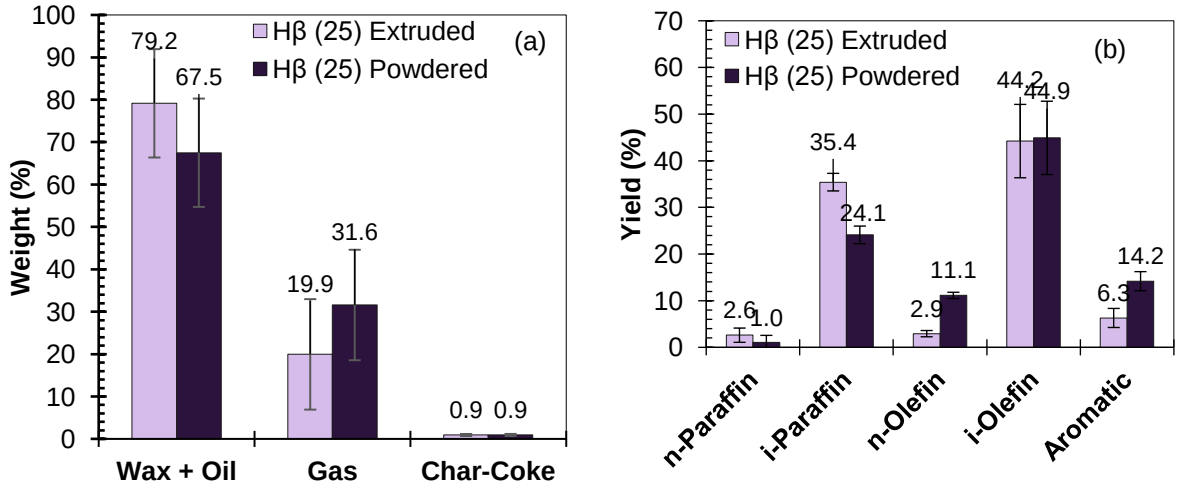

Figure 3.5. Yield result of pyrolysis of LLDPE with Hβ (25) (a) and composition of oil/wax (b) from the decomposition of LLDPE with Hβ (25) using powdered polymer (Powdered) or catalyst extruded with polymer (Extruded).

The wax+oil fraction is mainly composed of i-olefins and i-paraffins (**Figure 3.5** (b)). The small selectivity of aromatic compounds obtained in this part of the study is also reported by other authors [55]. On the other hand, the production of i-paraffins is higher with the Hβ/LLDPE extruded mixture (35.4 %) than with the powdered Hβ/LLDPE mixture (24.1 %) whereas the production of n-olefin and aromatic is lower. The high production of paraffins and the low production of aromatics found after pyrolysis of the Hβ/LLDPE extruded mixture demonstrate a tendency toward the random scission pathway reactions when the material is extruded.

A view of the carbon distribution (**Table 3.3**) of the wax+oil products shows that the amount of C_3-C_5 range is higher for the powdered Hβ/LLDPE mixture than for the Hβ/LLDPE extruded mixture. It means that the powdered mixture promotes the LLDPE cracking into the micropores, which is in line with the amount of gas produced that is higher. The extruded and powdered mixtures have high hydrocarbon selectivity from C_6 to C_{12}, especially the extruded mixture, in this zone are located the majority of monoaromatics. Indeed, the production of BTEX with zeolite Hβ is between 23 % and 62 % of the total aromatics. However, although the extruded mixture has a more extensive amount of hydrocarbons in this zone, the powdered mixture promotes a greater production of aromatics. Production of hydrocarbons with a carbon number ≥C_{13} is favoured with the extruded mixture. It may result from recombination reactions of higher molecular weight carbocations that did not enter the micropores due to limitations, which corroborates the inclination for random scission pathway reactions of this mixture.

Table 3.3 Carbon distribution by family of products from pyrolysis of LLDPE with Hβ (25) using powdered polymer (Powdered) or catalyst extruded with polymer (Extruded).

Catalyst	Carbon Distribution Range Peak Area %)		
	C_3-C_5	**C_6-C_{12}**	**≥C_{13}**
Hβ (25) Extruded	10.1 ± 0.1	84.8 ± 0.4	2.8 ± 0.3
Hβ (25) Powdered	18.0± 0.1	77.7± 0.4	1.5± 0.3
HZSM-5 (23) Extruded	4.6 ± 1.9	91.7 ± 1.9	0.6 ± 0.3
HZSM-5 (23) Powdered	3.8 ± 1.9	93.4 ± 1.9	0.9 ± 0.2

Catalytic pyrolysis of LLDPE using HZSM-5 (23)

At the opposite of what was observed for Hβ, the yields of gas/liquid/coke shown in **Figure 3.6** (a) do not differ depending on the preparation method used for the HZSM-5/polymer mixture. The low coke yield (<1 %) in both cases is related to the suitable cavities in ZSM-5 zeolites, avoiding the severe coking observed with other zeolites such as USY and HY[58].

On the other hand, aromatics are produced in large amounts, whatever the preparation methods, as shown in **Figure 3.6** (b) if we compare the results with Hβ. Inayat et al. [12] found similar results in LLDPE cracking with HZSM-5. This high selectivity in aromatics, especially in BTEX, is explained by Dai et al. [59] due to the acid properties, micropore size and structure of the ZSM-5 zeolite. Indeed, the initial cracking of the polyethylene occurs on the surface of the zeolite, in the acid sites, where shorter chain hydrocarbons are generated, many of them only evaporate, and others reach the micropores of the ZSM-5 zeolite [19], where more propagation and terminal reactions [60–62]. ZSM-5 zeolite favours a higher content of aromatic compounds in the oil phase from cyclic rings through hydrogen transfer reactions, especially of single-ring aromatics. This behaviour is mainly due to the pore size [44] and the strong Brønsted acid sites [12,16]. The latest promotes cracking and subsequent aromatisation [12].

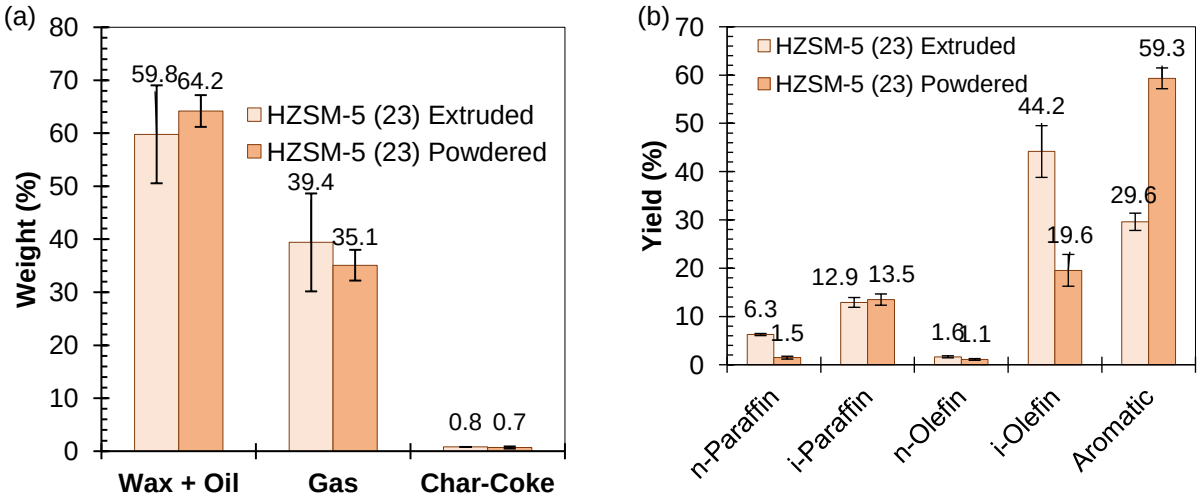

Figure 3.6. Yield result of pyrolysis of LLDPE with HZSM-5 (23) (a) and composition of oil/wax (b) from the decomposition of LLDPE with HZSM-5 (23) using powdered polymer (Powdered) or catalyst extruded with polymer (Extruded).

Figure 3.6 (b) also shows that i-olefins are the primary products obtained when the zeolite is extruded with the polymer, whereas aromatics are favoured when the catalyst is mixed as a powder with the polymer. This behaviour indicates that when the LLDPE is cracking, the extruded mixture favours random scission pathways, but subsequent reactions are limited by the size of the pore, which impedes hydrogenation reactions, producing high molecular weight molecules. Indeed, Zeolite HZSM-5 has a channel system of 10 rings interconnected, with two types of channels: straight and sinusoidal. The pore sizes of these channels are 5.6 × 5.6 A˚ and 5.1 × 5.5 A˚ [54]. Bimolecular reactions such as condensation or hydrogen transfer are sterically limited to form molecules of a higher molecular weight inside zeolite HZSM-5 [41,43,52]. The chain-end scission is the main reaction pathway for this zeolite due to its high acid strength, which means a more significant amount of light hydrocarbons (especially in the gas phase [44]) and aromatics are produced [63].

In contrast, when the zeolite is mixed with the polymer in powder form, fewer i-olefins are produced, and more aromatics are obtained to the detriment of n-olefins production through chain-end scission pathways [7,56], as explained above in the description of the LLDPE reaction mechanism. The olefin aromatisation is generated after LLDPE cracking through the Diels-Alder reaction [59].

More information on wax+oil carbon distribution is listed in **Table 3.3**. The light hydrocarbon zone (C_3-C_5) found a low production for both mixtures, especially for the powdered mixture, 3.8 % compared to 4.6 % of the extruded mixture. On the range of C_6-C_{12}, HZSM-5 zeolite is favourably selective in more than 90 %. In both cases, in this range, the composition of the liquid phase is mainly aromatics and i-olefins. The powder mixture generated 29.7 % more selectivity in aromatics, and when the extruded mixture was used, resulted in a higher selectivity of i-olefins (+24.6 %), showing the preference for random scission over chain-end scission pathway reactions from the pyrolysis with the extruded mixture, which may be limited by less accessibility to the acid sites. The carbon distribution of products with a carbon quantity greater than thirteen (>C_{13}) is insignificant for both cases, less than 1 %.

Characterisation of the catalyst after pyrolysis

It was shown that depending on the catalyst type, the preparation method may affect the pyrolysis differently. It is thus also interesting to characterize the catalyst after the pyrolysis to see if the preparation method may affect the coking differently by comparing Hβ and HZSM-5.

The quantity of coke in the zeolites Hβ and HZSM-5 after the reaction has been estimated from TG analyses (**Figure 3.7**). The weight loss between 50-350 °C can be attributed to water removal, while the weight loss between 350-700 °C is ascribed to coke oxidation. Beyond 700 °C, the dealumination of the zeolite can occur [64]. Based on the literature data, two kinds of coke can be distinguished. At low temperatures, well-structured coke species (soft coke) are oxidised, while at higher temperatures, polyaromatic coke species (hard coke) are burned [65,66]. The quantity of soft coke is similar for the two spent HZSM-5 catalysts but not for the two spent Hβ catalysts, where the difference is slight but clear, while more hard coke species are present when the zeolite is extruded initially with the polymer, independent of the zeolite. The pore system of HZSM-5 imposes more significant restrictions on condensation reactions, leading to reduced coke formation compared to Hβ zeolite [41].

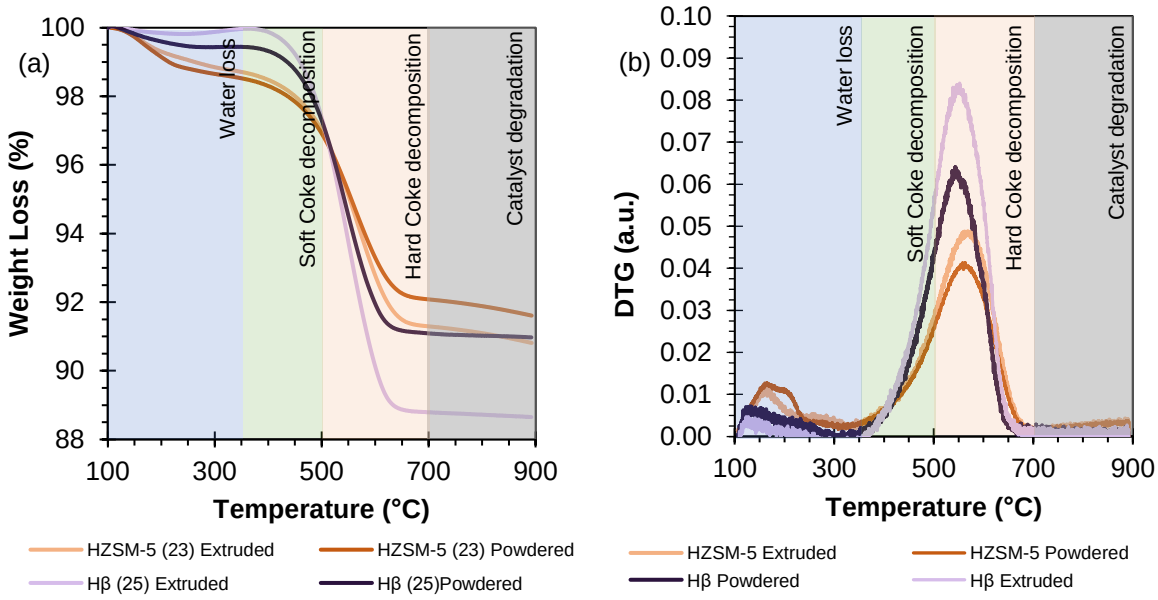

Figure 3.7. TG (a) and DTG (b) curves of Hβ (25) and HZSM-5 (23) zeolites after reaction using powdered catalyst-polymer mixture (Powdered) or catalyst extruded with polymer (Extruded) under air.

Figure 3.8 shows the XRD patterns of the fresh and spent Hβ (a) and HZSM-5 (b) samples. For the six zeolites, diffraction peaks for Bragg's angle between 5 and 55° can be observed and are characteristics of the tetragonal phase of the β zeolites framework (PDF-00-056-0467) for the Hβ samples (**Figure 3.8** (a)) and of the orthorhombic phase of the ZSM-5 zeolites framework (PDF-04-017-8707) for the HZSM-5 samples (**Figure 3.8** (b)). The two pairs of diffraction peaks of the HZSM-5 zeolites corresponding to the (3 3 2) and (0 5 1), and (8 0 4) and (0 1 0 0) lattice planes merged into a single peak at 2θ values of 23.2° and 45.1°, for the spent HZSM-5 zeolites, while for spent Hβ samples, a single peak at 2θ value

of 44.6° appears. After testing, this change in the crystallinity can be correlated with coke formation within the pores [67].

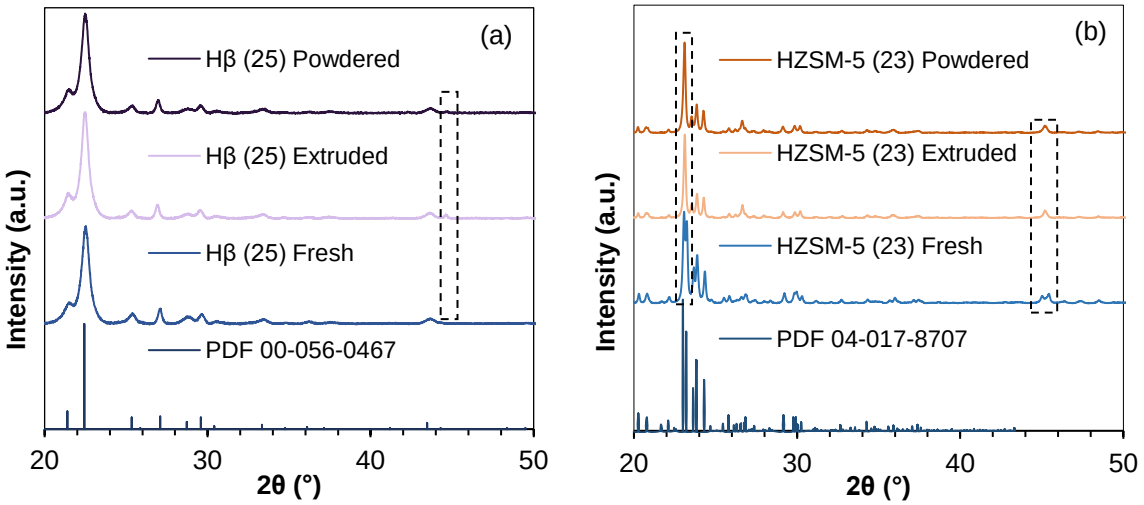

Figure 3.8. XRD of Hβ (25) (a) and HZSM-5 (23) (b) zeolites before reaction (Fresh) and after reaction using powdered catalyst-polymer mixture (Powdered) or catalyst extruded with polymer (Extruded).

The N_2-physisorption curves (not shown) obtained for the fresh and spent Hβ and HZSM-5 samples are type IV, with pronounced H4 hysteresis loops at P/P_0 greater than 0.4, according to the IUPAC nomenclature [68] and are generally observed with materials containing both micropores and mesopores [69]. The main textural data extracted from these curves are given in **Table 3.4**.

Table 3.4 Textural properties of Hβ (25) and HZSM-5 (23) zeolites before reaction (Fresh) and after reaction using powdered catalyst-polymer mixture (Powdered) or catalyst extruded with polymer (Extruded).

Catalyst	S_{BET} ($m^2 . g^{-1}$)	S_{EXT} ($m^2 . g^{-1}$)	S_{MICRO} ($m^2 . g^{-1}$)
HZSM-5 (23) Fresh	413	30	383
Hβ (25) Fresh	523	193	330
HZSM-5 (23) Extruded	90 (-78 %)	10 (-67 %)	80 (-79 %)
HZSM-5 (23) Powdered	178 (-57 %)	14 (-53 %)	165 (-57 %)
Hβ (25) Extruded	287 (-45 %)	156 (-19 %)	132 (-60 %)
Hβ (25) Powdered	330 (-37 %)	155 (-20 %)	175 (-47 %)

After the pyrolysis reactions, a significant decrease in the textural properties is observed. This decrease could be related to the coke formation in the zeolite, which blocks the pores [58]. Deactivation by coke can be generated directly in two ways: into the micropores, where only these are deactivated, or at the external surface, where the entrance to the micropores is blocked and therefore deactivated. Hβ (25) external surface is affected in equal proportion for the extruded and powdered mixture. Due to the large size of the pores of zeolite Hβ, it is easier to block the micropores than the pore entrances because its large pore size allows greater diffusion of by-products into the inside of the zeolite. It has been reported

that the coke in zeolite Hβ prefers to be located near strong acid sites, in the ultramicropores of the structure or blocking its access [70]. Hence, the external surface is less affected.

Indistinctively from zeolite, the micropores are more affected by deactivation by coke when extrusion is used, this effect being much more important for zeolite HZSM-5. This behaviour can be explained as a consequence of a polymer pre-degradation during the extrusion process in which the first cracks of the polymer at low temperature and the first pore blockages can be generated.

In the case of zeolite HZSM-5, the deactivation is more intense, possibly due to its pore size. In the powdered test, there is a higher coke formation on the surface because the deactivation is in the same proportion both on the external surface and in the micropores. The deactivation can be explained by considering that coke deposition on the external surface blocks access to the micropores and, therefore, the internal acid sites [71]. In other words, the smaller size of the pores enables a relatively straightforward obstruction of their entrances, concurrently deactivating all active sites within the pores. On the other hand, the extrusion method allows the diffusion of products in the micropores, where these products are exposed to more acid sites and an over-cracking, forming mainly polyaromatics (hard coke) [67]; in other words, there is an important migration of coke in the micropores which could restrict the aromatisation reaction of the olefins.

3.4.4. Effect of the ratio catalyst/polymer on the yield and selectivity of the pyrolysis reaction of LLDPE

It is also essential to emphasize that the extrusion process offers distinct advantages over existing literature. We can operate within a broader range of concentrations by employing extrusion, enabling greater flexibility in the experimental conditions. Moreover, the extrusion method allows for improved homogeneity control. This enhanced control over concentration and homogeneity enhances the reliability and accuracy of our experimental findings.

In order to be able to vary the catalyst:polymer ratio in a wide range and to study the effect of a small amount of catalyst, we proceeded with the extrusion method to prepare the mixtures, which allows the control at a very low catalyst:polymer ratio. The study was conducted on two catalysts, Hβ (25) and HZSM-5 (23).

Figure 3.9 (a) and (b) show the TG and DTG curves, respectively, obtained during the pyrolysis of pure LLDPE or in the presence of Hβ (25) zeolite at various ratios. Six different catalyst:polymer ratios have been investigated from 1:100 to 1:5. **Figure 3.10** (a) and (b) show the TG and DTG obtained for HZSM-5 (23) zeolite. In that case, three catalyst:polymer ratios have been investigated: 1:100, 1:50 and 1:10. The primary characteristic data are listed in **Table 3.5.**

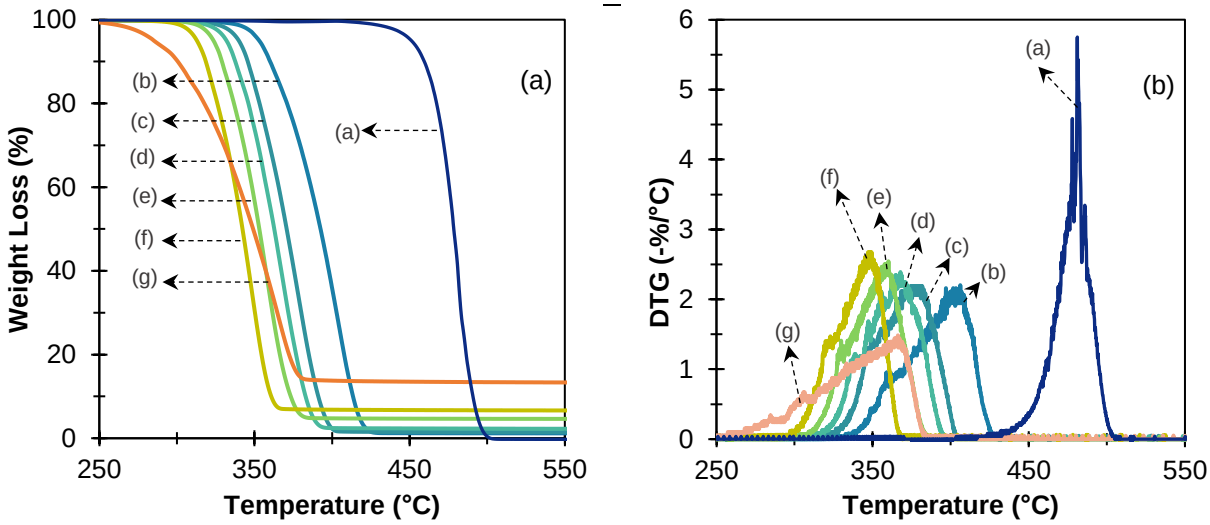

Figure 3.9. TG (a) and DTG (b) curves obtained during the pyrolysis of LLDPE under nitrogen atmosphere at 10 °C . min^{-1} with Hβ (25) zeolite using different catalyst: polymer ratios : (a) 0:100, (b) 1:100, (c) 1:50, (d) 1:30, (e) 1:20, (f) 1:10, (g) 1:5.

The relative activity (ΔT_{max}) is lower than 100 °C for all concentrations of HZSM-5 (23), making this zeolite less active than Hβ (25). For the optimum value of the catalyst:polymer ratio (1:10), a T_{max} difference of 55 °C is recorded in favour of Hβ (25), 132.6 °C compared to 77.3 °C for Hβ (25) and HZSM-5 (23), respectively. The shoulder in the principal peak at lower temperatures shown in **Figure 3.9** (b) and **Figure 3.10** (b) evidence two cracking steps, which are much less marked in the presence of HZSM-5 (23) and non-extruded conditions compared with the literature [23].

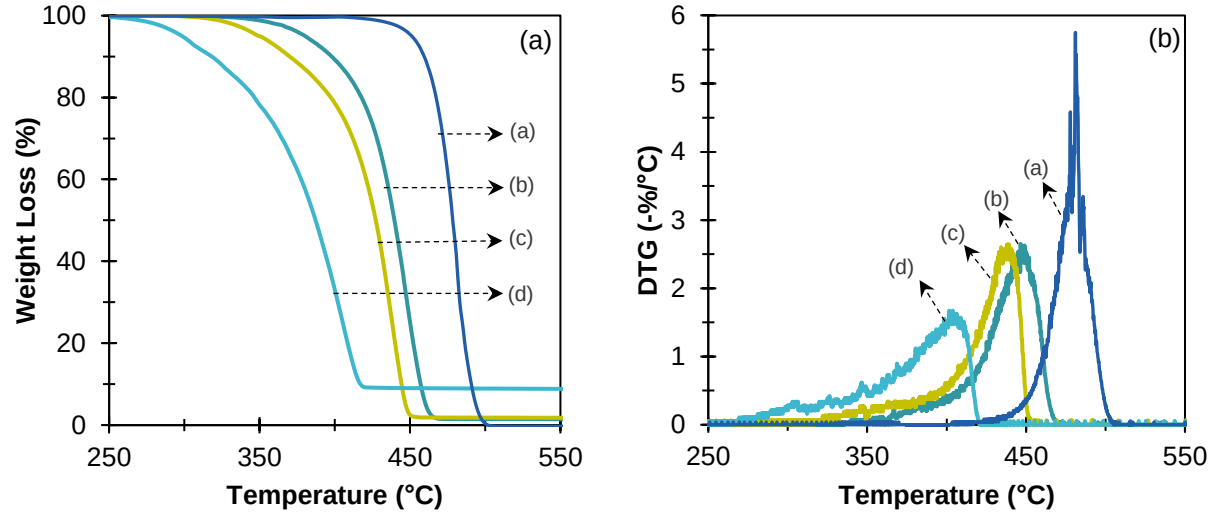

Figure 3.10. TG (a) and DTG (b) curves obtained during the pyrolysis of LLDPE under nitrogen atmosphere at 10 °C.min^{-1} with HZSM-5 (23) zeolite using different catalyst: polymer ratios: (a) 0:100, (b) 1:100, (c) 1:50, (d) 1:10.

The lowest external surface of HZSM-5 compared to Hβ (in proportions of ~6 times lower) [72–74] could explain this discrepancy. It must be pointed out that the $T_{5\,\%}$ values obtained in the presence of HZSM-5 (23) at catalyst:polymer ratio 1:100 is ~27 °C more compared to Hβ (25) at the same ratio, but the difference decreases with the increasing catalyst concentration, at 1:50 ratio this difference is ~9 °C and

at 1:10 ratio is ~3 °C, while $T_{95\ \%}$ values are much higher, more than 47 °C (**Table 3.5**). This suggests that HZSM-5 can initiate pyrolysis of LLDPE at a relatively low temperature despite its smaller external surface area.

Table 3.5 Data extracted from TG and DTG curves obtained in the course of the LLDPE pyrolysis (10 °C.min^{-1}) under nitrogen atmosphere (100 mL.min^{-1})

Catalyst:polymer ratio	Total weight loss (%)	T_{max} (°C)	ΔT_{max} (°C)	$T_{5\ \%}$ (°C)	$T_{95\ \%}$ (°C)
Extruded					
Hβ (25)					
1:100	98.9	406.1	75.0	352.9	412.9
1:50	98.6	380.7	100.4	339.7	394.2
1:30	97.8	367.8	113.3	331.8	385.3
1:20	95.4	360.1	121.0	323.2	374.0
1:10	93.4	348.5	132.6	312.4	359.7
1:5	86.7	366.2	114.9	282.8	374.6
HZSM-5 (23)					
1:100	98.6	446.6	34.5	380.0	459.5
1:50	98.2	438.0	43.1	348.7	446.1
1:10	91.2	403.8	77.3	315.0	427.2
Pure LLDPE	100	481.1	0.0	451.1	493.9
Powdered					
Hβ (25)					
1:10	89.8	401.9	78.5	358.2	410.7
HZSM-5 (23)					
1:10	91.3	407.5	72.9	322.5	415.4
Pure LLDPE	99.8	480.4	0.0	443.6	492.6

As shown more clearly in **Figure 3.10**, the maximum degradation temperature decreases when the amount of HZSM-5 increases. Nevertheless, the zeolites Hβ (25) seems to reach a possible saturation point (**Figure 3.11** (a)), which means that this increase in the amount of zeolite will reach a point where an additional quantity of catalyst has no additional effect or has a negative effect on the activity. The saturation point is found at catalyst:polymer ratio 1:10.

Marcilla et al. [23] did a similar study with a powdered mixture. Compared to our study, they did not observe a saturation point but a continuous increase in ΔT_{max} with catalyst concentration increase. Moreover, it must be pointed out that the preparation of the Hβ (25):polymer mixture by extrusion led to higher ΔT_{max} values in comparison values obtained by Marcilla et al. [23] with a powdered mixture. Such an effect is much less pronounced when HZSM-5 (23) is used as the catalyst.

This difference in behaviour between both zeolites can be explained by the difference in external surface area, which is ~6 times higher for Hβ (25) in comparison with HZSM-5 (23), suggesting that the mechanical effect of extrusion is experienced if the external surface of the zeolite is sufficiently high (193 $m^2.g^{-1}$).

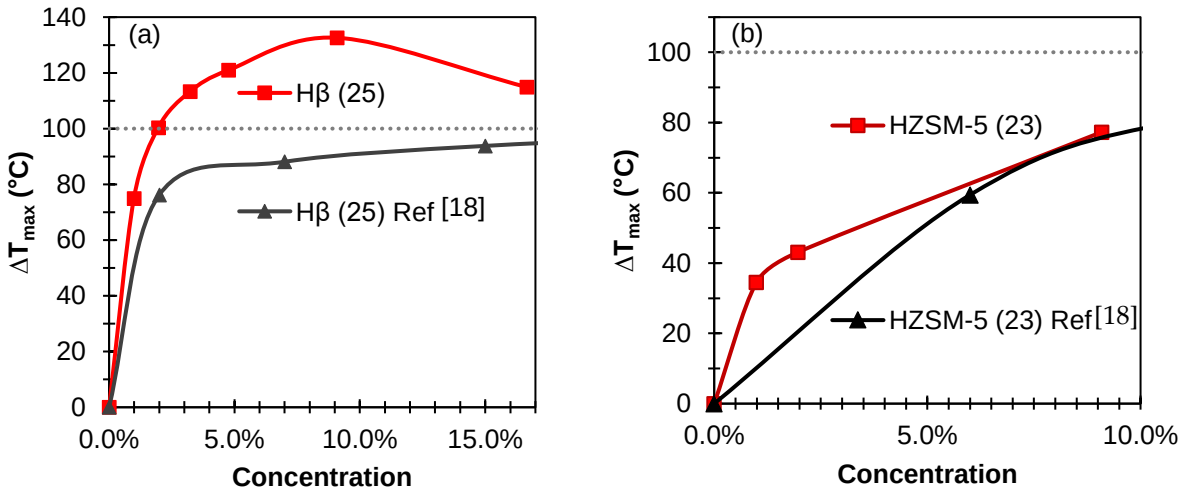

Figure 3.11. Comparison of the effect of the concentration of catalyst on the decomposition of LLDPE in the presence of Hβ (25) (a) and HZSM-5 (23) (b) zeolites on relative activity from the TG curves obtained in this study (red) and in ref [21] (black) at 10 °C . min^{-1} under nitrogen atmosphere.

3.5. Conclusions

In this study, we observed that the extrusion method for preparing zeolite-polymer mixtures has several noteworthy effects. It promotes random scission reactions, resulting in a notable increase in paraffin (17 % for Hβ (25) and 4.2 % for HZSM-5 (23)) and a significant increase of 25.1 % in olefin production for HZSM-5 (23) zeolite. On the other hand, it leads to a reduction in aromatic compound formation in the liquid phase by 7.7 % and 29.7 % for Hβ (25) and HZSM-5 (23), respectively. Furthermore, this method enhances the diffusion of products into micropores, resulting in more pronounced over-cracking and the formation of hard coke. Consequently, it deactivates a larger portion of the microporous surface compared to the powdered mixture method.

When comparing catalytic pyrolysis results, it is evident that the choice of zeolite significantly influences the impact of extrusion mixture cracking. Hβ zeolite, known for its extensive external surface (6 times that of HZSM-5) and larger pore size, yields 19.4 % and 3.3 % more liquid when subjected to extrusion and powdered mixture, respectively. In contrast, HZSM-5 (23) zeolite, with its strong Brønsted acid sites and smaller pore size, exhibits higher selectivity for aromatic compound production. Extrusion has a limited effect on liquid/gas/solid yields or soft coke production for HZSM-5 (23). However, it adversely affects the external surface and the microporous structure and leads to increased C_3-C_5 hydrocarbon production in the liquid phase.

The extrusion method was employed to reduce catalyst content, involving variations in zeolite Hβ (25) and HZSM-5 (23) concentrations within the extruded polymer. TGA revealed a two-step cracking process for Hβ (25), indicating an optimal 1:10 catalyst:polymer ratio. While HZSM-5 completes degradation at higher temperatures ($T_{95\,\%}$ = 427.2 °C compared to $T_{95\,\%}$ of Hβ (25) = 359.7 °C), the initial degradation temperature, $T_{5\,\%}$ equal to 315 °C, suggests it achieves decomposition at low temperatures, similar to Hβ (25) ($T_{5\,\%}$ = 312.4 °C), within the optimal catalyst:polymer ratio of 1:10.

3.6. References

[1] I. Vollmer, M.J.F. Jenks, M.C.P. Roelands, R.J. White, T. van Harmelen, P. de Wild, G.P. van der Laan, F. Meirer, J.T.F. Keurentjes, B.M. Weckhuysen, Beyond Mechanical Recycling: Giving New Life to Plastic Waste, Angew. Chemie Int. Ed. (2020). https://doi.org/10.1002/anie.201915651.

[2] A. Oasmaa, M.S. Qureshi, H. Pihkola, I. Deviatkin, J. Mannila, A. Tenhunen, H. Minkkinen, M. Pohjakallio, J. Laine-Ylijoki, Pyrolysis of Plastic Waste: Opportunities and Challenges, J. Anal. Appl. Pyrolysis. (2020) 104804. https://doi.org/10.1016/j.jaap.2020.104804.

[3] E.T. Aisien, I.C. Otuya, F.A. Aisien, Thermal and catalytic pyrolysis of waste polypropylene plastic using spent FCC catalyst, Environ. Technol. Innov. 22 (2021) 101455. https://doi.org/10.1016/j.eti.2021.101455.

[4] P. Kasar, D.K. Sharma, M. Ahmaruzzaman, Thermal and catalytic decomposition of waste plastics and its co-processing with petroleum residue through pyrolysis process, J. Clean. Prod. 265 (2020) 121639. https://doi.org/10.1016/j.jclepro.2020.121639.

[5] P.T. Williams, Hydrogen and Carbon Nanotubes from Pyrolysis-Catalysis of Waste Plastics: A Review, Waste and Biomass Valorization. (2020). https://doi.org/10.1007/s12649-020-01054-w.

[6] Y. Peng, Y. Wang, L. Ke, L. Dai, Q. Wu, K. Cobb, Y. Zeng, R. Zou, Y. Liu, R. Ruan, A review on catalytic pyrolysis of plastic wastes to high-value products, Energy Convers. Manag. 254 (2022) 115243. https://doi.org/10.1016/j.enconman.2022.115243.

[7] S. Kartik, H.K. Balsora, M. Sharma, A. Saptoro, R.K. Jain, J.B. Joshi, A. Sharma, Valorization of plastic wastes for production of fuels and value-added chemicals through pyrolysis – A review, Therm. Sci. Eng. Prog. 32 (2022) 101316. https://doi.org/10.1016/j.tsep.2022.101316.

[8] M.S. Abbas-Abadi, Y. Ureel, A. Eschenbacher, F.H. Vermeire, R.J. Varghese, J. Oenema, G.D. Stefanidis, K.M. Van Geem, Challenges and opportunities of light olefin production via thermal and catalytic pyrolysis of end-of-life polyolefins: Towards full recyclability, Prog. Energy Combust. Sci. 96 (2023) 101046. https://doi.org/10.1016/j.pecs.2022.101046.

[9] A.G. Buekens, H. Huang, Catalytic plastics cracking for recovery of gasoline-range hydrocarbons from municipal plastic wastes, Resour. Conserv. Recycl. 23 (1998) 163–181. https://doi.org/10.1016/S0921-3449(98)00025-1.

[10] G. Gałko, M. Rejdak, D. Tercki, M. Bogacka, M. Sajdak, Evaluation of the applicability of polymeric materials to BTEX and fine product transformation by catalytic and non-catalytic pyrolysis as a part of the closed loop material economy, J. Anal. Appl. Pyrolysis. 154 (2021). https://doi.org/10.1016/j.jaap.2021.105017.

[11] S.B. Lee, J. Lee, Y.F. Tsang, Y.-M.M. Kim, J. Jae, S.-C.C. Jung, Y.-K.K. Park, Production of value-added aromatics from wasted COVID-19 mask via catalytic pyrolysis, Environ. Pollut. 283 (2021) 117060. https://doi.org/10.1016/j.envpol.2021.117060.

[12] A.A.A. Inayat, A.A.A. Inayat, W. Schwieger, B. Sokolova, P. Lestinsky, Enhancing aromatics and olefins yields in thermo-catalytic pyrolysis of LDPE over zeolites: Role of staged catalysis and acid site density of HZSM-5, Fuel. 314 (2022) 123071. https://doi.org/10.1016/j.fuel.2021.123071.

[13] J. Wang, J. Jiang, X. Meng, M. Li, X. Wang, S. Pang, K. Wang, Y. Sun, Z. Zhong, R. Ruan, A.J. Ragauskas, Promoting Aromatic Hydrocarbon Formation via Catalytic Pyrolysis of Polycarbonate Wastes over Fe- And Ce-Loaded Aluminum Oxide Catalysts, Environ. Sci. Technol. 54 (2020) 8390–8400. https://doi.org/10.1021/acs.est.0c00899.

[14] K. Takuma, Y. Uemichi, A. Ayame, Product distribution from catalytic degradation of polyethylene over H-gallosilicate, Appl. Catal. A Gen. 192 (2000) 273–280. https://doi.org/10.1016/S0926-860X(99)00399-3.

[15] R. Bagri, P.T. Williams, Catalytic pyrolysis of polyethylene, J. Anal. Appl. Pyrolysis. 63 (2002) 29–41. https://doi.org/10.1016/S0165-2370(01)00139-5.

[16] J. Aguado, D.P. Serrano, G. San Miguel, Analysis of products generated from the thermal and catalytic degradation of pure and waste polyolefins using Py-GC/MS, J. Polym. Environ. 15 (2007) 107–118. https://doi.org/10.1007/s10924-007-0051-x.

[17] Y.H. Lin, M.H. Yang, T.F. Yeh, M.D. Ger, Catalytic degradation of high density polyethylene over mesoporous and microporous catalysts in a fluidised-bed reactor, Polym. Degrad. Stab. 86 (2004) 121–128. https://doi.org/10.1016/j.polymdegradstab.2004.02.015.

[18] D.P. Serrano, J. Aguado, J.M. Rodríguez, A. Peral, Catalytic cracking of polyethylene over nanocrystalline HZSM-5: Catalyst deactivation and regeneration study, J. Anal. Appl. Pyrolysis. 79 (2007) 456–464. https://doi.org/10.1016/j.jaap.2006.11.013.

[19] Y. Xue, P. Johnston, X. Bai, Effect of catalyst contact mode and gas atmosphere during catalytic pyrolysis of waste plastics, Energy Convers. Manag. 142 (2017) 441–451. https://doi.org/10.1016/j.enconman.2017.03.071.

[20] K. Akubo, M.A. Nahil, P.T. Williams, Aromatic fuel oils produced from the pyrolysis-catalysis of polyethylene plastic with metal-impregnated zeolite catalysts, J. Energy Inst. 92 (2019) 195–202. https://doi.org/10.1016/j.joei.2017.10.009.

[21] K. Ding, S. Liu, Y. Huang, S. Liu, N. Zhou, P. Peng, Y. Wang, P. Chen, R. Ruan, Catalytic microwave-assisted pyrolysis of plastic waste over NiO and HY for gasoline-range hydrocarbons production, Energy Convers. Manag. 196 (2019) 1316–1325. https://doi.org/10.1016/j.enconman.2019.07.001.

[22] M.S. Renzini, U. Sedran, L.B. Pierella, H-ZSM-11 and Zn-ZSM-11 zeolites and their applications in the catalytic transformation of LDPE, J. Anal. Appl. Pyrolysis. 86 (2009) 215–220. https://doi.org/10.1016/j.jaap.2009.06.008.

[23] A. Marcilla, A. Gómez-Siurana, F. Valdés, Catalytic cracking of low-density polyethylene over H-Beta and HZSM-5 zeolites: Influence of the external surface. Kinetic model, Polym. Degrad. Stab. 92 (2007) 197–204. https://doi.org/10.1016/j.polymdegradstab.2006.11.007.

[24] J. Aguado, D.P. Serrano, J.M. Escola, E. Garagorri, J.A. Fernández, Catalytic conversion of polyolefins into fuels over zeolite beta, Polym. Degrad. Stab. 69 (2000) 11–16. https://doi.org/10.1016/S0141-3910(00)00023-9.

[25] N. Miskolczi, T. Juzsakova, J. Sója, Preparation and application of metal loaded ZSM-5 and y-zeolite catalysts for thermo-catalytic pyrolysis of real end of life vehicle plastics waste, J. Energy Inst. 92 (2019) 118–127. https://doi.org/10.1016/j.joei.2017.10.017.

[26] G. Elordi, M. Olazar, G. Lopez, P. Castaño, J. Bilbao, Role of pore structure in the deactivation of zeolites (HZSM-5, Hβ and HY) by coke in the pyrolysis of polyethylene in a conical spouted bed reactor, Appl. Catal. B Environ. 102 (2011) 224–231. https://doi.org/10.1016/j.apcatb.2010.12.002.

[27] S.D. Anuar Sharuddin, F. Abnisa, W.M.A. Wan Daud, M.K. Aroua, A review on pyrolysis of plastic wastes, Energy Convers. Manag. 115 (2016) 308–326. https://doi.org/10.1016/j.enconman.2016.02.037.

[28] K. Moorthy Rajendran, V. Chintala, A. Sharma, S. Pal, J.K. Pandey, P. Ghodke, Review of catalyst materials in achieving the liquid hydrocarbon fuels from municipal mixed plastic waste (MMPW), Mater. Today Commun. 24 (2020) 100982.

https://doi.org/10.1016/j.mtcomm.2020.100982.

[29] M. Boronat, A. Corma, Factors Controlling the Acidity of Zeolites, Catal. Letters. 145 (2015) 162–172. https://doi.org/10.1007/s10562-014-1438-7.

[30] J.F. Mastral, C. Berrueco, M. Gea, J. Ceamanos, Catalytic degradation of high density polyethylene over nanocrystalline HZSM-5 zeolite, Polym. Degrad. Stab. 91 (2006) 3330–3338. https://doi.org/10.1016/j.polymdegradstab.2006.06.009.

[31] G. Lopez, M. Artetxe, M. Amutio, J. Bilbao, M. Olazar, Thermochemical routes for the valorization of waste polyolefinic plastics to produce fuels and chemicals. A review, Renew. Sustain. Energy Rev. 73 (2017) 346–368. https://doi.org/10.1016/j.rser.2017.01.142.

[32] M.S. Abbas-Abadi, M.N. Haghighi, H. Yeganeh, Evaluation of pyrolysis product of virgin high density polyethylene degradation using different process parameters in a stirred reactor, Fuel Process. Technol. 109 (2013) 90–95. https://doi.org/10.1016/j.fuproc.2012.09.042.

[33] M.S. Abbas-Abadi, M.N. Haghighi, H. Yeganeh, The effect of temperature, catalyst, different carrier gases and stirrer on the produced transportation hydrocarbons of LLDPE degradation in a stirred reactor, J. Anal. Appl. Pyrolysis. 95 (2012) 198–204. https://doi.org/10.1016/j.jaap.2012.02.007.

[34] V. Daligaux, R. Richard, M.H. Manero, Deactivation and regeneration of zeolite catalysts used in pyrolysis of plastic wastes—a process and analytical review, Catalysts. 11 (2021). https://doi.org/10.3390/catal11070770.

[35] S. Martey, B. Addison, N. Wilson, B. Tan, J. Yu, J.R. Dorgan, M.J. Sobkowicz, Hybrid Chemomechanical Plastics Recycling: Solvent-free, High-Speed Reactive Extrusion of Low-Density Polyethylene., ChemSusChem. 14 (2021) 4280–4290. https://doi.org/10.1002/cssc.202100968.

[36] A. Marcilla, M. del R. Hernández, Á.N. García, Study of the polymer-catalyst contact effectivity and the heating rate influence on the HDPE pyrolysis, J. Anal. Appl. Pyrolysis. 79 (2007) 424–432. https://doi.org/10.1016/j.jaap.2006.10.017.

[37] I. Muhammad, G. Manos, Simultaneous pretreatment and catalytic conversion of polyolefins into hydrocarbon fuels over acidic zeolite catalysts, Process Saf. Environ. Prot. 146 (2021) 702–717. https://doi.org/10.1016/j.psep.2020.12.012.

[38] V.P.S. Caldeira, A.G.D. Santos, D.S. Oliveira, R.B. Lima, L.D. Souza, S.B.C. Pergher, Polyethylene catalytic cracking by thermogravimetric analysis: Effects of zeolitic properties and homogenization process, J. Therm. Anal. Calorim. 130 (2017) 1939–1951. https://doi.org/10.1007/s10973-017-6551-6.

[39] D.P. Serrano, J. Aguado, J.M. Escola, E. Garagorri, Conversion of low density polyethylene into petrochemical feedstocks using a continuous screw kiln reactor, J. Anal. Appl. Pyrolysis. 58–59 (2001) 789–801. https://doi.org/10.1016/S0165-2370(00)00153-4.

[40] D.P. Serrano, J. Aguado, J.M. Escola, E. Garagorri, Performance of a continuous screw kiln reactor for the thermal and catalytic conversion of polyethylene-lubricating oil base mixtures, Appl. Catal. B Environ. 44 (2003) 95–105. https://doi.org/10.1016/S0926-3373(03)00024-9.

[41] M.S. Renzini, L.C. Lerici, U. Sedran, L.B. Pierella, Stability of ZSM-11 and BETA zeolites during the catalytic cracking of low-density polyethylene, J. Anal. Appl. Pyrolysis. 92 (2011) 450–455. https://doi.org/10.1016/j.jaap.2011.08.008.

[42] M. Heydariaraghi, S. Ghorbanian, A. Hallajisani, A. Salehpour, Fuel properties of the oils produced from the pyrolysis of commonly-used polymers: Effect of fractionating column, J. Anal. Appl. Pyrolysis. 121 (2016) 307–317. https://doi.org/10.1016/j.jaap.2016.08.010.

[43] A. Marcilla, A. Gómez-Siurana, F. Valdés, Catalytic pyrolysis of LDPE over H-beta and HZSM-5 zeolites in dynamic conditions. Study of the evolution of the process, J. Anal. Appl. Pyrolysis. 79 (2007) 433–442. https://doi.org/10.1016/j.jaap.2006.09.006.

[44] X. Tian, Z. Zeng, Z. Liu, L. Dai, J. Xu, X. Yang, L. Yue, Y. Liu, R. Ruan, Y. Wang, Conversion of

low-density polyethylene into monocyclic aromatic hydrocarbons by catalytic pyrolysis: Comparison of HZSM-5, Hβ, HY and MCM-41, J. Clean. Prod. 358 (2022) 131989. https://doi.org/10.1016/j.jclepro.2022.131989.

[45] I.C. Neves, G. Botelho, A. V. Machado, P. Rebelo, The effect of acidity behaviour of Y zeolites on the catalytic degradation of polyethylene, Eur. Polym. J. 42 (2006) 1541–1547. https://doi.org/10.1016/j.eurpolymj.2006.01.021.

[46] H. Wang, W. Xin, Surface acidity of H-beta and its catalytic activity for alkylation of benzene with propylene, Catal. Letters. 76 (2001) 225–229. https://doi.org/10.1023/A:1012244526995.

[47] A. Aho, N. Kumar, K. Eränen, T. Salmi, M. Hupa, D.Y. Murzin, Catalytic pyrolysis of biomass in a fluidized bed reactor: Influence of the acidity of h-beta zeolite, Process Saf. Environ. Prot. 85 (2007) 473–480. https://doi.org/10.1205/psep07012.

[48] Y. Miyamoto, N. Katada, M. Niwa, Acidity of β zeolite with different Si/Al2 ratio as measured by temperature programmed desorption of ammonia, Microporous Mesoporous Mater. 40 (2000) 271–281. https://doi.org/10.1016/S1387-1811(00)00264-X.

[49] J. Agullo, N. Kumar, D. Berenguer, D. Kubicka, A. Marcilla, A. Gómez, T. Salmi, D.Y. Murzin, Catalytic pyrolysis of low density polyethylene over H-β, H-Y, H-Mordenite, and H-Ferrierite zeolite catalysts: Influence of acidity and structures, Kinet. Catal. 48 (2007) 535–540. https://doi.org/10.1134/S002315840704009X.

[50] J. Aguado, D.P. Serrano, G.S. Miguel, J.M. Escola, J.M. Rodríguez, Catalytic activity of zeolitic and mesostructured catalysts in the cracking of pure and waste polyolefins, J. Anal. Appl. Pyrolysis. 78 (2007) 153–161. https://doi.org/10.1016/j.jaap.2006.06.004.

[51] P. Rex, V. Ganesan, V. Sivashankar, S. Tajudeen, Prospective review for development of sustainable catalyst and absorbents from biomass and application on plastic waste pyrolysis, Int. J. Environ. Sci. Technol. (2022). https://doi.org/10.1007/s13762-022-04292-8.

[52] S. Kumar, A.K. Panda, R.K. Singh, A review on tertiary recycling of high-density polyethylene to fuel, Resour. Conserv. Recycl. 55 (2011) 893–910. https://doi.org/10.1016/j.resconrec.2011.05.005.

[53] O. Dogu, M. Pelucchi, R. Van de Vijver, P.H.M. Van Steenberge, D.R. D'hooge, A. Cuoci, M. Mehl, A. Frassoldati, T. Faravelli, K.M. Van Geem, The chemistry of chemical recycling of solid plastic waste via pyrolysis and gasification: State-of-the-art, challenges, and future directions, Prog. Energy Combust. Sci. 84 (2021) 100901. https://doi.org/10.1016/j.pecs.2020.100901.

[54] G. Elordi, M. Olazar, G. Lopez, M. Amutio, M. Artetxe, R. Aguado, J. Bilbao, Catalytic pyrolysis of HDPE in continuous mode over zeolite catalysts in a conical spouted bed reactor, J. Anal. Appl. Pyrolysis. 85 (2009) 345–351. https://doi.org/10.1016/j.jaap.2008.10.015.

[55] S.T. Okonsky, J.V.J. Krishna, H.E. Toraman, Catalytic co-pyrolysis of LDPE and PET with HZSM-5, H-beta, and HY: experiments and kinetic modelling, React. Chem. Eng. 7 (2022) 2175–2191. https://doi.org/10.1039/d2re00144f.

[56] D. Fu, A. Lucini Paioni, C. Lian, O. van der Heijden, M. Baldus, B.M. Weckhuysen, Elucidating Zeolite Channel Geometry–Reaction Intermediate Relationships for the Methanol-to-Hydrocarbon Process, Angew. Chemie - Int. Ed. 59 (2020) 20024–20030. https://doi.org/10.1002/anie.202009139.

[57] Y.J. Lee, J.H. Kim, S.H. Kim, S.B. Hong, G. Seo, Nanocrystalline beta zeolite: An efficient solid acid catalyst for the liquid-phase degradation of high-density polyethylene, Appl. Catal. B Environ. 83 (2008) 160–167. https://doi.org/10.1016/j.apcatb.2008.02.013.

[58] A. Marcilla, M.I. Beltrán, F. Hernández, R. Navarro, HZSM5 and HUSY deactivation during the catalytic pyrolysis of polyethylene, Appl. Catal. A Gen. 278 (2004) 37–43. https://doi.org/10.1016/j.apcata.2004.09.023.

[59] L. Dai, N. Zhou, H. Li, Y. Wang, Y. Liu, K. Cobb, Y. Cheng, H. Lei, P. Chen, R. Ruan, Catalytic fast pyrolysis of low density polyethylene into naphtha with high selectivity by dual-catalyst tandem catalysis, Sci. Total Environ. 771 (2021) 144995.

https://doi.org/10.1016/j.scitotenv.2021.144995.

[60] J. Wang, J. Jiang, X. Wang, S. Pang, Y. Sun, X. Meng, M. Li, R. Ruan, A.J. Ragauskas, Enhanced BTEX formation via catalytic fast pyrolysis of styrene-butadiene rubber: Comparison of different catalysts, Fuel. 278 (2020). https://doi.org/10.1016/j.fuel.2020.118322.

[61] P. Gaurh, H. Pramanik, Production of benzene/toluene/ethyl benzene/xylene (BTEX) via multiphase catalytic pyrolysis of hazardous waste polyethylene using low cost fly ash synthesized natural catalyst, Waste Manag. 77 (2018) 114–130. https://doi.org/10.1016/j.wasman.2018.05.013.

[62] M. Cocchi, D. De Angelis, L. Mazzeo, P. Nardozi, V. Piemonte, R. Tuffi, S. Vecchio Ciprioti, Catalytic Pyrolysis of a Residual Plastic Waste Using Zeolites Produced by Coal Fly Ash, Catalysts. 10 (2020) 1113. https://doi.org/10.3390/catal10101113.

[63] D.P. Serrano, J. Aguado, J.M. Escola, J.M. Rodríguez, Influence of nanocrystalline HZSM-5 external surface on the catalytic cracking of polyolefins, J. Anal. Appl. Pyrolysis. 74 (2005) 353–360. https://doi.org/10.1016/j.jaap.2004.11.037.

[64] Q. Zhang, K. Qiu, B. Li, T. Jiang, X. Zhang, L. Ma, T. Wang, Isoparaffin production by aqueous phase processing of sorbitol over the Ni/HZSM-5 catalysts: Effect of the calcination temperature of the catalyst, Fuel. 90 (2011) 3468–3472. https://doi.org/10.1016/j.fuel.2011.06.046.

[65] S.J. Han, S.K. Kim, A. Hwang, S. Kim, D.Y. Hong, G. Kwak, K.W. Jun, Y.T. Kim, Non-oxidative dehydroaromatization of methane over Mo/H-ZSM-5 catalysts: A detailed analysis of the reaction-regeneration cycle, Appl. Catal. B Environ. 241 (2019) 305–318. https://doi.org/10.1016/j.apcatb.2018.09.042.

[66] M. Rahman, A. Infantes-Molina, A.S. Hoffman, S.R. Bare, K.L. Emerson, S.J. Khatib, Effect of Si/Al ratio of ZSM-5 support on structure and activity of Mo species in methane dehydroaromatization, Fuel. 278 (2020). https://doi.org/10.1016/j.fuel.2020.118290.

[67] Y. Zhang, S. Wu, X. Xu, H. Jiang, Ethane aromatization and evolution of carbon deposits over nanosized and microsized Zn/ZSM-5 catalysts, Catal. Sci. Technol. 10 (2020) 835–843. https://doi.org/10.1039/c9cy01903k.

[68] F.J. Sotomayor, K.A. Cychosz, M. Thommes, Characterization of Micro/Mesoporous Materials by Physisorption: Concepts and Case Studies, Acc. Mater. Surf. Res. 3 (2018) 34–50. https://www.hyomen.org/wp-content/uploads/papers/vol3_no2/sotomayor/sotomayor_40.pdf.

[69] C. Zhang, S. Li, S. Bao, Sustainable Synthesis of ZSM-5 Zeolite from Rice Husk Ash Without Addition of Solvents, Waste and Biomass Valorization. 10 (2019) 2825–2835. https://doi.org/10.1007/s12649-018-0356-0.

[70] J. Aguado, D.P. Serrano, J.M. Escola, L. Briones, Deactivation and regeneration of a Ni supported hierarchical Beta zeolite catalyst used in the hydroreforming of the oil produced by LDPE thermal cracking, Fuel. 109 (2013) 679–686. https://doi.org/10.1016/j.fuel.2013.03.011.

[71] X. Hou, L. Zhao, Z. Diao, Roles of Alkenes and Coke Formation in the Deactivation of ZSM-5 Zeolites During n-Pentane Catalytic Cracking, Catal. Letters. 150 (2020) 2716–2725. https://doi.org/10.1007/s10562-020-03173-4.

[72] Y. Fan, X. Bao, G. Shi, Hβ/HZSM-5 composite carrier supported catalysts for olefins reduction of FCC gasoline via hydroisomerization and aromatization, Catal. Letters. 105 (2005) 67–75. https://doi.org/10.1007/s10562-005-8007-z.

[73] P. Castaño, G. Elordi, M. Olazar, A.T. Aguayo, B. Pawelec, J. Bilbao, Insights into the coke deposited on HZSM-5, Hβ and HY zeolites during the cracking of polyethylene, Appl. Catal. B Environ. 104 (2011) 91–100. https://doi.org/10.1016/j.apcatb.2011.02.024.

[74] Y. Bi, X. Lei, G. Xu, H. Chen, J. Hu, Catalytic fast pyrolysis of kraft lignin over hierarchical HZSM-5 and Hβ zeolites, Catalysts. 8 (2018). https://doi.org/10.3390/catal8020082.

Chapter 4

4. Effect of zinc doping of ZSM-5 zeolite combined with multiphase catalytic pyrolysis on the cracking of polyethylene

4.1. Summary

This chapter explores the effect of HZSM-5 and ZnZSM-5 zeolites on the pyrolysis of LLDPE. The study is divided into two parts, with the global objective to maximise aromatic compound production. The initial segment encompasses a meticulous investigation involving three distinct operational arrangements at a temperature of 500 °C. These arrangements include Mix, Layer, and Mix/Layer arrangements, each focusing on elucidating the behaviour of liquid, vapour, and the combined liquid-vapour phases upon interaction with the powdered zeolite. Notably, the Mix/Layer arrangement exhibited superior performance in terms of aromatic compound production. Subsequently, the research compared LLDPE cracking at 450 °C and 500 °C, employing the previously identified Mix/Layer arrangement. Despite the anticipated preference for chain-end scission reactions at higher temperatures, it was observed that the more favourable aromatic yields were achieved at 450 °C. These investigations also showed the substantial influence of zeolite type on the outcomes. Specifically, utilising Zn-doped zeolite resulted in higher liquid yield, increased olefin production, and enhanced selectivity towards BTEX compounds. Notably, the acidity nature of the zeolite emerged as a critical factor impacting the overall activity, product distribution, and the complex process of aromatisation reactions. To gain a deeper understanding of the physicochemical differences, particularly concerning acid properties and their influence on LLDPE cracking, a comprehensive characterisation of HZSM-5 and ZnZSM-5 zeolites was undertaken; this entailed employing various analytical techniques, including XRD, N_2-physisorption, XPS, ICP-OES, EMPA, H_2-TPR, NH_3-TPD, Py-IR, and TGA.

4.2. Introduction

Zeolites find extensive utility as catalysts across diverse industrial processes, including the pyrolysis of waste plastics to yield valuable chemicals, notably aromatics [1]. Amongst the spectrum of zeolites explored in plastic waste pyrolysis, the ZSM-5 zeolite has garnered substantial attention. Its significance lies in its shape selectivity, which favours the production of aromatic compounds, and in its physical-chemical attributes and inherent stability [1], [2].

ZSM-5 zeolite boasts a unique pore structure, characterised by a pore size of approximately 0.55 nm, enabling the selective conversion of long-chain hydrocarbons into shorter-chain hydrocarbons and aromatics. This specificity extends to the selective formation of monoaromatics with a carbon number

of six or more. Additionally, ZSM-5 exhibits high acidity, which facilitates the cracking of long-chain hydrocarbons, further promoting the generation of aromatics [3], [4].

However, in the case of polyethylene, ZSM-5 zeolite's capacity to yield aromatic products can be constrained by its intrinsic acidity. Consequently, an emerging interest is enhancing zeolite catalytic properties by promoting it with metal ions [5]–[9]. Metal-doped ZSM-5 zeolites, which incorporate metals like Fe, Cu, Co, Ga, Mo, or Ni, can be prepared through diverse methods, including impregnation, ion exchange, structural incorporation, or precursor mixing followed by activation [5]–[10]. Irrespective of the preparation method, the desired catalytic outcomes can be achieved, although metal ion exchange often leads to more thermally stable, immobilised, non-volatile ionic species that do not reduce to zero-valent forms [8]. Incorporating metal ions moderates zeolite acidity, augmenting its catalytic capabilities [5]–[8].

Zinc, in particular, is a promoter of the ZSM-5 zeolite in different aromatisation reactions, such as in the aromatisation of 1-hexene, methanol, and ethylene, among others [10]–[14]. Zn also showed promising results in catalysts for this application, with zeolites different than ZSM-5 [9], [15]–[17], modifying zeolites properties by introducing new Lewis acid sites through Zn^{2+} [17], [18] without enhancing Brønsted acid sites [18], and thus increasing selectivity on aromatisation reactions [17]. Indeed, Lewis acid sites exhibit selectivity in forming aromatics through cyclisation and hydrogen transfer processes [17].

Pierella et al. [19] employed micro and mesoporous materials with Zn, Mo, or H as active sites in the catalytic cracking of HDPE, ultimately achieving an enhanced selectivity for BTX compounds, particularly pronounced with Zn-ZSM-11. Renzini et al. [16] conducted a comparative study involving H-ZSM-11 zeolite and Zn-ZSM-11 zeolite in the pyrolysis of LDPE. Their research revealed a notable increase in the liquid phase yield when employing Zn-ZSM-11, characterised by a substantial presence of C_6-C_9 aromatic hydrocarbons. This outcome was attributed to the heightened concentration of Lewis acid sites, which actively facilitated the aromatisation process. Later, Lerici et al. [17] conducted an extensive study on the stability of two zinc-doped zeolites in cracking low-density polyethylene (LDPE) to yield aromatic compounds. Their research demonstrated that Zn-ZSM-11 zeolite exhibited consistent stability throughout 11 reaction cycles. This remarkable stability suggested that the unique shape selectivity of Zn-ZSM-11 zeolite plays a pivotal role in mitigating deactivation due to coke deposition in the catalytic transformation of polymers. In contrast, Zn-BETA zeolite did not yield the same level of stability and performance as Zn-ZSM-11 zeolite.

In parallel to securing a catalyst aligned with aromaticity expectations, optimising the pyrolysis process is indispensable; this involves, among other considerations, improving catalyst-polymer contact to maximise aromatic production while mitigating potential catalyst damage. This result was clearly stated in the previous chapter, where extrusion was used as a pre-treatment for preparing the polymer/catalyst mixture. Numerous studies have explored configurations to yield optimal results. For instance, comparative investigations have favoured fixed bed systems over batch pyrolysis in static environments, where the polymer transitions from a liquid to a gas phase, delivering superior outcomes in both polymer

pyrolysis and aromatic compound selectivity [20]. Moreover, Gaurh and Pramanik [2] have explored various contact phases between waste polyethylene and ZSM-5 zeolite at different temperatures (from 500 to 800 °C) and the catalyst-to-polymer ratio of 1:20, highlighting one configuration that maximises aromatic yields, the multiphase at 700 °C, which means a combination of cracking phases: a first cracking is generated with half of the catalyst in contact with a polymer in liquid phase followed by a second cracking with the other half of the catalyst and the vapour phase generated in the first cracking.

Expanding upon the investigations outlined in the preceding chapter regarding the extrusion of polymer catalysts and their comparison with powdered configurations for optimising blend homogeneity, the present chapter embarks on a more profound inquiry. Its objectives encompass a comprehensive discussion of the attributes of HZSM-5 and zinc-ion-exchanged ZSM-5 zeolites and their applications within the field of polyethylene pyrolysis for the synthesis of aromatic compounds. In addition, the chapter aspires to refine this pyrolysis process through an extensive comparative analysis of three distinct scenarios: the interaction of liquid polyethylene with the catalyst (***Mix*** configuration), the interaction of gaseous polyethylene with the catalyst (***Layer*** configuration), and a hybrid configuration that amalgamates both of these modalities (***Mix/Layer*** configuration). The selection of ion exchange as the preferred method for preparing doped zeolites is underpinned by its capability to furnish the desired ion exchange capacity, stemming from introducing tetrahedral Zinc and creating a negative lattice charge [21].

4.3. Experimental

The Zn-doped zeolite, denoted as ZnZSM-5, was synthesised using the ion-exchange method, as detailed in section **2.6.3**. The doped zeolite and the protonated zeolite (HZSM-5) underwent calcination under dynamic conditions, following the procedure outlined in section **2.6.4**.

The pyrolysis of polyethylene in the presence of ZnZSM-5 and HZSM-5 zeolites was conducted as described in section **2.3**. Catalytic pyrolysis was carried out at 450 °C and 500 °C. A catalyst-to-polymer ratio of 1:10 was employed for these catalytic tests, using 1 g of LLDPE in pellet form as the feedstock. The different types of yields were evaluated, as shown in section **2.3**.

Various catalyst arrangements were implemented for the experiments carried out at 500 °C pyrolysis, each involving different placement of the catalyst components, as illustrated in **Figure 2.24**. The first arrangement (***Mix*** configuration) entailed the Mix of pelletised polymer and powdered catalyst, with the polymer assuming a liquid state during the reaction. In the second arrangement (***Layer*** configuration), the liquid-state polymer had initial contact with half of the powdered catalyst, followed by a second contact with the remaining catalyst to crack the resulting vapours from the first step. The third arrangement (***Mix/Layer*** configuration) involved allowing the vapours produced during the initial thermal cracking of the polymer to interact solely with the catalyst.

For the experiments carried out at 450 °C, only Mix/Layer arrangements were employed and compared to the results obtained when the pyrolysis is performed at 500 °C. The layer arrangement demands an

initial thermal cracking step, feasible only at temperatures exceeding 480 °C if a complete conversion of the LLDPE is to be achieved.

4.4. Results and Discussion

4.4.1. Zeolite characterisation

Structural properties

Figure 4.1 presents the XRD patterns of HZSM-5 and the doped zeolite, with NH_4^+ZSM-5 utilised as a reference. The relative crystallinity values of the ZSM-5 samples were calculated based on the height of the strongest peak at 2θ = 23.03°. The XRD patterns suggested that introducing Zinc by ion exchange did not affect the pristine structure of ZSM-5 zeolite [11]. However, the relative crystallinity results indicate a significant reduction in crystallinity upon zeolite doping, as detailed in **Table 4.1**. Other researchers who have introduced Zinc to zeolites have reported similar trends [17], [22]. The X-ray diffraction analysis revealed the absence of discernible ZnO crystallite diffraction peaks (associated with JCPD = 31.6°, 34.2°, 36.1°, 56.6°) within the zinc-doped zeolite. This observation suggests a high degree of dispersion for the Zn^{2+} cation species on the zeolite's surface [23].

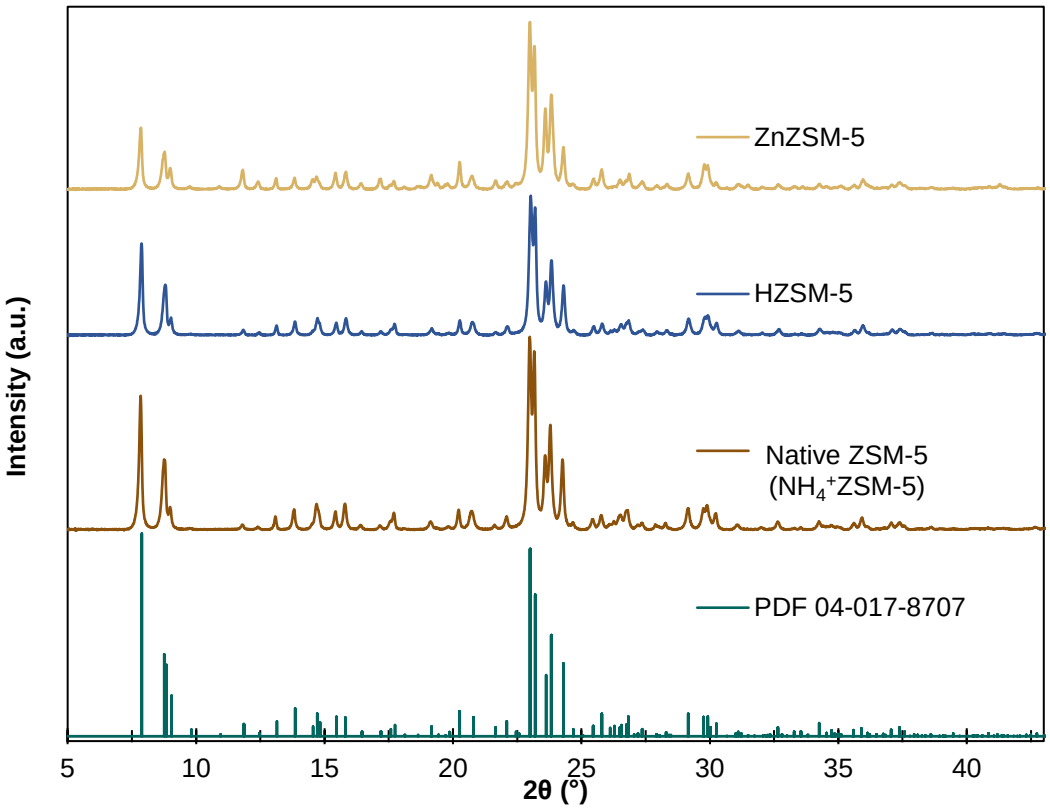

Figure 4.1. XRD patterns of HZSM-5 and ZnZSM-5 catalysts.

The textural characteristics of the zeolites were assessed via N_2 physisorption isotherms, as depicted in **Figure 4.2** (a). These findings have been compiled in **Table 4.1**. It is discernible from **Figure 4.2** (a)

that the N_2 physisorption isotherms for the catalysts exhibit typical Type IV isotherms, accompanied by a discernible H4 hysteresis loop. Following the incorporation of Zn, there is a noticeable reduction in physisorption, implying the successful insertion of Zn [1], [11]; this led to a reduction in both pore and surface area. Notably, the specific and external surface areas, along with the micropore volume of the HZSM-5 zeolite, experienced significant reductions. This trend of reduced surface area with the introduction of metal promoters has been well-documented in numerous studies [7], [11], [19]. This transformation is also reflected in the ZSM-5 micropore peak, as illustrated in **Figure 4.2** (b), which notably diminishes in the doped zeolite. Conversely, porosity within the 3–9 nm range (mesopores) and the 20–100 nm range (primarily macropores) maintains a comparable distribution in both doped and undoped zeolites.

Table 4.1 Textural properties and relative crystallinity of the ZSM-5 zeolites.

Catalyst	Specific surface ($m^2.g^{-1}$)			V_{micro*}	Relative
	S_{BET}	S_{ext}	S_{micro}*	($cm^3.g^{-1}$)	Crystallinity (%)**
HZSM-5	413	30	383	0.16	96
ZnZSM-5	369	20	350	0.14	87

**t-Plot Method.*

***Relative crystallinity considering the NH_4^+ZSM-5 sample as 100 % crystallinity.*

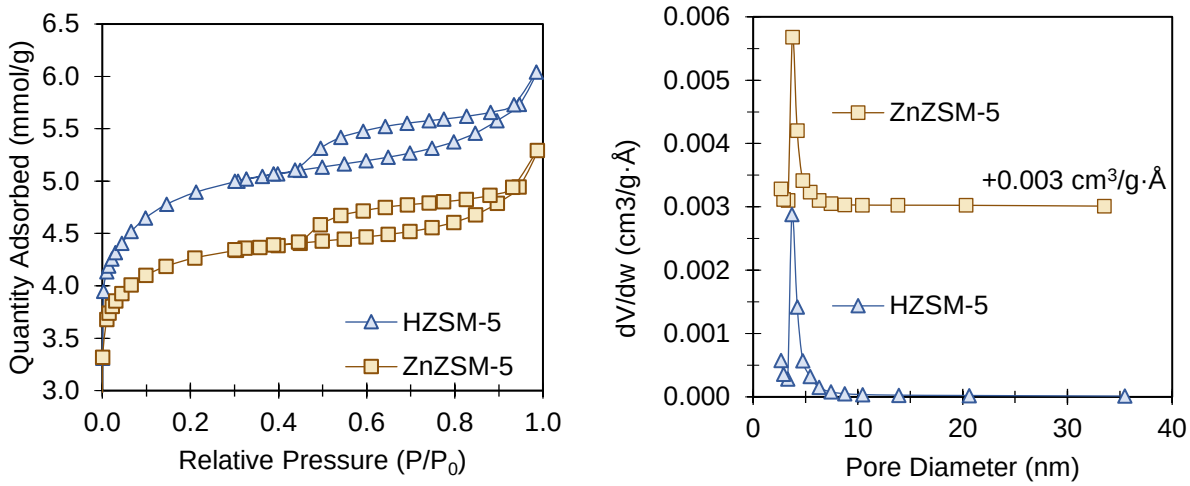

Figure 4.2. N_2-physisorption isotherms at -196 °C (a) and BJH pore size distribution (b) of HZSM-5 and ZnZSM-5 catalysts.

Chemical composition

The surface composition of the zeolites underwent thorough investigation via XPS analysis. The findings from the XPS analysis further substantiated the zinc-exchange process by confirming the presence of Zinc in a +2 valence state. This single charge state was notably characterised by the symmetrical and finely resolved XPS peaks at 1022.6 and 1045.7 eV (refer to **Figure 4.3** (a)), corresponding to the Zn

$2p_{3/2}$ and Zn $2p_{1/2}$ energy levels, respectively. [10], [14], [23]. These two are separated by 23.1 eV, in line with the reported results in the literature [24], [25].

In the case of both zeolites, it is noteworthy that the full width at half maximum (FWHM) of the Si 2p and O 1s photopeaks remained constant throughout the analysis (**Table 4.2**). In contrast, the FWHM of the Al 2p photopeaks exhibited a higher numerical count than those acquired from Si 2p and O 1s photopeaks. This observation strongly indicates the presence of aluminium species in a coordination state distinct from the conventional tetrahedral coordination [5], [6], and it will be better detailed in **Chapter 5.**

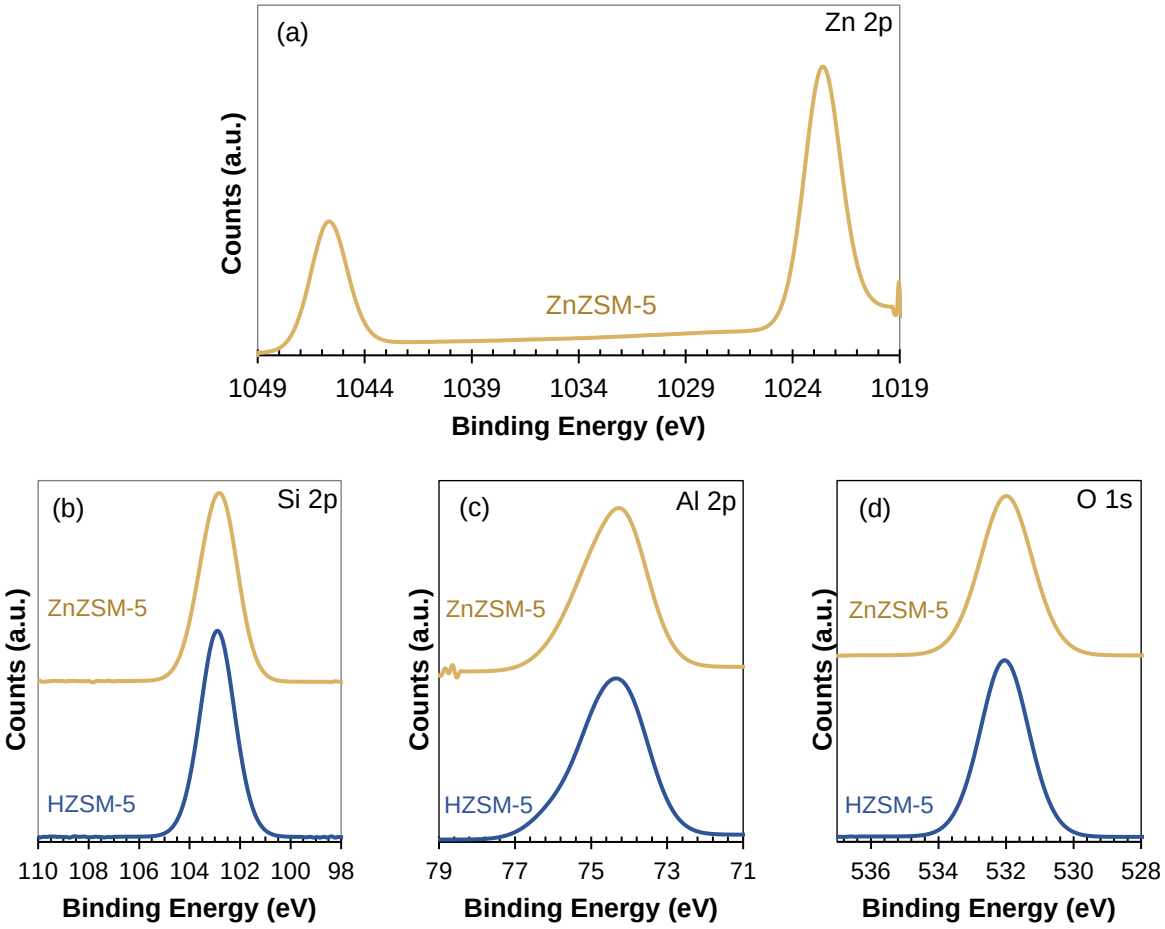

Figure 4.3. XPS core-level spectra of Zn 2p (a) of ZnZSM-5 and XPS core-level spectra of Si 2p (b), Al 2p (c) and O 1s (d) of the HZSM-5 and ZnZSM-5 zeolites.

Si/Al ratios and metal content were calculated and subsequently compared with the ICP analysis data of the bulk materials. As detailed in **Table 4.2**, it is apparent that the ionic exchange process had no discernible impact on the Si and Al content, aligning with the results obtained from XPS and ICP-OES analysis.

An intriguing observation pertains to the surface Zn deficiency relative to the bulk Zn content. This research sought to use a Si/Zn ratio of 32.7, corresponding to 2.5 wt. %. Zn introduced into the zeolite, ICP-OES analysis yielded a Si/Zn ratio of 30.4 (equivalent to 2.7 wt. % Zn), while XPS analysis indicated

a Si/Zn ratio of 105.8. This phenomenon could arise from the partial integration of Zn species within the inner surfaces of the zeolite crystals. Alternatively, it may be attributed, in part, to the intrinsic sensitivity of XPS to the surface region of the analysed zeolite crystals, potentially resulting in minor discrepancies in the relative quantitative analysis [26].

Table 4.2 XPS and ICP-OES results of ZSM-5 zeolites.

Catalyst	Si/Al		Si/Zn		Si 2p		Al 2p		O 1s		Zn 2p	
	XPS	ICP	XPS	ICP	BE (eV)	FWHM (eV)	BE (eV)	FWHM (eV)	BE (eV)	FWHM (eV)	BE (eV)	FWHM (eV)
HZSM-5	10.2	10.6	-	-	102.9	1.6	74.5	2.1	532.1	1.6	-	-
ZnZSM-5	10.2	10.5	105.8	30.4	102.9	1.7	74.2	2.0	531.9	1.7	1022.6 1045.7	2.0 2.0

Figure 4.4 displays electron microprobe images of both HZSM-5 and ZnZSM-5 zeolites. This analysis was conducted to examine the distribution of the metal within the zeolite structure. It is evident from the images that the dispersion of Zinc is non-uniform, and it agrees with XPS results.

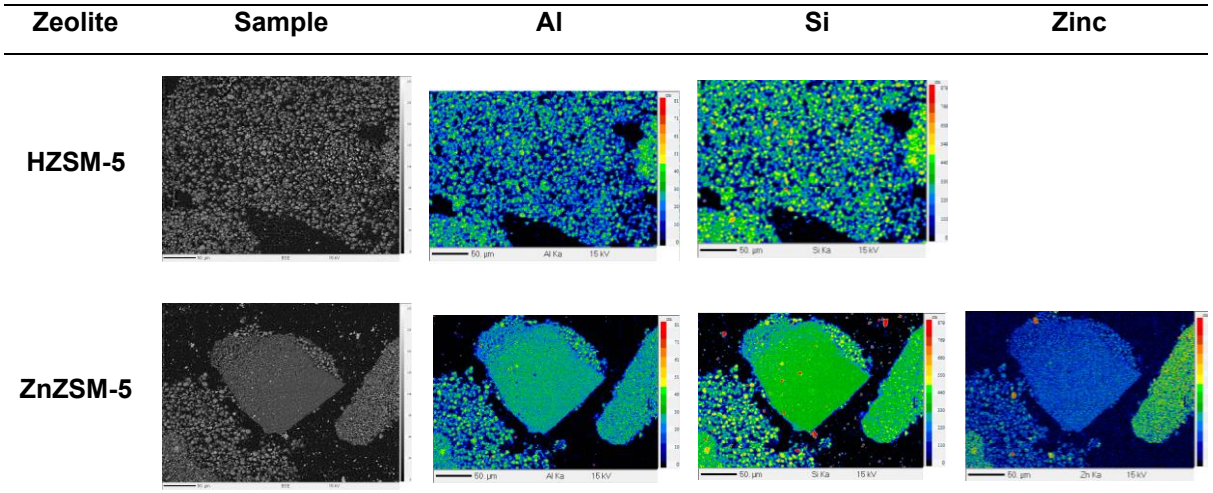

Figure 4.4. Electron microprobe images of HZSM-5 and ZnSM-5 zeolites.

The H_2-TPR analysis (profile not shown) exhibited a distinct absence of hydrogen consumption. This absence means Zn species are complex to reduce [25], suggesting that zinc species interact strongly with Si-OH-Al groups of ZSM-5 zeolite, so the Zn^{+2} ions become structurally stable and difficult to reduce. The absence of zinc reduction during the process also signifies nanosized zinc oxide's non-formation or zinc metal reduction throughout the ion-exchange phase [14]. Peaks associated with the reduction of these cations are discernible in samples containing transition metal ions [14] and usually start to reduce around 580 °C [21], [27].

Acidity

Ammonia temperature-programmed desorption measurements (NH_3-TPD) were performed to study the zeolite acidity. The NH_3-TPD profiles, as illustrated in **Figure 4.5**, were analysed to determine the overall acidity of Zn-doped and protonic zeolites. These TPD plots conform to the typical profile seen in MFI zeolites [3] and correspond to acid sites linked to the acidic Si-OH-Al group [28], [29] (Brønsted acid sites), along with extra-framework Al [29], [30] or stemming from framework defects [29] (Lewis acid sites). Two distinct NH_3 desorption peaks are observable. The peak located in the lower temperature range, approximately 300 °C, is attributed to weak acid sites, while the peak in the higher temperature range, approximately 450 °C, is associated with strong acid sites [11]. The NH_3-TPD profiles were integrated to calculate the acid strength distribution in both zeolites. The acquired peak data achieved this through Gaussian deconvolution [32]. The specific values for total acidity, weak acidity, and strong acidity are documented in **Table 4.3**.

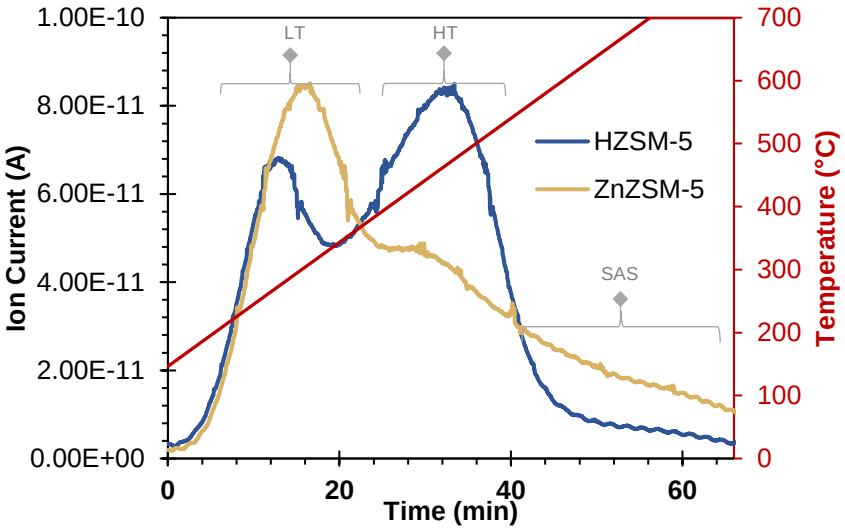

Figure 4.5. NH_3-TPD curves of HZSM-5 (blue) and ZnZSM-5 (yellow) zeolites.

Notably, the total acidity of HZSM-5 is lower by 0.17 $mmol.g^{-1}$ than that of ZnZSM-5. These total acidity values align with those reported in existing literature [31]–[34]. The findings underscore the profound impact of doping on acid site density and the equilibrium between weak and strong acidity (W-S) fractions. Notably, the W/S ratio for HZSM-5 remains visibly low, signifying its elevated strong acidity compared to weak acidity. Compared to protonated zeolite, Zinc doping increased approximately 32 % in weak acid sites and slightly over 15 % in strong acid sites per square meter. Notably, the LT peak exhibited a positive shift of 35 °C, signifying an enhancement in the acid strength of weak acid sites. Conversely, the HT peak displayed a lower temperature, registering a reduction of 39 °C. Nevertheless, it is apparent that upon concluding the analysis, the curve for this zeolite does not reach zero. This observation implies that ammonia remains adsorbed within the zeolite, conceivably within strongly acid sites (SAS) generated by incorporating zinc ions [10].

Table 4.3 NH_3-TPD results of HZSM-5 zeolites from different types of doping

Catalyst	Temperature (°C)		Acidity (mmol.g^{-1})			Acidity (µmol.m^{-2})			W/S Acidity
	LT Peak	HT Peak	Total	Weak	Strong	Total	Weak	Strong	
HZSM-5	274	475	**1.50**	0.45	1.06	**3.63**	1.11	2.52	**0.4**
ZnZSM-5	309	436	**1.67**	0.58	1.09	**4.52**	1.58	2.94	**0.5**

The NH_3-TPD, in conjunction with the Py-IR results, provided further insights into the acid properties of the two catalysts. The infrared (IR) spectra illustrating the pyridine adsorption on HZSM-5 and ZnZSM-5 zeolites after evacuation at temperatures of 150 °C, 250 °C, 350 °C, and 450 °C are depicted in **Figure 4.6**. In these spectra, two prominent bands at 1545 cm^{-1} and 1455 cm^{-1} correspond to pyridine adsorption on Brønsted and Lewis acid sites, respectively [22], [35]. Additionally, the band at 1490 cm^{-1} reflects the combined contribution of both types of acidity [35]. The Brønsted acid sites, associated with pyridine adsorbed at 1545 cm^{-1}, are primarily derived from tetrahedral configurations [36], constituting approximately 77 % and 48 % of the total acid sites for HZSM-5 and ZnZSM-5 zeolites, respectively (as detailed in **Table 4.4**.

Table 4.4 Total, Brønsted and Lewis acid sites of ZSM-5 Catalysts Measured by Pyridine FT-IR

Catalyst	Acidity (µmol.g^{-1})							B/L
	Total Acidity (B+L)	Brønsted (B)			Lewis (L)			
		Weak	Strong	Total	Weak	Strong	Total	
HZSM-5	686	126 (18 %)	405 (59 %)	531	97 (14 %)	61 (9 %)	158	3.4
ZnZSM-5	559	108 (19 %)	164 (29 %)	272	100 (18 %)	187 (33 %)	287	0.9

The densities of Brønsted and Lewis acid sites, as presented in **Table 4.4**, reveal a higher density of Brønsted acid sites in HZSM-5. This observation aligns with the findings of Anunziata et al. [37], who proposed that zinc ions are initially incorporated as counter ions, inhibiting strong Brønsted acidic sites. Indeed, the Zn^{2+} ions introduced into the zeolites localise to the negatively charged tetrahedral AlO_4^-, leading to a partial decrease of the Brønsted acid sites and possible blockage of the remaining OH groups [17], [22], [37]. Additionally, ZnZSM-5 has incorporated a heightened density of Lewis acid sites, especially strong Lewis acid sites, compared to the non-doped zeolite. Indeed, the Zn^{+2} introduction creates new and stronger Lewis acid sites [37]. It is hypothesised that Zinc is present as an O–Zn–O species, wherein a zinc atom substitutes two protons, as illustrated in **Figure 4.7**. This assumption aligns with the Py-IR findings, indicating the formation of Lewis acid sites by replacing two Brønsted acid sites. The Brønsted/Lewis acid site ratio is measured at 0.9 for ZnZSM-5 compared to 3.4 for the HZSM-5 zeolite. This trend has been previously documented with other zeolite types when subjected to zinc doping [11], [22].

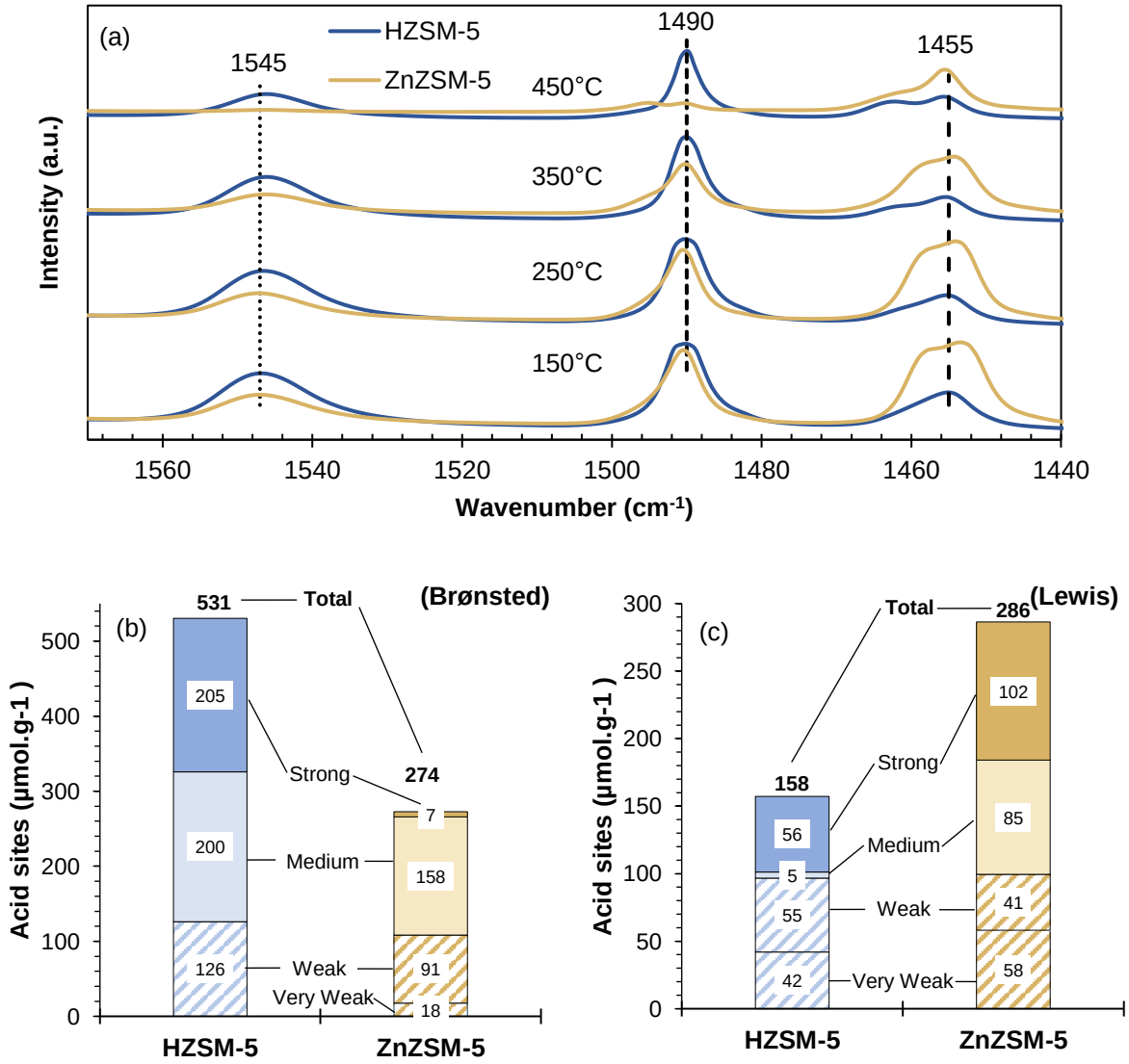

Figure 4.6. Pyridine FT-IR of HZSM-5 and ZnZSM-5 zeolites after desorption at 150, 250, 350, and 450 °C (a). And their respective Brønsted (b) and Lewis (c) acid sites distribution as functions of the strength of the acid site, very weak (150 °C), weak (250 °C), medium (350 °C) and strong (>450 °C).

Investigating the structural and chemical properties of doped ZSM-5 zeolite generated several significant findings. XRD, XPS, and H_2-TPR demonstrated that Zn^{2+} ions were correctly introduced via ion exchange, primarily located on the internal surface of the zeolite, and had insignificant impacts on the zeolite's crystalline structure. The disparity between the surface Zn content and the bulk Zn content could be attributed to a non-uniform distribution of Zinc, as shown by electron microprobe analyses. N_2-physisorption showed that the total surface area, especially the external surface, is decreased because of doping. Acidity analyses showed that introducing zinc ions created sites with stronger acidity, particularly of the Lewis type, potentially at the expense of Brønsted acid sites with a potential greater selectivity to aromatic compounds, especially BTEX. This will be studied in the following part of this chapter.

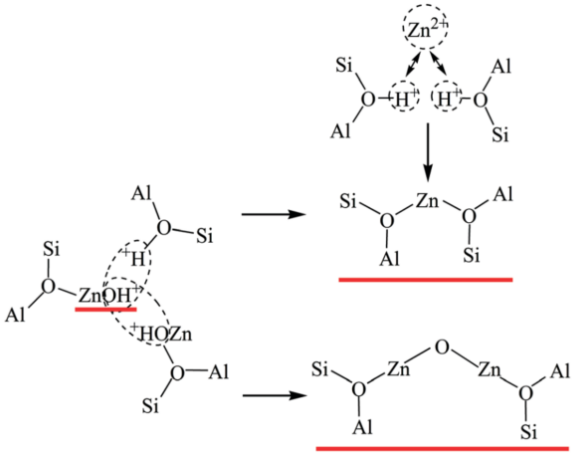

Figure 4.7. Zinc species reported in the literature from ref [13]

4.4.2. Pyrolysis of PE

Activity

The TG and DTG curves for both LLDPE and the corresponding LLDPE/Zeolite mixture, with a catalyst-to-polymer ratio of 1:10, are depicted in **Figure 4.8**. Detailed information, including total weight loss, relative activity, and specific degradation temperatures, can be found in **Table 4.5**.

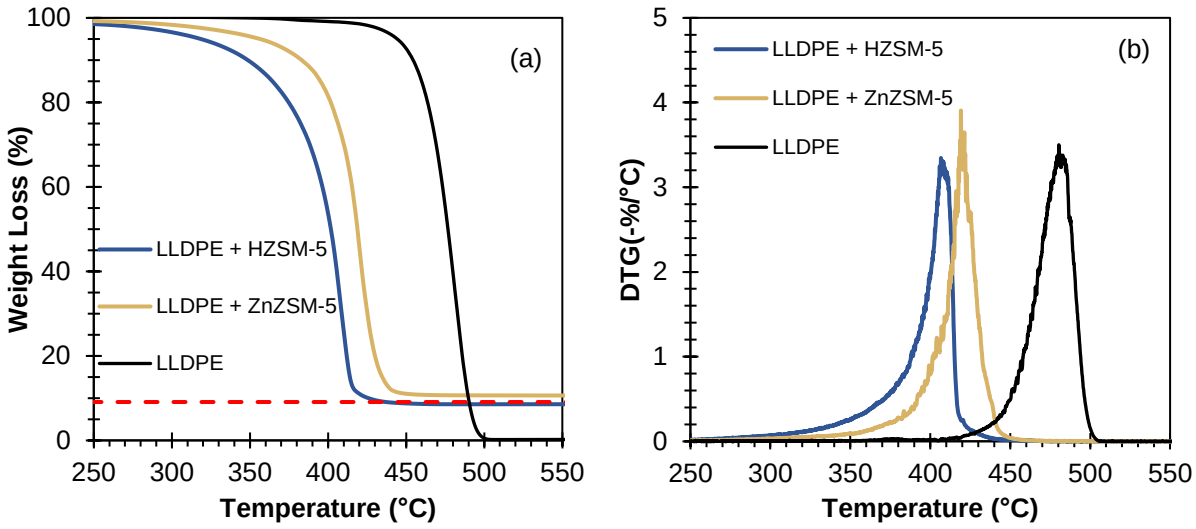

Figure 4.8. TG (a) and DTG (b) curves under N_2 of pure LLDPE the corresponding mixtures with ZSM-5 Zeolites.

Notably, the onset temperature for thermal decomposition differs among the samples. Pure LLDPE initiates thermal degradation at approximately 440 °C ($T_{5\,\%}$) without a catalyst. However, when HZSM-5 and ZnZSM-5 catalysts are introduced, the initiation temperatures drop to 321 °C and 355 °C, respectively. Indeed, the temperature at which the peak associated with the maximum decomposition of LLDPE (T_{max}) occurs is notably lower in the presence of zeolites, with a ΔT_{max} between 61.3 and 73.7 °C, mainly when HZSM-5 zeolite is employed. The same trends are found based on $T_{50\,\%}$ and $T_{95\,\%}$. This

variance can be attributed to the higher external surface area [38] and principally to the higher concentration of strong Brønsted acid sites [22], [38].

Table 4.5. Temperature of maximum decomposition rate and total weight loss of LLDPE and polymer mixtures with ZSM-5 zeolites.

Sample	Total weight loss (%)	T_{max} (ºC)	ΔT_{max} (ºC)	$T_{5\,\%}$ (ºC)	$T_{50\,\%}$ (ºC)	$T_{95\,\%}$ (ºC)
LLDPE + HZSM-5	90.9	406.7	73.7	320.8	399.9	415.4
LLDPE + ZnZSM-5	89.3	419.2	61.3	354.7	417.2	434.6
LLDPE	99.6	480.4	-	444.1	476.6	492.5

Pyrolysis of LLDPE at 500 °C

Experiments involving the multiphase pyrolysis of polyethylene, employing protonated and doped with zinc ZSM-5 zeolite, were conducted at a temperature of 500 °C. The resulting product yields are presented in **Table 4.6**, facilitating a qualitative and quantitative evaluation of product enhancements concerning liquid yield, gaseous yield, and solid residue.

Table 4.6 Yield result of pyrolysis of LLDPE with HZSM-5 and ZnZSM-5 zeolites at 500 °C.

Catalyst	Oil/Wax (wt. %)	Gas (wt. %)	Coke (wt. %)
HZSM-5 (Mix)	54.7	44.9	0.4
HZSM-5 (Mix/Layer)	51.0	48.6	0.4
HZSM-5 (Layer)	55.2	44.2	0.6
ZnZSM-5 (Mix)	58.8	40.6	0.6
ZnZSM-5 (Mix/Layer)	57.3	42.1	0.6
ZnZSM-5 (Layer)	66.8	32.7	0.5

Regardless of the catalyst used, during catalytic pyrolysis, the Mix/Layer arrangement demonstrates a slight reduction in liquid phase yield (between 1.5 and 3.7 %), consequently increasing the gas phase yield (the highest among all the arrangements). At the same time, the amount of coke remains relatively stable compared to the conventional Mix arrangement. Gaurh and Pramanik [2] suggest that a two-stage process involving the initial interaction of the catalyst with a liquid phase, followed by contact with a vapour phase, facilitates the catalytic conversion of lighter paraffins that may react in the first stage, generating more light gas hydrocarbons.

In contrast, the Layer arrangement, enabling direct interaction between thermal cracking gas products from LLDPE and the catalyst, yields a notably greater quantity of liquid phase products, particularly pronounced in the case of ZnZSM-5 zeolite, where this increase amounts to an additional 8 %; this could be explained by the difference in contact time of pyrolysis vapour with the zeolites [20]. Notably, this arrangement records the lowest gas phase yield for each catalyst, 44.2 % for HZSM-5 and 32.5 % for

ZnZSM-5. The quantity of coke residue, however, slightly varies, from 0.4 to 0.6 % observed for the HSM-5 zeolite and lower values from 0.6 to 0.5 % for the ZnZSM-5 zeolite when compared to the Mix arrangement, although these differences may fall within the range of experimental error.

Consequently, the order of Oil/Wax phase production follows the arrangement sequence: Mix/Layer < Mix < Layer and the results are similar for both catalysts.

When comparing each zeolite for a fixed arrangement, a general trend can be observed where the utilisation of doped zeolite leads to an increase in the liquid phase, such as reported in prior studies involving other types of Zn-doped zeolite [22]. Specifically, there is an increase of the liquid/was yield of 3.8 % in the Mix arrangement, 6.3 % in the Mix/Layer arrangement, and 11.6 % in the Layer arrangement compared to using protonated zeolite. Furthermore, the doped zeolite also appears to favour coke production, increasing by 0.1-0.2 %, whatever the arrangement. Several researchers have similarly documented heightened carbon deposition on metal-doped zeolites when contrasted with metal-free catalysts [7].

Composition of the pyrolysis oil for experiments carried out at 500°C – Effect of the arrangement

Examining the composition of the liquid phase in greater detail depending on the catalyst and arrangement reveals distinct patterns (**Figure 4.9** (a)). The choice of the arrangement follows a trend, but this trend depends on the used catalyst.

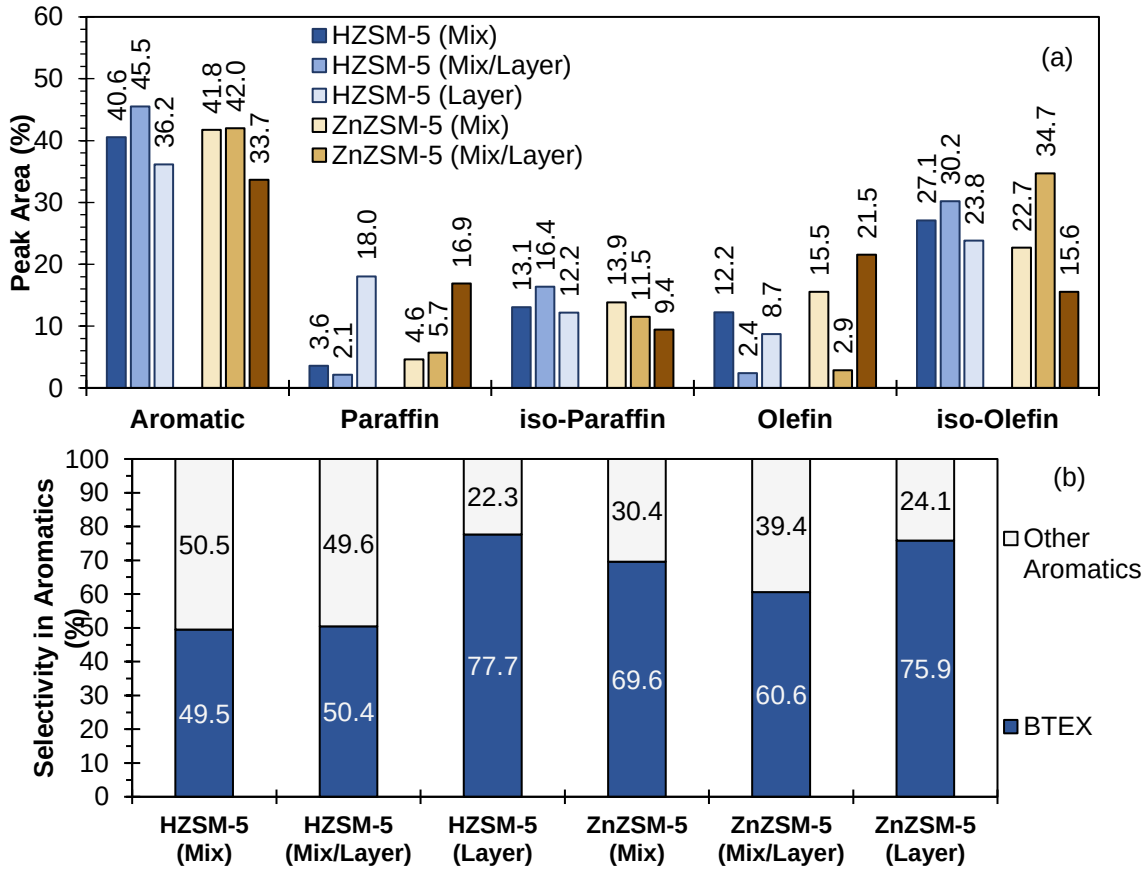

Figure 4.9. Liquid composition (a) and BTEX composition (b) results of pyrolysis of LLDPE with protonated (HZSM-5) and Zn-doped (ZnZSM-5) zeolites at 500 °C under nitrogen.

Firstly, comparing Mix and Mix/Layer arrangements, an increase in the production of aromatic compounds is observed for HZSM-5 with a rise of 5.9 %, whereas no difference is observed for ZnZSM-5 zeolite. However, considering the selectivity in BTEX (**Figure 4.9** (b)), a decrease of 9 % is observed for ZnZSM-5 zeolite, whereas no significant difference is observed for HZSM-5. Additionally, the production of olefins experienced a substantial reduction for both zeolites. The production of paraffinic, iso-paraffinic, and iso-olefinic compounds exhibited almost no variations except for ZnZSM-5 zeolite, demonstrating a significant increase in iso-olefin production (-12% comparing Mix with Mix/Layer). It can thus be concluded that the Mix/Layer arrangement notably enhances the production of aromatics when HZSM-5 was used at the expense of shorter-chain olefinic compounds.

Secondly, a significant increase in paraffin production in the Layer arrangement is observed with a rise of +14.4% and +12.3% comparing Mix with Layer arrangement, respectively, for protonated and doped zeolites. This contrasts with a decrease in the production of aromatics, iso-paraffins, and iso-olefins of 4.4 %, 0.9 %, and 3.3 % for HZSM-5 zeolite, and 8.1 %, 4.5 %, and 7.1 %, for ZnZSM-5 zeolite, respectively. However, despite lower aromatic production, the selectivity for BTEX increases by 28.2 % for HZSM-5 and 6.3 % for ZnZSM-5. This higher selectivity towards BTEX for a layer arrangement, and in particular in the case of HZSM-5, suggests increased diffusion of short-chain olefin compounds into the pores that come into contact with micropore acidic sites, resulting in the predominant formation of monoaromatic compounds. Steric constraints impede the formation of large-size polyaromatics within zeolite pores due to the requirement for bimolecular reactions, such as condensation and hydrogen transfer, among large molecules. These limitations effectively restrict the polymerisation of aromatic compounds in the zeolite's confined environment [17]. Olefin production is affected differently depending on the zeolite: the protonated zeolite reduced its production by 3.5 %, while the doped zeolite increased its production by 6 %.

It is widely acknowledged that the catalytic pyrolysis process of a polymer with an acid catalyst follows a carbocationic reaction mechanism. In this mechanism, carbenium ions are formed through reactions occurring at Lewis acid sites, or carbonium ions are generated through the protonation of hydrocarbons at Brønsted acid sites. Once these carbocations are produced, the catalyst facilitates secondary reactions involving isomerisation, oligomerisation, cyclisation, aromatisation, and cracking, ultimately producing an oily product rich in aromatics. Conversely, in thermal pyrolysis, where random cleavages of C-C bonds occur in the linear structure of the polymer, the cracking process yields hydrocarbon radicals, which are subsequently stabilised as paraffins and olefins, producing a wide array of hydrocarbons varying in size [7], [22], [31], [39].

Discussing the number of aromatic compounds generated, Gaurh and Pramanik [2] elucidate that, within the Mix/Layer arrangement, the smaller molecules in both the liquid and vapour phases come into contact with the ZSM-5 zeolite. This arrangement maximises the production of aromatic compounds, as it aligns with the known mechanisms of paraffin aromatisation in acidic catalysts. This is observed in our study in particular for HZSM-5. This process involves paraffin protolysis, carbonium ion cracking into paraffin and olefin, oligomerisation of olefins, cyclisation of oligomerised products, and the formation of aromatics from cyclic rings through hydrogen transfer. In contrast, the Layer arrangement only involves

interaction with vapour generated during prior thermal cracking and can have a reduced contact time between the pyrolysis vapours and catalyst particles [20]. Since thermal pyrolysis is inherently non-selective, the resulting product might not be ideal for vapour-phase aromatisation. This fundamental difference in configuration is why the Mix/Layer arrangement yields a significantly higher amount of aromatics than the Layer arrangement.

These distinctions can be attributed to each case's varying product phases interacting with the catalyst. In the Mix arrangement, the plastic initially undergoes a phase transition from solid to molten, followed by polymer chain reactions that form waxy compounds through a well-established carbocationic mechanism. Constrained by diffusion limitations, these waxy molecules subsequently locate the zeolite catalyst's acidic sites [17] that are available on the external surface of the catalyst or at the entrance to the pores.

Conversely, in the Layer arrangement, the plastic experiences prior cracking via a free radical mechanism, where the cleavages are random, favouring cracking at polymer structural defects. Although these vapours can more readily access the zeolite [2], they can also escape it. Consequently, a diverse range of compounds with varying carbon content is produced, comprising a higher proportion of paraffins stabilised through thermal cracking and a reduced quantity of aromatics.

The Mix/Layer arrangement, benefitting from both the molten polymer-catalyst interaction and the cracking-catalyst vapours, holds a distinct advantage. Specifically, the vapours resulting from the initial catalytic cracking exhibit selectivity, yielding smaller molecules than thermal cracking; this facilitates deeper penetration of these lighter hydrocarbons into the zeolite, fostering improved aromatisation reactions.

Composition of the pyrolysis oil for experiments carried out at 500°C – Effect of the zeolite

In the comparative analysis between the zinc-doped zeolite and the protonated variant, a noteworthy commonality emerges: an elevated production of olefins. The utilisation of ZnZSM-5 zeolite resulted in a substantial increase in olefin production when compared with HZSM-5, with increments of 3.3 %, 0.5 %, and 12.8 % observed for the Mix, Mix/Layer, and Layer arrangements. In catalytic cracking processes, it is typical for long-chain paraffins and olefins to be produced via carbenium ions on Lewis acid sites. These ions can yield olefins by extracting a hydride ion from paraffin, generating another carbenium ion to sustain the reaction, or by undergoing conversion into olefins through protolytic cracking. Alternatively, they can liberate H_2 if a proton interacts with the C-H bond. Furthermore, olefins can also be generated through a direct proton attack on a C-H bond within paraffin, producing H_2 and an olefin [1]. Reducing Brøsted acid sites by doping also enhances olefin yields by limiting hydrogen transfer reactions, thereby promoting dehydrogenative cracking [20].

In the case of other product families, a comparison between ZnZSM-5 and HZSM-5 revealed the following outcomes: For the Mix arrangement, there was a relatively modest increase of 1.2% in the production of aromatics and a slight 0.8% rise in iso-paraffins. In contrast, for the Mix/Layer and Layer arrangements, the utilization of doped zeolites led to a decline in performance. Specifically, a reduction

of 3.5 % and 4.9 % was observed for the Mix/Layer arrangement and 2.5 % and 2.8 % for the Layer arrangement in the production of aromatics and iso-paraffins, respectively. Concerning paraffin production, the Mix system experienced an increase of 1 %, while the Mix/Layer system exhibited a decrease of 1.1%. Similarly, the Layer system showed a decrease of 1.1%. Regarding the production of iso-olefins, the comparison of ZnZSM-5 with HZSM-5 demonstrated variations depending on the type of arrangement. There was a notable decrease of 4.4% and 8.2% in the Mix and Layer arrangements, while the Mix/Layer arrangement experienced a significant increase of 4.5%.

The higher selectivity in BTEX when ZnZSM-5 is used (+20.1 % in the Mix arrangement and +10.2 % in the Mix/Layer arrangement) may be attributed to the increased in Lewis acid sites content since it is reported that Lewis acid sites are more selective in forming C_6-C_9 aromatics through cyclisation processes [17]. Conversely, the selectivity remains similar in the Layer arrangement, where there is more extensive diffusion of previously cracked LLDPE gases; this suggests that in the first two arrangements, the initial cracking events transpiring on the external surface are substantially influenced by the presence of Lewis acid sites induced by the introduction of Zn^{+2} ions. Conversely, in the Layer arrangement, the impact of gas diffusion within the pores has to be more pronounced. In this case, gases do not necessarily require an initial cracking event on the external surface to permeate the zeolite. Instead, their progress is restricted by the microporous surface, reduced by 8.6 % for ZnZSM-5. The presence of Lewis acid sites probably offsets this limitation. Overall, using doped zeolites led to a reduction in aromatics production, coupled with an increase in the generation of olefins, which can potentially serve as precursors for aromatic compounds.

At this stage in the research, it was opted to follow the Mix/Layer arrangement. This decision was driven by the higher aromatics yield obtained in the liquid phase for both zeolites, even though the liquid yield is slightly lower compare to the Mix arrangement. With this arrangement, decreasing the reaction temperature becomes feasible, resulting in reduced energy consumption.

The subsequent section will thus compare the outcomes of both zeolites at 500 °C with the same catalytic cracking of LLDPE but at 450 °C. This comparative analysis serves a dual purpose: to investigate the influence of temperature and to elucidate the catalytic cracking process in two phases at 450 °C and 500 °C.

Mix/Layer arrangement study at 450 °C and 500 °C

Table 4.7 listed the distinct yields of Oil/Wax, Gas, and Coke resulting from the LLDPE cracking process in the presence of HZSM-5 and ZnZSM-5 zeolites, arranged in the Mix/Layer arrangement as previously outlined, at temperatures of 450 °C and 500 °C. The temperature variation exhibited a relatively minimal influence in all phases, particularly in the case of the ZnZSM-5 zeolite, despite the observation of a slight increase in gas production for HZSM-5. Moreover, it is also possible to assume that temperature contributes to the mitigation of coke formation. Notably, the reduction observed at 500 °C of 0.1 % can be attributed to the higher energy available at this temperature. This surplus energy enables an increased number of secondary reactions, which, in turn, curtail coke production [2], [40].

Table 4.7 Yield result of pyrolysis of LLDPE with HZSM-5 and ZnZSM-5 zeolites at 450 °C and 500 °C.

Catalyst	Oil/Wax (wt. %)	Gas (wt. %)	Coke (wt. %)
HZSM-5 (Mix/Layer) 450 °C	54.4	45.1	0.5
HZSM-5 (Mix/Layer) 500 °C	51.0	48.5	0.4
ZnZSM-5 (Mix/Layer) 450 °C	57.1	42.2	0.7
ZnZSM-5 (Mix/Layer) 500 °C	57.3	42.1	0.6

When comparing the effects of zeolites instead of temperature, at 450°C, there was a slight increase of 2.7 % in the liquid fraction when using the doped zeolite. However, at 500°C, the difference was more pronounced, with a 6.3 % increase in the liquid fraction for the ZnZSM-5 zeolite, while coke production showed a uniform increase of 0.2 %, regardless of the reaction temperature and a reduction in the gas phase. This outcome suggests that when employing ZnZSM-5, there is a diminished degree of cracking that results in less light-hydrocarbons falling within the C_1-C_4 range due to less Brønsted acid site content [19], [22].

Composition of the pyrolysis oil versus temperature

Figure 4.10 (a) provides a comprehensive overview of the content of various compounds constituting the Oil/Wax phase stemming from the LLDPE catalytic cracking process. The impact of temperature variation manifested differently across distinct compound families, with some reliant on both temperature and zeolite type. The influence of the zeolite type is conspicuously evident.

Irrespective of the zeolite used, elevating the temperature led to decreased paraffin production, with 0.4 % and 7.8 % reductions for HZSM-5 and ZnZSM-5, respectively. It can be explained by the favourability of wax cracking into lighter hydrocarbon at higher temperatures [1]. Conversely, iso-olefins production increased by 8.3 % and 0.7 % for HZSM-5 and ZnZSM-5, respectively. It could be suggested that this shift could be attributed to the thermal cracking of LLDPE at 500 °C, resulting in the conversion of branched polymer defects into molecules that were either not cracked with the catalyst or did not enter the zeolite.

In the case of HZSM-5 zeolite, elevated temperature (500 °C) correlated with a surge in iso-paraffin production by 6.3 %, while olefins and aromatics decreased by 4.8 % and 10 %, respectively. For ZnZSM-5 zeolite, an increase in temperature exhibited an inverse effect, causing a decrease in iso-paraffin production by 0.6 %, while olefins and aromatics increased by 0.8 % and 5.7 %, respectively. The elevation in aromatic compounds might be attributed to the increased energy availability observed at elevated temperatures [2], [40], [41]. Furthermore, selectivity toward BTEX compounds (**Figure 4.10** (b)) decreased with rising temperature for both zeolites, around 6-8 %.

A consistent trend emerged when comparing doped zeolite to protonated zeolite regardless of temperature. Doping increased the production of paraffins and iso-olefins, with the most pronounced differences observed at 450 °C, where production increased by 11 % and 12.1 %, respectively.

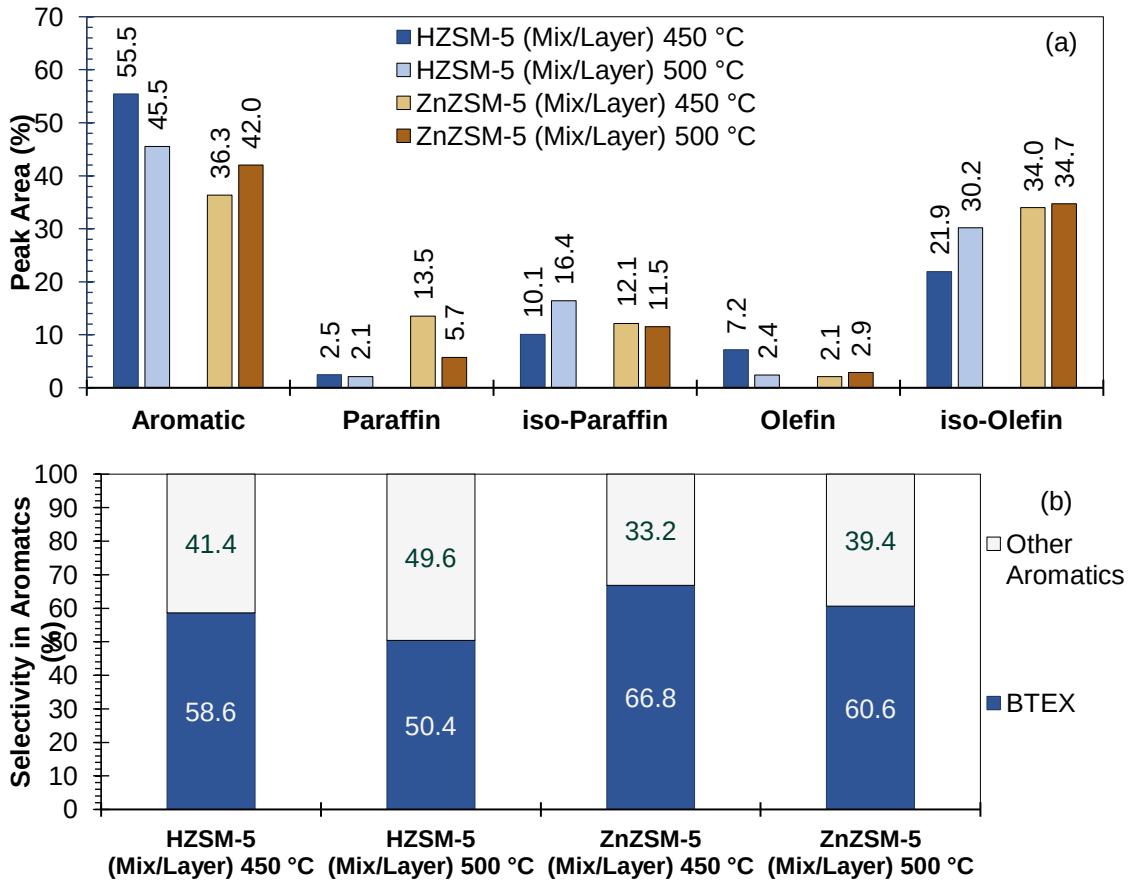

Figure 4.10. Liquid composition (a) and BTEX composition (b) results of pyrolysis of LLDPE with protonated (HZSM-5) and Zn-doped (ZnZSM-5) zeolites at 450 °C and 500 °C under nitrogen.

Conversely, doping led to a reduction in aromatics production, especially evident at 450 °C, with decreases of 19.2 %. Selectivity for BTEX compounds increased by approximately 8-10 % when doping is considered due to a more significant number of strong Lewis acid sites [19], [22]. At 450 °C, doped zeolite produced 2 % more iso-paraffins and 5.1 % less olefins than protonated zeolite. On the contrary, at 500 °C, doped zeolite produced 4.9 % fewer iso-paraffins and 0.5 % more olefins than protonated zeolite; this could be attributed to better end-chain scission selectivity with more available energy [2], [40], [41].

4.5. Conclusion

This research endeavour delved into multiphase pyrolysis, scrutinising polyethylene's transformation in two sequential parts. Initially, it was explored the multiphase pyrolysis of LLDPE and catalytic performance of protonated ZSM-5 zeolite alongside its zinc-doped counterpart at 500 °C. Subsequently, we assessed pyrolysis at two distinct temperatures, 450 °C and 500 °C, focusing on the most promising phase identified in the preliminary experimentation.

This inquiry encompassed multiple facets, unveiling critical insights into this complex process. It analysed the impact of arrangement, temperature, and catalyst on the polyethylene pyrolysis journey:

- **Arrangement of the polymer/catalyst mixture.**
  The arrangements played a pivotal role in dictating the product outcomes in the initial phase. Notably, the Mix/Layer arrangement, while exhibiting slightly subdued performance in the liquid phase, emerged as the vanguard in aromatic compound production. It is worth highlighting that the Layer arrangement, on the other hand, demonstrated superior selectivity in the production of BTEX compounds, emphasising the intricate trade-offs between these arrangements.

→ **Temperature effect.**
  The temperature variations had a discernible impact. While the distribution of the liquid, gas, and solid phases remained relatively unaffected, temperature adjustments notably influenced the paraffin and olefin content of the oil. This shift can be attributed to enhanced end-chain scission reactions facilitated by the increased energy available at elevated temperatures, ushering in changes in compound composition.

→ **Zeolite properties.**
  Within both the first and second parts, the choice of catalyst – whether doped with Zinc or protonated – wielded substantial influence. The zinc-doped catalyst exhibited superior performance in the liquid phase, attributed to its lower Brønsted acid site content and external surface area. This phenomenon was conspicuously reflected in the zeolite's overall catalytic activity, which was comparatively reduced. Furthermore, introducing zinc catalysts elevated the production of olefins, promising precursors of aromatic compounds. A remarkable increase in BTEX selectivity was also noted, albeit with a slightly reduced aromatics production, resulting from the creation of stronger Lewis acid sites, which were established for every two Brønsted sites. Detailed analyses through XRD, XPS, and H_2-TPR techniques meticulously validated the precise introduction of Zn^{2+} ions via ion exchange.

While the introduction of zinc-doped zeolite does indeed enhance the selectivity towards BTEX compounds, the production of aromatic compounds does not suffice to offset these advantages. Additionally, the differences in synthesis and production costs associated with zinc-doped zeolite render this approach less economically viable. As a result, the forthcoming chapter will pursue a different research trajectory. Continuing the investigations utilising the Mix/Layer arrangement with the HZSM-5 zeolite is imperative. This endeavour aims to engineer modifications in the zeolite's acidity by exploring alternative preparation methodologies. This strategic shift is underpinned by the quest for more efficient and cost-effective.

4.6. References

[1] L. Dai *et al.*, “Pyrolysis-catalysis for waste polyolefin conversion into low aromatic naphtha,” *Energy Convers. Manag.*, vol. 245, 2021, doi: 10.1016/j.enconman.2021.114578.

[2] P. Gaurh and H. Pramanik, “A novel approach of solid waste management via aromatization using multiphase catalytic pyrolysis of waste polyethylene,” *Waste Manag.*, vol. 71, pp. 86–96, 2018, doi: 10.1016/j.wasman.2017.10.053.

[3] A. López, I. de Marco, B. M. Caballero, M. F. Laresgoiti, A. Adrados, and A. Aranzabal, “Catalytic pyrolysis of plastic wastes with two different types of catalysts: ZSM-5 zeolite and

Red Mud," *Appl. Catal. B Environ.*, vol. 104, no. 3–4, pp. 211–219, 2011, doi: 10.1016/j.apcatb.2011.03.030.

[4] L. Dai *et al.*, "Chemical upcycling of waste polyolefinic plastics to low-carbon synthetic naphtha for closing the plastic use loop," *Sci. Total Environ.*, vol. 782, p. 146897, 2021, doi: 10.1016/j.scitotenv.2021.146897.

[5] M. Rahman, A. Infantes-Molina, A. S. Hoffman, S. R. Bare, K. L. Emerson, and S. J. Khatib, "Effect of Si/Al ratio of ZSM-5 support on structure and activity of Mo species in methane dehydroaromatization," *Fuel*, vol. 278, no. June, 2020, doi: 10.1016/j.fuel.2020.118290.

[6] J. Nishino, M. Itoh, H. Fujiyoshi, and Y. Uemichi, "Catalytic degradation of plastic waste into petrochemicals using Ga-ZSM-5," *Fuel*, vol. 87, no. 17–18, pp. 3681–3686, 2008, doi: 10.1016/j.fuel.2008.06.022.

[7] K. Akubo, M. A. Nahil, and P. T. Williams, "Aromatic fuel oils produced from the pyrolysis-catalysis of polyethylene plastic with metal-impregnated zeolite catalysts," *J. Energy Inst.*, vol. 92, no. 1, pp. 195–202, 2019, doi: 10.1016/j.joei.2017.10.009.

[8] C. M. Lok, J. Van Doorn, and G. Aranda Almansa, "Promoted ZSM-5 catalysts for the production of bio-aromatics, a review," *Renew. Sustain. Energy Rev.*, vol. 113, no. July, p. 109248, 2019, doi: 10.1016/j.rser.2019.109248.

[9] O. A. Anunziata and L. B. Pierella, "CONVERSION OF POLYETHYLENE INTO AROMATIC HYDROCARBONS USING MEL AND BEA ZEOLITES," *Stud. Surf. Sci. Catal.*, vol. 125, pp. 481–488, 1999.

[10] Y. Li, S. Liu, S. Xie, and L. Xu, "Promoted metal utilization capacity of alkali-treated zeolite: Preparation of Zn/ZSM-5 and its application in 1-hexene aromatization," *Appl. Catal. A Gen.*, vol. 360, no. 1, pp. 8–16, 2009, doi: 10.1016/j.apcata.2009.02.039.

[11] T. Fu *et al.*, "Synergistic Catalysis of Brønsted Acid, Al-Lewis Acid, and Zn-Lewis Acid on Steam-Treated Zn/ZSM-5 for Highly Stable Conversion of Methanol to Aromatics," *Ind. Eng. Chem. Res.*, vol. 62, no. 4, pp. 1865–1876, 2023, doi: 10.1021/acs.iecr.2c03873.

[12] R. Geng *et al.*, "Structure Evolution of Zn Species on Fresh, Deactivated, and Regenerated Zn/ZSM-5 Catalysts in Ethylene Aromatization," *ACS Catal.*, vol. 12, no. 23, pp. 14735–14747, 2022, doi: 10.1021/acscatal.2c04074.

[13] Y. Jia *et al.*, "Catalytic conversion of methanol to aromatics over nano-sized HZSM-5 zeolite modified by ZnSiF6·6H2O," *Catal. Sci. Technol.*, vol. 7, no. 8, pp. 1776–1791, 2017, doi: 10.1039/c7cy00143f.

[14] L. M. Lubango and M. S. Scurrell, "Light alkanes aromatization to BTX over Zn-ZSM-5 catalysts: Enhancements in BTX selectivity by means of a second transition metal ion," *Appl. Catal. A Gen.*, vol. 235, no. 1–2, pp. 265–272, 2002, doi: 10.1016/S0926-860X(02)00271-5.

[15] D. P. Serrano, J. Aguado, and J. M. Escola, "Developing Advanced Catalysts for the Conversion of Polyolefinic Waste Plastics into Fuels and Chemicals," *ACS Catal.*, vol. 2, no. 9, pp. 1924–1941, 2012, doi: 10.1021/cs3003403.

[16] M. S. Renzini, L. C. Lerici, U. Sedran, and L. B. Pierella, "Stability of ZSM-11 and BETA zeolites during the catalytic cracking of low-density polyethylene," *J. Anal. Appl. Pyrolysis*, vol. 92, no. 2, pp. 450–455, 2011, doi: 10.1016/j.jaap.2011.08.008.

[17] L. C. Lerici, M. S. Renzini, U. Sedran, and L. B. Pierella, "Tertiary recycling of low-density polyethylene by catalytic cracking over ZSM-11 and BETA zeolites modified with Zn2+: Stability study," *Energy and Fuels*, vol. 27, no. 4, pp. 2202–2208, 2013, doi: 10.1021/ef302099e.

[18] S. M. Auerbach, K. A. Carrado, and P. K. Dutta, *Handbook of Zeolite Science and Technology*, 1st Editio., vol. 126, no. 28. CRC Press, 2003.

[19] L. B. Pierella, S. Renzini, and O. A. Anunziata, "Catalytic degradation of high density polyethylene over microporous and mesoporous materials," *Microporous Mesoporous Mater.*, vol. 81, no. 1–3, pp. 155–159, 2005, doi: 10.1016/j.micromeso.2004.11.015.

[20] A. A. Inayat, A. A. Inayat, W. Schwieger, B. Sokolova, and P. Lestinsky, “Enhancing aromatics and olefins yields in thermo-catalytic pyrolysis of LDPE over zeolites: Role of staged catalysis and acid site density of HZSM-5,” *Fuel*, vol. 314, no. January, p. 123071, 2022, doi: 10.1016/j.fuel.2021.123071.

[21] H. G. Karge, *molecular sieves 5*. .

[22] M. S. Renzini, U. Sedran, and L. B. Pierella, “H-ZSM-11 and Zn-ZSM-11 zeolites and their applications in the catalytic transformation of LDPE,” *J. Anal. Appl. Pyrolysis*, vol. 86, no. 1, pp. 215–220, 2009, doi: 10.1016/j.jaap.2009.06.008.

[23] N. H. N. Kamarudin *et al.*, “Interaction of Zn 2+ with extraframework aluminum in HBEA zeolite and its role in enhancing n-pentane isomerization,” *Appl. Catal. A Gen.*, vol. 431–432, pp. 104–112, 2012, doi: 10.1016/j.apcata.2012.04.020.

[24] M. C. Biesinger, L. W. M. Lau, A. R. Gerson, and R. S. C. Smart, “Resolving surface chemical states in XPS analysis of first row transition metals, oxides and hydroxides: Sc, Ti, V, Cu and Zn,” *Appl. Surf. Sci.*, vol. 257, no. 3, pp. 887–898, 2010, doi: 10.1016/j.apsusc.2010.07.086.

[25] B. S. Liu *et al.*, “Characteristic and mechanism of methane dehydroaromatization over Zn-based/HZSM-5 catalysts under conditions of atmospheric pressure and supersonic jet expansion,” *J. Phys. Chem. C*, vol. 115, no. 34, pp. 16954–16962, 2011, doi: 10.1021/jp2027065.

[26] G. Greczynski and L. Hultman, “X-ray photoelectron spectroscopy: Towards reliable binding energy referencing,” *Prog. Mater. Sci.*, vol. 107, no. April 2019, p. 100591, 2020, doi: 10.1016/j.pmatsci.2019.100591.

[27] J. A. Biscardi, G. D. Meitzner, and E. Iglesia, “Structure and density of active Zn species in Zn/H-ZSM5 propane aromatization catalysts,” *J. Catal.*, vol. 179, no. 1, pp. 192–202, 1998, doi: 10.1006/jcat.1998.2177.

[28] Q. Zhang *et al.*, “Isoparaffin production by aqueous phase processing of sorbitol over the Ni/HZSM-5 catalysts: Effect of the calcination temperature of the catalyst,” *Fuel*, vol. 90, no. 11, pp. 3468–3472, 2011, doi: 10.1016/j.fuel.2011.06.046.

[29] J. Weitkamp and M. Hunger, “ACID AND BASE CATALYSIS ON ZEOLITES,” *Stud. Surf. Sci. Catal.*, vol. 168, pp. 787–835, 2007, doi: https://doi.org/10.1016/S0167-2991(07)80810-X.

[30] F. Benaliouche, Y. Boucheffa, P. Ayrault, S. Mignard, and P. Magnoux, “NH3-TPD and FTIR spectroscopy of pyridine adsorption studies for characterization of Ag- and Cu-exchanged X zeolites,” *Microporous Mesoporous Mater.*, vol. 111, no. 1–3, pp. 80–88, 2008, doi: 10.1016/j.micromeso.2007.07.006.

[31] N. Miskolczi, J. Sója, and E. Tulok, “Thermo-catalytic two-step pyrolysis of real waste plastics from end of life vehicle,” *J. Anal. Appl. Pyrolysis*, vol. 128, no. June, pp. 1–12, 2017, doi: 10.1016/j.jaap.2017.11.008.

[32] A. Marcilla, A. Gómez-Siurana, and F. Valdés, “Catalytic cracking of low-density polyethylene over H-Beta and HZSM-5 zeolites: Influence of the external surface. Kinetic model,” *Polym. Degrad. Stab.*, vol. 92, no. 2, pp. 197–204, 2007, doi: 10.1016/j.polymdegradstab.2006.11.007.

[33] A. A. A. Inayat, A. A. A. Inayat, W. Schwieger, B. Sokolova, and P. Lestinsky, “Enhancing aromatics and olefins yields in thermo-catalytic pyrolysis of LDPE over zeolites: Role of staged catalysis and acid site density of HZSM-5,” *Fuel*, vol. 314, no. January, p. 123071, 2022, doi: 10.1016/j.fuel.2021.123071.

[34] Y. K. Park, J. S. Jung, J. Jae, S. B. Hong, A. Watanabe, and Y. M. Kim, “Catalytic fast pyrolysis of wood plastic composite over microporous zeolites,” *Chem. Eng. J.*, vol. 377, no. August 2018, p. 119742, 2019, doi: 10.1016/j.cej.2018.08.128.

[35] A. M. Hernández-Giménez *et al.*, “Effect of Mesoporosity, Acidity and Crystal Size of Zeolite ZSM-5 on Catalytic Performance during the Ex-situ Catalytic Fast Pyrolysis of Biomass,” *ChemCatChem*, vol. 13, no. 4, pp. 1207–1219, 2021, doi: 10.1002/cctc.202001778.

[36] F. Jin and Y. Li, “A FTIR and TPD examination of the distributive properties of acid sites on ZSM-5 zeolite with pyridine as a probe molecule,” *Catal. Today*, vol. 145, no. 1–2, pp. 101–107, 2009, doi: 10.1016/j.cattod.2008.06.007.

[37] O. A. Anunziata and L. B. Pierella, “Nature of the active sites in H-ZSM-11 zeolite modified with Zn(2+) and Ga(3+),” *Catal. Letters*, vol. 19, no. 2–3, pp. 143–151, 1993, doi: 10.1007/BF00771749.

[38] A. Peral, J. M. Escola, D. P. Serrano, J. Přech, C. Ochoa-Hernández, and J. Čejka, “Bidimensional ZSM-5 zeolites probed as catalysts for polyethylene cracking,” *Catal. Sci. Technol.*, vol. 6, no. 8, pp. 2754–2765, 2016, doi: 10.1039/c5cy02075a.

[39] M. S. Abbas-Abadi *et al.*, “Challenges and opportunities of light olefin production via thermal and catalytic pyrolysis of end-of-life polyolefins: Towards full recyclability,” *Prog. Energy Combust. Sci.*, vol. 96, no. September 2022, p. 101046, 2023, doi: 10.1016/j.pecs.2022.101046.

[40] A. Lopez-Urionabarrenechea, I. De Marco, B. M. Caballero, M. F. Laresgoiti, and A. Adrados, “Catalytic stepwise pyrolysis of packaging plastic waste,” *J. Anal. Appl. Pyrolysis*, vol. 96, pp. 54–62, 2012, doi: 10.1016/j.jaap.2012.03.004.

[41] I. Vollmer *et al.*, “Beyond Mechanical Recycling: Giving New Life to Plastic Waste,” *Angew. Chemie Int. Ed.*, 2020, doi: 10.1002/anie.201915651.

Chapter 5

5. The effect of calcination conditions on the catalytic performances of HZSM-5 zeolite for the polyethylene pyrolysis

Note: This chapter will be published highlighting its scientific contribution and relevance

5.1. Summary

Two different calcination conditions of ZSM-5 zeolite, a dynamic air regime (DC) and a static air regime (SC), were evaluated, and both catalysts were used in the pyrolysis of polyethylene (PE). Calcination influenced the textural properties, the distribution of aluminium coordination and, therefore, the acidity of the zeolite. The distribution of Al evaluated by NMR showed that the aluminium naturally found in tetrahedral coordination shifted into octahedral and distorted coordination after calcination. This effect is more pronounced when the zeolite is calcined under static conditions. This shift in coordination influenced the acidity, which changes from a Brønsted to a Lewis type, which means that calcination can be used in modifying the nature of acidic active sites of the zeolite. Considering the pyrolysis of PE at 450 °C, the influence of the two zeolites was evaluated and compared with the thermal degradation of pure PE at 480 °C (a temperature where the conversion is total). HZSM-5 zeolite promotes cyclisation reactions, which increases the aromatic content of the pyrolysis oil, especially for zeolite calcined under dynamic conditions, which contains a more significant amount of Brønsted strong acid sites.

5.2. Introduction

In 2021, global plastics production reached 390.7 million tonnes (Mt), of which around 90 % comes from fossil resources [1]. This global production leads to a significant amount of plastic waste. The Organisation for Economic Co-operation and Development (OECD) data from 2019 revealed that only 9 % of post-consumer plastic waste was recycled, 19 % was incinerated, 49 % was landfilled, and 22 % underwent mismanagement or was uncollected [2]. The global problem is so serious that the Ellen McArthur Foundation estimates that by 2050 if no action is taken, there will be more plastic in the ocean than fish [3].

Mechanical recycling is generally considered the initial approach to plastics recycling, but it has its limitations when it comes to effectively processing post-consumer plastic waste. One of the main challenges is the presence of pollutants and/or inherited substances in the material, which hinders the recycling process. In addition, adequate sorting of plastic waste by type is crucial for efficient mechanical recycling. Another important limitation is the maximum number of recycling cycles a material can undergo before suffering structural degradation, which adversely affects its quality [4].

Chemical recycling has emerged as an alternative method to valorise plastic waste and produce monomers or oligomers that can be re-polymerised as well as molecules for the chemical industry. This approach enables waste plastics to be converted into high-value-added chemicals, thus contributing to a more sustainable and circular economy [5].

In recent decades, the conversion of plastic waste into chemicals by pyrolysis has attracted considerable attention and has been studied as an alternative to mechanical recycling [6]–[12]. Pyrolysis is currently considered one of the most promising ways of tackling plastic pollution. Under the influence of temperature and in the absence of oxygen, polymers produced from fossil resources are converted into various basic chemical products. Among these, hydrocarbon oils are the most interesting, as they can be the source of automotive and marine fuels, for example. Pyrolysis of plastics that are difficult to depolymerise, such as polyethylene, yields a wide range of chemical compounds. These include BTEX (Benzene, Toluene, Ethylbenzene and Xylenes), which are mono-aromatic volatile organic compounds widely used in various industries such as the petrochemical, cosmetics and pharmacochemical industries, entering in particular into the composition of essences, perfumes and medicines [13].

Catalytic pyrolysis offers several advantages over the non-catalytic route. Firstly, it significantly reduces the pyrolysis temperature by lowering the activation energy of the reaction. The presence of a catalyst can also direct the reaction towards desired products. In the plastic pyrolysis reaction, the pore structure and acidity of zeolites are suitable for increasing the yield of light hydrocarbon products and selectivity [6], [7], [11], [12]. Among zeolites, ZSM-5 has received particular attention due to its shape selectivity towards aromatic compounds and its high activity in the catalytic cracking of plastic waste [14]–[22]. ZSM-5 zeolites are usually synthesised by hydrothermal treatment. After the crystallisation stage, carried out at temperatures below 200 °C, calcination from 500 °C is employed to eliminate all organic precursors and impurities [23], [24]. For NH_4^+-zeolites, calcination is used to de-ammonate and therefore protonate the zeolite [25]–[28]. It is also used to decompose metal promoters [26], [29]–[33].

The acidity of ZSM-5 zeolites is a critical factor influencing their catalytic performance. Various methods can be used to modulate zeolite acidity. The Si/Al ratio defined at the synthesis [34]–[36], where Al^{3+} substitutes Si^{4+} to maintain charge neutrality, and metal promotion of zeolites [34], [35], [37], [38] are the most widely studied methods for modifying zeolite acidity. Nonetheless, alternative approaches for modifying acidity, such as the calcination process [23]–[33], [39], have received limited research attention. Parameters like temperature, duration, and atmospheric composition during calcination are the main determinants influencing the acidity of ZSM-5 zeolites.

Lu et al. [25] investigated the impact of calcination temperature (500-800 °C) on the total acidity of protonated ZSM-5 zeolite and found that the quantity of Brønsted acid sites decreases with an increase in temperature while the number of Lewis acid sites remained constant below 800 °C. Zhang et al. [32] observed a decrease in total acidity of Ni/HZSM-5 catalyst, especially strong acid sites, with increased calcination temperature from 400 to 700 °C. Tan et al. [31] studied the impregnated HZSM-5 with 2 wt. % molybdenum and found that acidity was affected after 700 °C. The loss of strong acid sites, mainly

related to Brønsted acid sites, was evident, and from 750 °C there were no strong acid sites. Romero et al. [30] found a direct relationship between decreased total acidity and higher calcination temperatures, primarily related to the thermal-dealumination caused by the decomposition of the zeolite structure at high temperatures. Pouria et al. [27] found that increasing calcination time (173-480 min) also negatively impacted the total acidity of the zeolite.

The composition of the carrier gas used for zeolite treatment can also affect its acidity. An air flow is generally used for the treatment. The presence of steam in the air flow led to the production of extra-lattice aluminium and to a decrease in Brønsted acidity, a consequence of dealumination caused by water vapour pressure [26], [28]. The substitution of air by pure nitrogen flow has an insignificant effect on the total acidity [27], regardless of the temperature of calcination of H-ZSM-5 (300 or 800 °C). Studying two different calcination procedures “directly under air atmosphere” or “following a two-step (nitrogen-air) treatment”, Serrano et al. [23] showed that the calcination procedure does not affect the properties of a reference ZSM-5 sample. However, when a hierarchical ZSM-5 material is employed, they observed a less pronounced decrease in the concentration of Brønsted acid sites when using a two-step nitrogen/air calcination, highlighting that the aluminium present in hierarchical ZSM-5 is very sensitive to the calcination conditions.

The effects of temperature and calcination time on the acidic properties of zeolites do not allow similar structural and textural properties to be maintained. Indeed, as calcination temperature increases, a decrease in specific surface area is generally observed, as well as profound changes in the zeolite structure at high temperatures. This approach makes it difficult to distinguish the effect of acidity from the effects of zeolite structure and texture in the pyrolysis reaction. Therefore, the aim of this study is to explore the modification of the acidity of a ZSM-5 zeolite calcined at 550 °C using two different calcination processes under static or dynamic air. These two processes are reported in the literature for the calcination of zeolites, but to our knowledge, the comparison of these two calcination processes and their effects on the acidity and catalytic performance of H-ZSM-5 zeolite in plastic pyrolysis have not been investigated. Various characterisation techniques, such as XRD, N_2-physisorption, ^{27}Al MAS NMR, FTIR of adsorbed pyridine, XPS, and TGA, were employed to understand the effects of the calcination process on the structural and textural properties, the aluminium distribution and the acidic properties of H-ZSM-5 and on the catalytic performances in the polyethylene pyrolysis.

5.3. Experimental

A commercial MFI zeolite in the ammonium form, NH_4^+-ZSM-5 (CBV23), provided by Zeolyst International, with a SiO_2/Al_2O_3 mole ratio of 23, was used as the starting material. In order to obtain the protonic form, the zeolite was calcined in flowing air (Alphagaz 1 Air Smartop from Air Liquide) at 100 $mL.min^{-1}$ or in static air. The calcination protocol used for each zeolite is described in section **2.6.4**. The samples were labelled DC or SC, depending on whether they were prepared under dynamic or static conditions, respectively. The experiments were carried out as described in section **2.3**. with half of the powdered zeolite in contact directly with the pellet polymer and the other half superposed between two layers of quartz wool, as illustrated in **Figure 2.24** (B). This arrangement will be noted as Mix/Layer. The

polymer reacts with the powdered catalyst, and the vapours from this first cracking react with the powdered zeolite layer. The analytical sampling follows the protocol description of section **2.4**.

5.4. Result and discussion

5.4.1. Effect on calcination conditions on structural and textural properties of HZSM-5

Figure 5.1 shows XRD patterns of the native NH_4^+-ZSM-5 zeolite and calcined HZSM-5 DC and HZSM-5 SC zeolites. For the three zeolites, diffraction peaks for 2θ Bragg's angle between 5° and 55° can be observed and are characteristics of the orthorhombic phase of the ZSM-5 zeolites framework (PDF-04-017-8707). The height of the most intense diffraction peak (051) at 2θ = 23.03° was used to calculate the relative crystallinity of the two calcined HZSM-5 samples compared to the native NH_4^+-ZSM-5 zeolite [33]. The results of the relative crystallinity of the zeolites are listed in **Table 5.1**. The calcination at 550 °C causes a moderate loss of crystallinity. Compared to the native NH_4^+-ZSM-5 sample, the calcined HZSM-5 DC and HZSM-5 SC samples lost ~ 4 % and ~ 8 % of their crystallinity, respectively.

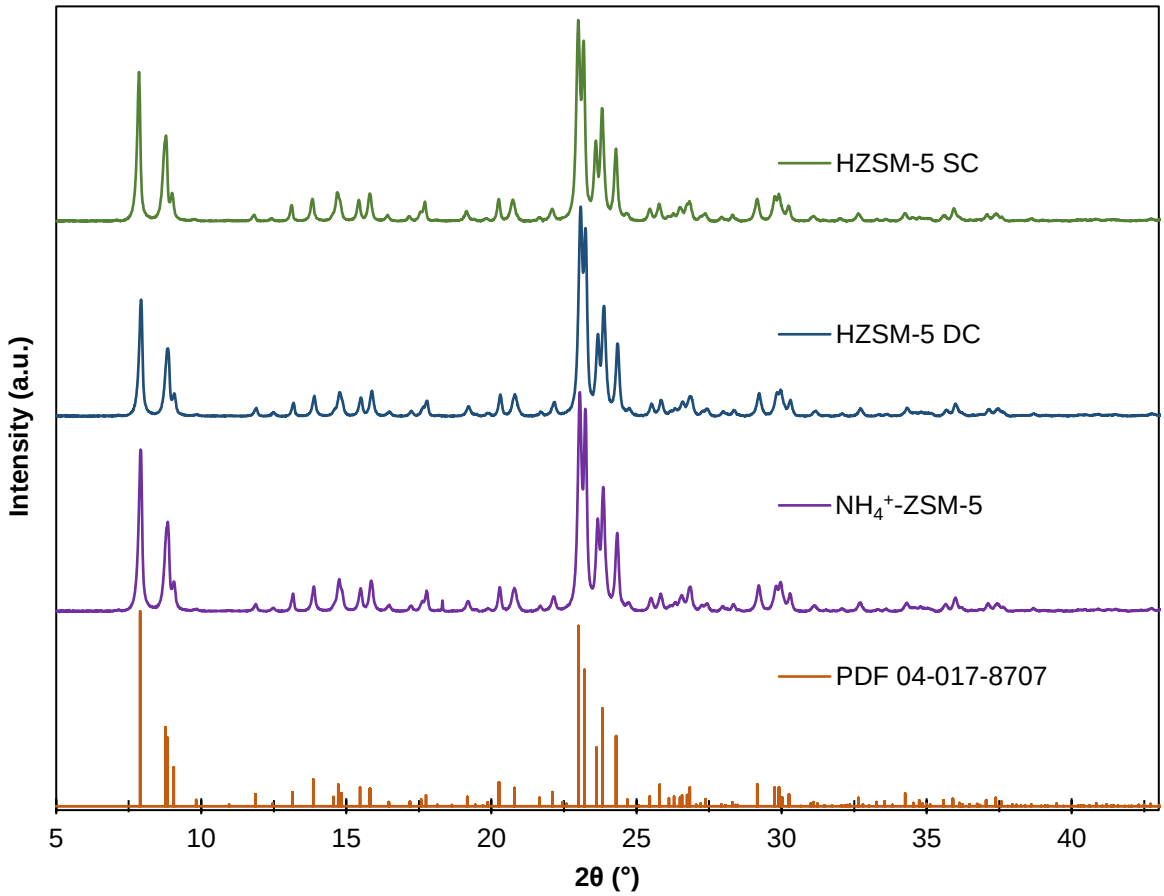

Figure 5.1. XRD patterns of the native NH_4^+-ZSM-5 zeolite and the calcined HZSM-5 DC and HZSM-5 SC zeolites.

The nitrogen physisorption curves for both calcined zeolites are given in **Figure 5.2** (a). The data extracted from these curves are gathered in **Table 5.1**. N_2 adsorption/desorption isotherms demonstrate that calcined ZSM-5 samples show the isotherms with hysteresis loop at P/P_0 in the range of 0.4–0.9.

This high-pressure hysteresis results from the aggregation of zeolite particles to form secondary mesopores combined with micropores [48].

The value of the specific surface area of the HZSM-5 DC zeolite is of the same order of magnitude as the value of the native NH_4^+-ZSM-5 zeolite (**Table 5.1**). The static calcination at 550 °C seems to induce a slight decrease in micropore surface area and volume (**Table 5.1**). Under static calcination conditions, the water vapour inside the zeolite is probably more difficult to remove because an air flow does not carry steam away, and some pores can remain blocked. Similar results were obtained by L. Bai et al. [33] when studying the calcination at 500 °C of a PtSnNaMg/ZSM-5 sample under airflow or static air. Moreover, whatever the calcination method used, the pore size distribution remains nearly identical (**Figure 2.4** (b)).

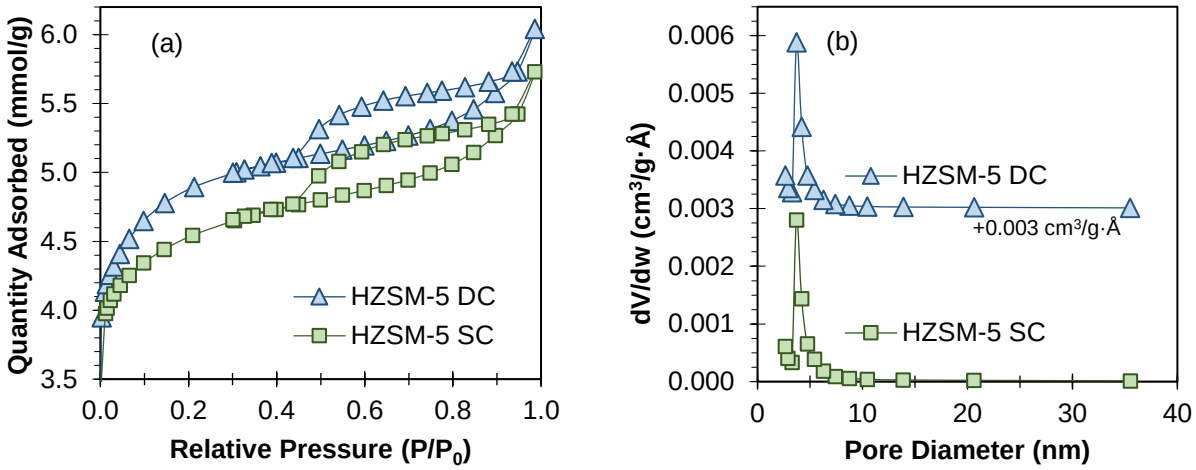

Figure 5.2. N_2 physisorption curves (a) and pore size distribution (b) of the calcined HZSM-5 DC and HZSM-5 SC zeolites.

The structural and textural properties of zeolites are slightly affected by the mode of calcination, static or dynamic. However, we note a lower microporosity for the sample calcined in static mode, which could result from a more difficult water removal in the microporosity.

Table 5.1 Textural properties and relative crystallinity of the calcined HZSM-5 DC and HZSM-5 SC zeolites.

Catalyst	Specific surface ($m^2.g^{-1}$)				Relative Crystallinity (%)
	S_{BET}	S_{ext}	S_{micro}	V_{micro*}	
NH_4^+-ZSM-5	425	-	-	-	100**
HZSM-5 DC	413	30	383	0.16	96
HZSM-5 SC	392	34	358	0.14	92

*t-Plot Method.

**Relative crystallinity considering the NH_4^+ZSM-5 sample as 100 % crystallinity.

5.4.2. Effect of calcination conditions on Al distribution in HZSM-5

The ^{27}Al MAS NMR spectra of the native NH_4^+-ZSM-5 zeolite and the calcined HZSM-5 DC and HZSM-5 SC zeolites are displayed in **Figure 5.3**. For native NH_4^+-ZSM-5 zeolite, only one signal at 54-56 ppm is observed. This signal is attributed to the presence of Al atoms in the framework in regular tetrahedral (Td) coordination. This aluminium is located in an oxygen environment and involved in structural Si–OH–Al groups. The signal at 0 ppm, arising after calcination, is attributed to octahedrally (Oh) coordinated extra-framework Al atoms. The signal at 54-56 ppm is also found for the calcined HZSM-5 DC and HZSM-5 SC zeolites. However, at lower frequencies, the main signal exhibits a shoulder that extends from 50 to 30 ppm. The ^{27}Al MAS NMR spectrum can be interpreted as the sum of three contributions (**Figure 5.3**). The contribution at around 40 ppm is more pronounced for HZSM-5 SC (27 % of the ^{27}Al MAS NMR signal) than for the HZSM-5 DC sample (13 % of the ^{27}Al MAS NMR signal) (**Table 5.2**). This contribution has been ascribed to highly distorted tetrahedral extra-framework aluminium–oxygen species [49], although the chemical shift is also consistent with 5-coordinate aluminium [50]. This could, therefore, represent a partial perturbation or release of Td framework Al atoms, creating framework defects due to steam zeolite dealumination [51].

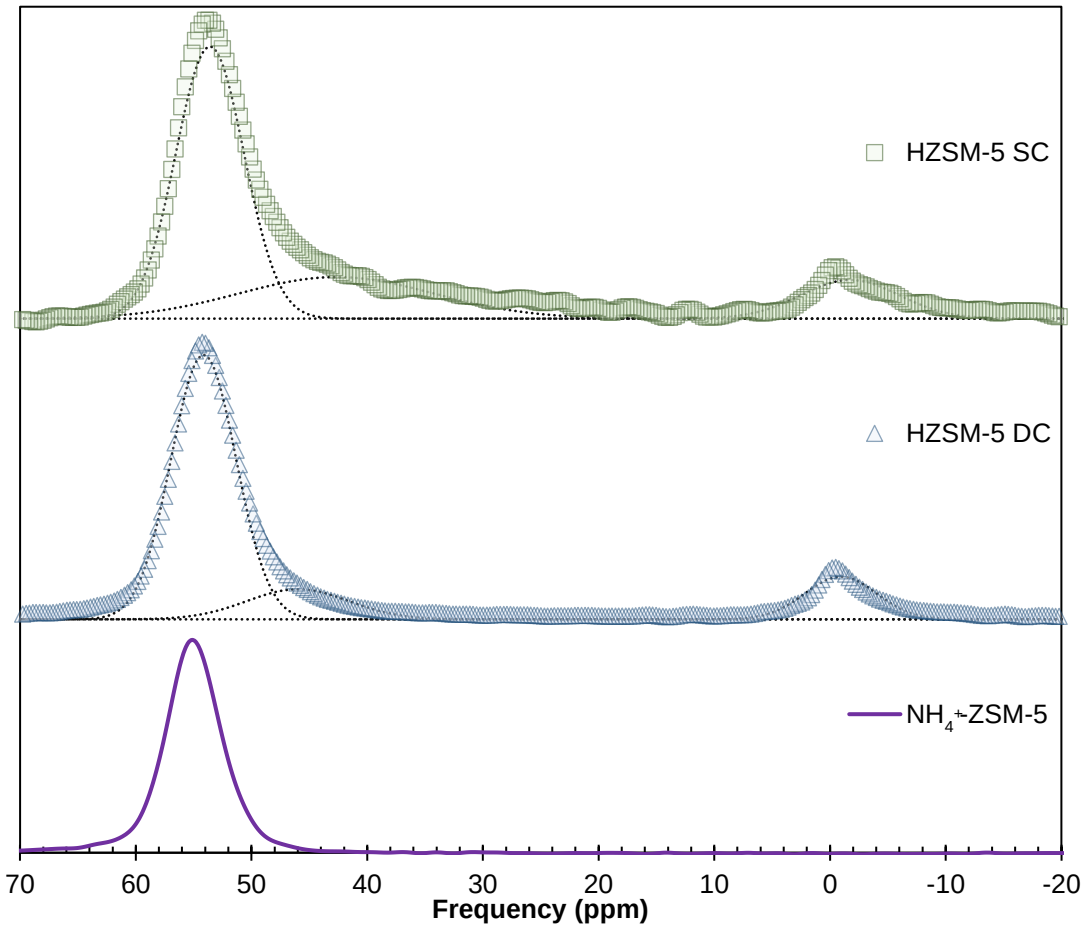

Figure 5.3. ^{27}Al MAS NMR of ZSM-5 samples: native NH_4^+-ZSM-5 (Purple), HZSM-5 DC (Blue), and HZSM-5 SC (Green).

The XPS analyses were conducted on the native NH_4^+-ZSM-5 zeolite and on the calcined HZSM-5 DC and HZSM-5 SC zeolites. The Si 2p, Al 2p and O 1s high-resolution photopeaks are shown in **Figure 5.4**. The surface Si/Al atomic ratio and Al atom distribution are listed in **Table 5.2**.

The calcination of the zeolite NH_4^+-ZSM-5 in static conditions increased the surface Si/Al ratio from 10.1 to 13.4 (**Table 5.2**). This increase can be explained by a partial dealumination occurring during the calcination process. The dealumination is not evident when the zeolite NH_4^+-ZSM-5 is calcinated in dynamic conditions since the ratio Si/Al value is 10.2 (**Table 5.2**). It is well known that using water vapour in the air for the calcination process favours the dealumination [52]. During the calcination process of the zeolite, water and other impurities are eliminated in the first stage at around 200 °C [53]. It can be suggested that in dynamic conditions, the flowing air allows efficient water draining from the micropores, while in static conditions, in the absence of flowing air, the water draining is probably less efficient. In this case, part of the water remaining inside the micropores will be eliminated at higher temperatures during the calcination process, causing a more pronounced dealumination of the zeolite ZSM-5. The dealumination process involves the surface removal of tetrahedral aluminium, generating additional extra-framework aluminium species. These species subsequently migrate into the intra-crystalline region or channels of the zeolite structure [54].

Table 5.2 Si/Al superficial ratio from XPS. Al atoms distribution from ^{27}Al MAS NMR and XPS. And Total, Brønsted and Lewis acid sites measured by Pyridine FT-IR in ZSM-5 zeolites.

Catalyst	Si/Al	Td Al (%)		Distorted Al (%)		Oh Al (%)		Acidity (μmol.g^{-1})		
		^{27}Al MAS NMR	XPS	^{27}Al MAS NMR	XPS	^{27}Al MAS NMR	XPS	Total Acidity (B+L)	Brønsted (B)	Lewis (L)
NH_4^+-ZSM-5	10.1	100	85.2	-	14.8	-	-			
HZSM-5 DC	10.2	74	49.7	13	40.1	13	10.2	689	531 (77 %)	158 (23 %)
HZSM-5 SC	13.4	61	43.1	27	50.6	12	6.4	645	425 (66 %)	220 (34 %)

A similar O 1s BE of 532.2 eV is found for the three samples (**Figure 5.4** (c)), and this value can be related to lattice oxygens in Si-O-Si, and Si-O-Al bonds [55]. The Al 2p BE value of 74 eV and the low Al 2p photopeak full width at half maximum, FWHM, (1.5 eV) for the NH_4^+-ZSM-5 sample (**Figure 5.4** (a)) suggest the main presence of one type of aluminium mainly in 4-fold coordination (tetrahedral aluminium) [40], [56]. However, for the calcinated samples, while Si 2p and O 1s photopeaks FWHM remain constant, Al 2p photopeak FWHM significantly increases. The broadening of the Al 2p photopeak for the calcined samples suggests the existence of aluminium species in another coordination state [57], [58]. Based on the NMR results, three Gaussian-Lorentzian lines have been used to fit the Al 2p spectra, as shown in **Figure 5.4** (b). For the Al 2p spectral fitting, the value of the FWHM for the three components was imposed close to 1.5 eV.

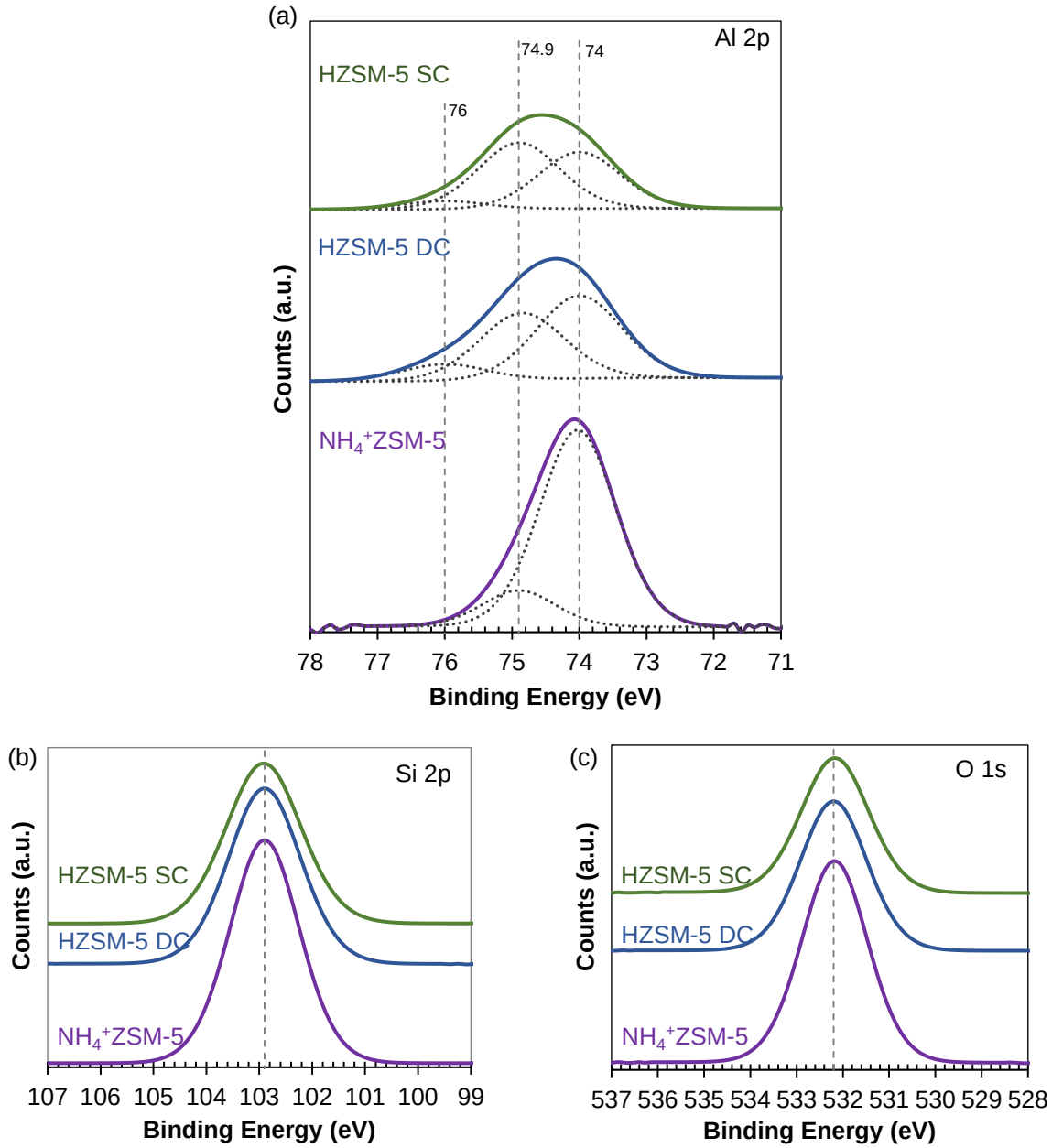

Figure 5.4. XPS core-level spectra of Si 2p (a), Al 2p (b) and O 1s (c) of the native NH_4^+-ZSM-5 zeolite and the calcined HZSM-5 DC and HZSM-5 SC zeolites.

As aforementioned, the contribution at 74 eV is due to the presence of Al atoms in regular tetrahedral coordination (Td Al). The Al 2p BE value of 76 eV found for the third component in the calcinated samples agrees with the presence of extra-framework aluminium in 6-fold coordination (Oh Al) [57], [59]. The intermediate contribution at 74.9 eV can be attributed to the highly distorted tetrahedral aluminium species observed by ^{27}Al MAS NMR. The percentages of each aluminium species are listed in **Table 5.2**. Analysis of the distribution of aluminium species on the surface shows that, compared with NMR analysis, more highly distorted Al extra-framework species are present. This result can be explained by the presence of these species on the surface of the native zeolite prior to the calcination step (Figure 5.5 A). As previously observed by NMR, highly distorted Al extra-framework species are more abundant at the surface of HZSM-5 SC in comparison with HZSM-5 DC (**Table 5.2**).

Both ^{27}Al MAS NMR and XPS analyses showed that calcination caused the formation of octahedrally (Oh) coordinated extra-framework Al atoms and highly distorted Al extra-framework species. Highly distorted Al extra-framework species are clearly more abundant after a calcination process in static conditions. This results from the dealumination process caused by steam exposition during the heating [51], the calcination in static conditions favouring this process.

5.4.3. Effect of calcination conditions on HZSM-5 acid properties

Pyridine FTIR is a helpful method for evaluating the relative acid strength at a catalyst surface for both Brønsted- and Lewis-acid sites at different temperatures (150-450 °C). Pyridine FTIR spectra of HZSM-5 DC and HZSM-5 SC zeolites after desorption at 150 °C, 250 °C, 350 °C, and 450 °C are shown in **Figure 5.5** (a). After desorption at 150 °C, three bands located at ~1455, 1490 and 1545 cm^{-1} are found for the two zeolites. The peak at ~1455 cm^{-1} is due to pyridine coordinated with Lewis acid. The peak at ~1490 cm^{-1} is assigned to pyridine adsorbed on Lewis and Brønsted acid sites. The peak at ~1545 cm^{-1} is attributed to the C-C stretching vibration of the pyridinium ions resulting from pyridine protonation on Brønsted acid sites [44].

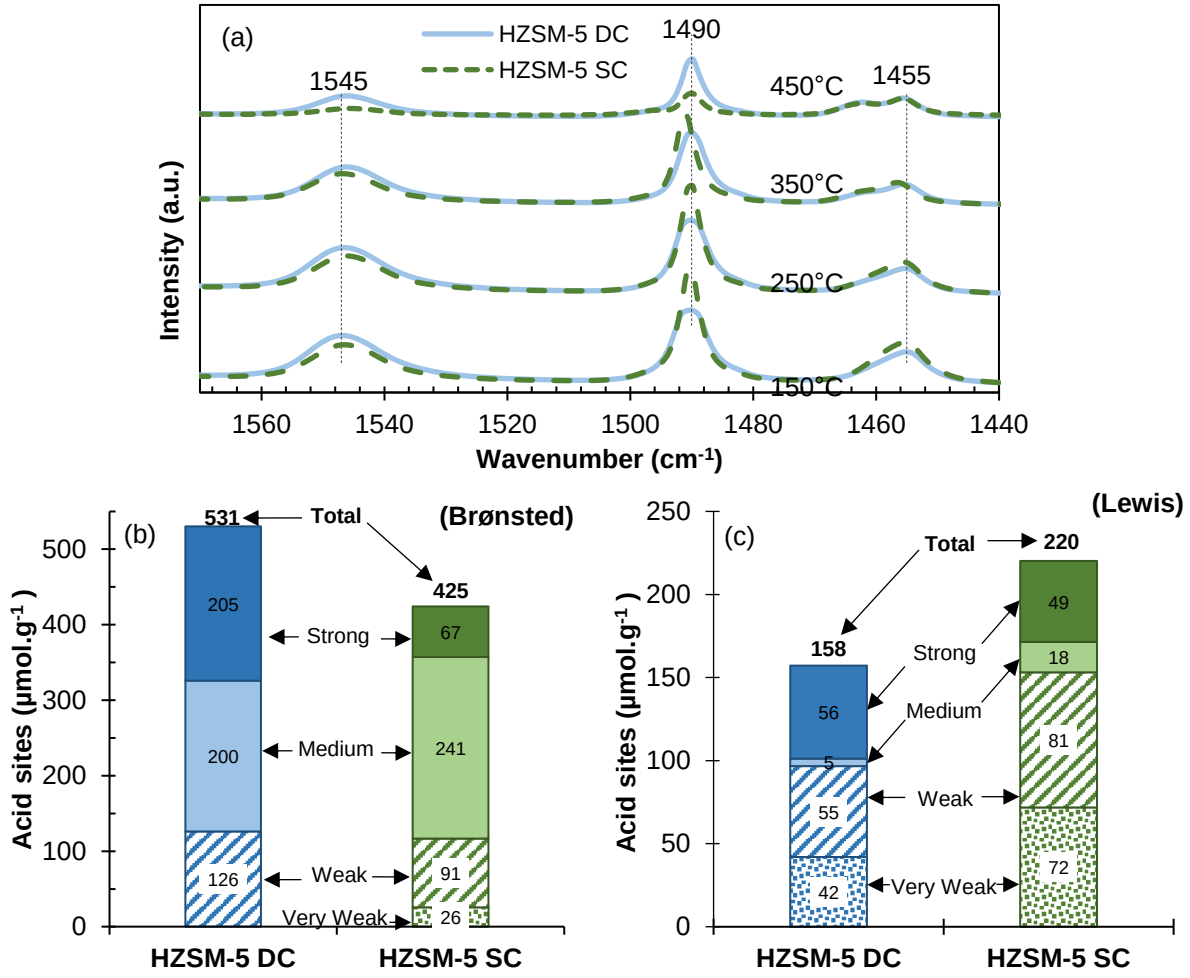

Figure 5.5. Pyridine FT-IR of HZSM-5 DC and HZSM-5 SC zeolites after desorption at 150, 250, 350, and 450 °C (a). And their respective Brønsted (b) and Lewis (c) acid sites distribution as functions of the strength of the acid site, very weak (150 °C), weak (250 °C), medium (350 °C) and strong (>450 °C).

Brønsted and Lewis acid sites quantification has been done along the intensity of the peaks at 1545 cm^{-1} and 1455 cm^{-1}, respectively. The intensity of the three bands decreased with the temperature increase from 150 to 450 °C (**Figure 5.5** (a)). The quantity of desorbed pyridine can be calculated at each temperature, allowing the evaluation of the acid sites distribution as a function of the strength of the acid site (**Figure 5.5** (b and c)). Compared to HZSM-5 SC, HZSM-5 DC zeolite exhibited much more Brønsted acid sites. The difference in Brønsted acid sites is emphasised in the medium and strong acid sites. In contrast, more Lewis acid sites are found in HZSM-5 SC compared to HZSM-5 DC. The difference in Lewis acid sites is highlighted in the very weak and weak acid sites. The relative ratio of the Brønsted and Lewis acid sites is given in **Table 5.2**. The Brønsted acid sites represent 77 % and 66 % of the total acid sites of zeolites calcinated in dynamic and static conditions, respectively. The highest proportion of Lewis acid sites in HZSM-5 DC zeolite can be explained by the dehydroxylation of Brønsted sites promoted by steam autogenerated [60]. These values well agree with the values found by NMR and are attributed to tetrahedral lattice aluminium (Td Al) in HZSM-5 DC (74 %) and HZSM-5 DC (61 %).

This study shows that the calcination conditions alter the Lewis/Brønsted acid sites ratio (0.30 for HZSM-5 DC and 0.52 for HZSM-5 SC) and amend the strength of Brønsted acid sites (3 times less strong sites for HZSM-5 SC).

5.4.4. Effect of calcination conditions on LLDPE catalytic pyrolysis

Thermogravimetric studies on the thermal and catalytic degradation of LLDPE have been first conducted. **Figure 5.6** shows TG and DTG curves obtained for the pyrolysis under N_2 flow of the pure LLDPE and the LLDPE/HZSM-5 mixtures. The different temperatures of LLDPE decomposition (5 %, 50 % and 95 %) obtained with or without a catalyst are listed in **Table 5.3**.

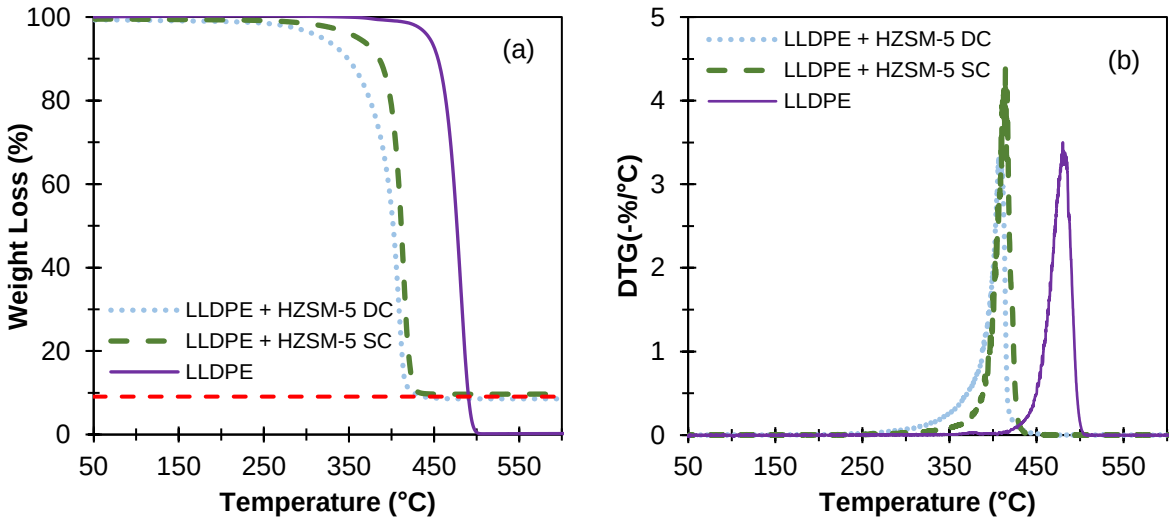

Figure 5.6. TG (a) and DTG (b) curves under N_2 of LLDPE and the corresponding mixtures with the HZSM5 Zeolites.

The catalytic effect for HZSM-5 DC and HZSM-5 SC is significant. Based on the $T_{5\ \%}$, the temperature of LLDPE decomposition is lowered by 106 °C and 68 °C in the presence of HZSM-5 DC and HZSM-5 SC, respectively. The same trends are found based on $T_{50\ \%}$, $T_{95\ \%}$ and T_{max}, but the difference between the two catalysts is getting smaller. In the presence of ZSM-5 zeolites, the DTG curves exhibited a low-temperature shoulder, suggesting a two-step process for the degradation of LDPE. Due to the microporous nature of zeolite, only a small number of external acid sites are initially accessible to the large polymer molecules. In other words, the first step of the reaction takes place on the external surface of the zeolite. As the cracking reaction progresses, smaller and smaller polymer fragments are formed, and the fragments can more easily access the internal acid sites. This first cracking facilitates a second step corresponding to the complete degradation of the polymer fragments. Peral et al. [61] found a direct linear relationship between the number of Brønsted acid sites and the catalytic activity of LDPE cracking on the external surface. Therefore, the highest activity of HZSM-5 DC compared to HZSM-5 SC, in the temperature range of 300-400 °C, can be related to the highest amount of Brønsted acid sites at the external surface in this zeolite (**Figure 5.5** (b)).

Table 5.3 Temperature of maximum, 5 %, 50 % and 95 % of decomposition and total weight loss of LLDPE and polymer mixtures with both HZSM5.

Sample	Total Weight loss (%)	T_{max} (ºC)	ΔT_{max} (ºC)	$T_{5\ \%}$ (ºC)	$T_{50\ \%}$ (ºC)	$T_{95\ \%}$ (ºC)
LLDPE + HZSM-5 SC	91.7 ± 2.8	413.7 ± 4.6	68.1 ± 4.6	377.0 ± 19.4	409.3 ± 4.8	419.9 ± 4.7
LLDPE + HZSM-5 DC	90.3 ± 1.2	407.8 ± 3.1	73.8 ± 3.1	339.8 ± 59.9	400.1 ± 12.1	414.9 ± 3.1
LLDPE	99.8 ± 0.53	481.7 ± 8.7	-	445.4 ± 6.5	476.2 ± 5.0	491.0 ± 9.0

Thermal and catalytic pyrolysis of LLDPE (Mix/Layer arrangement) have also been performed in a tubular reactor to evaluate solid/liquid/gas yields and the product composition in the liquid phase. The results of the wax + oil/gas/coke yields of thermal and catalytic pyrolysis of LLDPE are shown in **Figure 5.7**. Both zeolites show a decrease in oil/wax yield and higher gas production compared to the thermal pyrolysis of LLDPE. These expected results confirm a more volatile and short-chain hydrocarbon formation in the catalytic process compared to the thermal one. HZSM-5 SC catalyst led to the highest gas yield compared to HZSM-5 DC. While the Brønsted acid sites catalyse C-C cracking reactions, Lewis acid sites have a strong preference for C-H activation and, to a greater extent, for dehydrogenation reactions [62]. Therefore, HZSM-5 SC, which exhibited the highest amount of Lewis acid sites (**Figure 5.5**), will favour dehydrogenative cracking, which in turn improves the yield of light olefins [63], [64].

Figure 5.8 (a) shows the carbon distribution from C_3 to C_{21} in the liquid phase obtained after the thermal and catalytic PE pyrolysis. Carbon distribution differs significantly between thermal and catalytic pyrolysis. Heavier condensable products ranging from C_{12} to C_{21} are mainly found after the thermal process. In this case, thermal polyethylene cracking initiates via a radical mechanism [22]. This mechanism initiates principally through random chain scissions and chain-end scission. Random scission produces long-chain hydrocarbons [65] and well explains the observed carbon distribution (mainly $\geq C_{13}$). With HZSM-5 catalysts, the main carbon number composition of the liquid phase is found

between C_3 and C_{12}. When the catalyst is involved, competition between thermal and catalytic cracking occurs. With an acid catalyst, the cracking initiates via a carbocationic mechanism. The initiation can occur strongly by adding protons in the C-C bonds through Brønsted acid sites producing carbonium ions or weakly in Lewis acid sites (electron donor-acceptor, EDA) by subtracting hydride ions, creating carbenium ions [10], [45]. As expected, HZSM-5 SC leads to the production of more light hydrocarbons (C_3-C_5) in comparison with HZSM-5 DC due to its lower Brønsted acid sites. In contrast, HZSM-5 DC leads to the production of more liquid products in the range of C_6-C_{12}. According to Inayat et al. [66], the enhancement in the yield of light hydrocarbons is driven by dehydrogenative cracking. This is a result of the reduction in the content of Brønsted acid sites within the zeolite, thereby suppressing hydrogen transfer reactions.

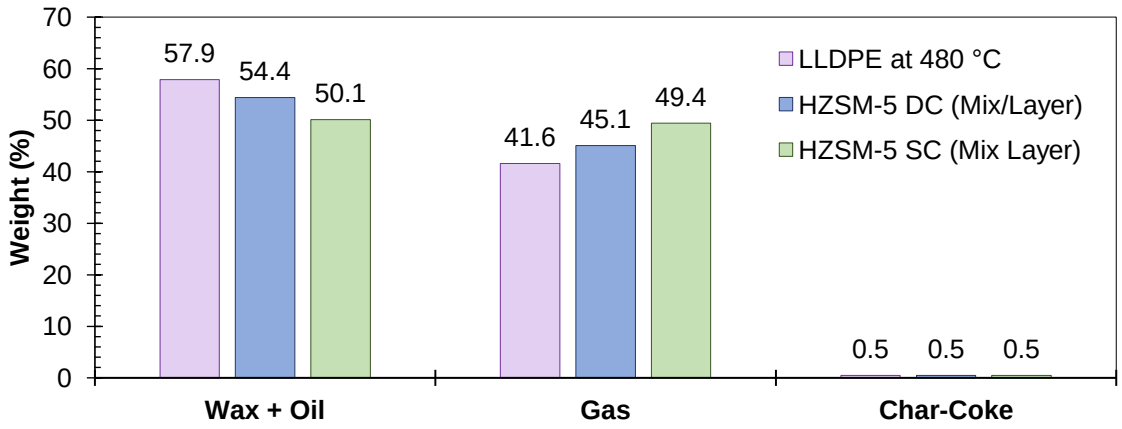

Figure 5.7. Yield result of pyrolysis of LLDPE at 480 °C (Purple), LLDPE + HZSM-5 DC (Blue), and LLDPE + HZSM-5 SC (Green).

Figure 5.8 (b) shows the composition of the liquid phase obtained after the thermal and catalytic PE pyrolysis. The liquid composition was gathered into aromatics, paraffins, iso-paraffins, olefins (including alkenes, alkadienes and alkynes) and iso-olefins.

Through the free radical mechanism, thermal pyrolysis promotes the production of olefins and paraffins from C_1 to C_{40}. Aromatic compounds were negligibly low, under 500 °C (random scission). Paraffins result from H-abstraction, olefines from β-scission, and iso-paraffins and iso-olefins from isomerisation.

When carbocations are generated in the zeolite acid sites, subsequent cracking reactions, such as isomerisation, oligomerisation aromatisation, or alkylation reactions, can occur [10], [22]. Macromolecules degrade on the acid sites at the external surface, producing shorter intermediaries. The catalyst adsorbs these molecules, and subsequent chemical reactions occur. Paraffins are limited, such as bimolecular reaction by the pore size of HZSM-5 zeolites, where β-scission and isomerisation are predominant reactions. Cyclisation and aromatisation are possible through hydrogen transfer reactions [10]. In the cracking of polymers using zeolites, the main responsible for aromaticity (especially monoaromatics production [67]) is the Brønsted acid sites [64]. However, the moderated presence of Lewis acid sites can increase the aromatic selectivity [45], [67].

The aromatic hydrocarbon production increases by 55.5 % and 42.6 %, with HZSM-5 DC and HZSM-5 SC catalysts, respectively, compared to thermal cracking. HZSM-5 DC zeolite production is less than 4.3 % paraffins, 8.6 % in iso-paraffins and 8.6 % iso-olefins compared to HZSM-5 SC zeolite; olefins and iso-olefins are the primary precursors in the Diels Alder reaction, aromatisation from alkenes and dienes [68]. Improved contact between the acid sites of the micropores and the short-chain hydrocarbons generated during the initiation reactions, the aromatisation reactions that use olefins as precursors are increased; these reactions occur at the micropores [68] and will depend on the density of Brønsted acid sites. In this experiment, the different roles played by the external and microporous surfaces combined with the nature of acid sites in the cracking of the polymer are evident. While the former is responsible for the first catalytic cracking and is the connection between the products of this first cracking and the micropores, the latter is influenced by the diffusion rate, the type of acidity and the number of available acid sites linked to the amount of microporous surface [69]. The most significant amount of aromatics produced with the HZSM-5 DC zeolite is caused by strong Brønsted acids [64], [67]. On the external surface, these sites cause catalytic cracking [61] at lower temperatures, and in the micropores, they are responsible for aromatisation.

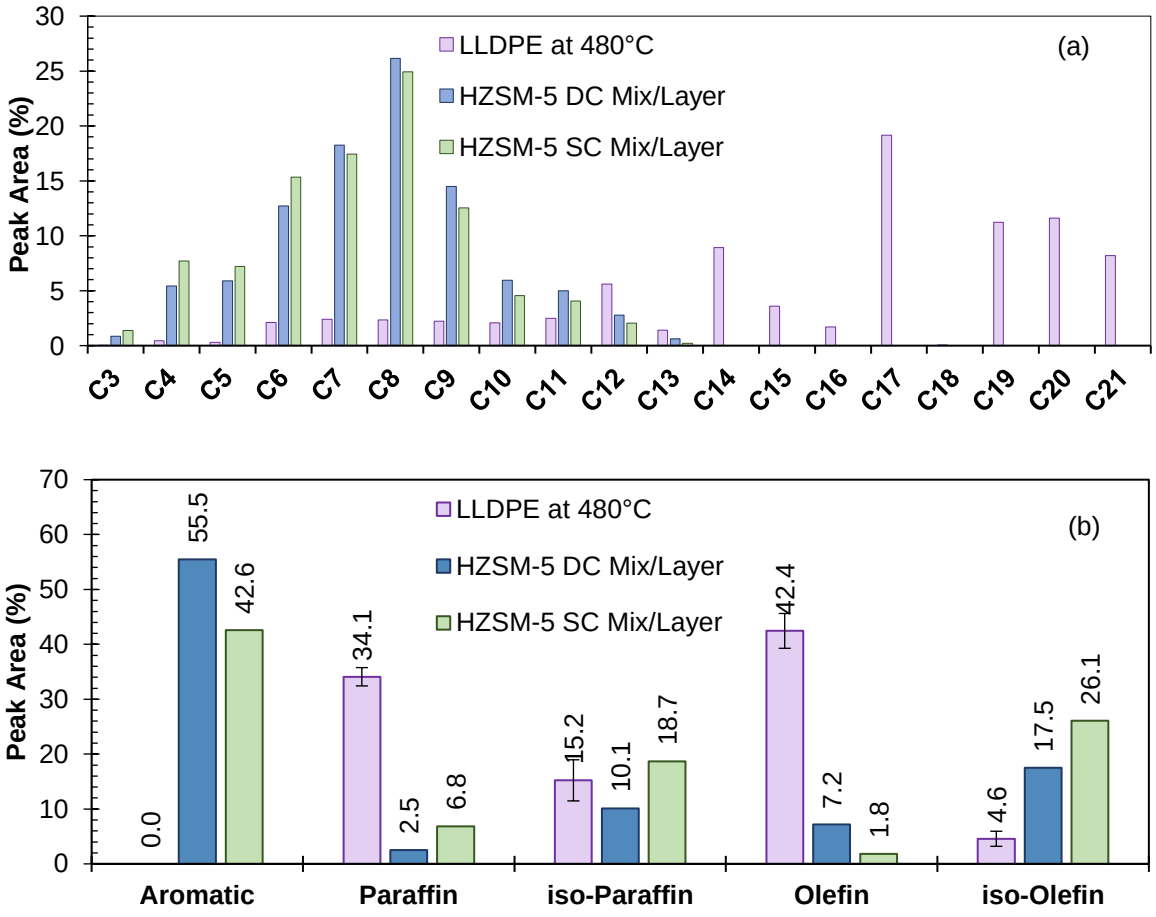

Figure 5.8. Product carbon distribution (a) and composition (b) of the oil/wax from the decomposition of LLDPE at 480 °C (Purple), LLDPE + HZSM-5 DC (Blue), and LLDPE + HZSM-5 SC (Green).

5.5. Conclusions

The effect on LLDPE pyrolysis of ZSM-5 zeolite calcined under two conditions: dynamic (DC), where there is an airflow and static (SC), where there is no airflow during calcination, was studied. The physicochemical characteristics show a significant difference between both calcination conditions. XRD patterns reveal that both calcined samples have lost some crystallinity compared to the native NH^{4+}-ZSM-5 zeolite. The specific surface area of the HZSM-5 SC zeolite is similar to the value of the HZSM-5 DC zeolite, but a slight decrease in micropore surface area was observed, 6.5 % less compared to HZSM-5 DC. The pore size distribution remains nearly identical, regardless of the calcination method. The ^{27}Al MAS NMR spectra show that calcination creates framework defects and partially perturbs Al^{4+} in the zeolites; the calcined HZSM-5 SC sample has a more pronounced framework defect due to steam zeolite dealumination. The XPS analyses indicate that the surface of the HZSM-5 SC zeolite is depleted in aluminium compared to the surface of ammonium-exchanged and HZSM-5 DC zeolites. The acid properties of the zeolites were evaluated using pyridine FTIR, and it was found that HZSM-5 DC has more Brønsted acid sites than HZSM-5 SC, while HZSM-5 SC has more Lewis acid sites than HZSM-5 DC. These differences in acid sites are attributed to the dehydroxylation of Brønsted sites promoted by steam. The results from different techniques were consistent and provided valuable insights into the change of the nature of the acidity of the ZSM-5 zeolite using calcination as a modification method.

The catalytic effect of the HZSM-5 zeolites significantly reduces the starting temperature of LLDPE thermal decomposition. The HZSM-5 DC zeolite exhibited a higher activity in catalytic cracking than HZSM-5 SC. The catalytic pyrolysis of LLDPE using HZSM-5 zeolites showed a decrease in wax/oil yield and increased gas production compared to thermal pyrolysis, indicating the generation of more volatile, short-chain hydrocarbons. This study also analysed the composition and carbon distribution of the liquid phase. HZSM-5 zeolites increased the production of aromatics, especially for HZSM-5 DC zeolite, which was attributed to the Brønsted acid sites of the micropores of the structure and the short-chain hydrocarbons generated during the initiation reactions.

5.6. References

[1] P. Europe, “Plastics – the Facts 2022,” *PlasticEurope*, no. October, p. 80, 2022.

[2] “Plastic pollution is growing relentlessly as waste management and recycling fall short, says OECD.” https://www.oecd.org/newsroom/plastic-pollution-is-growing-relentlessly-as-waste-management-and-recycling-fall-short.htm (accessed Jun. 23, 2023).

[3] Ellen MacArthur Foundation and World Economic Forum, “The New Plastics Economy: Rethinking the future of plastics,” *Ellen MacArthur Found.*, no. January, p. 120, 2016.

[4] I. Vollmer *et al.*, “Beyond Mechanical Recycling: Giving New Life to Plastic Waste,” *Angew. Chemie Int. Ed.*, 2020, doi: 10.1002/anie.201915651.

[5] I. Vollmer *et al.*, “Beyond Mechanical Recycling: Giving New Life to Plastic Waste,” *Angew. Chemie - Int. Ed.*, 2020, doi: 10.1002/anie.201915651.

[6] R. Miandad, M. A. Barakat, A. S. Aburiazaiza, M. Rehan, and A. S. Nizami, “Catalytic pyrolysis of plastic waste: A review,” *Process Saf. Environ. Prot.*, vol. 102, pp. 822–838, 2016, doi:

10.1016/j.psep.2016.06.022.

[7] L. O. Mark, M. C. Cendejas, and I. Hermans, “The Use of Heterogeneous Catalysis in the Chemical Valorization of Plastic Waste,” *ChemSusChem*, vol. 13, no. 22, pp. 5808–5836, 2020, doi: 10.1002/cssc.202001905.

[8] E. Butler, G. Devlin, and K. McDonnell, “Waste polyolefins to liquid fuels via pyrolysis: Review of commercial state-of-the-art and recent laboratory research,” *Waste and Biomass Valorization*, vol. 2, no. 3, pp. 227–255, 2011, doi: 10.1007/s12649-011-9067-5.

[9] J. Aguado, D. P. Serrano, and J. M. Escola, “Fuels from Waste Plastics by Thermal and Catalytic Processes: A Review,” *Ind. Eng. Chem. Res.*, vol. 47, no. 21, pp. 7982–7992, 2008, doi: 10.1021/ie800393w.

[10] D. P. Serrano, J. Aguado, and J. M. Escola, “Developing Advanced Catalysts for the Conversion of Polyolefinic Waste Plastics into Fuels and Chemicals,” *ACS Catal.*, vol. 2, no. 9, pp. 1924–1941, 2012, doi: 10.1021/cs3003403.

[11] S. D. Anuar Sharuddin, F. Abnisa, W. M. A. Wan Daud, and M. K. Aroua, “A review on pyrolysis of plastic wastes,” *Energy Convers. Manag.*, vol. 115, pp. 308–326, 2016, doi: 10.1016/j.enconman.2016.02.037.

[12] B. Kunwar, H. N. Cheng, S. R. Chandrashekaran, and B. K. Sharma, “Plastics to fuel: a review,” *Renew. Sustain. Energy Rev.*, vol. 54, pp. 421–428, 2016, doi: 10.1016/j.rser.2015.10.015.

[13] W. A. Sweeney and P. F. Bryan, “BTX Processing,” *Kirk-Othmer Encycl. Chem. Technol.*, no. X, 1990, doi: 10.1002/0471238961.02202419230505.a01.pub2.

[14] Q. Zhou, Y. Z. Wang, C. Tang, and Y. H. Zhang, “Modifications of ZSM-5 zeolites and their applications in catalytic degradation of LDPE,” *Polym. Degrad. Stab.*, vol. 80, no. 1, pp. 23–30, 2003, doi: 10.1016/S0141-3910(02)00378-6.

[15] A. Durmuş, S. N. Koç, G. S. Pozan, and A. Kaşgöz, “Thermal-catalytic degradation kinetics of polypropylene over BEA, ZSM-5 and MOR zeolites,” *Appl. Catal. B Environ.*, vol. 61, no. 3–4, pp. 316–322, 2005, doi: 10.1016/j.apcatb.2005.06.009.

[16] J. F. Mastral, C. Berrueco, M. Gea, and J. Ceamanos, “Catalytic degradation of high density polyethylene over nanocrystalline HZSM-5 zeolite,” *Polym. Degrad. Stab.*, vol. 91, no. 12, pp. 3330–3338, 2006, doi: 10.1016/j.polymdegradstab.2006.06.009.

[17] A. Marcilla, M. del R. Hernández, and Á. N. García, “Study of the polymer-catalyst contact effectivity and the heating rate influence on the HDPE pyrolysis,” *J. Anal. Appl. Pyrolysis*, vol. 79, no. 1–2, pp. 424–432, 2007, doi: 10.1016/j.jaap.2006.10.017.

[18] A. Marcilla, A. Gómez-Siurana, and F. J. Valdés, “Influence of the final ‘ageing’ temperature on the regeneration behaviour and location of the coke obtained in the HZSM-5 and USY zeolites during the LDPE cracking,” *Appl. Catal. A Gen.*, vol. 334, no. 1–2, pp. 20–25, 2008, doi: 10.1016/j.apcata.2007.07.042.

[19] G. Elordi *et al.*, “Catalytic pyrolysis of HDPE in continuous mode over zeolite catalysts in a conical spouted bed reactor,” *J. Anal. Appl. Pyrolysis*, vol. 85, no. 1–2, pp. 345–351, 2009, doi: 10.1016/j.jaap.2008.10.015.

[20] N. Miskolczi, F. Ateş, and N. Borsodi, “Comparison of real waste (MSW and MPW) pyrolysis in batch reactor over different catalysts. Part II: Contaminants, char and pyrolysis oil properties,” *Bioresour. Technol.*, vol. 144, pp. 370–379, 2013, doi: 10.1016/j.biortech.2013.06.109.

[21] “Thermoplastics :: PlasticsEurope.” https://www.plasticseurope.org/en/about-plastics/what-are-

plastics/large-family/thermoplastics (accessed May 27, 2021).

[22] Y. Xue, P. Johnston, and X. Bai, “Effect of catalyst contact mode and gas atmosphere during catalytic pyrolysis of waste plastics,” *Energy Convers. Manag.*, vol. 142, pp. 441–451, 2017, doi: 10.1016/j.enconman.2017.03.071.

[23] D. P. Serrano, R. A. García, M. Linares, and B. Gil, “Influence of the calcination treatment on the catalytic properties of hierarchical ZSM-5,” *Catal. Today*, vol. 179, no. 1, pp. 91–101, 2012, doi: 10.1016/j.cattod.2011.06.029.

[24] D. J. Kim and H. S. Chung, “Synthesis and characterization of ZSM-5 zeolite from serpentine,” *Appl. Clay Sci.*, vol. 24, no. 1–2, pp. 69–77, 2003, doi: 10.1016/S0169-1317(03)00149-2.

[25] J. Lu, Z. Zhao, C. Xu, A. Duan, and P. Zhang, “Effects of calcination temperature on the acidity and catalytic performances of HZSM-5 zeolite catalysts for the catalytic cracking of n-butane,” *J. Nat. Gas Chem.*, vol. 14, no. 4, pp. 213–220, 2005, doi: 10.1016/j.ijfoodmicro.2004.12.017.

[26] D. A. Bulushev, L. Kiwi-minsker, and A. Renken, “N2O decomposition over Fe / ZSM-5 catalysts : effects of high-temperature calcination and steaming,” *Ind. Eng. Chem. Res.*, vol. 211, no. 2002, p. 2004, 2004.

[27] R. Pouria, L. Vafi, and R. Karimzadeh, “Propane catalytic cracking on pretreated La-ZSM-5 zeolite during calcination for light olefins production,” *J. Rare Earths*, vol. 35, no. 6, pp. 542–550, 2017, doi: 10.1016/S1002-0721(17)60946-3.

[28] S. . Campbell, D. . Bibby, J. . Coddington, and R. . Howe, “Dealumination of HZSM-5 Zeolites,” *J. Catal.*, vol. 161, no. 1, pp. 350–358, 1996, doi: 10.1006/jcat.1996.0192.

[29] L. R. Raddi De Araujo and M. Schmal, “The Calcination effects on Pt/HZSM-5 catalysts in the aromatization of propane,” *Appl. Catal. A Gen.*, vol. 203, no. 2, pp. 275–284, 2000, doi: 10.1016/S0926-860X(00)00487-7.

[30] M. D. Romero, J. A. Calles, A. Rodriguez, and J. C. Cabanelas, “The influence of calcination treatment over bifunctional Ni/HZSM-5 catalysts,” *Ind. Eng. Chem. Res.*, vol. 37, no. 10, pp. 3846–3852, 1998, doi: 10.1021/ie980143i.

[31] P. L. Tan, Y. L. Leung, S. Y. Lai, and C. T. Au, “The effect of calcination temperature on the catalytic performance of 2 wt. % Mo/HZSM-5 in methane aromatization,” *Appl. Catal. A Gen.*, vol. 228, no. 1–2, pp. 115–125, 2002, doi: 10.1016/S0926-860X(01)00955-3.

[32] Q. Zhang *et al.*, “Isoparaffin production by aqueous phase processing of sorbitol over the Ni/HZSM-5 catalysts: Effect of the calcination temperature of the catalyst,” *Fuel*, vol. 90, no. 11, pp. 3468–3472, 2011, doi: 10.1016/j.fuel.2011.06.046.

[33] L. Bai, Y. Zhou, Y. Zhang, H. Liu, X. Sheng, and Y. Duan, “Effect of calcination atmosphere on the catalytic properties of PtSnNaMg/ZSM-5 for propane dehydrogenation,” *Catal. Commun.*, vol. 10, no. 15, pp. 2013–2017, Sep. 2009, doi: 10.1016/j.catcom.2009.07.020.

[34] R. Hull *et al.*, *Characterization and Design of Zeolite Catalysts*, vol. 141. Berlin, Heidelberg: Springer Berlin Heidelberg, 2010.

[35] M. S. Abbas-Abadi *et al.*, “Challenges and opportunities of light olefin production via thermal and catalytic pyrolysis of end-of-life polyolefins: Towards full recyclability,” *Prog. Energy Combust. Sci.*, vol. 96, no. September 2022, p. 101046, 2023, doi: 10.1016/j.pecs.2022.101046.

[36] T. Xayachak *et al.*, “Pyrolysis for plastic waste management: An engineering perspective,” *J. Environ. Chem. Eng.*, vol. 10, no. 6, p. 108865, 2022, doi: 10.1016/j.jece.2022.108865.

[37] L. C. Lerici, M. S. Renzini, U. Sedran, and L. B. Pierella, “Tertiary recycling of low-density polyethylene by catalytic cracking over ZSM-11 and BETA zeolites modified with Zn2+: Stability study,” *Energy and Fuels*, vol. 27, no. 4, pp. 2202–2208, 2013, doi: 10.1021/ef302099e.

[38] A. Smiešková, P. Hudec, N. Kumar, T. Salmi, D. Y. Murzin, and V. Jorík, “Aromatization of methane on Mo modified zeolites: Influence of the surface and structural properties of the carriers,” *Appl. Catal. A Gen.*, vol. 377, no. 1–2, pp. 83–91, 2010, doi: 10.1016/j.apcata.2010.01.021.

[39] K. S. MAZDIYASNI and L. M. BROWN, “Influence of Dynamic Calcination on Crystallite Growth of Submicron Rare-Earth Oxides,” *J. Am. Ceram. Soc.*, vol. 54, no. 10, pp. 479–483, 1971, doi: 10.1111/j.1151-2916.1971.tb12183.x.

[40] T. L. Barr, “The nature of the relative bonding chemistry in zeolites: An XPS study,” *Zeolites*, vol. 10, no. 8, pp. 760–765, 1990, doi: 10.1016/0144-2449(90)90058-Y.

[41] P. Decyk, K. K. Do, and I. W. Seong, “Poisoning effect of SO2 on NO reduction by i-butane over Fe/ZSM-5 prepared by sublimation method,” *J. Catal.*, vol. 203, no. 2, pp. 369–374, 2001, doi: 10.1006/jcat.2001.3346.

[42] T. L. Barr and M. A. Lishka, “ESCA Studies of the Surface Chemistry of Zeolites,” *J. Am. Chem. Soc.*, vol. 108, no. 12, pp. 3178–3186, 1986, doi: 10.1021/ja00272a004.

[43] J. B. Nagy *et al.*, “Aluminium distribution and cation location in various M-ZSM-5-type zeolites (M {double bond, long} Li, Na, K, Rb, Cs, NH4),” *Zeolites*, vol. 8, no. 3, pp. 209–220, 1988, doi: 10.1016/S0144-2449(88)80310-5.

[44] A. M. Hernández-Giménez *et al.*, “Effect of Mesoporosity, Acidity and Crystal Size of Zeolite ZSM-5 on Catalytic Performance during the Ex-situ Catalytic Fast Pyrolysis of Biomass,” *ChemCatChem*, vol. 13, no. 4, pp. 1207–1219, 2021, doi: 10.1002/cctc.202001778.

[45] M. S. Renzini, U. Sedran, and L. B. Pierella, “H-ZSM-11 and Zn-ZSM-11 zeolites and their applications in the catalytic transformation of LDPE,” *J. Anal. Appl. Pyrolysis*, vol. 86, no. 1, pp. 215–220, 2009, doi: 10.1016/j.jaap.2009.06.008.

[46] M. S. Renzini, L. C. Lerici, U. Sedran, and L. B. Pierella, “Stability of ZSM-11 and BETA zeolites during the catalytic cracking of low-density polyethylene,” *J. Anal. Appl. Pyrolysis*, vol. 92, no. 2, pp. 450–455, 2011, doi: 10.1016/j.jaap.2011.08.008.

[47] M. Heydariaraghi, S. Ghorbanian, A. Hallajisani, and A. Salehpour, “Fuel properties of the oils produced from the pyrolysis of commonly-used polymers: Effect of fractionating column,” *J. Anal. Appl. Pyrolysis*, vol. 121, pp. 307–317, 2016, doi: 10.1016/j.jaap.2016.08.010.

[48] C. Zhang, S. Li, and S. Bao, “Sustainable Synthesis of ZSM-5 Zeolite from Rice Husk Ash Without Addition of Solvents,” *Waste and Biomass Valorization*, vol. 10, no. 10, pp. 2825–2835, Oct. 2019, doi: 10.1007/s12649-018-0356-0.

[49] A. Samoson, E. Lippmaa, G. Engelhardt, U. Lohse, and H. G. Jerschkewitz, “Quantitative high-resolution 27Al NMR: tetrahedral non-framework aluminium in hydrothermally treated zeolites,” *Chem. Phys. Lett.*, vol. 134, no. 6, pp. 589–592, 1987, doi: 10.1016/0009-2614(87)87199-3.

[50] D. Coster and J. J. Fripiat, “Memory Effects in Gel-Solid Transformations: Coordinately Unsaturated Al Sites in Nanosized Aluminas,” *Chem. Mater.*, vol. 5, no. 9, pp. 1204–1210, 1993, doi: 10.1021/cm00033a004.

[51] P. Sazama *et al.*, “FTIR and 27Al MAS NMR analysis of the effect of framework Al- and Si-defects in micro- and micro-mesoporous H-ZSM-5 on conversion of methanol to hydrocarbons,” *Microporous Mesoporous Mater.*, vol. 143, no. 1, pp. 87–96, 2011, doi: 10.1016/j.micromeso.2011.02.013.

[52] C. Coutanceau, J. Da Silva, M. Alvarez, F. Ribeiro, and M. Guisnet, “Dealumination of zeolites,” *J. Chim. Phys.*, vol. 94, no. 0191, pp. 765–781, 1997, doi: 10.1051/jcp/1997940765.

[53] S. Klaimy *et al.*, “Flash Catalytic Pyrolysis of Polyethylene over (Alumino)silicate Materials,” *ChemCatChem*, vol. 12, no. 4, pp. 1109–1116, 2020, doi: 10.1002/cctc.201901819.

[54] H. Xiao *et al.*, “A highly efficient Ga/ZSM-5 catalyst prepared by formic acid impregnation and in situ treatment for propane aromatization,” *Catal. Sci. Technol.*, vol. 5, no. 8, pp. 4081–4090, 2015, doi: 10.1039/c5cy00665a.

[55] D. Stacchiola *et al.*, “Synthesis and structure of ultrathin aluminosilicate films,” *Angew. Chemie - Int. Ed.*, vol. 45, no. 45, pp. 7636–7639, 2006, doi: 10.1002/anie.200602670.

[56] W. Choopun and S. Jitkarnka, “Catalytic activity and stability of HZSM-5 zeolite and hierarchical uniform mesoporous MSU-SZSM-5 material during bio-ethanol dehydration,” *J. Clean. Prod.*, vol. 135, pp. 368–378, 2016, doi: 10.1016/j.jclepro.2016.06.110.

[57] R. B. Borade, A. Adnot, and S. Kaliaguine, “Acid sites in Al-ZSM-22 and Fe-ZSM-22,” *Zeolites*, vol. 11, no. 7, pp. 710–719, 1991, doi: 10.1016/S0144-2449(05)80177-0.

[58] M. Todea, E. Vanea, S. Bran, P. Berce, and S. Simon, “XPS analysis of aluminosilicate microspheres bioactivity tested in vitro,” *Appl. Surf. Sci.*, vol. 270, pp. 777–783, 2013, doi: 10.1016/j.apsusc.2013.01.178.

[59] T. L. Barr, S. Seal, K. Wozniak, and J. Klinowski, “ESCA studies of the coordination state of aluminium in oxide environments,” *J. Chem. Soc. - Faraday Trans.*, vol. 93, no. 1, pp. 181–186, 1997, doi: 10.1039/a604061f.

[60] J. Weitkamp and M. Hunger, “ACID AND BASE CATALYSIS ON ZEOLITES,” *Stud. Surf. Sci. Catal.*, vol. 168, pp. 787–835, 2007, doi: https://doi.org/10.1016/S0167-2991(07)80810-X.

[61] A. Peral, J. M. Escola, D. P. Serrano, J. Přech, C. Ochoa-Hernández, and J. Čejka, “Bidimensional ZSM-5 zeolites probed as catalysts for polyethylene cracking,” *Catal. Sci. Technol.*, vol. 6, no. 8, pp. 2754–2765, 2016, doi: 10.1039/c5cy02075a.

[62] N. Rane, A. R. Overweg, V. B. Kazansky, R. A. van Santen, and E. J. M. Hensen, “Characterization and reactivity of Ga+ and GaO+ cations in zeolite ZSM-5,” *J. Catal.*, vol. 239, no. 2, pp. 478–485, 2006, doi: 10.1016/j.jcat.2006.03.004.

[63] D. K. Ratnasari, M. A. Nahil, and P. T. Williams, “Catalytic pyrolysis of waste plastics using staged catalysis for production of gasoline range hydrocarbon oils,” *J. Anal. Appl. Pyrolysis*, vol. 124, pp. 631–637, 2017, doi: 10.1016/j.jaap.2016.12.027.

[64] A. A. A. Inayat, A. A. A. Inayat, W. Schwieger, B. Sokolova, and P. Lestinsky, “Enhancing aromatics and olefins yields in thermo-catalytic pyrolysis of LDPE over zeolites: Role of staged catalysis and acid site density of HZSM-5,” *Fuel*, vol. 314, no. January, p. 123071, 2022, doi: 10.1016/j.fuel.2021.123071.

[65] S. T. Okonsky, J. V. J. Krishna, and H. E. Toraman, “Catalytic co-pyrolysis of LDPE and PET with HZSM-5, H-beta, and HY: experiments and kinetic modelling,” *React. Chem. Eng.*, vol. 7, pp. 2175–2191, 2022, doi: 10.1039/d2re00144f.

[66] A. A. Inayat, A. A. Inayat, W. Schwieger, B. Sokolova, and P. Lestinsky, “Enhancing aromatics and olefins yields in thermo-catalytic pyrolysis of LDPE over zeolites: Role of staged catalysis and acid site density of HZSM-5,” *Fuel*, vol. 314, no. January, p. 123071, 2022, doi: 10.1016/j.fuel.2021.123071.

[67] Nishu *et al.*, “A review on the catalytic pyrolysis of biomass for the bio-oil production with ZSM-5: Focus on structure,” *Fuel Process. Technol.*, vol. 199, no. July 2019, p. 106301, 2020, doi:

10.1016/j.fuproc.2019.106301.

[68] L. Dai *et al.*, “Catalytic fast pyrolysis of low density polyethylene into naphtha with high selectivity by dual-catalyst tandem catalysis,” *Sci. Total Environ.*, vol. 771, p. 144995, 2021, doi: 10.1016/j.scitotenv.2021.144995.

[69] P. Gaurh and H. Pramanik, “A novel approach of solid waste management via aromatization using multiphase catalytic pyrolysis of waste polyethylene,” *Waste Manag.*, vol. 71, pp. 86–96, 2018, doi: 10.1016/j.wasman.2017.10.053.

Chapter 6

6. Study of cycles effect on the performances of HZSM-5 zeolite in the polyethylene catalytic pyrolysis

6.1. Introduction

In the pyrolysis of PE, the use of a catalyst, especially catalysts of an acid nature, such as zeolites, decreases the cracking temperature and improves the quality and selectivity of the products, and this depends on the textural properties, such as the acid strength of the catalyst [1]–[4]. However, coke is inevitable during cracking production [5], provoking active site poisoning and selectivity changes [6]. The undesired formation of carbonaceous materials (poor in hydrogen compared to initial macromolecules) produced by consecutive cracking reactions, especially those that drive olefins intermediaries into oligomers and multi-cyclised species and then transformed into aromatics that eventually conform the coke species [5], [7], [8], are deposited on the catalyst surface and plays a significant role in deactivation. Coke formation can manifest either internally within the pores of the zeolite or externally on its surface (**Figure 6.1**). The location of coke deposition is contingent upon various zeolite parameters, including pore size and acid strength, as well as reaction parameters such as reaction temperature.[5]. Consequently, many studies have been carried out on coke formation and location on the zeolite HZSM-5 on different cracking reactions [5] but few on cracking of PE, especially after consecutive use. This information is essential for developing an optimal regeneration method and can positively impact the industry from a process and economic point of view.

Preliminary studies of the deactivation of ZSM-5 zeolite by LDPE pyrolysis via TGA were first led in the 2000s by Professor Marcilla using a proportion of catalyst-polymer equal to 1:10. Among the critical findings of the first study made in 2004 [9], the experiments began with a relative activity of 72.8 °C and ended in a thirteenth run of reuse of the zeolite with a reduced relative activity of 28.9 °C. It should be noted that the relative activity is based on the difference between the maximum degradation temperature of the polymer alone and its maximum degradation temperature accompanied, in this case, by a catalyst. It was shown that the loss of activity is linked to the deactivation of the active acid sites, the coke formed, and after thirteen runs, the zeolite contained 8.2 % coke; this coke deposition in the acid sites represented a loss of the total acidity of 46 %, with a high representation of loss of strong sites (65 %). In a consecutive study [10], more information was gained employing the TG/FT-IR technique on the nature of the gaseous products during these thirteen runs, finding a decrease in the intensity of the characteristic bands of aromatic, olefins and -CH_3 of paraffins compounds, in contrast to an increase in the -CH_2 band intensity of paraffins. A consecutive study [6] made in a batch reactor with a relation of HZSM-5 zeolite and polyethylene of 1/10 was carried out in a batch reactor heated to 550 °C. They compared LDPE and HDPE cracking over the zeolite; in the LDPE system, they observed that the overall

yield of condensed and non-condensed products remains relatively stable during the initial four cycles. However, there are substantial changes in gas composition, coke deposition, acidity, relative activity, and textural properties over these cycles. Beyond the fifth cycle, the composition of all products gradually converges toward that observed in the absence of a catalyst. Their findings suggest the involvement of both strong and weak acid sites in catalytic pyrolysis. Deactivation appears to stem from a reduction in the quantity and strength of these acid sites. Within the framework of HZSM-5 zeolite, the generation of insoluble coke through various polymer cracking runs and its potential presence on the external surface may underlie the notable pore occlusion observed in this particular zeolite [11]. This study was completed with another article [12], in which the global kinetics of this reaction was studied until the fourth run. A progressive decrease in total acidity was observed, especially in the strong acid sites, with a maximum decrease of 47 %.

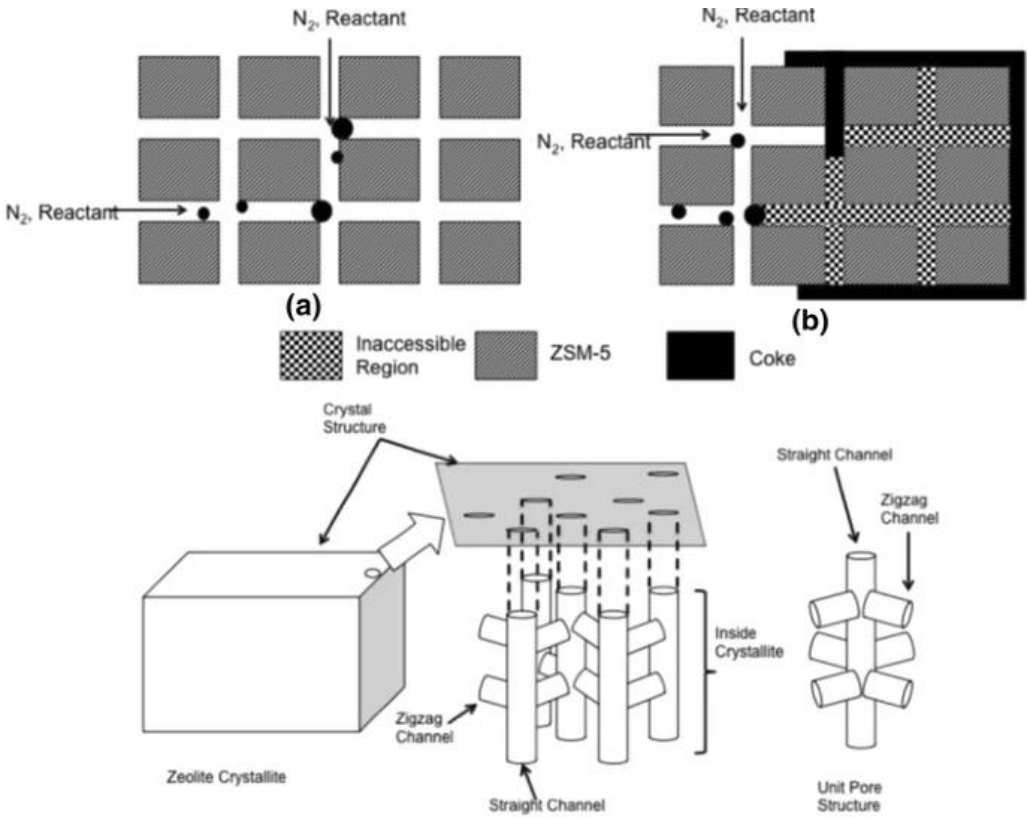

Figure 6.1. Possible states of deactivation of acid sites of the zeolite after coke deposition from ref. [13].

In 2007, Serrano et al. [14] synthesised two nanocrystalline HZSM-5 zeolites with different textural and acidity properties. The nanocrystalline HZSM-5 zeolites, unlike the hierarchical HZSM-5 zeolites, have a larger external surface. With a catalyst:polymer ratio of 1:20 for the catalyst with an external surface area of 74 $m^2.g^{-1}$ and 1:50 for the catalyst with an external surface area of 218 $m^2.g^{-1}$, the experiments took place in a stirred batch reactor at 340 °C for 6 hours. Five runs were made where a conversion from 60 % to 10 % and 45 % to 2.5 % was passed for these two catalysts. After three runs, the total paraffins and olefins produced with the fresh catalyst remained around 70 wt. % for both zeolites. Artetxe et al. [15] studied the effect of the amount of coke deposited on the catalyst on the activity using a two-step system, where the fixed catalyst reacts continuously with the product of polyethylene thermal

cracking. On the other hand, Ibáñez et al. [16], in a system very similar to the previous one, studied the type of coke generated during 5 hours.

This chapter aims to study the cycle effect and, therefore, the loss of activity of HZSM-5 zeolite and evaluate if this catalyst could be used over different cycles for the pyrolysis of polyethylene in a one-step batch system. The pyrolysis performance and characterisation of the HZSM-5 over the cycles are presented in this work and will elucidate the nature and type of the coke deposition.

6.2. Experimental

The pyrolysis experiments were performed as described in section **2.3** in a Mix arrangement (**Figure 2.24 (A)**), using Linear low-density polyethylene (LLDPE) in pellet and HZSM-5 calcinated under dynamic conditions (section **2.6.4**)**.** In brief, catalytic experiments were carried out at 450 °C with a nitrogen flow rate of 200 mL min^{-1}. Under these conditions, the LLDPE was fully converted to gaseous, liquid or waxy products, and no solid residue apart from the coke deposited on the zeolite was observed after each test. The catalyst was reused without any regeneration process five times. Each catalyst has been labelled with the number of catalytic experiments carried out. So when the catalyst HZSM-5 DC has been used three times, both the experiment and the catalyst have been labelled with “3- cycle”. HZSM-5 DC before and after one and five cycles of reactions were characterised by TGA (under oxygen), RAMAN spectroscopy, XPS, SEM-EDS, XRD, N_2-physisorption and NH_3-TPD as described in section **2.7.**

6.3. Catalytic performances of HZSM-5 up to five pyrolysis reaction cycles

Figure 6.2 shows, for the consecutive 5 cycles, the evolution of the yield of wax+oil/gas/coke obtained for the catalytic pyrolysis of LLDPE at 450 °C. The yield of coke refers to the total amount of coke accumulated on the zeolite in all the cycles, which has been estimated by TG analysis (see part **6.4.1**). The wax-oil yield increases from 54 % (after 1 cycle) to 65 % (after three cycles), but it does not evolve significantly after 3 cycles. The char-coke yield remains low, with a maximum obtained after 4 cycles (3.4 %). Similar results were obtained by Marcilla et al. [6], studying the pyrolysis of HZSM-5/LLDPE mixture in a batch reactor. The authors observed an increase of liquid and coke phase in detriment to the gas phase occurring through consecutive 10 cycles.

Figure 6.3 shows, for the consecutive 5 cycles, the carbon distribution of the wax-oil of LLDPE pyrolysis. After one cycle of reaction, the cracking of the polyethylene chains yields high amounts of molecular weight compounds with 7 and 8 carbon atoms. With the increase of consecutive cycles, the proportion of such compounds decreases to the benefit of compounds containing 5 and 6 carbon atoms and compounds containing more than 13 carbon atoms.

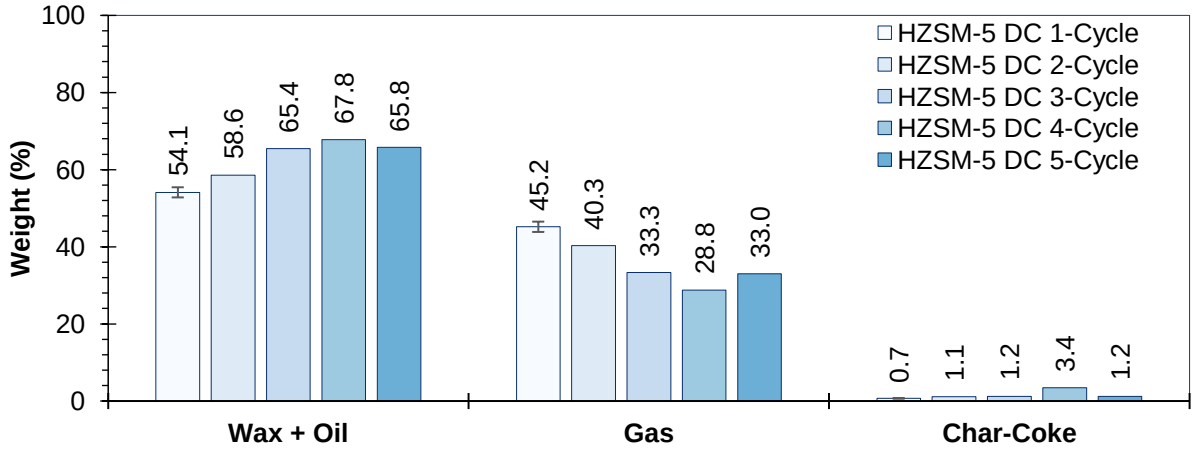

Figure 6.2. Yield result of pyrolysis of LLDPE with HZSM5 zeolite after first use (1-cycle) and after using it five times (5-cycle).

Figure 6.4 (a) shows, for the consecutive 5 cycles, the compound types in the oil/wax phase (i.e., aromatic, paraffin, iso-paraffin, olefin and iso-olefin). Significant differences are observed in the evolution of aromatic and iso-olefin compounds. The quantity of aromatics, major compounds after the first cycle, decreased with the number of cycles, while the iso-olefin compounds became preponderant with the increase of the number of cycles.

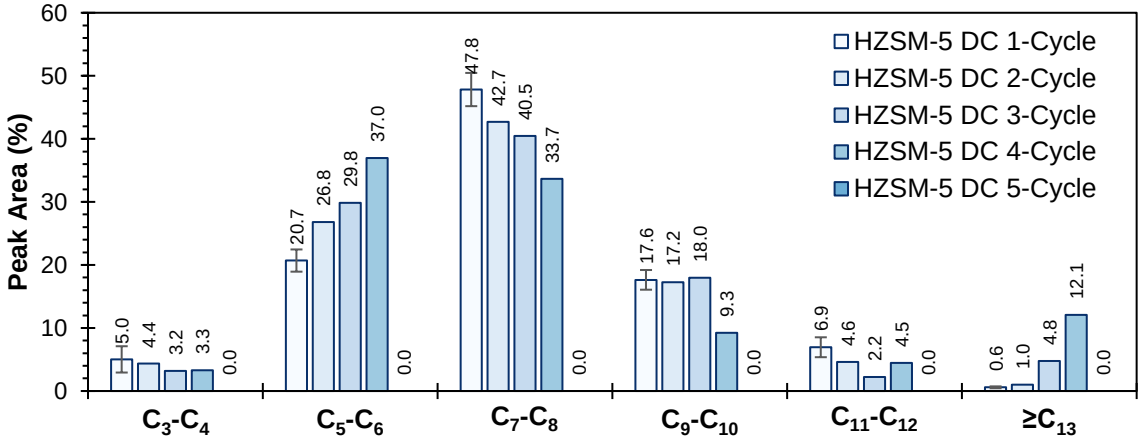

Figure 6.3. Carbon distribution of the wax+oil of pyrolysis of LLDPE with HZSM5 zeolite after first use (1-cycle) and after using it five times (5-cycle).

This behaviour can be explained by coke deposition on the catalyst surface, leading to the deactivation of acid sites [17]. Consequently, random scissions become more favourable compared to chain-end scissions [18], thereby enhancing the production of iso-olefins. This increase is achieved through isomerisation and cracking reactions. Concurrently, deactivating acid sites imposes limitations on hydrogen transfer reactions, consequently limiting aromatisation reactions [19].

The aromatic compounds obtained after five cycles primarily consist of BTEX (benzene, toluene, ethylbenzene, and xylene). However, owing to the constraints imposed on aromaticity reactions following five cycles, the selectivity towards BTEX experienced an increase from 55.1 % on the first cycle to 86.7 % on the fifth cycle using HZSM-5, benzene and toluene formation being not observed in

the last cycle, **Figure 6.4** (b). This higher selectivity can be rationalised by the sequence of BTEX formation preceding polyaromatics and occurring on a relatively smaller total surface area after five cycles, thus constraining polycondensation reactions to generate polyaromatic compounds [3], [20], [21].

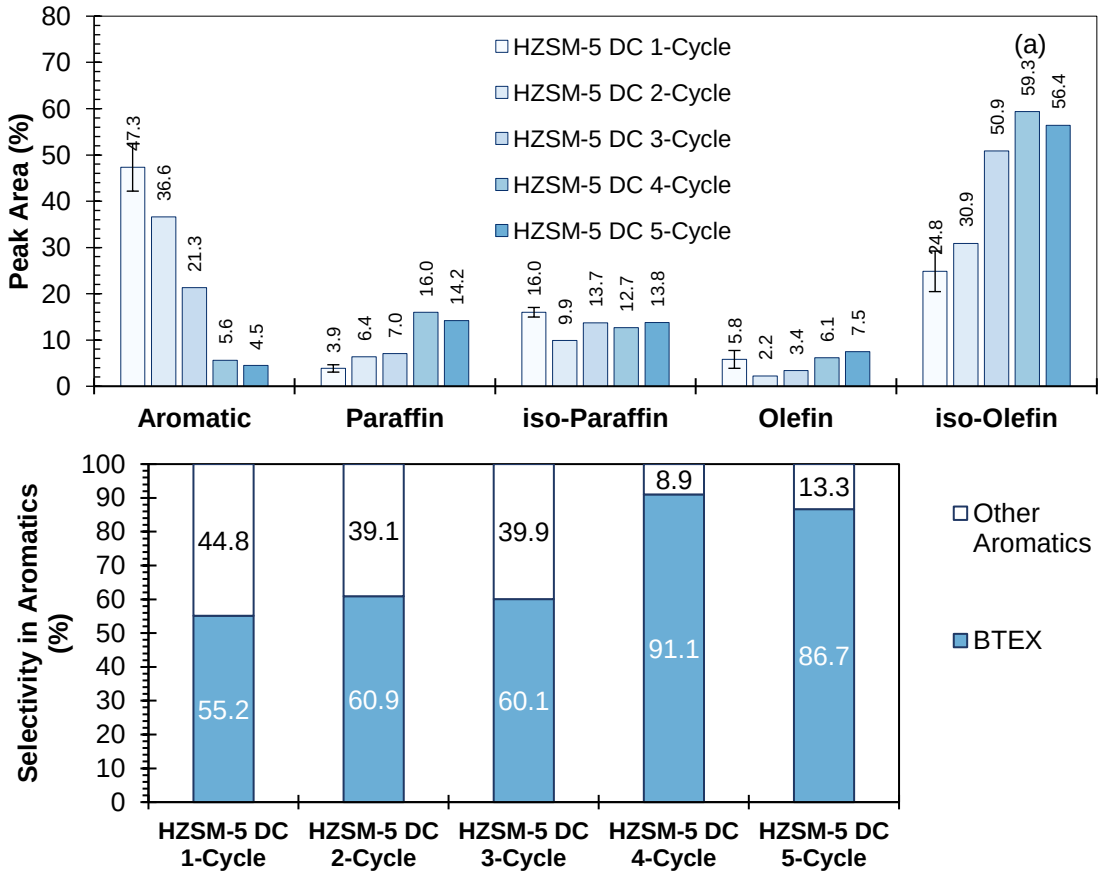

Figure 6.4. Composition of oil/wax product (a) and total BTEX (b) from liquid yield composition of catalytic pyrolysis of LLDPE after fifth use of HZSM-5 DC catalyst.

In order to better understand the catalytic results, the spent catalysts have been characterized.

6.4. Characterisation of spent catalysts

6.4.1. TG analysis

The amount of coke deposited in HZSM-5 zeolite after the first and fifth reaction cycles has been estimated by performing thermogravimetric analysis under air (**Figure 6.5**). The weight loss between 50-350 °C is explained by water removal; the weight loss observed within the temperature range of 350-700 °C is attributed to coke oxidation. Above 700 °C, the dealumination of the zeolite occurs [22]. The temperature range in which coke oxidation takes place can be divided into two parts. Between 350-500 °C (low temperature), well-structured hydrogen-rich coke species, also called "soft coke", are oxidised, while between 500-700 °C (high temperature), condensed polyaromatic coke species, called "hard coke", are degraded [23], [24].

As expected, the HZSM-5 DC fresh sample presents one main weight loss up to 200 °C, corresponding to water removal. The TG analyses of HZSM-5 DC samples after 1 and 5 cycles of reaction also evidence the water removal but in lower proportion compared to fresh HZSM-5 zeolite. Additionally, weight losses corresponding to coke oxidation are observed for both spent zeolites. From these weight losses, the quantity of coke can be estimated to be 6.5 % and 10.8 % for HZSM-5 DC 1-cycle and HZSM-5 DC 5-cycle, respectively, highlighting the increase of coking with the number of cycles. However, the proportion of soft coke versus hard coke differs. Indeed, for HZSM-5 DC 1-cycle, the percentage of soft coke is 31.7 %, while for HZSM-5 DC 5-cycle it is only 16.9 %. This finding indicates that more hard coke is produced by prolonged exposure of the catalyst to the pyrolysis reaction. The DTG analysis (Figure 6.5) underlines that the maximum oxidation temperature of hard coke is shifted to a higher temperature (from 567 °C after the first cycle to 595 °C after five cycles). This hard coke becomes more difficult to oxidise owing to probably its incorporation with time into the micropores of the zeolite [25], [26].

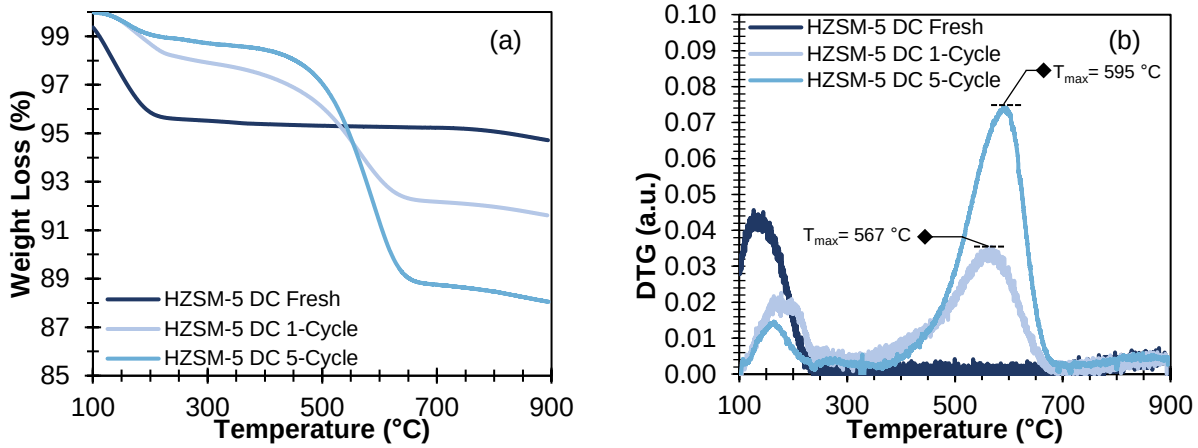

Figure 6.5. TG (a) and DTG (b) curves of HZSM-5 DC zeolites after one and five reactions under air.

6.4.2. RAMAN Spectroscopy

The Raman spectra of the fresh and spent HZSM-5 DC zeolites are shown in **Figure 6.6**. For fresh zeolite, no Raman lines are observed in the Raman shift range 1000 – 1700 cm^{-1}. In contrast, for HZSM-5 DC 1-cycle and HZSM-5 DC 1-cycle five lines at 1200, 1380, 1440, 1570 and 1620 cm^{-1} are observed.

The line at 1200 cm^{-1} is attributed to vibrations of C-H bond [23], [27]–[29]. The D_1-line at 1380 cm^{-1} is known as the disorder line or the defect line. It represents a ring breathing mode from sp2 carbon rings, although to be active, the ring must be adjacent to a graphene edge or a defect. If the D_1-line is significant, it indicates that there are a lot of defects in the material. The intensity of the D_1-line is directly proportional to the level of defects in the sample [23], [27]–[30]. The D_3 line at 1440 cm^{-1} is attributed to structural defects of aromatics clusters or CH deformation modes of paraffinic species. The G-line at ~1570 cm^{-1} features ideal graphitic vibrations with E_{2g} symmetry, which can be observed in graphitic rings and chains made of sp2 C atoms [31]. The D_2 line at 1620 cm^{-1} is ascribed to the disordered aromatic structure or polyolefinic and/or polyaromatic species [21], [25]–[28].

The contribution of these peaks, the precise peak position of the G line (P_G), and the integrated intensity ratio (I_G/I_{D1}) are listed in **Table 6.1**.

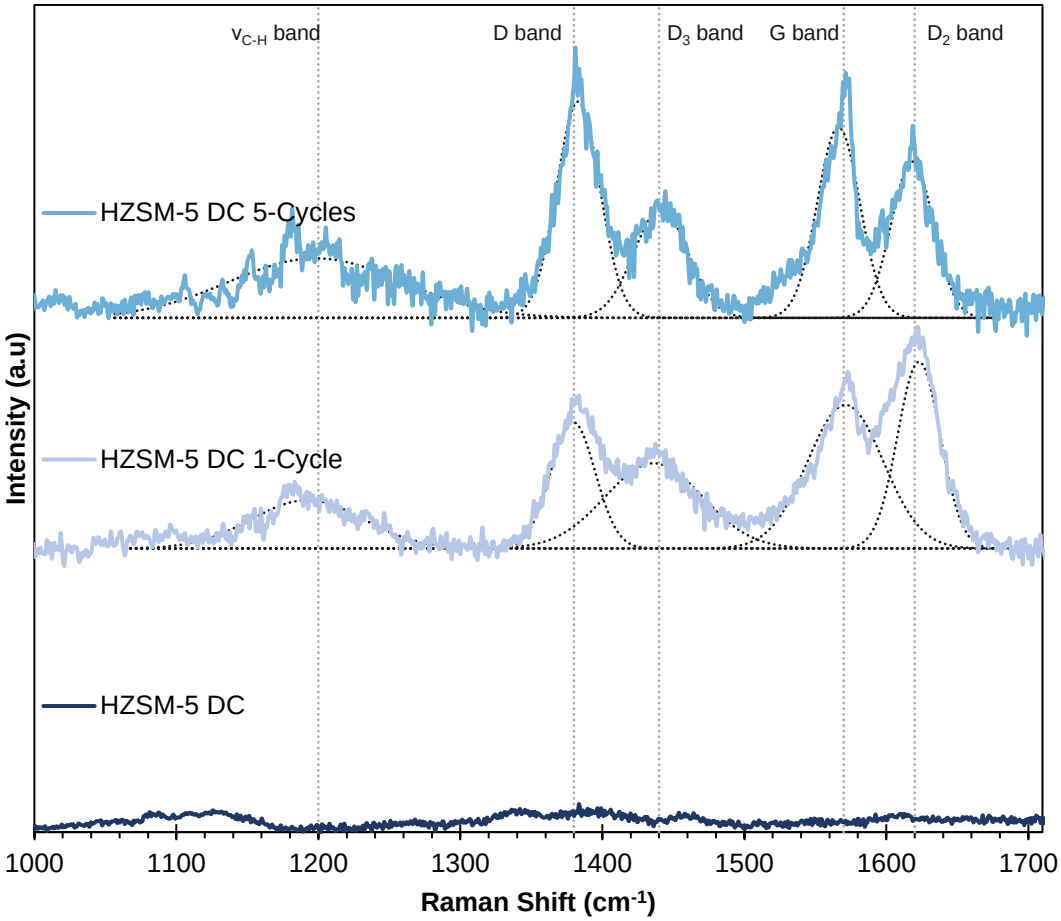

Figure 6.6. RAMAN Spectroscopy curves of HZSM-5 DC fresh and after one and five cycles of reaction.

Table 6.1 Characteristic fraction of deconvoluted area of lines assignee in the Raman spectra and peak position of the spent HZSM-5 DC zeolite after one and five reaction cycles.

Catalyst	ν_{C-H} (%)	D_1 (%)	D_3 (%)	G (%)	D_2 (%)	P_G (cm^{-1})	I_G/I_D
HZSM-5 DC 1-Cycle	14.1 %	14.7 %	21.7 %	28.5 %	20.9 %	1571	1.9
HZSM-5 DC 5-Cycle	25.6 %	23.3 %	14.5 %	20.1 %	16.4 %	1566	0.9

The increase of the contribution of C-H and D_1 lines in HZSM-5 DC 5-cycle compared to HZSM-5 DC 1-cycle is observed. This suggests a higher concentration of aliphatic compounds, particularly paraffins, and aromatic compounds within the coke matrix [28], [30]. Conversely, the percentages of D_3 and D_2 lines decrease with the number of cycles, indicating a lower content of deformed-paraffinic and polyolefin species [30]. Furthermore, the peak corresponding to the G line (P_G) shifts slightly to a lower wavenumber, signifying an increased sp^3:sp^2 hybridization ratio as the reaction cycles progress. This

shift indicates a greater proportion of saturated hydrocarbons within the coke structure [28]. The ratio of I_G/I_D serves as a quantitative measure of the degree of disorder in the coke structure. A lower I_G/I_D ratio corresponds to a more disordered coke structure, while a higher I_G/I_D ratio indicates a well-developed structure [29]. Notably, the I_G/I_D ratio decreases as the number of reaction cycles increases, revealing a higher degree of structural disorder within the coke after five cycles of reaction [25].

6.4.3. XPS

XPS analysis was conducted on the HZSM-5 DC material before and after five reaction cycles. **Figure 6.7** shows the different high-resolution Si 2p, Al 2p, O 1s and C1s photopeaks. According to the deposition of carbon element at the surface of HZSM-5 DC 5-cycles and compared to fresh ZSM-5 DC, the C 1s photopeak intensity increased while the intensity of other photopeaks (Si 2p, Al 2p and O1s) decreased. The surface atomic ratios Si/Al and C/Si of the HZSM-5 DC materials are provided in **Table 6.2**. The C/Si ratio of the fresh catalyst was less than unity. The main contribution of the C 1s signal at 284.3 eV can be attributed to the presence of adventitious carbon (AdC) [32]. After five reaction cycles, the C/Si ratio increased from 0.7 to 2.7. Studying the coke distribution on HZSM-5 by XPS, Sexton et al. [33] showed that at low coke levels (<8 wt %), the carbon is uniformly distributed throughout the zeolite structure, and an internal coking is suggested. At levels from 8 to about 14 wt % coke, some extra external coking occurred in parallel with channel filling (internal coking). Therefore, with the total coke content of 11 % after five cycles, it is reasonable to conclude the presence of both external and internal coke. After five reaction cycles, the Si/Al ratio increased from 10.2 to 11.1. This result can be explained by the accumulation of coke on Si-OH-Al tetrahedra (acid site) rather than on silanol groups. Compared to Si, less Al species are visible by XPS, leading to an increase of Si/Al atomic ratio.

Table 6.2 XPS surface atomic concentration of the fresh and used catalysts after five cycles.

Catalyst	Si/Al	C/Si	Si 2p		Al 2p		O 1s		C 1s	
			BE (eV)	FWHM (eV)	BE (eV)	FWHM (eV)	BE (eV)	FWHM (eV)	BE (eV)	FWHM (eV)
HZSM-5 DC	10.2	0.7	102.9	1.6	74.5	2.1	532.1	1.6	284.2	1.5
HZSM-5 DC 5-Cycle	11.1	2.7	102.9	1.8	74.3	2.3	532.0	1.8	284.1	1.6

BE of Si 2p at 102.9 eV has been used as a reference for the calculation of other BEs. The binding energy, at which the signal intensity of the C1s photopeak is highest, is slightly higher (0.3 eV) for the sample HZSM-5 DC 5-Cycle (**Table 6.2**). This result could be interpreted by an experimental challenge in the case of insufficient conductivity of materials, the alignment between the XPS spectrometer's Fermi levels (FL) and the sample being difficult to achieve [32]. This outcome may stem from distinctions in the carbon environment between the adventitious carbon and the coke. The lingering carbon noticed on the catalyst's fresh surface might be attributed to the adsorption of CO_2 and/or other carbon-containing compounds during sample storage, signifying contaminating carbon [34], [35]. The generation of coke

is conspicuously marked by the emergence of a peak at 284.6 eV, indicative of aromatic constituents [36], with a notably robust intensity.

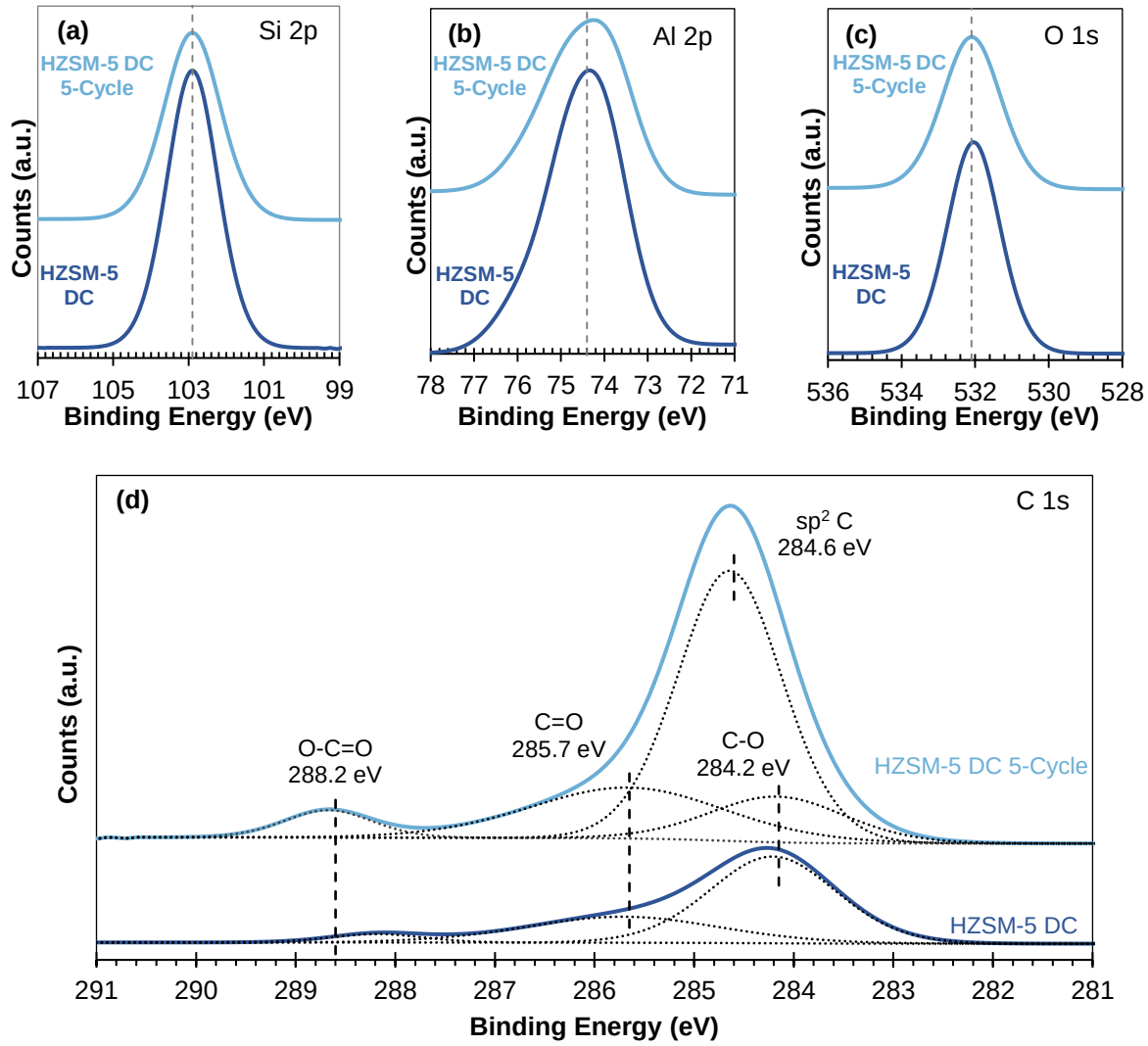

Figure 6.7. XPS core-level spectra of Si 2p (a), Al 2p (b), O 1s (c) and C 1s (d) of HZSM-5 DC fresh and after five cycles of reaction

6.4.4. SEM-EDS

The surface morphology of the fresh zeolite and its counterpart following five reaction cycles is shown in **Figure 6.8**. In the fresh sample, well-defined crystalline rectangular grains with varying sizes from 80 to 1099 nm, characteristic of HZSM-5 zeolites, are prominently observed. However, after subjecting the zeolites to five pyrolysis cycles, noticeable modifications occur on the surface morphology. The crystalline grains transform, exhibiting the presence of coke deposits that form more amorphous structures (**Figure 6.8** (b). Indeed, the particle size distribution, initially heterogeneous, exhibits an increasing degree of heterogeneity. It modifies from an average size of 223 nm, encompassing particles ranging from 80 nm in length to an average size of 301 nm, including particles ranging from 29 nm in length. This average particle size was determined by analysing 100 particles.

(a) **Fresh HZSM-5 DC** (b) **HZSM-5 DC 5-Cycle**

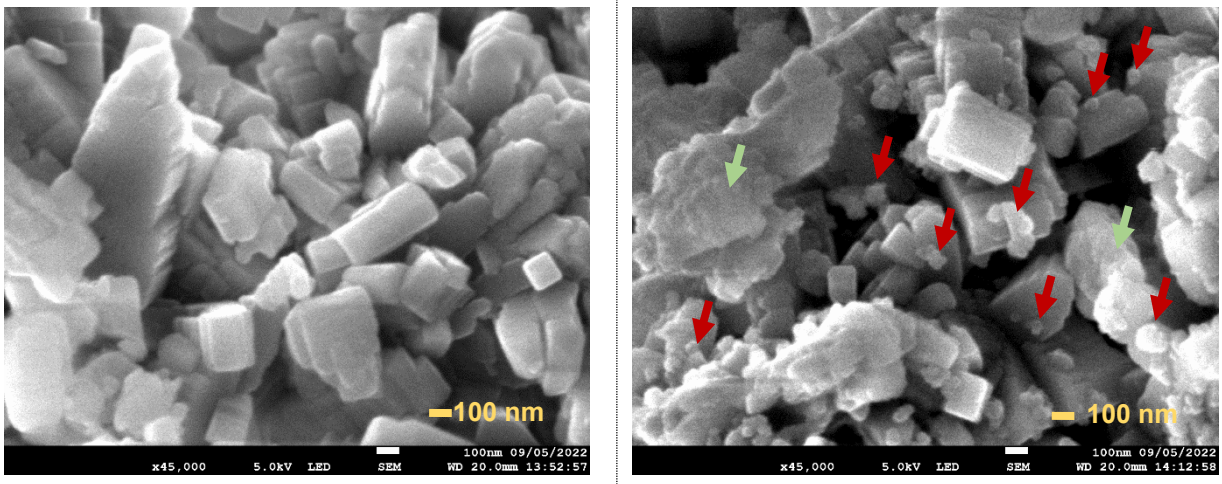

Figure 6.8. SEM images of fresh (a) and spent HZSM-5 DC zeolite after five cycles (b).

6.4.5. XRD

The X-ray diffraction (XRD) patterns of the fresh and spent HZSM-5 DC samples (after one and five cycles) are shown in **Figure 6.9**. In all materials, distinct diffraction peaks within Bragg's angle range of 5 to 55° are observed, indicative of the orthorhombic phase characteristic of the ZSM-5 zeolite framework (PDF-04-017-8707). From the first reaction cycle, three pairs of diffraction peaks associated with HZSM-5 DC zeolites at 2θ values of 23°-23.2°, 26.7°-26.8°, and 45°-45.4° undergo merging, resulting in a single peak observed at 2θ values of 23.1°, 26.7°, and 45.2°. This change in crystallinity is closely associated with coke formation, causing lattice distortions in zeolite. Indeed, some authors attributed the phase change from orthorhombic to tetragonal to the deposition of carbonaceous material within the zeolitic pores [7], [26], [37]–[39] [40]. Lattice cell dimensions and volume of zeolite crystals are altered, and shifts in the positions of XRD peaks are observed [5], [7], [26], [39], [41].

6.4.6. N_2-physisorption

The N_2-physisorption data obtained for both the fresh and spent HZSM-5 DC samples are shown in **Figure 6.10** (a). According to the IUPAC classification, the isotherms exhibit a Type IV profile, which is a characteristic feature of materials possessing a combination of micropores and mesopores [42]; this is evident from the distinct H4 hysteresis loops observed at P/P_0 values exceeding 0.4.

After one cycle of reaction, the BET (Brunauer-Emmett-Teller) surface area of HZSM-5 DC zeolite decreased by impacting both the external surface and the microporous surface (**Figure 6.10** (c)). Following five cycles of reactions, the decrease in the BET surface area of HZSM-5 DC zeolite is much more pronounced (**Figure 6.10** (c)). Proportionally, the reduction in specific surface area is much more marked for the microporous surface than for the external surface. This drop in surface area can be primarily attributed to coke formation at the pore entrances on the external surface of the zeolite, thereby obstructing the pores [5]. It is well-established that aromatisation reactions predominantly occur within

the micropores. Consequently, these reactions and the production of polyaromatic-like coke are closely linked, explaining the relatively lower extent of coke deposition on the external surface.

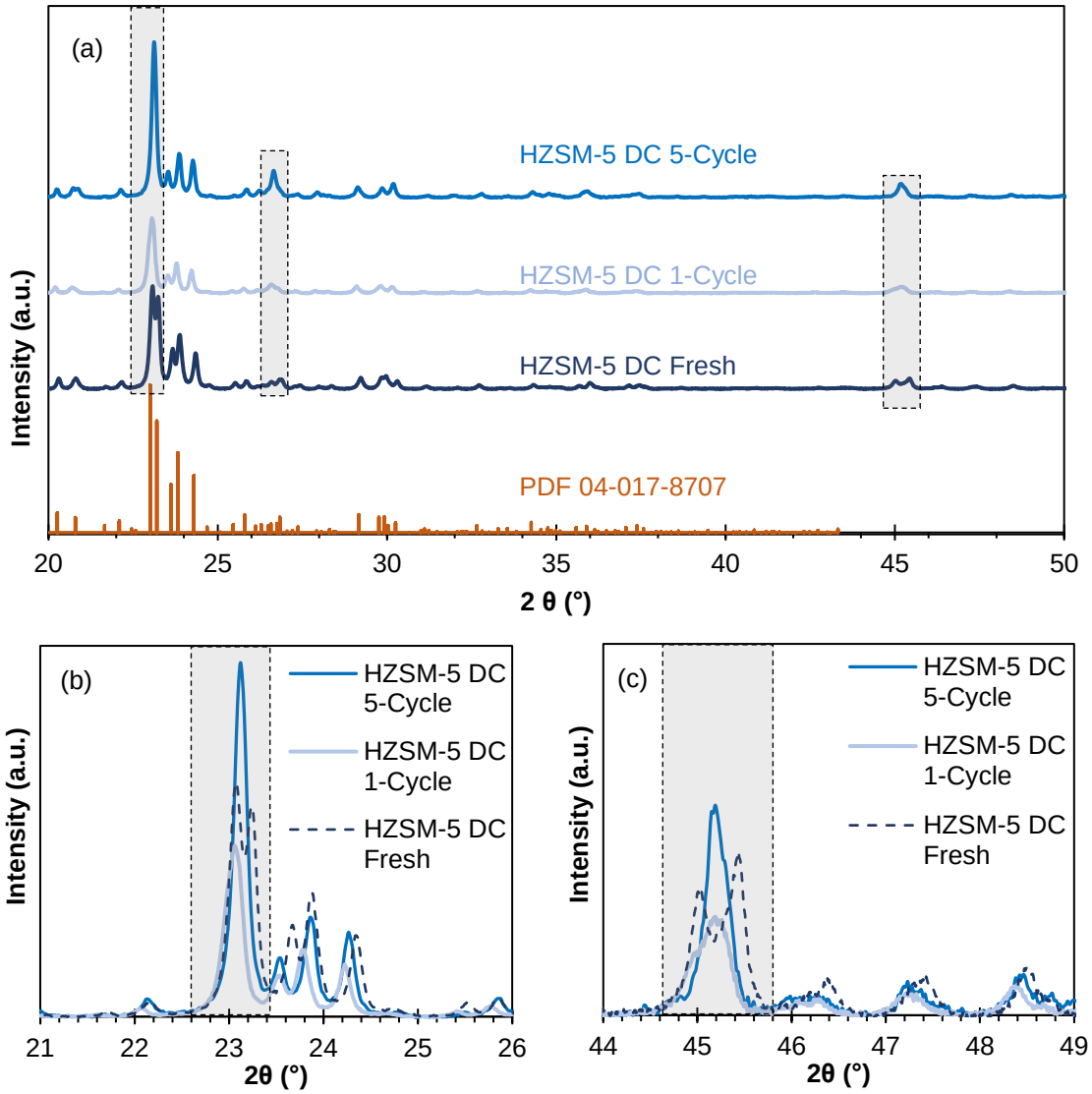

Figure 6.9. XRD of HZSM-5 DC zeolite before reaction (Fresh) and after one and five cycles of reaction.

6.4.7. Acidity by NH_3-TPD

The NH_3-TPD (temperature-programmed desorption) profiles of the fresh and spent zeolites following five cycles of pyrolysis reactions are presented in **Figure 6.11**. The NH_3-TPD profiles were subjected to integration to calculate overall acidity and further analysis of the acidity (quantity and strength) distribution of the zeolites over the cycles by Gaussian deconvolution of the peaks [43]. The analysis of these profiles reveals a reduction in the total acidity of one gram of HZSM-5 DC zeolite after 5 cycles, with a decrease of 39 % (**Table 6.3**). The decrease in the number of weak acid sites (first peak LT at 257 °C) is highly pronounced after 5 cycles of reaction, with a decrease of 61 %. For HZSM-5 DC 5-Cycle, the width of the second signal at 450 °C is much greater than for HZSM-5 DC. This result underlines a wider distribution of the number of strong acid sites after 5 cycles of reaction.

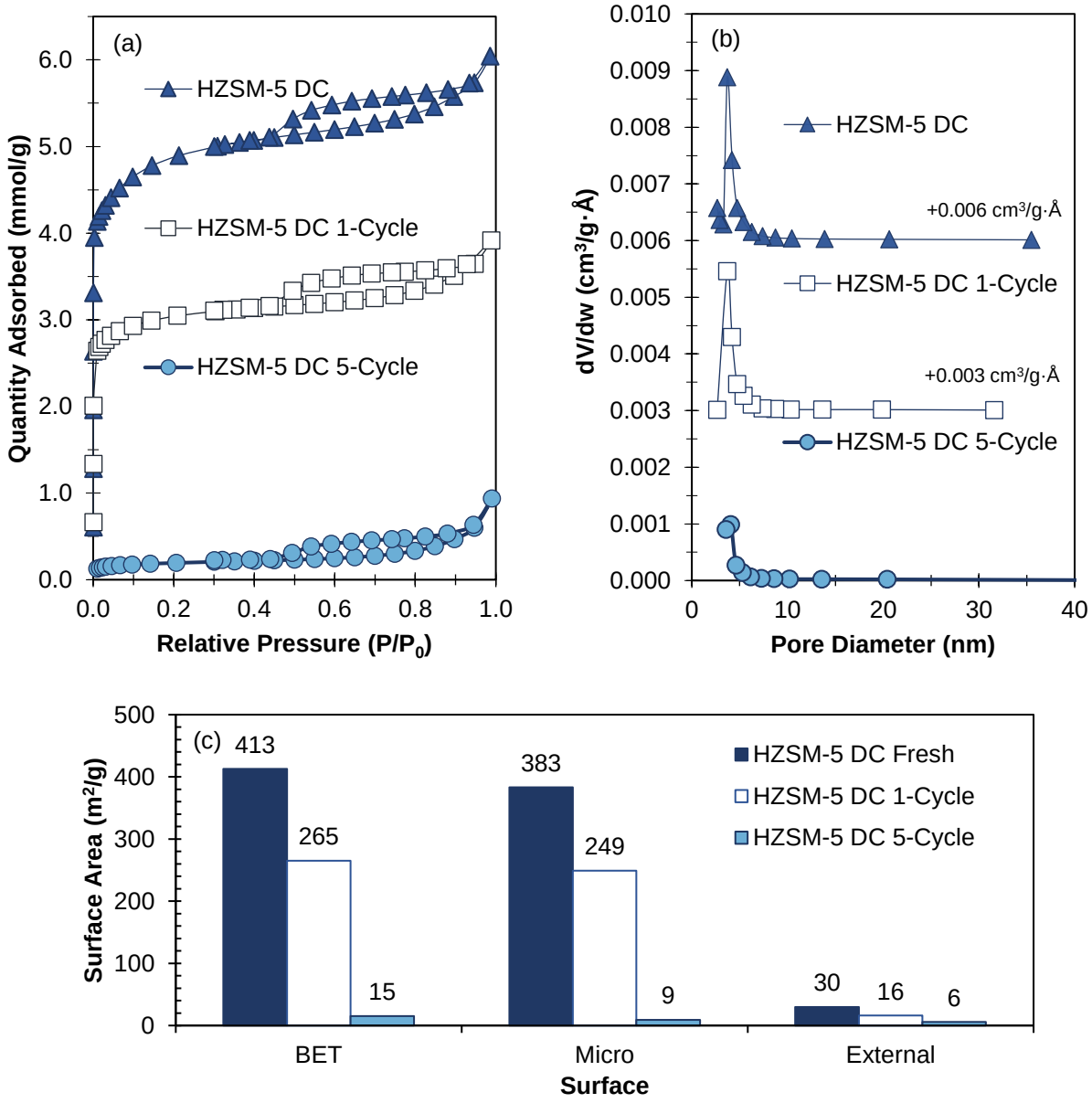

Figure 6.10. N_2-physisorption isotherms at -196 °C (a) and BJH pore size distribution (b) and total specific surface area (BET surface), external and micropore surface area (c) of HZSM-5 zeolites before reaction (Fresh) and after five reaction cycles.

The loss of acidity can be attributed to the presence of coke, which covers the acid sites dosed with the NH_3 probe molecule. Moreover, it should be pointed out that the sample HZSM-5 DC 5-Cycle has lost almost all its microporous surface, as demonstrated by the physisorption study mentioned above. Besides, the total acidity of one square meter of HZSM-5 DC zeolite increased for the HZSM-5 DC 5-Cycle sample (**Table 6.3**). Clearly, the presence of coke interferes with the measurement of zeolite acid sites.

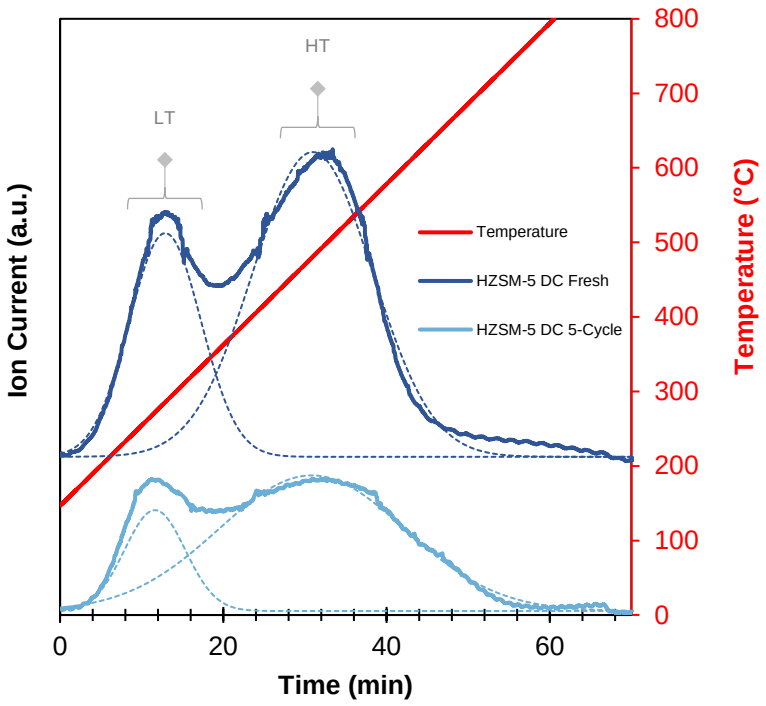

Figure 6.11. NH_3-TPD curves of HZSM-5 fresh and after five cycles of reactions

Table 6.3 NH_3-TPD and pore volume results of fresh and spent (after five cycles) HZSM-5 zeolite.

Catalyst	Temperature (°C)		Acidity (mmol.g^{-1})			Acidity (µmol.m^{-2})			W/S Acidity	Micropore Volume (cm^3.g^{-1})
	LT Peak	HT Peak	**Total**	Weak	Strong	**Total**	Weak	Strong		
HZSM-5 DC	274	475	**1.50**	0.46	1.04	**3.63**	1.11	2.52	**0.44**	**0.1585**
HZSM-5 DC 5-Cycle	257	450	**0.92** **(-39 %)**	0.18 (-61 %)	0.74 (-29 %)	**6.13** **(+68.9 %)**	1.20 (+8.1 %)	4.93 (+95.6 %)	**0.29**	**0.0042** **(-97 %)**

Song et al. studied the 1,3-dimethylcyclopentenyl carbenium ion adsorbed on H-ZSM-5. They showed theoretically that the coadsorption of basic molecules led to deprotonation of the carbenium ion to produce the neutral diene only when the base used had an affinity for protons greater than the enthalpy of deprotonation of the ion [44]. This replacement has been experimentally described for zeolites coked in m-xylene transformation [45]. Using pyridine as a strong base molecule for probing the acidity, the authors demonstrated that pyridine can replace a substantial amount of coke molecules owing to its very high proton affinity (930 kJ/mol). With a proton affinity of 846 kJ.mol^{-1} [46], we can assume that NH_3 species are also able to replace a large amount of coke molecules during the TPD analysis, contributing to the apparent high acidity of HZSM-5 DC 5-Cycle. This interpretation can also justify the wider distribution in the strong acidity range (HT).

6.5. Discussion and conclusions

During the five cycles of LLDPE pyrolysis, the ZSM-5 zeolite, which was calcined under dynamic conditions with airflow, exhibited significant degradation in its physicochemical characteristics. Analysis through TG and RAMAN spectroscopies revealed that coke formation became harder with successive reaction cycles. Continuous cyclisation and aromatisation of linear hydrocarbons into small aromatics or polymerisation of aromatic into polyaromatic hydrocarbons (PAH) played a role in the deactivation process. It has been reported [5], [7] that the first reaction deposits coke, particularly within the micropores where aromatics are formed. In contrast, the polymerisation reactions are free to develop bulky polyaromatic compounds at the external surface where no particular constraints of pore size exist (**Figure 6.12**). Micropore acid sites were covered by coke deposits, obstructing the diffusion of reactants, becoming less accessible over time, possibly affecting the durability of the catalyst [8] and leading to limitation in hydrogen transfer and bimolecular reactions, resulting in reduced formation of aromatics and cyclic hydrocarbons.

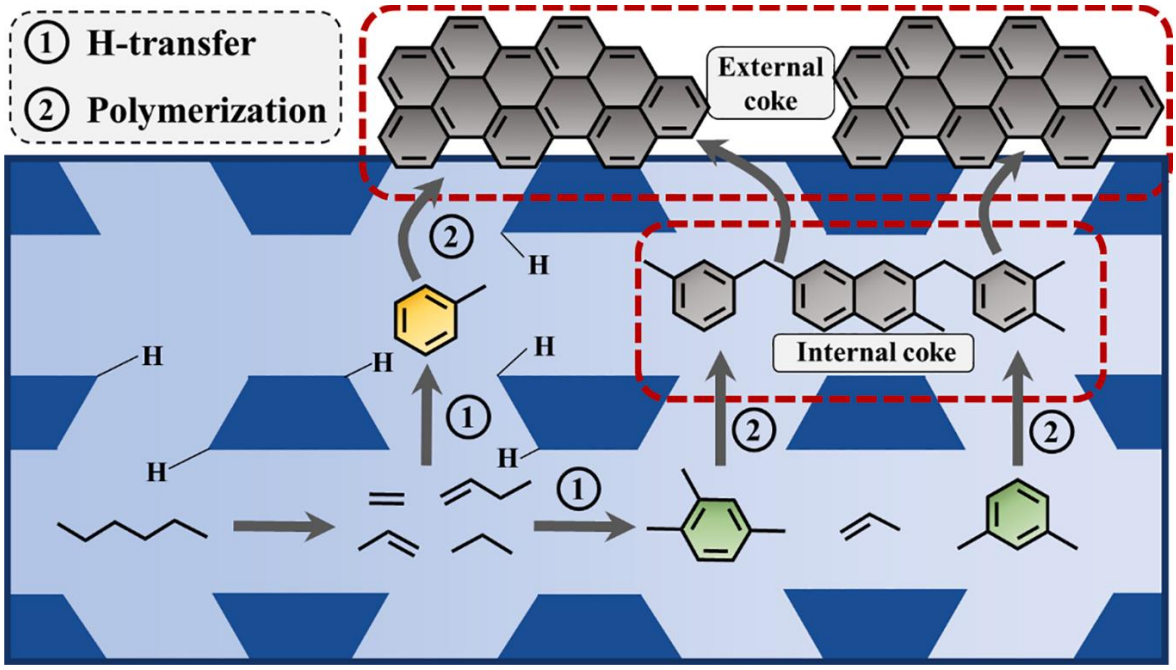

Figure 6.12. Schema of coke formation from reference [5].

The external surface of the zeolite was less impacted, with approximately 80 % deactivation compared to the substantial ~98 % deactivation observed in the micropore surface area; this 80 % may be responsible for the blockage by accumulation of coke at the entrance of the pores, this phenomenon can be attributed to the enhanced activity of internal acid sites compared to their external ones, likely resulting from their lower deprotonation enthalpies and their potent capacity to stabilise intermediate reactions within the microporous structure of the zeolite [7]; this indicated that even after five cycles, the catalyst continued to facilitate LLDPE cracking, corroborating the relationship that exists between the external surface and the activity of the zeolite described in the literature [6], although with hindered diffusion in the micropores.

Interestingly, while less than 4 % of the total surface area remained accessible, only 39 % of the acidity was affected. It has been suggested that light carbocations, in our case generated during LLDPE cracking, were adsorbed by acid sites and readily replaced by ammonia ions during NH_3-TPD analysis [46]–[48]. This process persisted because strong acid sites are typically responsible for LLDPE cracking. TPD with ammonia or another method involving the adsorption of strong bases, such as Py-IR, is not suitable for accurately measuring the acidity of a coked zeolite. This is because a portion of the coke is replaced by these bases, leading to misleading acidity results. A more informative approach would involve conducting ^{13}C and ^{1}H NMR studies before and after reaction cycles to establish a correlation between the adsorbed coke molecules and the acidic sites.

XPS analysis revealed fewer aluminium atoms on the surface and increased carbon atom content, indicating coke deposition and the blocking of Si-OH-Al acid sites, especially at the internal surface.

The coke deposition, evident in the zeolite characterisation after five reaction cycles, significantly affects LLDPE cracking. It restricted product diffusion and secondary reactions, particularly at the micropore surface area. Liquid distribution analysis indicated a reduction in aromatics formation, with increased production of paraffins and iso-olefins. These iso-olefins serve as precursors for aromatic compounds. The heightened activity of the external surface area was reflected in the increased presence of C_5-C_6 hydrocarbons in LLDPE cracking. Initially, carbocations are generated and undergo secondary reactions, ultimately producing cyclic or aromatic compounds. Due to limitations in diffusion within zeolite micropores and constraints in hydrogen transfer and bimolecular reactions, C_5-C_6 carbocations are stabilised as light olefins before entering the zeolite structure. These C_5-C_6 carbocations act as precursors for monoaromatic compounds.

Coke formation can induce structural modification of the zeolite, resulting in irreversible deactivation [20]. Therefore, it is crucial to determine the optimal timing and conditions for zeolite regeneration. Several regeneration methods exist, including coke combustion with air and pure oxygen (the most traditional approach), ozonation, hydrogen peroxide oxidation (Fenton Process), hydrogenation, and, more recently, the use of Non-Thermal Plasma (NTP). Among these methods, coke combustion and hydrogenation are the most commonly employed regeneration methods [20], [49]. In the case of combustion, data obtained from thermogravimetric Analysis in an oxidative environment can assist in establishing preliminary regeneration parameters. This includes determining the ideal temperature for water desorption to prevent zeolite dealumination and for coke combustion without reaching temperatures that degrade the zeolite. Additionally, it helps identify the optimal duration for each step of the process. The study of the regeneration process considering deactivation levels and economic feasibility represents an important outlook of this work.

6.6. References

[1] M. Sekar, V. K. Ponnusamy, A. Pugazhendhi, S. Nižetić, And T. R. Praveenkumar, “Production And Utilization Of Pyrolysis Oil From Solidplastic Wastes: A Review On Pyrolysis Process And Influence Of Reactors Design,” *J. Environ. Manage.*, Vol. 302, No. October 2021, 2022, Doi:

10.1016/J.Jenvman.2021.114046.

[2] S. Kartik *Et Al.*, “Valorization Of Plastic Wastes For Production Of Fuels And Value-Added Chemicals Through Pyrolysis – A Review,” *Therm. Sci. Eng. Prog.*, Vol. 32, No. March, P. 101316, 2022, Doi: 10.1016/J.Tsep.2022.101316.

[3] M. S. Abbas-Abadi *Et Al.*, “Challenges And Opportunities Of Light Olefin Production Via Thermal And Catalytic Pyrolysis Of End-Of-Life Polyolefins: Towards Full Recyclability,” *Prog. Energy Combust. Sci.*, Vol. 96, No. September 2022, P. 101046, 2023, Doi: 10.1016/J.Pecs.2022.101046.

[4] R. Mishra, A. Kumar, E. Singh, And S. Kumar, “Recent Research Advancements In Catalytic Pyrolysis Of Plastic Waste,” *Acs Sustain. Chem. Eng.*, Vol. 11, No. 6, Pp. 2033–2049, 2023, Doi: 10.1021/Acssuschemeng.2c05759.

[5] M. He *Et Al.*, “Study On The Deactivation Mechanism Of Hzsm-5 In The Process Of Catalytic Cracking Of N-Hexane,” *Chem. Eng. J.*, Vol. 451, No. August 2022, 2023, Doi: 10.1016/J.Cej.2022.138793.

[6] A. Marcilla, M. I. Beltrán, And R. Navarro, “Study Of The Deactivation Process Of Hzsm5 Zeolite During Polyethylene Pyrolysis,” *Appl. Catal. A Gen.*, Vol. 333, No. 1, Pp. 57–66, 2007, Doi: 10.1016/J.Apcata.2007.09.004.

[7] S. Lee And M. Choi, “Unveiling Coke Formation Mechanism In Mfi Zeolites During Methanol-To-Hydrocarbons Conversion,” *J. Catal.*, Vol. 375, Pp. 183–192, 2019, Doi: 10.1016/J.Jcat.2019.05.030.

[8] Z. Wan, G. K. Li, C. Wang, H. Yang, And D. Zhang, “Relating Coke Formation And Characteristics To Deactivation Of Zsm-5 Zeolite In Methanol To Gasoline Conversion,” *Appl. Catal. A Gen.*, Vol. 549, No. September 2017, Pp. 141–151, 2018, Doi: 10.1016/J.Apcata.2017.09.035.

[9] A. Marcilla, M. I. Beltrán, F. Hernández, And R. Navarro, “Hzsm5 And Husy Deactivation During The Catalytic Pyrolysis Of Polyethylene,” *Appl. Catal. A Gen.*, Vol. 278, No. 1, Pp. 37–43, 2004, Doi: 10.1016/J.Apcata.2004.09.023.

[10] A. Marcilla, M. I. Beltrán, And R. Navarro, “Tg/Ft-Ir Analysis Of Hzsm5 And Husy Deactivation During The Catalytic Pyrolysis Of Polyethylene,” *J. Anal. Appl. Pyrolysis*, Vol. 76, No. 1–2, Pp. 222–229, 2006, Doi: 10.1016/J.Jaap.2005.11.008.

[11] A. Marcilla, A. Gómez, And F. J. Valdés, “Evolution Of The Deactivation Mode And Nature Of Coke Of Hzsm-5 And Usy Zeolites In The Catalytic Cracking Of Low-Density Polyethylene During Successive Cracking Runs,” *Appl. Catal. A Gen.*, Vol. 352, No. 1–2, Pp. 152–158, 2009, Doi: 10.1016/J.Apcata.2008.10.001.

[12] A. Marcilla, M. I. Beltrán, A. Gómez, R. Navarro, And F. Valdés, “A Global Kinetic Model As A Tool To Reproduce The Deactivation Behaviour Of The Hzsm-5 Zeolite In The Catalytic Cracking Of Low-Density Polyethylene,” *Appl. Catal. A Gen.*, Vol. 328, No. 2, Pp. 124–131, 2007, Doi: 10.1016/J.Apcata.2007.05.038.

[13] B. Liu *Et Al.*, “Advances In The Study Of Coke Formation Over Zeolite Catalysts In The Methanol-To-Hydrocarbon Process,” *Appl. Petrochemical Res.*, Vol. 6, No. 3, Pp. 209–215, 2016, Doi: 10.1007/S13203-016-0156-Z.

[14] D. P. Serrano, J. Aguado, J. M. Rodríguez, And A. Peral, “Catalytic Cracking Of Polyethylene Over Nanocrystalline Hzsm-5: Catalyst Deactivation And Regeneration Study,” *J. Anal. Appl. Pyrolysis*, Vol. 79, No. 1-2 Spec. Iss., Pp. 456–464, 2007, Doi: 10.1016/J.Jaap.2006.11.013.

[15] M. Artetxe, G. Lopez, M. Amutio, J. Bilbao, And M. Olazar, “Kinetic Modelling Of The Cracking

Of Hdpe Pyrolysis Volatiles On A Hzsm-5 Zeolite Based Catalyst," *Chem. Eng. Sci.*, Vol. 116, Pp. 635–644, 2014, Doi: 10.1016/J.Ces.2014.05.044.

[16] M. Ibáñez *Et Al.*, "Identification Of The Coke Deposited On An Hzsm-5 Zeolite Catalyst During The Sequenced Pyrolysis-Cracking Of Hdpe," *Appl. Catal. B Environ.*, Vol. 148–149, Pp. 436–445, 2014, Doi: 10.1016/J.Apcatb.2013.11.023.

[17] L. C. Lerici, M. S. Renzini, U. Sedran, And L. B. Pierella, "Tertiary Recycling Of Low-Density Polyethylene By Catalytic Cracking Over Zsm-11 And Beta Zeolites Modified With Zn2+: Stability Study," *Energy And Fuels*, Vol. 27, No. 4, Pp. 2202–2208, 2013, Doi: 10.1021/Ef302099e.

[18] S. T. Okonsky, J. V. J. Krishna, And H. E. Toraman, "Catalytic Co-Pyrolysis Of Ldpe And Pet With Hzsm-5, H-Beta, And Hy: Experiments And Kinetic Modelling," *React. Chem. Eng.*, Vol. 7, Pp. 2175–2191, 2022, Doi: 10.1039/D2re00144f.

[19] A. Angyal, N. Miskolczi, L. Bartha, And I. Valkai, "Catalytic Cracking Of Polyethylene Waste In Horizontal Tube Reactor," *Polym. Degrad. Stab.*, Vol. 94, No. 10, Pp. 1678–1683, 2009, Doi: 10.1016/J.Polymdegradstab.2009.06.024.

[20] V. Daligaux, R. Richard, And M. H. Manero, "Deactivation And Regeneration Of Zeolite Catalysts Used In Pyrolysis Of Plastic Wastes—A Process And Analytical Review," *Catalysts*, Vol. 11, No. 7, 2021, Doi: 10.3390/Catal11070770.

[21] S. P. Da S. Ribeiro *Et Al.*, "Influence Of The Zeolite Acidity On Its Synergistic Action With A Flame-Retarding Polymeric Intumescent Formulation," *J. Mater. Sci.*, Vol. 55, No. 2, Pp. 619–630, 2020, Doi: 10.1007/S10853-019-04047-W.

[22] Q. Zhang *Et Al.*, "Isoparaffin Production By Aqueous Phase Processing Of Sorbitol Over The Ni/Hzsm-5 Catalysts: Effect Of The Calcination Temperature Of The Catalyst," *Fuel*, Vol. 90, No. 11, Pp. 3468–3472, 2011, Doi: 10.1016/J.Fuel.2011.06.046.

[23] S. J. Han *Et Al.*, "Non-Oxidative Dehydroaromatization Of Methane Over Mo/H-Zsm-5 Catalysts: A Detailed Analysis Of The Reaction-Regeneration Cycle," *Appl. Catal. B Environ.*, Vol. 241, No. April 2018, Pp. 305–318, 2019, Doi: 10.1016/J.Apcatb.2018.09.042.

[24] M. Rahman, A. Infantes-Molina, A. S. Hoffman, S. R. Bare, K. L. Emerson, And S. J. Khatib, "Effect Of Si/Al Ratio Of Zsm-5 Support On Structure And Activity Of Mo Species In Methane Dehydroaromatization," *Fuel*, Vol. 278, No. June, 2020, Doi: 10.1016/J.Fuel.2020.118290.

[25] I. Hussain *Et Al.*, "New Insights On The Effect Of The H2/Co Ratio For Enhancement Of Co Methanation Over Metal-Free Fibrous Silica Zsm-5: Thermodynamic And Mechanistic Studies," *Energy Convers. Manag.*, Vol. 199, No. September, 2019, Doi: 10.1016/J.Enconman.2019.112056.

[26] Y. Zhang, S. Wu, X. Xu, And H. Jiang, "Ethane Aromatization And Evolution Of Carbon Deposits Over Nanosized And Microsized Zn/Zsm-5 Catalysts," *Catal. Sci. Technol.*, Vol. 10, No. 3, Pp. 835–843, 2020, Doi: 10.1039/C9cy01903k.

[27] P. Castaño, G. Elordi, M. Olazar, A. T. Aguayo, B. Pawelec, And J. Bilbao, "Insights Into The Coke Deposited On Hzsm-5, Hβ And Hy Zeolites During The Cracking Of Polyethylene," *Applied Catalysis B: Environmental*, Vol. 104, No. 1–2. Pp. 91–100, 2011, Doi: 10.1016/J.Apcatb.2011.02.024.

[28] C. Song *Et Al.*, "Effect Of Cofeeding N-Butane With Methanol On Aromatization Performance And Coke Formation Over A Zn Loaded Zsm-5/Zsm-11 Zeolite," *Appl. Catal. A Gen.*, Vol. 470, Pp. 15–23, 2014, Doi: 10.1016/J.Apcata.2013.10.036.

[29] X. Hou, L. Zhao, And Z. Diao, "Roles Of Alkenes And Coke Formation In The Deactivation Of

Zsm-5 Zeolites During N-Pentane Catalytic Cracking," *Catal. Letters*, Vol. 150, No. 9, Pp. 2716–2725, 2020, Doi: 10.1007/S10562-020-03173-4.

[30] H. G. Karge And J. Weitkamp, *Molecular Sieves: Characterization Ii*, Vol. 5. Berlin, Heidelberg: Springer Berlin Heidelberg, 2007.

[31] A. C. Ferrari And J. Robertson, "Interpretation Of Raman Spectra Of Disordered And Amorphous Carbon," *Phys. Rev. B*, Vol. 61, No. 20, Pp. 14095–14107, May 2000, Doi: 10.1103/Physrevb.61.14095.

[32] G. Greczynski And L. Hultman, "X-Ray Photoelectron Spectroscopy: Towards Reliable Binding Energy Referencing," *Prog. Mater. Sci.*, Vol. 107, No. April 2019, P. 100591, 2020, Doi: 10.1016/J.Pmatsci.2019.100591.

[33] B. A. Sexton, A. E. Hughes, And D. M. Bibby, "An Xps Study Of Coke Distribution On Zsm-5," *J. Catal.*, Vol. 109, No. 1, Pp. 126–131, 1988, Doi: 10.1016/0021-9517(88)90190-X.

[34] A. Guo *Et Al.*, "Low-Temperature And Low-Pressure Non-Oxidative Activation Of Methane For Upgrading Heavy Oil," *Catal. Sci. Technol.*, Vol. 6, No. 4, Pp. 1201–1213, 2016, Doi: 10.1039/C5cy00947b.

[35] B. S. Liu, L. Jiang, H. Sun, And C. T. Au, "Xps, Xaes, And Tg/Dta Characterization Of Deposited Carbon In Methane Dehydroaromatization Over Ga-Mo/Zsm-5 Catalyst," *Appl. Surf. Sci.*, Vol. 253, No. 11, Pp. 5092–5100, 2007, Doi: 10.1016/J.Apsusc.2006.11.031.

[36] Y. H. Mo, Y. J. Choi, H. Choi, And S. E. Park, "Aromatization Of Iso-Butanol With Co2 As An Enhancer Over Zsm-5 Catalysts," *Res. Chem. Intermed.*, Vol. 43, No. 12, Pp. 7223–7239, 2017, Doi: 10.1007/S11164-017-3070-9.

[37] Y. Tian, S. Hu, X. De Jing, J. Xue, Y. Song, And X. Lan, "Desulfurization Performances Of Activated Coke Prepared From Fine Blue-Coke," *Water. Air. Soil Pollut.*, Vol. 231, No. 2, 2020, Doi: 10.1007/S11270-019-4390-8.

[38] M. A. Uguina, D. P. Serrano, R. Van Grieken, And S. Vènes, "Adsorption, Acid And Catalytic Changes Induced In Zsm-5 By Coking With Different Hydrocarbons," *Appl. Catal. A, Gen.*, Vol. 99, No. 2, Pp. 97–113, 1993, Doi: 10.1016/0926-860x(93)80093-6.

[39] A. M. Hernández-Giménez *Et Al.*, "Effect Of Mesoporosity, Acidity And Crystal Size Of Zeolite Zsm-5 On Catalytic Performance During The Ex-Situ Catalytic Fast Pyrolysis Of Biomass," *Chemcatchem*, Vol. 13, No. 4, Pp. 1207–1219, 2021, Doi: 10.1002/Cctc.202001778.

[40] S. Bhatia, J. Beltramini, And D. D. Do, "Deactivation Of Zeolite Catalysts," *Catal. Rev.*, Vol. 31, No. 4, Pp. 431–480, 1989, Doi: 10.1080/01614948909349937.

[41] A. G. Alvarez, H. Viturro, And R. D. Bonetto, "Structural Changes On Deactivation Of Zsm-5. A Study By X-Ray Powder Diffraction," *Mater. Chem. Phys.*, Vol. 32, No. 2, Pp. 135–140, 1992, Doi: 10.1016/0254-0584(92)90269-E.

[42] F. J. Sotomayor, K. A. Cychosz, And M. Thommes, "Characterization Of Micro/Mesoporous Materials By Physisorption: Concepts And Case Studies," *Acc. Mater. Surf. Res*, Vol. 3, No. 2, Pp. 34–50, 2018, [Online]. Available: Https://Www.Hyomen.Org/Wp-Content/Uploads/Papers/Vol3_No2/Sotomayor/Sotomayor_40.Pdf.

[43] M. D. Romero, J. A. Calles, A. Rodriguez, And J. C. Cabanelas, "The Influence Of Calcination Treatment Over Bifunctional Ni/Hzsm-5 Catalysts," *Ind. Eng. Chem. Res.*, Vol. 37, No. 10, Pp. 3846–3852, 1998, Doi: 10.1021/Ie980143i.

[44] W. Song, J. B. Nicholas, And J. F. Haw, "Acid-Base Chemistry Of A Carbenium Ion In A Zeolite Under Equilibrium Conditions: Verification Of A Theoretical Explanation Of Carbenium Ion

Stability," *J. Am. Chem. Soc.*, Vol. 123, No. 1, Pp. 121–129, 2001, Doi: 10.1021/Ja002775d.

[45] H. S. Cerqueira, P. Ayrault, J. Datka, And M. Guisnet, "Influence Of Coke On The Acid Properties Of A Ushy Zeolite," *Microporous Mesoporous Mater.*, Vol. 38, No. 2–3, Pp. 197–205, 2000, Doi: 10.1016/S1387-1811(99)00304-2.

[46] H. D. B. Jenkins And D. F. C. Morris, "Proton Affinity Of Gaseous Ammonia," *J. Chem. Soc. Faraday Trans. 2 Mol. Chem. Phys.*, Vol. 80, No. 9, Pp. 1167–1169, 1984, Doi: 10.1039/F29848001167.

[47] A. Feller, I. Zuazo, A. Guzman, J. O. Barth, And J. A. Lercher, "Common Mechanistic Aspects Of Liquid And Solid Acid Catalyzed Alkylation Of Isobutane With N-Butene," *J. Catal.*, Vol. 216, No. 1–2, Pp. 313–323, 2003, Doi: 10.1016/S0021-9517(02)00068-4.

[48] A. Feller, J. O. Barth, A. Guzman, I. Zuazo, And J. A. Lercher, "Deactivation Pathways In Zeolite-Catalyzed Isobutane/Butene Alkylation," *J. Catal.*, Vol. 220, No. 1, Pp. 192–206, 2003, Doi: 10.1016/S0021-9517(03)00251-3.

[49] M. Guisnet And F. R. Ribeiro, *Deactivation And Regeneration Of Zeolite Catalysts*, Vol. 9. Imperial College Press, 2011.

General Conclusion and Prospect for Future Work

I. The main conclusions of this thesis

Having conducted an in-depth analysis of the catalytic pyrolysis of polyethylene while manipulating the catalyst's acidity and the interaction between the polymer and the catalyst, the following key findings and contributions of this thesis can be summarised:

1. ***Activity vs Efficiency and Selectivity***: The Hβ zeolite, with approximately six times more external surface area than the HZSM-5 zeolite, exhibits a relative activity about 8 °C higher than that of HZSM-5 (catalyst:polymer ratio, 1:1). This is attributed to the increased accessibility of Brønsted sites for the initial polyethylene cracking. However, the shape-selectivity of HZSM-5 results in higher aromatics production, ranging from 23.3 % to 45.1 %, and a lower formation of hard coke compared to Hβ zeolite.

2. ***Preparation of the material using extrusion:*** Extrusion proves to be an advantageous preparation method in terms of activity, but the external surface area of the zeolite constrains it. The more external surface area corresponds to higher activity. Extrusion promotes the diffusion of products into the micropores, leading to an over-cracking and, consequently, an increased formation of coke, which is a source of aggressive deactivation.

3. ***Mix/Layer Arrangement:*** The Mix/Layer arrangement involves two stages of contact—first between polymer-liquid and catalyst, and second between cracking gas and catalyst—combining the advantages of arrangements focusing solely on polymer-liquid/catalyst and cracking gas/catalyst interactions. This arrangement results in a lower cracking temperature (450 °C instead of 500 °C) and facilitates greater diffusion of gaseous products of low molecular weight into the zeolite's micropores, leading to higher aromatics production.

4. ***Zinc Doping:*** The introduction of zinc in the zeolite increases the liquid fraction due to a combined effect of a reduced number of Brønsted sites and external surface area (though with an elevated quantity of Lewis acid sites); this leads to a decreased production of aromatics, but enhances the selectivity of BTEX within the aromatic compounds, thanks to the presence of new Lewis acid sites.

5. ***Dynamic Calcination Conditions***: Dynamic conditions involving a continuous airflow, as opposed to static conditions conducted with the air confined within the calcination chamber, present several advantages. It results in less dealumination due to water vapour drained from the zeolite before calcination, preserving Brønsted acid sites while reducing the generation of

Lewis acid sites during calcination. HZSM-5 zeolite calcined under dynamic conditions exhibits more significant activity and increased production of aromatic compounds.

6. ***Consecutive Use and Deactivation:*** The sequential utilisation of this HZSM-5 zeolite calcined under dynamic conditions has significant implications for polyethylene pyrolysis and zeolite deactivation. After three consecutive reaction cycles, the production of the oil fraction remains constant. However, the product distribution undergoes notable changes, with increasing production of iso-olefins and reduced aromatics production. The coke accumulates throughout the cycles, gradually transforming into hard coke of polyaromatic origin. Due to continuous cyclisation and aromatisation reactions, this coke forms within the zeolite's acid sites. It obstructs the pores, blocking accessible acid sites and impeding the diffusion and contact of compounds with these sites, affecting primarily the microporous surface.

II. The main contributions of this thesis to the catalytic pyrolysis of polyethylene

The preceding conclusions offer valuable insights into the practical implications of the catalytic pyrolysis of polyethylene. The primary contributions of this study align with the objectives outlined in the thesis plan of **section I** in the ***General Introduction*** and are summarised as follows:

1. ***Impact of Polymer-Catalyst Contact:*** The interaction between the polymer and the catalyst plays a pivotal role, particularly in the context of the experimental conditions of this thesis, where the polymer transitions into a liquid state before undergoing cracking. Under identical operational parameters, this distinctive contact exerts varying influences on different cracking fractions, product distribution within the oil fraction, coke quality, and, subsequently, the degree of zeolite deactivation.
2. ***Doping Effects:*** The introduction of dopants may have a favourable impact on the aromaticity of the final products of polyethylene catalytic pyrolysis. In the case of zinc introduced through ion exchange with the objective to enhance the quantity of Lewis acid sites, it influences the selectivity regarding BTEX production, increasing their presence among the aromatic compounds. However, the overall yield of aromatics remained relatively modest.
3. ***Calcination Conditions:*** The conditions of zeolite calcination have an important effect on both the catalyst properties and, thus, the pyrolysis oil yield and composition, in particular regarding the aromatic content.
4. ***Deactivation:*** It is crucial to study the catalytic pyrolysis reaction of polyethylene over multiple cycles. Reaction cycles impact product distribution since coking of the catalyst occurs rapidly, and the nature of coke varies over the cycle. A thorough understanding of coke characteristics is vital for selecting appropriate catalyst regeneration methods, an inherent aspect of the process. Effective regeneration is critical to preserving the physicochemical properties of the zeolite and averting rapid degradation.

5. ***NH_3-TPD Limitations:*** Methods such as NH_3-TPD, which involve the absorption of a strongly basic molecule, are unreliable for assessing the acidity of a coked zeolite; this is due to these basic entities' partial replacement of coke (carbenium ions) adsorbed on acidic sites.

These findings contribute to a comprehensive understanding of the complexities associated with catalytic polyethylene pyrolysis under real-world conditions. They shed light on various factors that need to be considered when optimising the process and ensuring the longevity of the zeolite catalyst.

III. Perspective for future work

Following extensive experimentation, results, and thorough analysis, it is evident that catalytic polyethylene cracking through pyrolysis represents a valuable technique for the recycling of plastic waste. To further enhance the efficiency of the catalytic pyrolysis process, the following research directions should be explored:

1. ***Gas Phase Characterisation:*** A deeper understanding of the gas phase, including product distribution, is essential. This knowledge will aid in elucidating reaction mechanisms and exploring the potential use of this gas as an energy source through combustion or other value-added processes.
2. ***Realistic Sample Analysis:*** Extend the application of this process to more representative samples, such as actual plastic waste, which typically consists of a mixture of PE, PP, PET, PVC, PS, and other plastics. Analysing real-world waste can provide insights into the challenges and opportunities of scaling up the process.
3. ***Multiphase Mix/Layer System:*** Investigate implementing a multiphase system utilising various zeolites at different stages, whether doped or not. This approach involves placing a zeolite with enhanced cracking capacity in the initial stage and another with superior favouring aromaticity in the subsequent stage, where aromatic propagation reactions are prevalent.
4. ***Optimised Calcination Variables:*** Explore diverse calcination variables, including temperature, heating rate, and duration. Conduct additional characterisations after pyrolysis to identify the most suitable calcination conditions that minimise any adverse effects on catalyst degradation. The aim is to enhance its performance in polyethylene pyrolysis.
5. ***Zeolite Regeneration Comparative Analysis:*** Compare various methods of zeolite regeneration, such as coke combustion with air, pure oxygen, ozonation, hydrogen peroxide oxidation, hydrogenation, Non-Thermal Plasma (NTP), or microwave assistance. Additionally, it will assess different regeneration variables, including temperature and regeneration duration, to understand their impact on zeolite degradation or dealumination.
6. ***Optimal Reaction Cycle for Regeneration:*** Determine the correct reaction cycle for implementing zeolite regeneration without incurring irreversible degradation. Finding the right balance is critical for sustaining the catalyst's effectiveness.